

**Gelatin Nanoparticles for
Targeted Oligonucleotide Delivery to Kupffer Cells**

—

Analytics, Formulation Development, Practical Application

Dissertation

zur Erlangung des Doktorgrades
der Fakultät für Chemie und Pharmazie der
Ludwig-Maximilians-Universität München

vorgelegt von

Jan Carl Zillies
aus Hamburg

2007

ERKLÄRUNG

Diese Dissertation wurde im Sinne von § 13 Abs. 3 bzw. 4 der Promotionsordnung vom 29. Januar 1998 von Herrn Prof. Dr. Gerhard Winter betreut.

EHRENWÖRTLICHE VERSICHERUNG

Diese Dissertation wurde selbstständig, ohne unerlaubte Hilfe erarbeitet.

München, am 12. Januar 2007

Jan Carl Zillies

Dissertation eingereicht am: 12. Januar 2007

1. Gutachter: Prof. Dr. Gerhard Winter

2. Gutachter: Prof. Dr. Wolfgang Frieß

Tag der mündlichen Prüfung: 02. Februar 2007

For my parents

Acknowledgements

The present thesis has been prepared between January 2003 and February 2007 at the Department of Pharmacy Pharmaceutical Technology and Biopharmaceutics of the Ludwig-Maximilians-University (LMU) Munich, Germany.

Foremost, I would like to express my honest gratitude to my supervisor Prof. Dr. Gerhard Winter for giving me the opportunity to be a member of his working group and to prepare this thesis. I am especially grateful for his guidance that allowed me to work independently and for the numerous successful scientific discussions driven by his impressive experience and knowledge. Furthermore, I always enjoyed his commitment to achieve the great working atmosphere we experienced at his chair.

I would like to thank my tutor Dr. Conrad Coester for his support during my work and the loyalty to his research team. Special thanks go to his efforts at presenting our work on international congresses and promoting my research stay at the University of Colorado.

Many thanks go to Prof. Dr. Angelika Vollmar and her research team at the Department of Pharmaceutical Biology (LMU Munich) for the great cooperation within the DFG project. PD Dr. Stefan Zahler is acknowledged for assisting me with FACS analysis, fluorescence microscopy, and monocyte isolation. My special appreciation goes to Florian Hoffmann for being more than my cooperation partner.

I am extremely grateful to Prof. Dr. Thomas J. Anchordoquy for giving me the chance to work in his lab at the School of Pharmacy of the University of Colorado and for his decisive contribution to the successful development of my research work. Within his team I especially would like to thank Marion Molina for providing me with the know-how about freeze-drying, for helping me with the analytics of my samples, and for joining me for lunch.

Special thanks go to Dr. Torsten Göppert (formerly Department of Pharmaceutical Technology at the Free University of Berlin) for the pleasant and successful 2D-PAGE cooperation.

I would like to thank Dr. Wolfgang Fraunhofer for telling me the secrets of AF4.

The teams of Postnova Analytics and Wyatt Technology are acknowledged for their always immediate and uncomplicated help with all kinds of problems concerning AF4 and light scattering analysis.

I am very thankful to Andrea Hawe, Florian Hoffmann, Rainer Lang, and Klaus Zwioerek for the quick and helpful proofreading of this thesis, which was essential to finish my work in time.

I would like to thank all the former and present colleagues of our department for the great times we had in- and outside the lab. I always enjoyed working with all of you and it was a pleasure to be member of the team. Especially, I want to highlight Klaus Zwioerek, who had to cope with my wordy attendance and became a good friend, after all the years sharing the lab. Special thanks go to Imke Leitner who always assisted me in supervising the students' practical course in biopharmaceutics, Alice Hirschmann for the great supply with lab consumables, Patricia Plath and Sabine Kersting for providing me with literature, as well as Gabi Hartl for their pleasant help with the administration.

Finally, I would like to thank my parents, my siblings, and my grandma for being my family. And, I would like to thank Stefanie!

TABLE OF CONTENTS

GENERAL INTRODUCTION	1
References	5
CHAPTER I	
Asymmetrical Flow Field-Flow Fractionation (AF4) in the Analytical	
Description of Gelatin Nanoparticles	7
1.1 Introduction	9
1.2 Materials and Methods	13
Reagents	13
AF4 Running buffers	13
Preparation and surface modification of gelatin nanoparticles	14
PEGylation of gelatin nanoparticles	15
Characterization of nanoparticles	16
Analysis of the gelatin bulk material	16
Quantification of oligonucleotide-loading onto the surface of gelatin nanoparticles	17
Quantification of gelatin nanoparticle PEGylation	19
Atomic force microscopy analysis of plain and PEGylated gelatin nanoparticles	20
1.3 Analysis of Gelatin Bulk Material Applied for the Manufacturing of Gelatin Nanoparticle Drug Delivery Systems Using Asymmetrical Flow Field-Flow Fractionation (AF4) and Multi-Angle Light Scattering (MALS)	
Detection	21
1.3.1 Introduction	21
1.3.2 Results and discussion	25
1.3.3 Summary	28
1.4 Quantifying the Oligonucleotide-Loading of Gelatin Nanoparticle Drug Delivery Systems Using Asymmetrical Flow Field-Flow Fractionation (AF4) and UV Detection	29
1.4.1 Introduction	29
1.4.2 Results and discussion	31

Characterization of nanoparticles	31
Single-stranded oligonucleotide loading	31
Double-stranded oligonucleotide loading	33
1.4.3 Summary	39
1.5 Quantifying the PEGylation of Gelatin Nanoparticle Drug Delivery Systems Using Asymmetrical Flow Field-Flow Fractionation (AF4) and Refractive Index (RI) Detection	41
1.5.1 Introduction	41
1.5.2 Results and discussion	44
Characterization of nanoparticles	44
Quantification of the PEGylation reaction via AF4	45
Visualization of the PEGylation reaction via AFM	51
1.5.3 Summary	52
1.6 Concluding Remarks	53
1.7 References	55
CHAPTER II	
Formulation Development of Freeze-Dried Gelatin Nanoparticles	63
2.1 Introduction	65
2.2 Materials and Methods	69
Reagents	69
Preparation and surface modification of gelatin nanoparticles	70
Oligonucleotide-loading of gelatin nanoparticles	70
Freeze-drying of empty and oligonucleotide-loaded gelatin nanoparticles	70
Storage conditions during stability studies	72
Characterization of gelatin nanoparticles	72
Karl-Fischer titration	73
Differential scanning calorimetry (DSC)	73
In vivo hepatic lipopolysaccharide (LPS) (sepsis) rat model	75
2.3 Results and Discussion	77
2.3.1 Applicability of freeze-drying for gelatin nanoparticle suspensions	77
Characterization of nanoparticles	77
Initial freeze-drying experiments	78

2.3.2	Storage stability tests of freeze-dried empty and oligonucleotide-loaded gelatin nanoparticles	90
	Empty gelatin nanoparticles	91
	Oligonucleotide-loaded gelatin nanoparticles	109
2.4	Summary	115
2.5	References	119
2.6	Annex	125
2.6.1	Stability data of empty gelatin nanoparticles	125
	Photon correlation spectroscopy (PCS) data	125
	Karl-Fischer titration data	127
	Differential scanning calorimetry (DSC) data	129
2.6.2	Stability data of oligonucleotide-loaded gelatin nanoparticles	132
	Photon correlation spectroscopy (PCS) data	132
CHAPTER III		
Gelatin Nanoparticles for Targeted Oligonucleotide Delivery to Kupffer Cells During Hepatic Ischemia Reperfusion (I/R) Injury		
		133
3.1	Introduction	135
3.1.1	Anatomic fundamentals	136
3.1.2	Pathophysiological mechanisms	137
3.1.3	Therapeutic options	140
	Surgical options	140
	Interruption of pathophysiological signal transduction pathways	140
3.1.4	Therapeutic strategy – Gelatin nanoparticles for targeted delivery of an NF- κ B decoy oligonucleotide to Kupffer cells	143
3.2	Proof of Principle – Kupffer Cell Targeting	147
3.2.1	Materials and methods	147
	Reagents	147
	Cell culture	148
	Fluorescent staining	148
	Solutions	149
	Preparation and surface modification of gelatin nanoparticles	149
	Preparation of fluorescent cationic gelatin nanoparticles	150

Oligonucleotide-loading of gelatin nanoparticles	150
Characterization of nanoparticles	150
Isolation and purification of Kupffer cells	150
Kupffer cell uptake studies	151
In vivo biodistribution experiments	151
CLSM imaging	152
3.2.2 Results and discussion	155
Characterization of nanoparticles	155
Biodistribution of intravenously and intraportally applied gelatin nanoparticles	155
Intracellular distribution of gelatin nanoparticles in Kupffer cells	158
3.2.3 Summary	161
3.3 Excursus – Comparing Plasma Protein Adsorption Pattern and Biodistribution of Gelatin Nanoparticles and Solid Lipid Nanoparticles (SLN)	163
3.3.1 Introduction	163
In vivo fate of colloidal drug carrier systems	163
Two dimensional polyacrylamide gel electrophoresis (2D-PAGE)	165
3.3.2 Materials and methods	167
Reagents	167
Fluorescent dyes	168
2D-PAGE analysis	168
Preparation and surface modification of gelatin nanoparticles	169
Preparation of fluorescent cationic gelatin nanoparticles	169
Oligonucleotide-loading of gelatin nanoparticles	169
Manufacturing of SLN	170
Manufacturing of fluorescent-labeled SLN	170
Characterization of nanoparticles	170
In vivo biodistribution experiments	171
CLSM imaging	171
FACS analysis of rat whole blood and plasma	171
2D-PAGE experiments	172

3.3.3	Results and discussion	175
	Characterization of nanoparticles	175
	Plasma protein adsorption patterns – gelatin nanoparticles vs. SLN	177
	Biodistribution	183
3.3.4	Summary	190
3.4	NF-κB Inhibition During Hepatic Ischemia Reperfusion Injury	191
3.4.1	Materials and methods	191
	Reagents	191
	Fluorescent staining	192
	Electrophoretic Mobility Shift Assay (EMSA)	192
	Preparation and surface modification of gelatin nanoparticles	193
	Oligonucleotide-loading of gelatin nanoparticles	194
	Freeze dried formulation of empty and oligonucleotide loaded gelatin nanoparticles	194
	Preparation of NF- κ B decoy oligonucleotide loaded liposomes	195
	Characterization of liposomes and nanoparticles	196
	In vivo biodistribution experiments	196
	CLSM imaging	196
	In vivo Hepatic Ischemia Reperfusion rat model	197
	In vivo hepatic LPS (sepsis) rat model	197
	Electrophoretic Mobility Shift Assay (EMSA)	198
3.4.2	Results and discussion	201
	Characterization of gelatin nanoparticles and liposomes	201
	Hepatic Ischemia Reperfusion model in rat	201
	Lipopolysaccharide (LPS) induced hepatic NF- κ B response in rat	206
	Liposomal vs. gelatin nanoparticulate delivery of the NF- κ B decoy oligonucleotide to Kupffer cells	207
3.4.3	Summary	211
3.5	Concluding Remarks	213
3.6	References	215
	FINAL CONCLUSION	225

LIST OF ABBREVIATIONS

2-DE	Two-dimensional electrophoresis
2D-PAGE	Two-dimensional polyacrylamide gel electrophoresis
AF4	Asymmetrical flow field-flow fractionation
AFM	Atomic force microscopy
ALT	Alaninaminotransferase
APS	Ammonium persulfate
AST	Aspartataminotransferase
ATP	Adenosine triphosphate
AUC	Area under the curve
BSA	Bovine serum albumin
CHAPS	3-[(3-Cholamidopropyl) dimethylammonio]-1-propanesulfonate
CLSM	Confocal laser scanning microscopy
DFG	Deutsche Forschungsgemeinschaft
DLS	Dynamic light scattering
DMEM	Dulbecco's modified eagle medium
DMF	Dimethylformamide
DNA	Desoxyribonucleic acid
DOPC	1,2-dioleoyl-sn-glycero-3-phosphocholine
DOTAP	1,2-dioleoyl-3-trimethylammonium-propane
ds	Double-stranded
DSC	Differential scanning calorimetry
DTE	1,4-dithioerythritol
DTT	Dithiothreitol
EDC	1-ethyl-3-(3-dimethyl-aminopropyl) carbodiimide hydrochloride
EMSA	Electrophoretic Mobility Shift Assay
FACS	Fluorescence-activated cell sorting
FBS	Fetal bovine serum
FDA	U.S. Food and Drug Administration
FFF	Field-flow fractionation

FT-IR	Fourier-transformation infrared spectroscopy
G-CSF	Granulocyte colony stimulating factor
G-NP	Gelatin nanoparticles
G-NP pos	Surface-modified (cationized) gelatin nanoparticles
G-NP pos + O	Oligonucleotide-loaded surface-modified gelatin nanoparticles
hmw	High molecular weight
HPLC	High pressure liquid chromatography
HSA	Human serum albumin
I/R	Ischemia / reperfusion
IEF	Isoelectric focussing
IEP	Isoelectric point
Ig	Immunoglobulin
IPG	Immobilized pH gradient
lmw	low molecular weight
LPS	Lipopolysaccharide
M	Mannitol
MALS	Multi angle light scattering
MELANIE	Medical Electrophoresis Analysis Interactive Expert System
mp	Melting point
MPS	Mononuclear phagocytosis system
MS	Mannitol-sucrose
ODN	Oligonucleotide
P188-SLN	Poloxamer 188 solid lipid nanoparticles
PAGE	Polyacrylamide gel electrophoresis
PBS	Phosphate-buffered saline
PCL	Polycaprolactone
PCS	Photon correlation spectroscopy
PDI	Polydispersity index
PEG	Polyethylenglycol
PEI	Polyethylenimin
PLA	Poly lactide
PLGA	Poly (lactide-co-glycolide)

PMSF	Phenylmethanesulfonyl fluoride
PTO	Phosphorothioate
RH	Relative Humidity
RI	Refractive index
RNA	Ribonucleic acid
ROS	Reactive oxygen species
S	Sucrose
SDS	Sodium dodecyl sulfate
SE-HPLC	Size exclusion high pressure liquid chromatography
SEM	Scanning electron microscopy
siRNA	Small interfering ribonucleic acid
SLN	Solid lipid nanoparticles
ss	Single-stranded
STE	Sodium chloride / Tris / EDTA buffer
T	Trehalose
T ₀	Temperature of “zero” mobility
TBE	Tris / borate / EDTA buffer
T _c	Collapsing temperature
TEMED	N, N, N', N' tetramethyl ethylene diamine
T _g	Glass transition temperature
T _g '	Glass transition of the maximally freeze-concentrated solution
TRIS	Tris(hydroxymethyl)aminomethane
UV	Ultraviolet

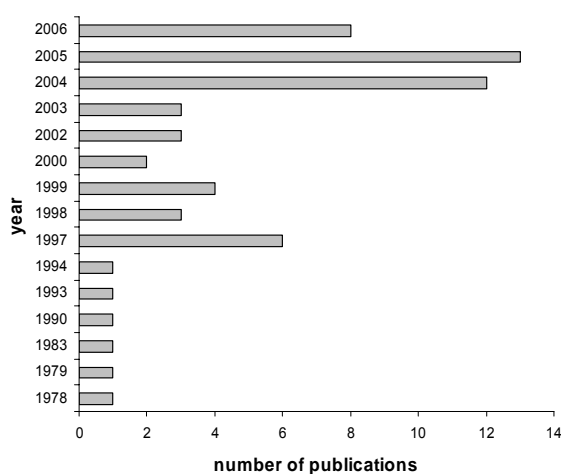
GENERAL INTRODUCTION

Today, nanoparticle-mediated drug delivery and drug targeting is intensively researched. Within the growing field of nanomedicine, drug delivery accounts for more 50 % of all publications and patent filings worldwide [Wagner et al., 2006], whereas nanoparticulate delivery is still mostly part of basic research. The need for nanoparticles as biodegradable and non toxic drug delivery system was firstly formulated in 1978 by Marty [Marty et al., 1978]. Since then, numerous synthetic and natural polymers were adopted for the production of biodegradable nanoparticles. Poly- ϵ -caprolactone (PCL), poly(lactic acid) (PLA), poly(glycolic acid) (PGA), and their co-polymers poly(lactide-co-glycolide) (PLGA) are the most widely used starting materials [Hans et al., 2006]. Applied natural polymers are proteins (albumin and gelatin) [Kaul et al., 2005] and polysaccharides (dextran, alginate, and chitosan) [Chorny et al., 2004]. Scholes summarized the requirements for an ideal targeting system as follows: i) biocompatibility, biodegradability, and low antigenicity, ii) protection of the drug, iii) maintenance of the integrity till the target is reached, iv) avoidance of side effects, v) membrane passage, vi) target recognition and association, vii) controlled drug release, and viii) elimination upon drug release [Scholes et al., 1997].

Among natural polymers gelatin offers some advantageous material properties. Due to its proteinaceous nature it is readily accessible for chemical modifications either of the bulk material or the finished nanoparticles via the functionalities of the amino acid residues [Djagny et al., 2001]. And, beside these technological aspects gelatin is known for its good biodegradability and biocompatibility [Yamamoto et al., 2001; Stevens et al., 2002] accompanied with low immunogenicity [Schwick et al., 1969; Kuijpers et al., 2000]. These beneficial characteristics are not only expressed in long clinical usage of gelatin as plasma expander [Tabata et al., 1998] and as sealant for vascular prosthesis [Kuijpers et al., 2000] but also led to the acceptance of gelatin as “Generally Recognized as Safe” (GRAS) substance in the

area of food additives by the U.S. Food and Drug Administration (FDA)*. The application of gelatin in controlled release devices for bioactive molecules like proteins or plasmid DNA was recently reviewed [Young et al., 2005] and the emerging interest in gelatin nanoparticles as drug delivery system can be drawn from the increasing number of scientific contributions published in last five years (Figure 1).

Figure 1 Number of publications containing gelatin nanoparticles for drug delivery and drug targeting (source: Chemical Abstract Service; search criteria: „gelatin“ AND „nanoparticles“ AND „drug delivery“ OR „drug targeting“)



The present work is based on the achievements in the preparation of stable gelatin nanoparticles exhibiting a homogenous size distribution described by Coester [Coester et al., 2000]. It was the objective of this thesis to technologically advance this colloidal drug carrier system in order to provide the basis for further *in vitro* and *in vivo* applications.

In the end of the performed research work on gelatin nanoparticles the obtained results are here discussed in three discrete chapters covering analytical aspects, formulation development, and *in vivo* application. In **CHAPTER I** the introduction of asymmetrical flow field-flow fractionation (AF4) in the analysis of colloidal drug carrier systems is described. The impact of gelatin bulk material on the preparation of gelatin nanoparticles, the drug loading of gelatin nanoparticles with single- and double-stranded oligonucleotides, and the PEGylation of the nanoparticles were intensively studied. **CHAPTER II** explores the applicability of freeze-drying for the stabilization of gelatin nanoparticles. Different common freeze-drying excipients

*<http://www.cfsan.fda.gov/~dms/opascogc.html#ftn2>

were employed and assessed for their protection of empty and oligonucleotide-loaded nanoparticles during lyophilization and short term stability stress testing. The investigation of the role that NF- κ B, released from Kupffer cells, plays during hepatic ischemia reperfusion (I/R) injury, was subject of the work summarized in **CHAPTER III**. Conducted in cooperation, together with the chair of Pharmaceutical Biology of the Ludwig-Maximilians-University Munich the interruption of NF- κ B activation within Kupffer cells was addressed in an animal model. Thereby a drug targeting approach with NF- κ B decoy oligonucleotide-loaded gelatin nanoparticles was utilized. The selective Kupffer cell uptake of the nanoparticles, the correlation between their biodistribution and corresponding plasma protein adsorption patterns, and the NF- κ B decoy efficacy are reviewed.

The NF- κ B decoy oligonucleotide forms the brace that thematically links the work. It is applied during AF4 studies; it is part of the freeze-drying formulation development; and it is the center of the ischemia reperfusion injury cooperation project.

References

- Chorny, M., Cohen-Sacks, H., Fishbein, I., Danenberg, H. D., and Golomb, G.; Biodegradable nanoparticles as drug delivery systems for parenteral administration; *Tissue Engineering and Novel Delivery Systems*, 2004, 393-422
- Coester, C. J., Langer, K., Von Briesen, H., and Kreuter, J.; Gelatin nanoparticles by two step desolvation-a new preparation method, surface modifications and cell uptake; *Journal of Microencapsulation*, 2000, 17(2), 187-193
- Djagny, K. B., Wang, Z., and Xu, S.; Gelatin: A valuable protein for food and pharmaceutical industries: Review; *Critical Reviews in Food Science and Nutrition*, 2001, 41(6), 481-492
- Hans, M. L. and Lowman, A. M.; Nanoparticles for drug delivery; in *Nanomaterials Handbook*, CRC Press, LLC., Boca Raton, FL, 2006, 637-664
- Kaul, G. and Amiji, M.; Protein nanoparticles for gene delivery; in *Polymeric Gene Delivery: Principles and Applications*, CRC Press, LLC., Boca Raton, FL, 2005, 429-447
- Kuijpers, A. J., Engbers, G. H., Krijgsveld, J., Zaat, S. A., Dankert, J., and Feijen, J.; Cross-linking and characterisation of gelatin matrices for biomedical applications; *Journal of Biomaterials Science. Polymer edition*, 2000, 11(3), 225-243
- Marty, J. J., Oppenheim, R. C., and Speiser, P.; Nanoparticles - a new colloidal drug delivery system; *Pharmaceutica Acta Helveticae*, 1978, 53(1), 17-23
- Scholes, P. D., Coombes, A. G. A., Davies, M. C., Illum, L., and Davis, S. S.; Particle engineering of biodegradable colloids for site-specific drug delivery; *Controlled Drug Delivery*, 1997, 73-106
- Schwick, H. G. and Heide, K.; Immunochemistry and immunology of collagen and gelatin; *Bibliotheca Haematologica (Basel)*, 1969, 33, 111-125
- Stevens, K. R., Einerson, N. J., Burmania, J. A., and Kao, W. J.; In vivo biocompatibility of gelatin-based hydrogels and interpenetrating networks; *Journal of Biomaterials Science, Polymer Edition*, 2002, 13(12), 1353-1366
- Tabata, Y. and Ikada, Y.; Protein release from gelatin matrixes; *Advanced Drug Delivery Reviews*, 1998, 31(3), 287-301
- Wagner, V., Dullaart, A., Bock, A. K., and Zweck, A.; The emerging nanomedicine landscape; *Nature Biotechnology*, 2006, 24(10), 1211-1217
- Yamamoto, M., Ikada, Y., and Tabata, Y.; Controlled release of growth factors based on biodegradation of gelatin hydrogel; *Journal of Biomaterials Science. Polymer edition*, 2001, 12(1), 77-88

Young, S., Wong, M., Tabata, Y., and Mikos, A. G.; Gelatin as a delivery vehicle for the controlled release of bioactive molecules; *Journal of Controlled Release*, 2005, 109(1-3), 256-274

CHAPTER I

Asymmetrical Flow Field-Flow Fractionation (AF4) in the Analytical Description of Gelatin Nanoparticles

Abstract

Asymmetrical flow field-flow fractionation (AF4) offers unique separation properties for macromolecules, colloids, particles, and even cells from human or animal origin. At the same time the characterization of non viral colloidal drug delivery systems by means of AF4 is barely described in literature. Here, three different analytical tasks investigating gelatin nanoparticles as drug delivery system were executed utilizing AF4 coupled with multi-angle light scattering (MALS), UV, and refractive index (RI) detection respectively. In a comparative study, several batches of gelatin bulk material were characterized for their molecular weight distribution. Based on these data the exact requirements on gelatin for the realized development of a one-step desolvation process for gelatin nanoparticle synthesis could be described. Following the loading of surface-modified gelatin nanoparticles with a double-stranded oligonucleotide revealed systematical limits of the analytical approach. And finally, the quantification of the PEGylation of gelatin nanoparticles could successfully be completed. In sum, the presented results demonstrate the versatile applicability of asymmetrical flow field-flow fractionation also in the field of colloidal drug delivery systems.

Keywords: field-flow fractionation, multi-angle light scattering, gelatin, nanoparticulate drug delivery systems, PEGylation

1.1 Introduction

Field-flow fractionation (FFF) was proposed in 1966 as separation concept especially exhibiting advantages in separating macromolecules and colloids [Giddings, 1966]. Since then FFF was developed to one of the most versatile families of separation techniques known [Giddings, 2000] and its potential in the analysis of high molecular weight specimen even up to human and animal cells was demonstrated [Reschiglian et al., 2005; Kowalkowski et al., 2006; Ratanathanawongs-Williams et al., 2006]. The theory behind and the basic mechanisms of AF4 are discussed elsewhere [Wahlund et al., 1987; Litzen et al., 1991; Colfen et al., 2000; Schimpf et al., 2000] and are thus in the following only summarized in brief. During an FFF sample run a liquid carrier is transported through a hollow separation channel forming a parabolic flow profile with layers of different velocities. Perpendicular to this laminar carrier flow a field of separation is applied. With respect to the source of this field (symmetrical, asymmetrical, and hollow fiber) flow (F)FFF, thermal (Th)FFF, sedimentation (Sd)FFF, electrical and dielectric (E/DI)FFF, as well as magnetic (Mg)FFF are differentiated. During asymmetrical flow field-flow fractionation (AF4) the separation field is erected by another liquid flow, called cross-flow, which contributes to the distribution of the analytes in the different areas of velocity of the laminar channel flow, finally leading to their fractionated elution. The cross-flow leaves the channel through an ultrafiltration membrane covering the bottom (= accumulation) wall of the channel. The analyte's diffusion coefficient is thereby the critical number the cross-flow has to compensate. The Stokes-Einstein equation expresses the relationship between the diffusion coefficient D of a spherical particle and its hydrodynamic radius R_h in a medium with a given viscosity η :

$$D = \frac{kT}{6\pi\eta R_h} \quad (1-1)$$

where k is the Boltzmann constant and T is the absolute temperature. Together cross-flow V_c and diffusion coefficient D determine the elution (retention) time t_r of the analytes as it is shown in the following equation:

$$t_r = \frac{t_0 V_c w^2}{6DV_0} \quad (1-2)$$

where t_0 is the retention time of an unretained solute, V_0 is the volume of the separation channel, and w is the channel height. This means that larger particles with a smaller diffusion coefficient (eq. 1-1) are stronger influenced by the actual cross-flow. Therefore they are concentrated in areas of the laminar flow closer to the accumulation wall exhibiting lower velocities, which finally leads to prolonged retention (eq. 1-2). Due to the open architecture of the separation channel species ranging from 1 nm up 100 μ m are accessible for separation by field-flow fractionation [Giddings, 1993].

The described strengths in the fractionation of macromolecules, colloids, particles, and cells are thereby reflected in the applications of FFF ranging from industrial [Schimpf et al., 2000] and environmental [Gimbert et al., 2003] to biotechnological [Reschiglian et al., 2005] and (bio)pharmaceutical [Fraunhofer et al., 2004a] tasks. However, despite the growing implementation of the different field-flow fractionation subtechniques over the last two decades [Kowalkowski et al., 2006] and the general recognition of field-flow fractionation for the characterization of nanoparticles [Haskell, 2006] only little is reported about employing FFF for the characterization of non viral colloidal drug delivery systems. Investigation of size and size distribution via (flow) FFF of gelatin [Fraunhofer et al., 2004b], PLGA [Augsten et al., 2005] and solid lipid nanoparticles [Jores et al., 2004] as well as virus like particles [Lang et al., 2006] and lipid-DNA complexes [Lee et al., 2001] were just recently described. The characterization of liposomes via SdFFF and FFFF is in turn already known for more than 20 years [Caldwell et al., 1981; Moon et al., 1993]. In addition, Andersson described the influence of several surface modifications on size distribution and mass of polystyrene nanoparticles utilizing SdFFF [Andersson et al., 2005].

In this context, it was the objective of the present work to illustrate how asymmetrical flow field-flow fractionation can be used as high resolution technique

for the analytical description of nanoparticulate drug delivery systems. In continuation of the basic work accomplished by Wolfgang Fraunhofer at this chair [Fraunhofer, 2003] three different applications of AF4 in the work with gelatin nanoparticles are introduced. Gelatin bulk material used for the nanoparticle synthesis was investigated for its molecular weight distribution via the combination of AF4 and multi-angle light scattering (MALS) detection, drug loading of surface-modified gelatin nanoparticles with a double-stranded oligonucleotide was followed with AF4 and UV-detection, and in the end PEGylation of gelatin nanoparticles was quantified after AF4 separation from refractive index (RI) detection signals.

1.2 Materials and Methods

Reagents

Reagent	Description	Supplier
Acetone	p.a.	VWR International GmbH (Ismaning, Germany)
Cholaminechloride hydrochloride	(2-aminoethyl)-trimethyl-ammoniumchloride hydrochloride	Sigma-Aldrich GmbH (Taufkirchen, Germany)
ds NF- κ B decoy ODN	5'-AGT TGA GGG GAC TTT CCC AGG C-3' phosphorothioate	biomers.net GmbH (Ulm, Germany)
EDC	1-ethyl-3-(3-dimethyl-aminopropyl) carbodiimide hydrochloride	Sigma-Aldrich GmbH (Taufkirchen, Germany)
Gelatin type A	175 Bloom	Sigma-Aldrich GmbH (Taufkirchen, Germany)
Gelatin PN307779	Portion of peptides with MW < 65 kDa below 40 %	Gelita AG (Eberbach, Germany)
Gelatin VP433	Portion of peptides with MW < 65 kDa below 40 %; enriched portion of high molecular weight fractions > 10 ⁴ kDa	Gelita AG (Eberbach, Germany)
Gelatin VP306/VP413-2	Portion of peptides with MW < 65 kDa below 20 %	Gelita AG (Eberbach, Germany)
Glutaraldehyde	25 % aqueous solution	Sigma-Aldrich GmbH (Taufkirchen, Germany)
HCl	2 N	VWR International GmbH (Ismaning, Germany)
PEG 5000 (mPEG-NH ₂)	Methoxy-poly(ethyleneglycol)-amine MW 5,884 Da	Nektar Therapeutics (Huntsville, AL, USA)
ss ODN	5'-TCG-CTC-GAT-AGC-TCG-ATC-3'	MWG-Biotech AG (Ebersberg, Germany)

AF4 Running buffers

Solution	Components*	Concentration
Dulbecco's PBS pH 7.3	KCl	2.67 mM
	KH ₂ PO ₄	1.47 mM
	NaCl	137.93 mM
	Na ₂ HPO ₄ X 7H ₂ O	8.06 mM

Solution	Components*	Concentration
PBS pH 6.0	NaCl	14 mM
	Na ₂ HPO ₄ x 2H ₂ O	2 mM
	NaOH/HCl	q.s.
PBS pH 7.0	NaCl	150 mM
	Na ₂ HPO ₄ x 2H ₂ O	30 mM
	NaH ₂ PO ₄ x 2H ₂ O	20 mM
	NaOH/HCl	q.s.
PBS pH 7.4	NaCl	140 mM
	Na ₂ HPO ₄ x 2H ₂ O	2 mM
	NaOH/HCl	q.s.

*All buffer salts were purchased from Sigma-Aldrich GmbH (Taufkirchen, Germany)

Preparation and surface modification of gelatin nanoparticles

Gelatin nanoparticles were prepared by the two-step desolvation method [Coester et al., 2000]: 1.25 g gelatin were dissolved in water (5% [w/w]) under stirring (500 rpm) and heating up to 50°C. The resulting solution was fractionated in a first desolvation step by quickly adding 25 mL of acetone. The supernatant was discarded and the remaining sediment –containing the high molecular weight fraction of gelatin – was dissolved in another 25 mL of water. After adjusting the pH with 110 µL hydrochloric acid nanoparticles emerged in a second desolvation step by dropwise adding 50 mL of acetone under constant stirring (500 rpm). After 5 min of stirring, the in situ formed particles were stabilized by crosslinking with 43.8 µg glutaraldehyde. Nanoparticles were 4 times purified by centrifugation for 20 min at 20.000 g (SIGMA 4K15, SIGMA Laborzentrifugen GmbH, Osterode, Germany) and redispersion in highly purified water. Finally, the concentration of the nanoparticle dispersions was determined gravimetrically by drying three aliquots of 100 µL each to weight constancy.

Surface modification (cationization) of gelatin nanoparticles was performed with the quaternary amine cholamine in a modified procedure based on the method previously described by Coester [Coester, 2003]: after preparation and purification, the nanoparticles were suspended in highly purified water to a volume of 25 mL followed by adjusting the pH to 4.20 and dissolving 50 mg cholamine in the resulting suspension. After 5 minutes of stirring, 50 mg EDC were added to the reaction vessel

in order to activate the free carboxyl groups on the surface of the unmodified nanoparticles for the coupling with cholamine. Beside the activated carboxyl groups cholamin reacts with aldehyde groups of mono-functionally bound glutaraldehyde derived from crosslinking. After 3 h the reaction was abandoned and the nanoparticles were purified as described above.

PEGylation of gelatin nanoparticles

For PEGylation 50 μL of an aqueous nanoparticle dispersion (20 mg/mL) were incubated for 2 h under constant shaking (800 rpm; 25°C; Thermomixer comfort, Eppendorf, Hamburg, Germany) with various amounts of an mPEG-NH₂ solution in borate buffer pH 8.4 (20 mg/mL). Thereby, mPEG-NH₂ reacts with residual aldehyde groups on the surface of the gelatin nanoparticles (Figure 1.2.1). After incubation the total volume was completed with highly purified water to 1 mL resulting in a nanoparticle concentration of 1 mg/mL. An aliquot was transferred to AF4 analysis and the remaining particles were washed by 3-fold centrifugation and redispersion in PBS pH 7.4. PEGylation of gelatin nanoparticles is described and was conducted by Klaus Zwiorek [Zwiorek, 2006].

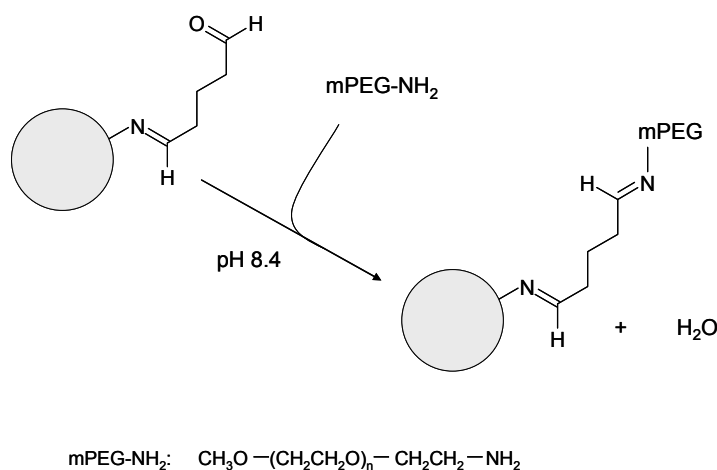


Figure 1.2.1 PEGylation reaction scheme of gelatin nanoparticles

PEGylated nanoparticles used in atomic force microscopy (AFM) experiments demanded furthermore a cationic surface charge to enable fixation on the anionic sample grid and were surface-modified as described above subsequent to PEGylation.

Characterization of nanoparticles

Size and zeta potential of the applied gelatin nanoparticle batches were determined by dynamic light scattering (DLS) using a Zetasizer Nano ZS (Malvern Instruments, Worcestershire, UK). Zeta potential measurements were conducted under standardized ionic conditions in 10 mM NaCl at pH 7.0.

Analysis of the gelatin bulk material

Samples of different gelatin batches were dissolved under heating (50 °C) in highly purified water and diluted to a final concentration of 2.5 mg/mL, which is sufficient to avoid gelation upon cooling down to room temperature. In addition, gelatin sediment derived from the first desolvation step from the manufacturing process of the gelatin nanoparticles was diluted in highly purified water to an equivalent final concentration. Samples were transferred to AF4 analysis without further preparation.

AF4 studies were performed using a HRFFF-10.000 AF4 system (Postnova Analytics GmbH, Landsberg a. L., Germany). The channel height was set at 350 μm ; the applied ultrafiltration membrane was a regenerated cellulose membrane with 5 kDa cut-off (Nadir Filtration, Wiesbaden, Germany). PBS pH 6.0 was chosen as running buffer. The channel flow rate accounted for 1 mL/min, the cross-flow was adjusted to 0.05 mL/min over 30 min (cp. Figure 1.2.2 for complete cross-flow profile), and the measurement period amounted to 40 min.

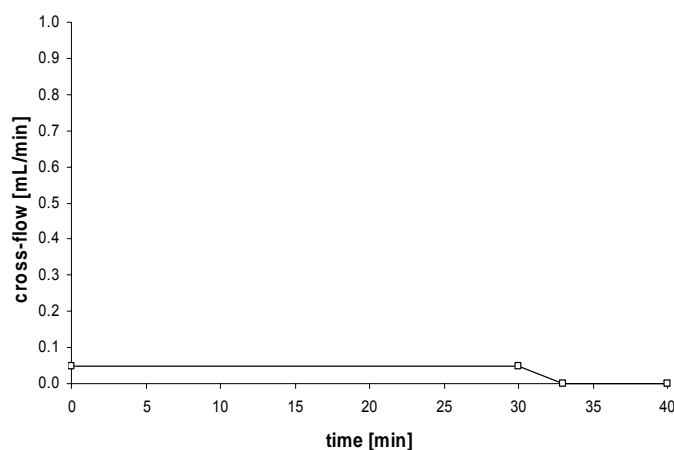


Figure 1.2.2 Cross-flow profile applied for the AF4 analysis of aqueous gelatin solutions

On-line detection was done UV-spectrophotometrically at a wavelength of 220 nm (Spectra System UV 1000, Thermo Separation Products, Germany) coupled

with multi-angle light scattering (MALS) detection using a miniDAWNTM light scattering detector (Wyatt Technology Europe GmbH, Dernbach, Germany). For molar mass determination of gelatin the refractive index increment was set to 0.174 mL/g and the second virial coefficient was set to 0. The whole study was repeated three times.

Quantification of oligonucleotide-loading onto the surface of gelatin nanoparticles

Single-stranded oligonucleotide loading: 185 μ L of an aqueous nanoparticle dispersion containing 1.0 mg surface-modified gelatin nanoparticles were incubated with 10 μ L of an aqueous oligonucleotide (ODN) solution containing 0.1 mg single-stranded ODN (i.e., 10 % [w/w]) in PBS pH 7.4 adjusted to a final volume of 1.0 mL for 2 h at 22 °C and 800 rpm under constant shaking (Thermomixer Comfort, Eppendorf AG, Hamburg, Germany). The amount of loaded oligonucleotide was calculated from unbound oligonucleotide determined UV-spectrophotometrically at a wavelength of 260nm (UV1, Thermo Spectronic, Dreieich, Germany) in the supernatant of the reaction media after separating the nanoparticles by centrifugation for 50 min at 14000g (neo lab 16/18, Hermle Labortechnik GmbH, Wehingen, Germany). In addition blanks of oligonucleotide and gelatin nanoparticles at their own were accordingly prepared in PBS pH 7.4. All samples were afterwards directly transferred to AF4 analysis. AF4 studies were performed using a HRFFF-10.000 AF4 system (Postnova Analytics GmbH, Landsberg a. L., Germany). The channel height was set at 500 μ m; the applied ultrafiltration membrane was a regenerated cellulose membrane with 1 kDa cut-off (Nadir Filtration, Wiesbaden, Germany). PBS pH 7.4 was chosen as running buffer. The channel flow rate accounted for 1 mL/min and the cross-flow was initially adjusted to 1.86 mL/min and gradually decreased down to 0 mL/min after 13 min (cp. Figure 1.2.3 for complete cross-flow profile). The measurement period amounted to 40 min. On-line detection was done UV-spectrophotometrically at a wavelength of 260 nm (Spectra System UV 1000, Thermo Separation Products, Germany). ODN loading was quantified by comparing the AUCs of oligonucleotide and nanoparticles from their respective peaks in the resulting fractograms before and after the loading process. The results from UV-spectroscopy were thereby used as positive control for the AF4 experiments. The whole study was repeated three times.

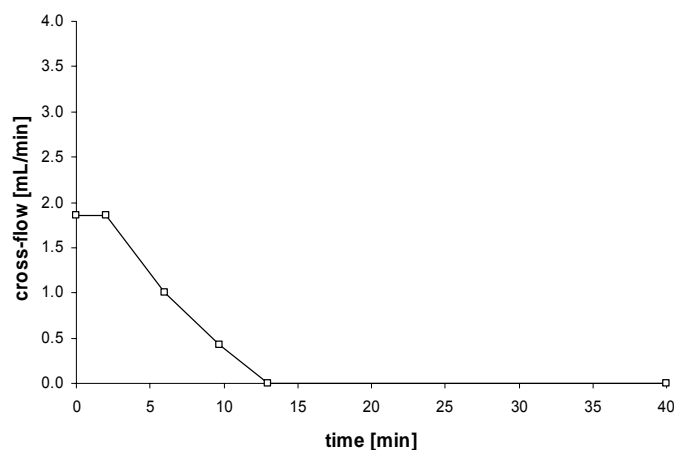


Figure 1.2.3 AF4 cross-flow profile applied for the quantification of the loading of gelatin nanoparticles with single-stranded oligonucleotide

Experiments were conducted together with Wolfgang Fraunhofer. According data are as well described in his thesis and have already been published elsewhere [Fraunhofer, 2003; Zillies et al., 2003; Fraunhofer et al., 2004b].

Double-stranded oligonucleotide loading: 95 μL of an aqueous nanoparticle dispersion containing 1.4 mg surface-modified gelatin nanoparticles were incubated with 100 μL of an aqueous oligonucleotide solution containing 0.07 μg double-stranded ODN (i.e., 5 % [w/w]) in highly purified water adjusted to a final volume of 1.0 mL for 2 h at 22 $^{\circ}\text{C}$ and 800 rpm under constant shaking (Thermomixer Comfort, Eppendorf AG, Hamburg, Germany). The oligonucleotide-loading was UV-spectrophotometrically assessed as already described for the single-stranded oligonucleotide-loaded gelatin nanoparticles. Again blanks from oligonucleotide and gelatin nanoparticles at their own were accordingly prepared in highly purified water and all samples were then directly transferred to AF4 analysis. AF4 studies were performed using a Wyatt Eclipse2 AF4 system (Wyatt Technology Europe GmbH, Dernbach, Germany). The channel height was set at 350 μm ; the applied ultrafiltration membranes were a regenerated cellulose membrane and a polyethersulfone (PES) membrane each with 5 kDa cut-off. Isocratic HPLC pump, autosampler, degasser, and UV-detector are parts of the Agilent 1100 series (Agilent Technologies, Palo Alto, CA, United States). Dulbecco's PBS pH 7.3 was chosen as running buffer. The channel flow rate accounted for 1 mL/min, the cross-flow was adjusted to 2.5 mL/min over 10 min (cp. Figure 1.2.4 for complete cross-flow profile), and the measurement period amounted to 51 min. On-line detection was done UV-spectrophotometrically at a wavelength of 260 nm.

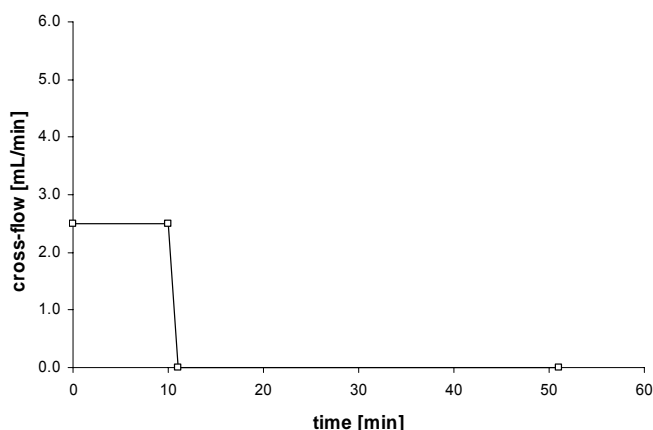


Figure 1.2.4 AF4 cross-flow profile applied for the quantification of the loading of gelatin nanoparticles with double-stranded oligonucleotide

Quantification of gelatin nanoparticle PEGylation

The study was performed using a Wyatt Eclipse2 AF4 system (Wyatt Technology Europe GmbH, Dernbach, Germany). The channel height was set at 350 μm ; the applied ultrafiltration membrane was a regenerated cellulose membrane with 5 kDa cut-off. Isocratic HPLC pump, autosampler, degasser, refractive index (RI) -, and UV-detector are parts of the Agilent 1100 series (Agilent Technologies, Palo Alto, CA, United States). PBS pH 7.0 was chosen as running buffer. The channel flow rate accounted for 1 mL/min, the cross-flow was adjusted to 3 mL/min over 10 min (cp. Figure 1.2.5 for complete cross-flow profile), and the measurement period amounted to 29 min.

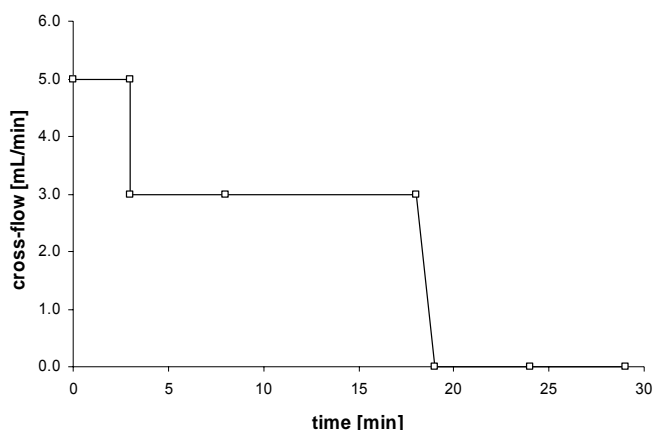


Figure 1.2.5 AF4 cross-flow profile applied for the quantification of the PEGylation of gelatin nanoparticles

On-line detection was done UV-spectrophotometrically (gelatin nanoparticles) and via refractive index (PEG 5000). The amount of detected PEG was calculated

from the AUC of its respective peaks in the resulting fractograms via a calibration curve. The PEGylation was quantified by comparing the AUCs of PEG before and after the PEGylation process. The whole study was repeated three times.

Atomic force microscopy analysis of plain and PEGylated gelatin nanoparticles

Size and surface morphology of cationized plain and PEGylated gelatin nanoparticles were analyzed by atomic force microscopy (AFM) in cooperation with Christian Löbbe (JPK Instruments, Berlin, Germany). Thereby, a JPK NanoWizard™ Life science version (JPK Instruments) was used in intermittent contact (ic) mode with a super sharp silicon (SSS) cantilever (NanoWorld, Schaffhausen, Switzerland). These special cantilevers were chemically etched and end with a slim 200 nm long and 2 nm radius tip. The cantilevers had a spring constant of about 42 N/m. Measurements in water were utilized with softer cantilevers having spring constants of about 0.2 N/m (10-15 nm-radius tip). In both cases the cantilever was excited close to its resonance frequency (air: ~300 kHz; water: ~12 kHz).

1.3 Analysis of Gelatin Bulk Material Applied for the Manufacturing of Gelatin Nanoparticle Drug Delivery Systems Using Asymmetrical Flow Field-Flow Fractionation (AF4) and Multi-Angle Light Scattering (MALS) Detection

1.3.1 Introduction

Due to its unique gel-forming ability, gelatin has long been used in food and pharmaceutical industry [Djagny et al., 2001]. Thus, intensive research was rendered to elucidate the chemical composition and structure of gelatin to understand its functional properties. Basically, gelatin is derived from collagen, the chief structural protein of the body [Friess, 1998], extracted from animal sources. In the meantime there are 27 types of collagen described [Brinckmann, 2005], but only collagen type I originating from skin and bone, type II originating from hyaline vessels, and type III as well originating from skin are used as source for gelatin production [Babel, 1996]. Related to the manufacturing process two types of gelatin are differentiated. Gelatin type A (acid) is obtained by an acidic hydrolysis of pig skin collagen, whereas the amide groups of the amino acid residues asparagine and glutamine remain unaffected causing an isoelectric point (IEP) of the finished product comparable to that of collagen between pH 7.0 to 8.5. During the alkaline processing of ossein from bovine origin and cattle hide to gelatin type B these amide groups are hydrolyzed and the resulting acidic amino acids aspartate and glutamate squeeze the IEP down to values between pH 4.5 and 5.0 [Bauer et al., 2006]. The exact chemical composition of gelatin was already intensively investigated and accurately described in the 1950ies [Djagny et al., 2001] and revealed a composition of 33 % glycine, 22 % proline and 4-hydroxyproline, and 45 % further 17 amino acids [Babel, 1996]. As seen for collagen the repetitive triplet Gly-X-Y can be assumed to form the primary structure of gelatin with proline almost exclusively occupying position X and 4-hydroxyproline predominantly occupying position Y [Friess, 1998]. The secondary structure of gelatin consists of α -chains. Based on those, several fractions of different molecular weight exhibiting fragments and multimers are known to build up the bulk material of gelatin [Farrugia et al., 1999]. Thus, gelatin shows in contrast to soluble collagen a broad molar mass distribution in solution [Meyer et al., 2003]. Describing

this molecular heterogeneity, size exclusion chromatography (SE-HPLC) is the analytical method routinely used for process control and development in gelatin industry [Meyer et al., 2003]. Molecular weights ranging from 10^4 Da up to more than 10^6 Da are reported by several authors [Farrugia et al., 1999; Meyer et al., 2003; Fraunhofer et al., 2004b].

Besides the well established application in foods and pharmaceuticals, gelatin was firstly described as base material for the production of nanoparticles to be used as drug delivery system in the 1970s [Speiser et al., 1974; Marty et al., 1978]. During the manufacturing of nanoparticles from gelatin its high molecular weight fraction (hmw) plays a major role [Zwiorek, 2006; Ahlers et al., 2006]. This was already assumed by Farrugia [Farrugia et al., 1999], who systematically investigated the desolvation process described by Marty for the production of gelatin nanoparticles [Marty et al., 1978]. Their assumption was finally corroborated by the development of the two-step desolvation technique [Coester et al., 2000]. During two-step desolvation gelatin bulk material is fractionated, whereas the low molecular weight fraction (lmw) is discarded and nanoparticles can be manufactured from the hmw fraction with a remarkable homogenous size distribution. Former results derived from SE-HPLC and AF4 analysis provided detailed information about the molecular weight distribution of gelatin bulk material and gelatin sediment – comprising the high molecular weight fraction obtained from two-step desolvation – revealing up to ~27 % [w/w] hmw protein molecules present in the sediment [Fraunhofer et al., 2004b]. A number of 100 kDa marking the border line between low and high molecular weight fraction was determined and molecular weights ranging from 20 kDa to 10,000 kDa were characterized to constitute gelatin bulk material. Followed from these findings it can be assumed that the application of gelatin possessing reduced amounts of its low molecular weight fraction should enable the production of homogenous nanoparticles by a one-step desolvation procedure i.e., the direct preparation of gelatin nanoparticles from gelatin bulk material omitting its initial fractionation. Accordingly, four customized gelatin batches developed from the Gelita AG (Eberbach, Germany), one of the world's largest gelatin manufacturers, were provided to investigate their potential in terms of successful one-step desolvation. The four batches were prepared with reduced amounts of peptides < 65 kDa accounting for < 40 % [w/w] (batch PN307779 / VP433) and

< 20 % [w/w] (batches VP306 / VP413-2) respectively. Batch VP433 was additionally spiked with a high molecular weight fraction $> 10^7$ Da in order to estimate the impact of pronounced present hmw fractions in comparison to the further reduced peptide portions in batches VP306 and VP413-2. Due to its strengths in resolving samples of macromolecules and polymers [Giddings, 2000] and the possibility of absolute determination of molar masses [White, 1997] the analytical description of this material via AF4 coupled with multi-angle light scattering (MALS) detection was the aim of this study.

The absolute molar mass determination derived from light scattering detection is based on the everyday phenomenon of static or classical light scattering emanating from analytes upon exposure to light as a function of size and molecular weight. Thereby, the ratio between the intensity of scattered light and the intensity of incident light of a certain wavelength is detected. The resulting excess Rayleigh ratio $R(\theta)$ defined by

$$R(\theta) = f_{geom} \frac{I(\theta) - I_s(\theta)}{I_0} \quad (1-3)$$

where I_0 is the incident light intensity, f_{geom} is a geometrical calibration constant that is a function of solvent and scattering cell's refractive index and geometry, and $I(\theta)$ and $I_s(\theta)$ are the normalized intensities of scattered light detected at angle θ with respect to the illuminated solution and solvent respectively. For generally assumed vanishing small concentrations and negligible interactions between sample and solvent the following proportionality can be described

$$\frac{K \cdot c}{R(\theta)} \approx \frac{1}{M_w \cdot P(\theta)} \quad (1-4)$$

where K is a constant representing the refractive index increment of the analyte, c is the sample concentration, M_w is the weight average molar mass, and $P(\theta)$ is the scattering function, which is 1 for sample molecules smaller than $\lambda/20$ (λ is the vacuum wavelength of the incident light = 690 nm for the applied miniDAWNTM detector). This proportionality reveals the relation between the samples' light scattering properties and its molar mass providing the basis for molecular weight determination from light scattering data. It is important to note that the scattering

properties of samples exhibiting a bigger diameter than $\lambda/20$ e.g., nanoparticles are shifted from an isotropic to an anisotropic behavior (Figure 1.3.1). For accurate molar mass determination it is then necessary to detect light scattering at up to 18 angles directed around the scattering cell; in this case 3 angles are employed at 45° , 90° , and 135° , which is sufficient for polymer analysis.

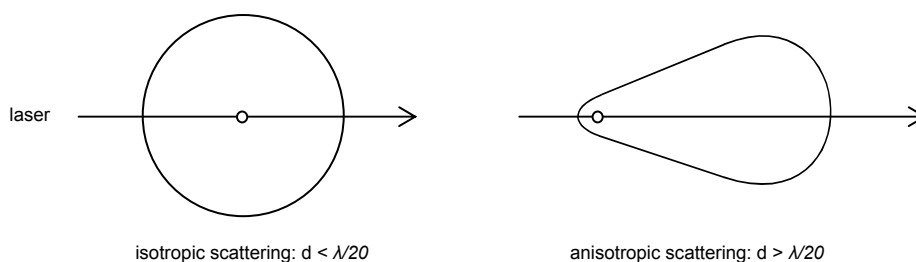


Figure 1.3.1 Dependence of light scattering from sample size; if the sample size exceeds $\lambda/20$ the pattern of the scattered light will change from an isotropic to a forwarded anisotropic manner

It has to be confined that MALS is only able to provide exact data for the analysis of sample populations which consist of identical specimens. Consequently, the necessity of sample fractionation into distinct slices prior to detection becomes evident and is in this study achieved by AF4.

Basic theoretical considerations to light scattering detection are summarized from according literature [Arndt et al., 1996; White, 1997; Wyatt, 1998].

Data from AF4/MALS analysis should help to understand failure or success of the respective gelatin batches while developing a one-step desolvation procedure for the synthesis of gelatin nanoparticles. Experiments were conducted in comparison to regularly applied gelatin bulk material purchased from Sigma-Aldrich and gelatin sediment obtained from two-step desolvation. Particle manufacturing via one-step desolvation was evaluated by Klaus Zwioerek; for a detailed description of the corresponding experimental conditions it is referred to his thesis [Zwioerek, 2006].

1.3.2 Results and discussion

At first gelatin bulk material purchased from Sigma-Aldrich was analyzed to gain a benchmark for the following investigations. The molar mass of the applied batch was determined to comprise sizes ranging from 10 kDa to above 10,000 kDa (Figure 1.3.2), which confirms the data reported by Fraunhofer [Fraunhofer et al., 2004b] and exceeds the findings from SE-HPLC/MALS analysis [Meyer et al., 2003; Fraunhofer et al., 2004b] by more than one order of magnitude. The discrepancy between sizing data obtained from SE-HPLC and AF4 reflects the fundamental differences between these two separation techniques. While SE-HPLC separation takes place in a packed column AF4 utilizes an open channel leading to lower hydrostatic pressure and therewith lower shear forces the samples are encountered during analysis.

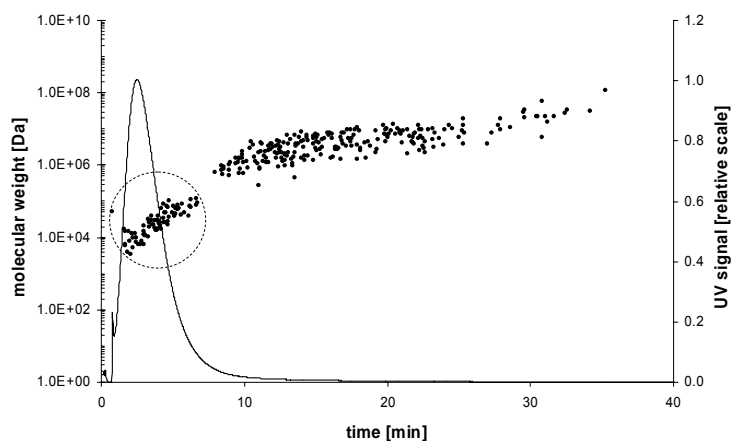


Figure 1.3.2 UV signal (continuous line) and molecular weight (dots) calculated from respective UV and MALS data resulting from AF4 analysis of gelatin bulk material purchased from Sigma-Aldrich; the circle marks the low molecular weight fraction

Particularly high molecular weight specimens suffer from degradation by increased shear forces and are thus preserved and can be detected during AF4 analysis [Myers, 1997]. The displayed diagram showing the high molecular weight fraction of gelatin almost eluting over the whole experimental period, expresses the chosen cross-flow conditions displayed in Figure 1.2.2. Due to the broad variety of molecules all possessing different molar masses present in gelatin bulk material a baseline separation of particular portions is excluded. Thus it was decided to only apply a weak separation force in order to expand the elution of the blend of

molecules over a prolonged period and thereby visualizing the heterogeneous nature of gelatin.

Gelatin from Sigma-Aldrich is characterized by a broad molecular weight distribution as displayed in Figure 1.3.2. As solely its high molecular weight fraction can be used for the preparation of homogenous nanoparticles (cp. chapter 1.3.1) it generally has to be processed by two-step desolvation. Manufacturing experiments in turn, conducted with two of the four customized Gelita batches (VP306 / VP413-2) that possessed less than 20 % [w/w] peptides < 65 kDa resulted in successful one-step desolvation synthesis of gelatin nanoparticles exhibiting equivalent size and size distribution [Zwiorek, 2006]. Batch PN307779 that exhibited peptides < 65 kDa only reduced to amounts < 40 % [w/w] failed in this context as well as batch VP433 containing an identically reduced peptide fraction but at the same time an expanded amount of hmw components > 10⁴ kDa. These findings reveal the restriction that has especially to be made for the presence of low molecular weight portions in gelatin batches designated to one-step desolvation.

Compared to gelatin from Sigma-Aldrich the molar mass distribution of the Gelita batches is altered, which can be followed during AF4/MALS analysis. In Figure 1.3.3 results are exemplarily displayed for batch VP413-2.

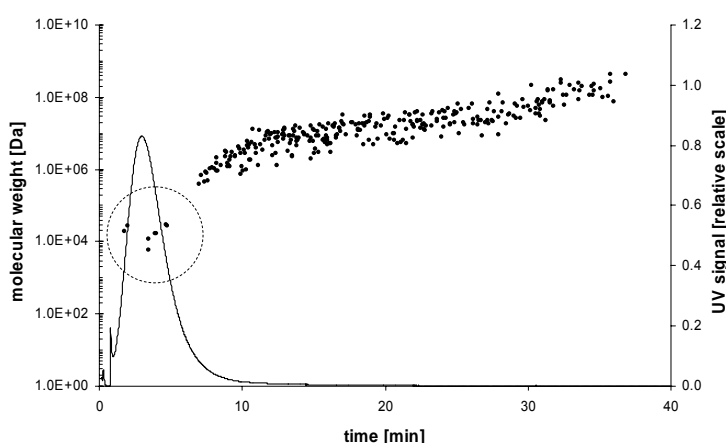


Figure 1.3.3 UV signal (continuous line) and molecular weight (dots) calculated from respective UV and MALS data resulting from AF4 analysis of gelatin bulk material VP413-2 developed and provided from Gelita; the circle marks the low molecular weight fraction

Highlighted by the circle (cp. Figure 1.3.2) the successful depletion of the low molecular weight fraction of gelatin is demonstrated. In addition, gelatin sediment obtained from two-step desolvation after the first desolvation step – as the result from fractionation and used for the preparation of nanoparticles – was transferred to

AF4 analysis. Data from these experiments and from gelatin bulk material are displayed as function of their mean molecular weight and opposed in Figure 1.3.4. Interestingly the clear shift of the mean molecular weight of the gelatin sediment (4) by more than one order of magnitude compared to the bulk material (1) must not be stated as necessity in terms of successful one-step desolvation. Even a mean molecular weight between 400 and 500 kDa determined for the Gelita batches VP306 and VP413-2 was sufficient.

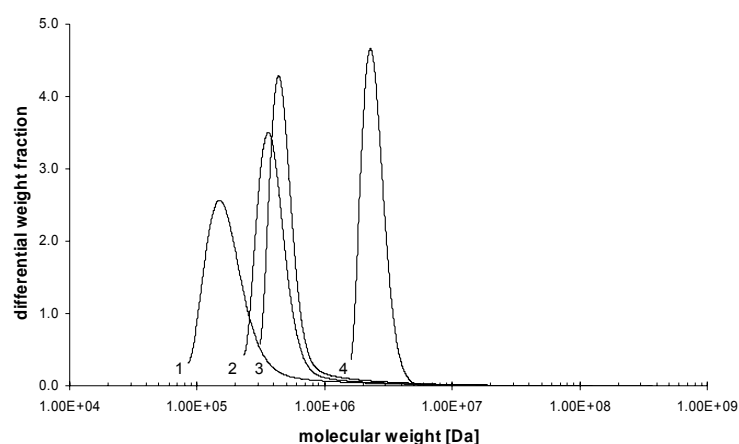


Figure 1.3.4 Mean molecular weight fractions calculated from respective UV and MALS data resulting from AF4 analysis of gelatin bulk material purchased from Sigma-Aldrich (1), of gelatin bulk material VP306 (2) and VP413-2 (3) developed and provided from Gelita, and of gelatin sediment obtained after the first desolvation step from the manufacturing process of the gelatin nanoparticles (4)

Thus, derived from these findings and the specification of the applied gelatin batches a mean molecular weight of ~ 500 kDa and a threshold of maximum 20 % [w/w] for the portion of low molecular weight fractions < 65 kDa could be defined as prerequisite for the successful manufacturing of gelatin nanoparticles by a one-step desolvation procedure.

The mean molecular weight of gelatin sediment ranges clearly above the one of the Gelita batches, which may not only be attributed to even more reduced amounts of peptides < 65 kDa far below 20 % in the sediment. Thus, the fractionation of gelatin bulk material during two-step desolvation supposedly led to a depletion of molecular weight fractions bigger than 65 kDa.

1.3.3 Summary

The analysis of gelatin bulk material by the combination of asymmetrical flow field-flow fractionation and multi-angle light scattering was accomplished in continuation of preliminary studies from Fraunhofer [Fraunhofer et al., 2004b]. At first, their basic results obtained for gelatin bulk material applied for the manufacturing of gelatin nanoparticles by two-step desolvation could be confirmed. Secondly, mean molecular weights of customized gelatin batches from the Gelita AG characterized by the depletion of low molecular weight fractions during production could be successfully classified in between the mean molecular weight determined for gelatin bulk material from Sigma-Aldrich and gelatin sediment obtained from two-step desolvation. These results demonstrated the impact of the low molecular weight fraction of gelatin for the manufacturing of gelatin nanoparticles and contributed to further understanding and description of gelatin nanoparticle synthesis by desolvation. This was at least feasible in a one-step attempt utilizing particular batches of the customized Gelita material [Zwiorek, 2006]. The one-step desolvation is not only straightforward in terms of technological aspects as it simplifies the manufacturing procedure but also especially interesting for regulatory considerations. One of the major drawbacks of the two-step desolvation is that gelatin nanoparticles are produced with not exactly defined bulk material obtained from the first desolvation step i.e., bulk material resulting from an indeed validated but “hand made” fractionation with varying outcome. The successful application of the one-step desolvation for gelatin nanoparticle synthesis circumvents this problem.

Finally, concerning the restrictions for certain molecular weight fractions of gelatin, necessary for the one-step desolvation, together with the Gelita AG a patent application could be filed to the authorities [Ahlers et al., 2006].

1.4 Quantifying the Oligonucleotide-Loading of Gelatin Nanoparticle Drug Delivery Systems Using Asymmetrical Flow Field-Flow Fractionation (AF4) and UV Detection

1.4.1 Introduction

Basically, drug loading of nanoparticulate carrier system is either conducted during manufacturing or afterwards by binding the respective substances onto the surface of the finished product [Soppimath et al., 2001]. Thereby matrix systems exhibiting homogeneously distributed drug molecules and core-shell like structures emerge. Subsequent conducted assessment of the drug loading efficiency has thus to be accordingly adapted. The preparation techniques of gelatin nanoparticles that are described in literature admit both the incorporation of drugs during manufacturing as well as a later binding onto the nanoparticles' surface. Due to the various applications in drug delivery and drug targeting gelatin nanoparticles are developed for, there is a multiplicity of analytical approaches utilized for the quantification of their drug load. In the following these approaches revealing the current status of drug-loaded gelatin nanoparticle research are summarized in brief.

Applying W/O emulsions nanoparticles are formed within the aqueous phase which optionally contains the drug substance at the same time. After purification drug loading can be UV spectrophotometrically determined from the remaining reaction medium [Gupta et al., 2004] or from dissolved nanoparticles [Cascone et al., 2002]. Bajpai described a gravimetric approach for gelatin nanoparticles drug-loaded by swelling the dried particles till equilibrium in a freshly prepared drug solution, as he determined the weight of the same dried nanoparticle aliquot before and after drug loading [Bajpai et al., 2005]. Originally dating from the work of Marty [Marty et al., 1978] several desolvation procedures are described for the incorporation of drug substances in gelatin nanoparticles. To quantify the respective drug loading UV spectroscopy [Leo et al., 1997] and HPLC [Vandervoort et al., 2004] are employed for the analysis of the supernatant after separating the nanoparticles. Labhasetwar reported a dialysis approach for the extraction of incorporated metronidazole [Labhasetwar et al., 1990] and the group of Amiji determined the amount of plasmid DNA after enzymatic digestion of gelatin

nanoparticles via a PicoGreen[®] assay [Kaul et al., 2005; Kommareddy et al., 2005]. Self-assembled nanoparticulate DNA-polycation i.e., gelatin systems were identically processed [Leong et al., 1998; Truong-Le et al., 1999] and Lu combined a HPLC protocol with preceding digestion of nanoparticles [Lu et al., 2004]. Gelatin nanoparticles prepared by two-step desolvation were drug-loaded by physical entrapment of a low molecular weight substance into the nanoparticles and after surface activation with reactive sulfhydryl groups by NeutrAvidin[™] mediated coupling with biotinylated antibodies or peptide nucleic acids (PNAs). Drug loading was determined after centrifugation from the supernatant containing unbound drug by UV spectroscopy [Verma et al., 2005] as well as reversed phase HPLC and immunoblotting / fluorimetry respectively [Langer et al., 2000; Dinauer et al., 2005].

In the present study drug loading of gelatin nanoparticles obtained from two-step desolvation with single- and double-stranded DNA oligonucleotides was performed by electrostatic interactions comparable to the mechanism driving the self-assembling synthesis of DNA-polycation complexes. To permit the adsorption of negatively charged oligonucleotide molecules onto gelatin nanoparticles a permanent positive surface charge is crucial. It can be achieved by the covalent introduction of cholamin, bearing a quaternary amino group, via the carboxyl residues present on the surface of gelatin nanoparticles, whereas a clear pH independent positive surface charge arises [Coester, 2003; Zwioerek et al., 2004]. This oligonucleotide-loading procedure is routinely quantified via UV spectroscopical detection of unbound oligonucleotide staying within the incubation medium after removing the nanoparticles [Zillies et al., 2004]. The verification of these data by utilizing asymmetrical flow field-flow fractionation (AF4) coupled with UV detection was aspired during this study. Based on the well known strengths of AF4 in resolving macromolecular and particulate matter [Giddings, 2000] its ability to separate gelatin nanoparticles from biopolymers i.e., proteins or oligonucleotides should be demonstrated. It was intended to develop a fractionation protocol that provides the in situ quantification of the oligonucleotide-loading of gelatin nanoparticles concurrently omitting further sample preparation.

1.4.2 Results and discussion

Characterization of nanoparticles

Both nanoparticle formulations applied during AF4 experiments exhibited the same homogenous size distribution with polydispersity indices (PDIs) clearly below 0.050. The slightly varying sizes can be stated as negligible in the present analytical context. Zetapotential differences between the two batches utilized for oligonucleotide-loading are in accordance to the requirements for single and double-stranded ODN loading. Equivalent amounts i.e., 5 % [w/w] can be loaded under identical conditions (in highly purified water) of the single-stranded oligonucleotide onto batch G-NP_{ZW} 03-121 pos and of the double-stranded oligonucleotide onto batch G-NP 06-027 pos.

Table 1.4.1 Size, polydispersity, and surface charge of nanoparticle formulations applied for the quantification of single-stranded[#] and double-stranded[§] oligonucleotide-loading

	[#] Surface-modified gelatin nanoparticles (G-NP _{ZW} 03-121 pos)	[§] Surface-modified gelatin nanoparticles (G-NP 06-027 pos)
size [nm]	255.7	365.0
PDI	0.028	0.043
ZP [mV]	+2.3	+16.4

Single-stranded oligonucleotide loading

Before the single-stranded oligonucleotide-loading onto gelatin nanoparticles could be evaluated, adequate AF4 separation conditions for the oligonucleotide and the gelatin nanoparticles were developed and the linear relation of sample concentration and UV detection signal was proven. UV detection was chosen since the analytes were not accessible by refractive index (RI) detection. Initiatory experiments demonstrated the separation of gelatin nanoparticles from several macromolecules exhibiting declining molecular weights. An immunoglobulin (IgG₁, 147 kDa), human serum albumin (HSA, 66.4 kDa), granulocyte colony stimulating factor (G-CSF, 19.6 kDa), and insulin (5.8 kDa) were successfully fractionated from gelatin nanoparticles. Especially the separation from insulin was important as the

oligonucleotide exhibited a similar molecular weight of 5.5 kDa. Thus, the developed cross-flow profile (Figure 1.2.3) could also be applied for quantifying the oligonucleotide loading. All experiments were performed together with Wolfgang Fraunhofer. For a detailed description of the corresponding data it is referred to his thesis [Fraunhofer, 2003]. Here, the final results of these studies are shown in Figure 1.4.1 as they illustrate the goal that was aimed at during the development of an AF4 separation protocol for quantifying the double-stranded oligonucleotide-loading onto gelatin nanoparticles without previous sample preparation.

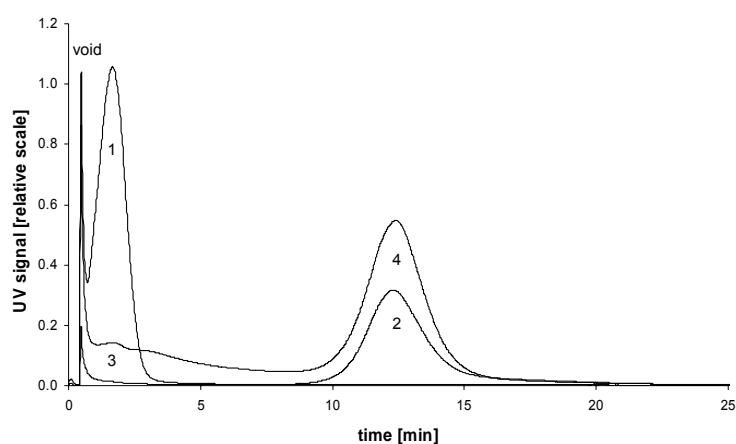


Figure 1.4.1 UV signals resulting from AF4 analysis of the single-stranded oligonucleotide before loading (1) and after loading (3) onto gelatin nanoparticles as well displayed before (2) and after oligonucleotide-loading (4); originally published data from Fraunhofer [Fraunhofer, 2003]

The graphs summarize the AF4 runs separately performed before oligonucleotide-loading with the oligonucleotide (1) and the nanoparticles (2) and at once performed after oligonucleotide-loading with both (3) / (4). The alterations thereby observed for the respective UV signals showed a clear downsizing of the ODN peak and concurrently a commensurate growth of the nanoparticle peak. Calculated from the corresponding AUCs an amount of ~50 % of the applied single-stranded oligonucleotide could be determined to be bound representing a loading capacity of the gelatin nanoparticles of 5 % [w/w]. These findings met expectations as they were confirmed by data from centrifugation / UV-spectroscopy. Regarding the size of the oligonucleotide, it has to be mentioned that its molecular weight marks the lower limit of sample sizes which can be effectively handled during AF4 analysis [Giddings, 1993]. This is also expressed by the void peak merging the oligonucleotide peak (Figure 1.4.1). The void peak inherent in AF4 occurs after the time required to flush out the channel volume and contains non-retained parts of the

injected sample that did not interact with the separation field [Giddings et al., 1977; Klein et al., 1998].

Based on the completed quantification of single-stranded oligonucleotide loading, double-stranded oligonucleotide-loading onto gelatin nanoparticles was evaluated via AF4/UV in the next step.

Double-stranded oligonucleotide loading

Due to their size and molecular weight gelatin nanoparticles are affected by very low cross-flow intensities [Giddings, 1993; Colfen et al., 2000], which became obvious during the first AF4 experiments. Thus, to achieve sufficient separation during oligonucleotide-loading quantification studies it could be concentrated on the development of cross-flow conditions providing adequate elution of the respective oligonucleotide; whereas nanoparticles are retained within the separation channel until the cross flow was completely abandoned. For the experiments assessing the double-stranded ODN loading the cross-flow was slightly increased compared to the formerly applied profile (Figure 1.2.3) as a thinner channel was applied and kept constant over 10 min (Figure 1.2.4). The applied settings comprising cross-flow, ultrafiltration membrane, and running buffer provided reproducible detection signals of a symmetrical shape (Figure 1.4.2). Furthermore, due to its higher molecular weight of 14.1 kDa the double-stranded ODN could sufficiently be baseline-separated from the void peak allowing a more precise determination of the resulting AUC.

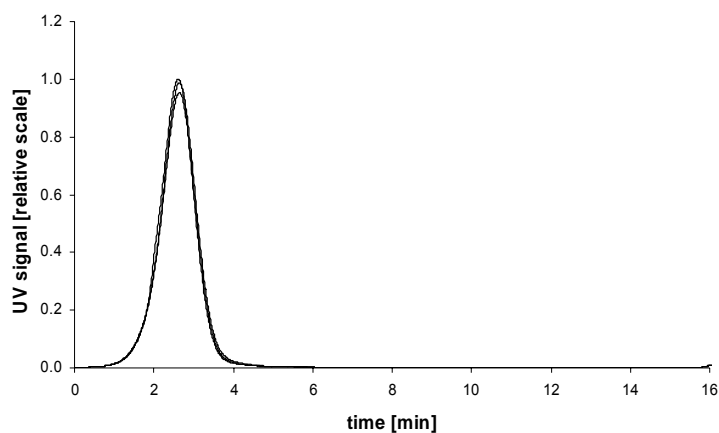


Figure 1.4.2 UV signals arising from the double-stranded oligonucleotide after AF4 analysis; identical concentrations were injected 3 times under the same conditions (Dulbecco's PBS pH 7.3 / regenerated cellulose ultrafiltration membrane 5kDa cut-off)

Subsequently, gelatin nanoparticles were investigated for their elution behavior by applying the same instrumental set-up. The obtained fractograms are displayed in Figure 1.4.3 a). Despite repeated injection no congruent detection signals could be gained. The picture shows the nanoparticles' UV signals arising from the first three injections. Along the stepwise appearance membrane saturation with nanoparticles was assumed that finally led to bouncing peak heights and excluded reproducible AUC calculation (data not shown).

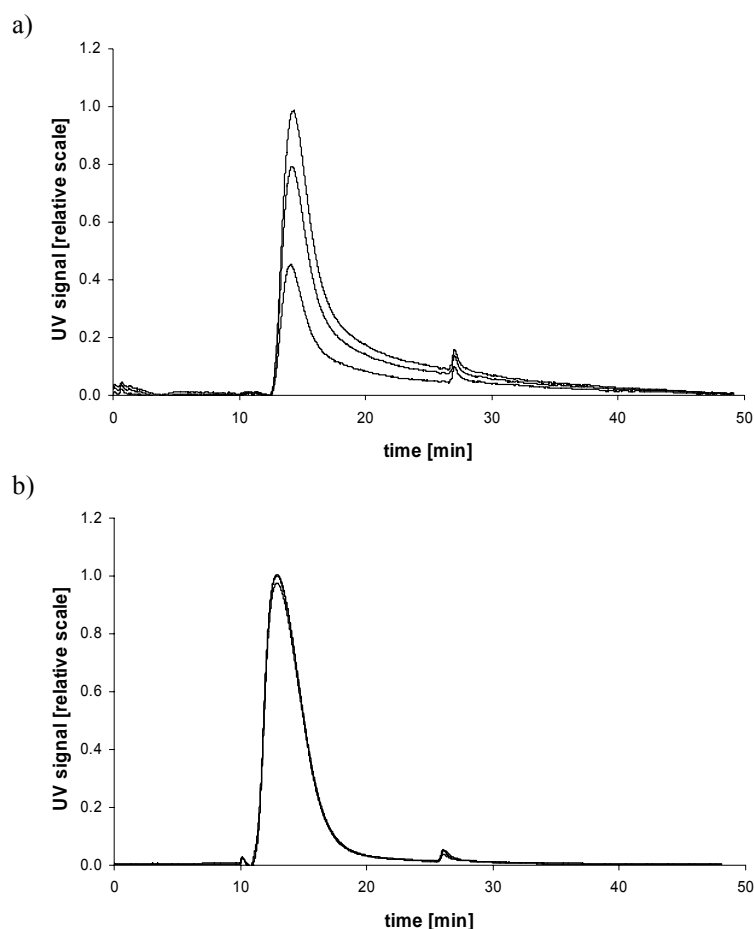


Figure 1.4.3 UV signals arising from gelatin nanoparticles after AF4 analysis; identical concentrations of a) surface-modified nanoparticles and b) plain nanoparticles were injected 3 times each under the same conditions (Dulbecco's PBS pH 7.3 / regenerated cellulose ultrafiltration membrane 5kDa cut-off)

The applied surface-modified gelatin nanoparticles exhibited a clear positive surface charge necessary for loading the double-stranded oligonucleotide onto their surface. Presumably, electrostatic interactions emerging between the positively charged nanoparticles and the negatively charged cellulose residues of the ultrafiltration membrane delayed the elution of the nanoparticles from the separation channel and led to nanoparticles persisting on the membrane. This hypothesis could

be proven when *not* surface-modified gelatin nanoparticles were examined under identical conditions. These particles produced already after the first sample run congruent UV detection signals (Figure 1.4.3 b). The small peak appearing after 27 min in both fractograms of Figure 1.4.3 originates from flushing the injection valve and will not disturb calculation of the AUCs, especially as it can be omitted or initiated later. Concerning the nanoparticles used for the single-stranded oligonucleotide-loading the observed discrepancy might be explained by their lower surface charge which seems to be in a way abolished by the ionic environment of the PBS running buffer that allows unaffected elution. The disappointing results from the surface-modified gelatin nanoparticles were in turn also obtained with oligonucleotide-loaded nanoparticles revealing the positive surface charge partially remaining after oligonucleotide-loading (cp. chapter 3.3.3, Table 3.3.1). And, as nanoparticles accumulating within the separation channel disturb propelling others by electrostatic interactions via the bound oligonucleotide, the quantification of the oligonucleotide-loading process only from the excellent oligonucleotide detection signal was not possible.

Thus, in the following changes of the instrumental setup were implemented in order to achieve the aspired quantification of the double-stranded oligonucleotide loading. At first the material of the ultrafiltration membrane was changed from regenerated cellulose to polyethersulfone. Due to the missing negatively charged cellulose residues ionic interactions between the membrane material and the surface-modified gelatin nanoparticles should therewith be excluded. However, this time the oligonucleotide exhibited certain membrane adsorption. This was expressed in stepwise appearing UV detection signals (Figure 1.4.4) comparable to those seen for the nanoparticles on the regenerated cellulose membrane (Figure 1.4.3 a). Again this problem could not be circumvented by repeated injections in order to obtain stable membrane saturation, whereas interactions with subsequent injected nanoparticles either empty or ODN loaded would corrupt this attempt. Intensive focusing or high initial cross-flow commonly known to evoke adsorption phenomena during AF4 analysis [Wahlund, 2000] can be excluded as the cause of the problem as these parameters remained unchanged. But, in contrast to membranes made of regenerated cellulose polyethersulfone membranes do not exhibit negatively charged side chains of the applied polymer.

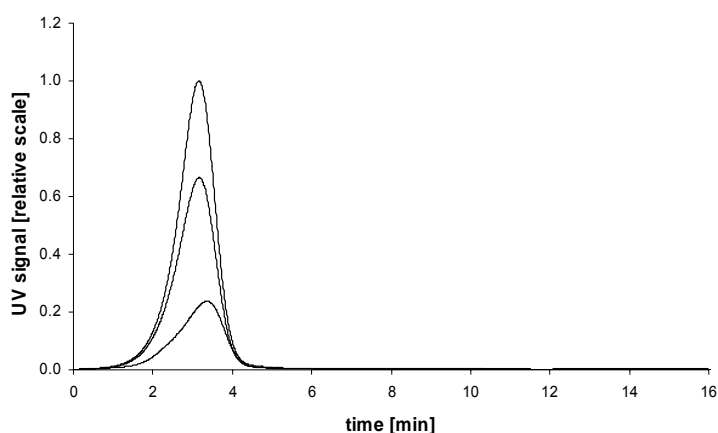


Figure 1.4.4 UV signals arising from the double-stranded oligonucleotide after AF4 analysis; identical concentrations were injected 3 times under the same conditions (Dulbecco's PBS pH 7.3 / polyethersulfone ultrafiltration membrane 5kDa cut-off)

Thus electrostatic repulsion driven by equal charge of analyte and membrane material is missing and consequently hydrophilic interactions were assumed to be responsible for the observed irregular elution. Suggesting, that ionic shielding of the nanoparticles' surface charge explains the good results from single-stranded ODN loading the augmentation of the ionic strength within the running buffer was obvious. Therefore the NaCl concentration was adjusted to 0.6 mol/L, phosphate content and pH were maintained unaltered, and the membrane material was changed back to regenerated cellulose. Corresponding results obtained for the double-stranded oligonucleotide and the gelatin nanoparticles are summarized in Figure 1.4.5. For both analytes the chosen combination of membrane material and running buffer evidently provided optimum separation conditions. Congruent detection signals were observed after triple injection and with respect to the corresponding elution times a sufficient separation could be expected analyzing oligonucleotide and gelatin nanoparticles together in one run subsequent to loading.

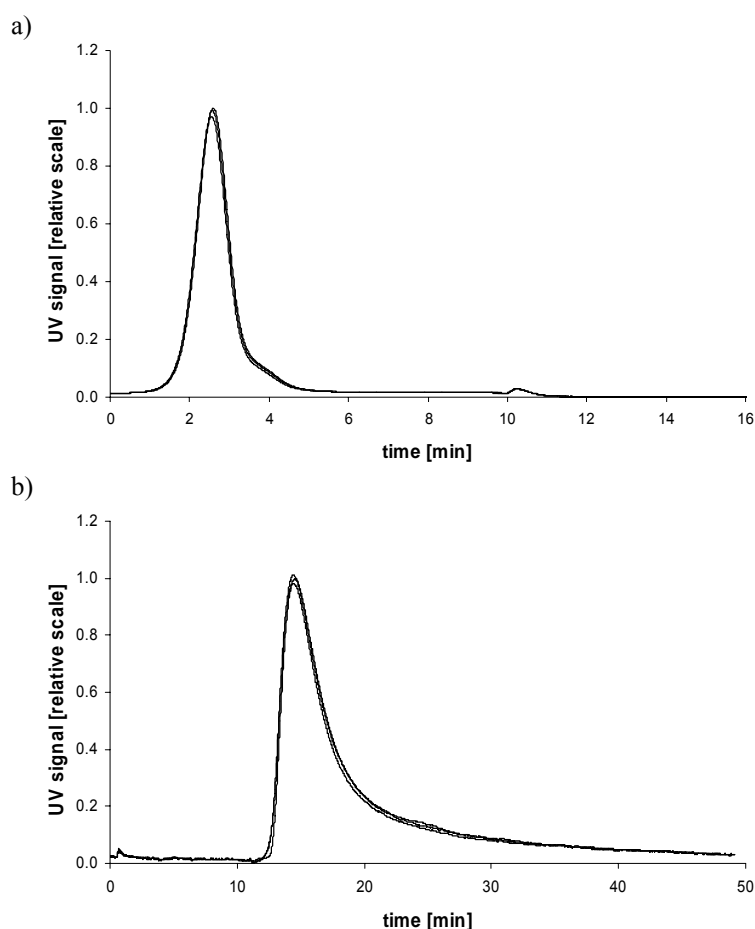


Figure 1.4.5 UV signals arising from a) the double-stranded oligonucleotide and b) surface-modified gelatin nanoparticles after AF4 analysis; respective identical concentrations were injected 3 times under the same conditions (Dulbecco's PBS pH 7.3 containing 0.6 mol/L NaCl / regenerated cellulose ultrafiltration membrane 5kDa cut-off)

In fact, a baseline separation was achieved (Figure 1.4.6) but with respect to the aim of the study these final sample runs failed. As nanoparticles were incubated with 5 % [w/w] double-stranded oligonucleotide for what centrifugation / UV-spectroscopy data revealed complete loading, its UV signal should have been totally erased. In discussing this phenomenon, the ionic strength of the running buffer has to be taken into account. Utilizing electrostatic attractive forces loading will be more stable the stronger the electrostatic interactions are. Working in buffered media with its elevated ionic strength, net charges of the involved analytes are partially or even completely compensated. This is successfully used for the prevention of membrane adsorption during AF4 analysis as discussed above but abrogates at the same time also the attractive forces between nanoparticles and oligonucleotide. Thus, the raised NaCl concentration within the running buffer was

indeed able to prevent membrane adsorption but finally led to the release of the oligonucleotide-loading of gelatin nanoparticles.

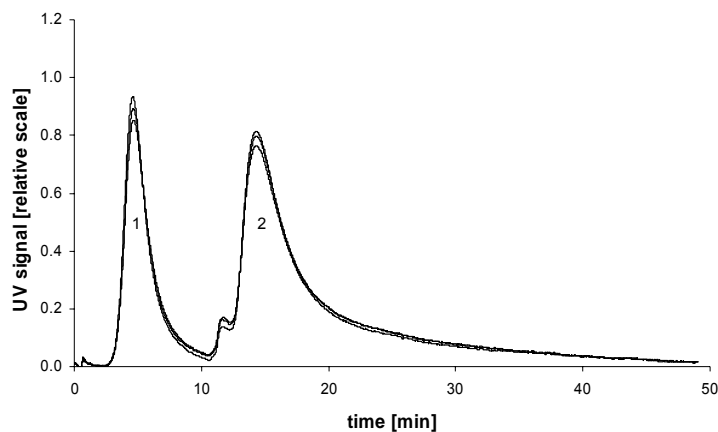


Figure 1.4.6 UV signals arising from the double-stranded oligonucleotide (1) and surface-modified gelatin nanoparticles (2) – after incubating the nanoparticles for 2 h with the ODN – subsequent to AF4 analysis; identical concentrations were injected 3 times under the same conditions (Dulbecco's PBS pH 7.3 containing 0.6 mol/L NaCl / regenerated cellulose ultrafiltration membrane 5kDa cut-off)

Similar observations were already made during former studies evaluating the siRNA loading of gelatin nanoparticles when the medium was changed upon incubation from highly purified water to PBS [Zillies et al., 2004]. Regarding the ODN release from gelatin nanoparticles *in vivo*, the same mechanism can be assumed, whereas an immediate release right after injection before reaching the respective target is not desirable. Here, a sodium chloride concentration of 0.6 mol/L was finally applied which is about four times higher than isotonic i.e., physiological values (~ 0.15 mol/L). In a comparable *in vitro* setup, Tondelli reported about almost complete release of electrostatically bound ODN from PMMA nanoparticles in the presence of 1 mol/L sodium chloride. 0.1 mol/L NaCl in turn governed a release up to 78 % over eight days depending on the total amount of bound oligonucleotide [Tondelli et al., 2003]. These data were further confirmed by our findings from biodistribution studies in rats with fluorescent-labeled NF- κ B decoy oligonucleotide-loaded gelatin nanoparticles that did not reveal a rapid release of the oligonucleotide (cp. chapter 3.4.2). Thus, a release of electrostatically bound oligonucleotide from nanoparticles by (partially) compensated attractive forces in buffered media can be stated, whereas the degree of release seems to be determined by the ionic strength of the particular medium. Derived from the present data it can be stated that sufficient AF4 separation settings can be described even for charged analytes. This is achieved

by compensating the involved charges by accordingly adjusting the ionic strength of the running buffer, which is in general recommended for samples exhibiting charged surfaces [Ratanathanawongs-Williams, 2000]. This in turn causes the dilemma: if there were conditions applied that provided stable oligonucleotide-loading membrane adsorption took place and if the chosen conditions inhibited this, oligonucleotide-loading was destabilized. Nevertheless, the unique capability of AF4 to separate soluble specimens from suspended material was once more highlighted still leaving it attractive for the work with colloidal drug carriers in general and gelatin nanoparticles in special.

1.4.3 Summary

Followed from former studies demonstrating the potential of asymmetrical flow field-flow fractionation for the separation of dissolved biopolymers and gelatin nanoparticles the quantification of double-stranded oligonucleotide-loading onto gelatin nanoparticles via AF4 was assessed. The conducted experiments proved the known high resolution power but lastly failed in terms of a successful quantification. Neither replacing the ultrafiltration membrane nor varying the ionic strength of the running buffer could solve this problem. Due to the involved high surface charges of the analytes it was not possible to develop adequate separation conditions for the three investigated specimens double-stranded oligonucleotide, surface-modified gelatin nanoparticles, and oligonucleotide-loaded gelatin nanoparticles at once. High surface charges on the one hand require high ionic strength of the running buffer on the other hand. This methodical restriction lastly led to the ODN-loaded formulation eluting either in a non reproducible manner or releasing the oligonucleotide during AF4 analysis. Thus, direct quantification of the oligonucleotide-loading without previous sample preparation was not feasible. Thereby, the release mechanism of electrostatically bound oligonucleotide from nanoparticles was elucidated. Elevated concentrations of sodium chloride led to immediate oligonucleotide release, whereas as a sustained effect can be assumed under *in vivo* conditions with a roughly four times reduced ionic strength compared to the respective AF4 running buffer.

In sum, the results describe the limits of this analytical approach but do not basically challenge the advantages of AF4 in colloidal analysis.

1.5 Quantifying the PEGylation of Gelatin Nanoparticle Drug Delivery Systems Using Asymmetrical Flow Field-Flow Fractionation (AF4) and Refractive Index (RI) Detection

1.5.1 Introduction

The growing experience with colloidal drug carrier systems led to a detailed understanding of their in vivo fate subsequent to intravenous application. Hence, it is nowadays well known that foreign material with a molecular weight higher than the renal threshold is sequestered in the mononuclear phagocytic system (MPS) organs [Owens et al., 2006]. The involved phagocytotic cells recognize colloidal structures like liposomes and nanoparticles due to the rapid opsonization immediately occurring after application [Yan et al., 2005; Owens et al., 2006]. The resulting low plasma half life minimizing most therapeutic effects led to an intensive research in order to overcome this problem. Ruling out the extensive plasma protein adsorption during opsonization should consequently provide a certain macrophage resistance expressed in a reduced MPS accumulation and a prolonged circulation time. Followed from this idea long circulating liposomes and nanoparticles have been developed [Peracchia, 2003; Yan et al., 2005; Owens et al., 2006]. These systems possess a “molecular cloud” of polymer chains esp. polyethylene glycol (PEG) chains grafted onto their surface, which sterically protect them from opsonization and enable prolonged circulation. Despite the long circulation properties opsonization even of these systems cannot be completely excluded and is meanwhile critically discussed [Moghimi et al., 2003; Yan et al., 2005]. Due to this successful approach the concept of PEG grafting is widely applied for drug carriers as liposomes [Yan et al., 2005], nanoparticles based on synthetic [Peracchia et al., 1999; Owens et al., 2006] and natural polymers [Lin et al., 1999; Kaul et al., 2002; Owens et al., 2006], and polyplexes [Ogris et al., 1999; Walker et al., 2005] as wells as for drug molecules at their own, namely proteins [Fee et al., 2005; Veronese et al., 2005] and in the field of transfusion medicine for red blood cells [Garratty, 2004].

Besides the grafting process the quantification of the introduced PEG is a matter of interest as the grade of PEGylation is decisive for a successful shielding [Veronese, 2001; Moghimi et al., 2003; Yan et al., 2005] and a homogenous product

is a necessary prerequisite during the regulatory process [Chamberlain et al., 2003]. Quantifying PEG is in general an analytical challenge. The lack of any chromophores and its transparent and non-fluorescent appearance excludes the direct spectrophotometrical detection. Indirect methods like the determination of unreacted functionalities of the reaction counterpart will not provide a precise evaluation of the number of polymer chains bound. So, due to the various PEGylated systems numerous analytical approaches have been proposed quantifying the PEGylation. The first successful attempts utilizing colorimetric assays by introducing an UV active staining into the PEG molecule, were described in the 1970s [Childs, 1975; Skoog, 1979]. The formed PEG barium iodide complex produces a band at 535nm which can be used for quantitative measurements. This complex formation was transferred to SDS-PAGE [Kurfurst, 1992] and is still in use for the evaluation of PEGylation efficiencies [Natarajan et al., 2005; Zhang et al., 2006]. Another colorimetric assay without initial extraction of PEG could be developed based on the partitioning of a chromophore present in aqueous ammonium ferrothiocyanate from an aqueous to an organic phase in the presence of PEG [Nag et al., 1996]. However, despite rapidness, accuracy, and sensitivity these methods suffer from the high values of the blanks. Finally, derivatization techniques have been used to produce UV active PEG species like PEG dibenzoates [Murphy et al., 1981]. Besides these PEG modifying assays, detecting PEG without any changes of the molecule is nowadays extensively described in literature: flame ionisation detection [Kwong et al., 1995], dynamic surface tension detection [Miller et al., 2000], nuclear magnetic resonance spectrometry [Leenheer et al., 1991; Mazarin et al., 2006], mass spectrometry [Fakt et al., 1997; Crescenzi et al., 1997; Nielen et al., 1999; Na et al., 2004b], and refractive index detection [Delahunty et al., 1986; Kirkland et al., 1992b; Oliva et al., 1994; Benincasa et al., 2001] are applied for the quantitative (and qualitative) evaluation of PEG of different molecular weights. The separation of PEGylated from non-PEGylated compounds and PEG, required prior to any kind of detection, is feasible by different chromatographic techniques as well as flow field-flow fractionation (FFFF). Due to the amphiphilic properties of PEG, RP-HPLC [Oliva et al., 1994; Crescenzi et al., 1997] and organic FFFF [Kirkland et al., 1992a] are likewise applied as conventional SEC-HPLC [Delahunty et al., 1986; Miller et al., 2000; Fee et al., 2005] and aqueous FFFF [Kirkland et al., 1992b; Benincasa et al.,

2001]. Furthermore, capillary electrophoresis is applied for sample separation [Na et al., 2004a; Na et al., 2004b]. Working with PEGylated colloidal drug carrier systems the adoption of the field-flow fractionation combined with subsequent PEG determination appears especially interesting, as separation takes place in a hollow channel, allowing the concurrent fractionation of undissolved i.e. suspended colloidal structures and dissolved samples like PEG within a broad molecular weight range of $\sim 10^4$ - 10^{18} Da = 1 nm – 100 μ m (cp. chapter 1.1) [Giddings, 1993].

The present study describes an AF4 separation method for PEGylated gelatin nanoparticles and PEG as well as the determination of the PEGylation efficiency of gelatin nanoparticles via the concentration of non-reacted PEG residues in the reaction media. Beyond the quantitative description of this process we were interested in visualizing the successful PEGylation of the nanoparticles. Therefore plain and PEGylated gelatin nanoparticles were investigated in atomic force microscope (AFM) experiments. During AFM experiments samples are mechanically scanned with a special cantilever resulting in a resolution of nanometre sized structures like the helical morphology of DNA double strands [LaVan et al., 2002; Ravi Kumar, V et al., 2004], which makes AFM the method of choice in this context.

1.5.2 Results and discussion

Characterization of nanoparticles

Prior to AFM measurements, nanoparticles had to be fixed on the sample grid as scans performed with mobile analytes will not guarantee optimum resolution of subtle morphological changes like the investigated PEGylation of gelatin nanoparticles. Fixation was accomplished via electrostatic interactions comparable to the above investigated oligonucleotide-loading procedure (chapter 1.4). Since the sample grid had a negatively charged coating, the nanoparticles had to be cationized to ensure sufficient fixation. During AF4 analysis this additional surface modification was not necessary. Furthermore, the PEGylation is accomplished via the free aldehyde groups of mono-functionally bound glutaraldehyde derived from crosslinking present at the surface of the nanoparticles. As the aldehyde groups are beside free carboxyl groups as well reaction counterpart during cationization, the resulting competitive situation may lead to released PEG during subsequent conducted cationization. With respect to the aim of the AF4 study, to reproducibly quantify a maximum amount of PEG that can be bound onto the surface of gelatin nanoparticles, experiments were conducted without cationization. Thus, cationization differentiates nanoparticles applied during AFM studies from the nanoparticles analyzed via AF4. It was assumed that the modification with cholamine, a low molecular weight substance (Mw 175.10 Da) should not have a crucial impact on the particle's morphology.

Table 1.5.1 Size and polydispersity of nanoparticle formulations applied for AF4 and AFM analysis of the PEGylation

	non-PEGylated gelatin nanoparticles (G-NP _{zw} AF)		PEGylated gelatin nanoparticles (G-NP _{zw} AF-PEG)	
	plain	cationized	plain	cationized
	size [nm]	179.7	180.4	185.2
PDI	0.041	0.064	0.072	0.097

Otherwise, it was thereby exemplified, that both modifications (cationization and PEGylation) can be performed on one nanoparticle batch. Dynamic light scattering (DLS) revealed that neither cationization or PEGylation nor cationization and

PEGylation led to changes in the particle homogeneity as indicated by the polydispersity index; all batches still exhibited PDIs below 0.1.

Quantification of the PEGylation reaction via AF4

During the intended quantification of the PEGylation of gelatin nanoparticles there are two requirements to be met in order to succeed. First, the baseline separation of the analytes has to be guaranteed and second, the linear relation between PEG and its detection signal intensity has to be proven.

Figure 1.5.1 shows the cross-flow profile of the separation procedure developed for the fractionation of PEG and gelatin nanoparticles and the resulting RI signal of PEG. Refractive index detection was chosen due to the poor spectrophotometric properties of PEG. The squares indicate the changes in the instrument's running mode and in the cross-flow strength respectively.

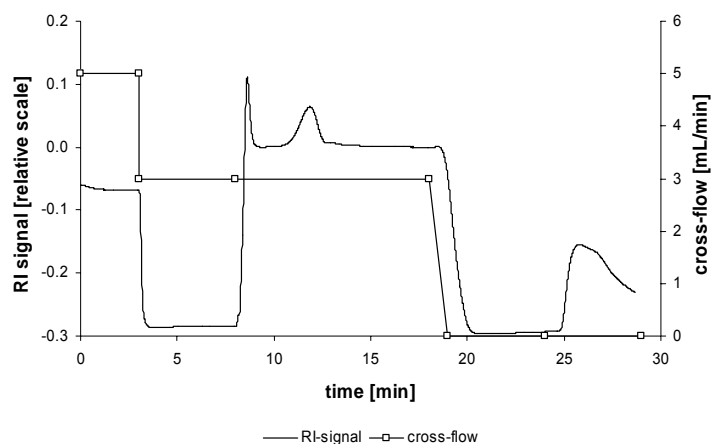


Figure 1.5.1 Cross-flow profile and resulting RI signal of PEG 5000

Note that in comparison to cross flow-profiles displayed in Figure 1.2.3 and Figure 1.2.4 for the oligonucleotide-loading quantification experiments the cross flow is as well plotted for injection (0 - 3 min) and focusing (3 - 5 min) both taking place during AF4 analysis prior to separation, which starts after 8 min. This presentation was chosen to highlight the pressure sensitivity of the RI signal [Colfen et al., 2000]. It is reflected by a baseline shift at 3, 9, and 19 min as well as peaks at 8 min and 25 min. The chosen cross-flow conditions provide a constant baseline in a time frame between 9 and 19 min, necessary for a reproducible calculation of the AUC and finally the quantification of PEG (Figure 1.5.2 a and b).

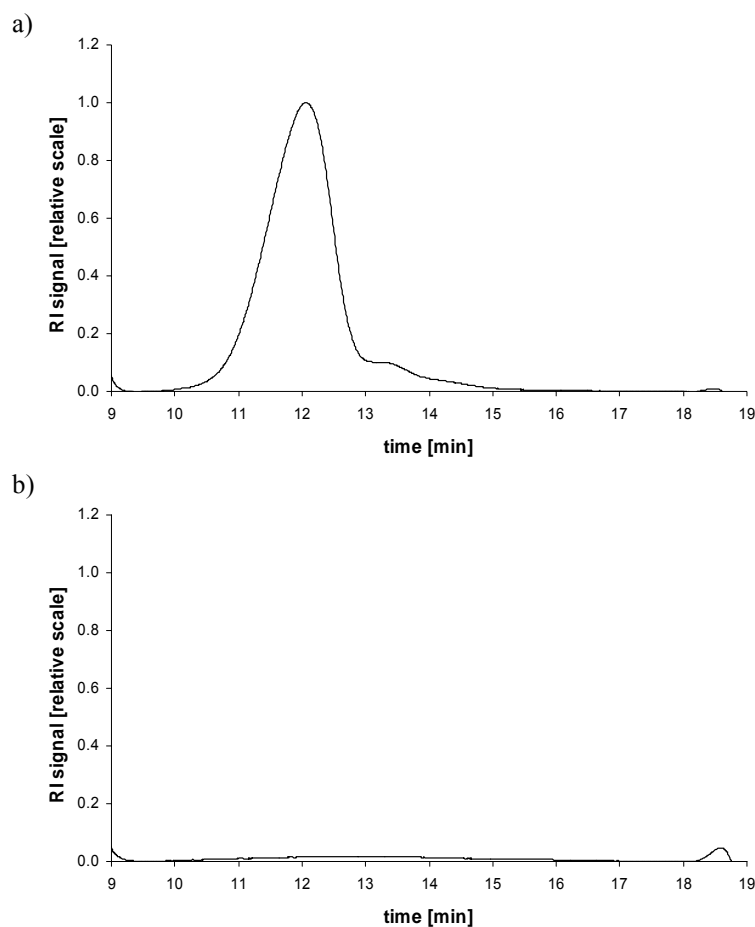


Figure 1.5.2 The fractogram section showing a) the peak of PEG 5000, $c = 1$ mg/mL and b) the respective baseline recorded with water

Before terminating the cross-flow after the period of 10 min of a constant baseline the analyte is completely eluted. The graph exhibits a shoulder on the descending arm of the peak indicating the presence of higher molecular weight compounds than PEG 5000 and therefore certain heterogeneity of the PEG size distribution. These data are confirmed by the specification from the manufacturer. Due to its anionic polymerization PEG has a certain variance in the number of ethylene oxide units [Nektar Therapeutics, 2006]. Since the whole amount of unbound PEG present in the particular reaction medium should be quantified, there was no emphasis laid on a further separation of the PEG sample specimens. The separation of unbound PEG from its reaction partner, the gelatin nanoparticles, is especially important, as the nanoparticles show certain RI response and are therefore able to disturb the PEG quantification. After adjusting the cross-flow aiming at a good PEG peak symmetry the afterwards reduced cross-flow enables the controlled

elution of the nanoparticles sufficiently separated from PEG. Figure 1.5.3 shows the successful separation of PEG and gelatin nanoparticles. Since there is only a weak RI signal arising from the gelatin nanoparticles an overlay of UV and RI detection is shown. Compared with the basic method shown in Figure 1.2.5 it was now modified to the point of a prolonged elution step (plus 10 min) after abandoning the cross-flow. This prolonged duration enables a more complete elution of the nanoparticles from the AF4 channel subsequent to separation.

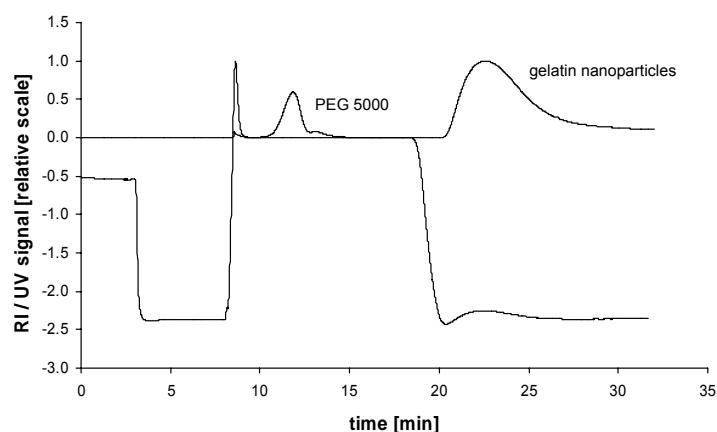


Figure 1.5.3 Separation of PEG 5000, $c = 1$ mg/mL and gelatin nanoparticles highlighted by the overlay of the concurrently recorded UV_{260} (gelatin nanoparticles) and RI (PEG 5000) signal.

To achieve a calibration curve describing the correlation of the detection signal intensity with the PEG concentration a row of PEG containing solutions with rising concentrations was investigated. Figure 1.5.4 displays the stepwise appearance of the fractograms related to the increasing mass of PEG per sample.

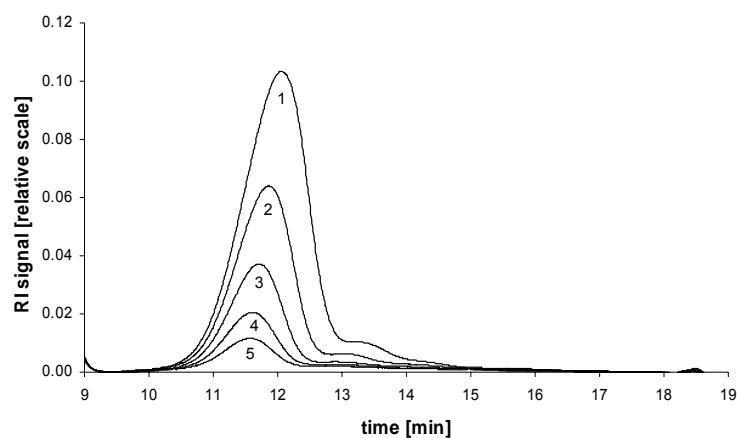


Figure 1.5.4 The fractogram section showing the peak of PEG 5000; peak height and AUC are decreasing with injecting reduced amounts of PEG; concentrations of the injected samples were adjusted to 1 mg/mL (1), 0.5 mg/mL (2), 0.25 mg/mL (3), 0.125 mg/mL (4), and 0.0625 mg/mL (5)

Plotting the resulting AUC of each peak versus the according PEG concentration the expected linear relation could be proven and a straight calibration curve ($R^2 = 0.9992$) was obtained (Figure 1.5.5). After establishing the analytical basis, the PEGylation reaction was conducted with four different initial PEG concentrations “offered” to a constant amount of gelatin nanoparticles. The idea behind was to determine a threshold of PEG above which a further PEGylation will not take place even with increasing amounts of PEG.

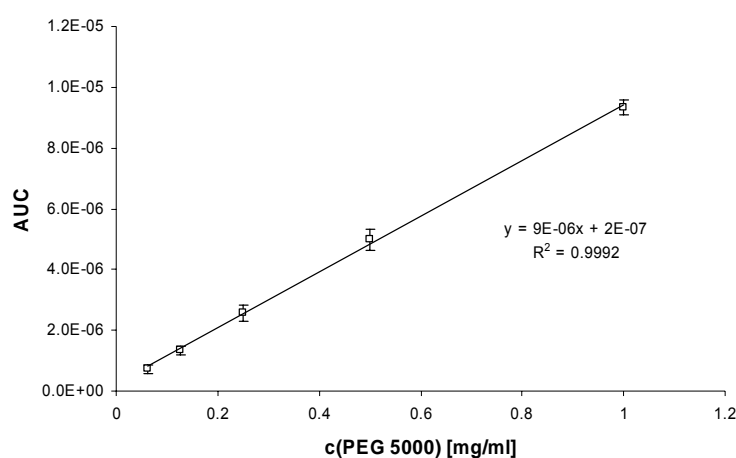


Figure 1.5.5 Calibration curve of PEG 5000 based on the AUCs calculated from the respective fractograms displayed in Figure 1.5.4

To follow the course of the PEGylation reaction PEG was analyzed twice. A defined amount of PEG was first determined in the absence of gelatin nanoparticles and in a second step PEG was measured directly in the reaction media after separation from the now PEGylated gelatin nanoparticles. Based on the calibration curve the respective mass of PEG could be calculated from the obtained AUCs.

The decrease of the AUC determined for PEG caused by its consumption during the PEGylation reaction is visualized in Figure 1.5.6. Exemplarily shown for two of the investigated concentrations, the comparison of the fractograms recorded before and after the PEGylation reveals this consumption. In contrast to the single-stranded oligonucleotide-loading studies the according detection signal of the nanoparticles could not be exploited in terms of a grown AUC in response to the PEGylation. On the one hand PEG is inaccessible for UV detection and on the other hand the RI detection signal of the nanoparticles arises only weakly direct upon to a baseline shift (Figure 1.5.3) caused by the cross-flow gradient (Figure 1.5.1), which negatively affects reproducibility.

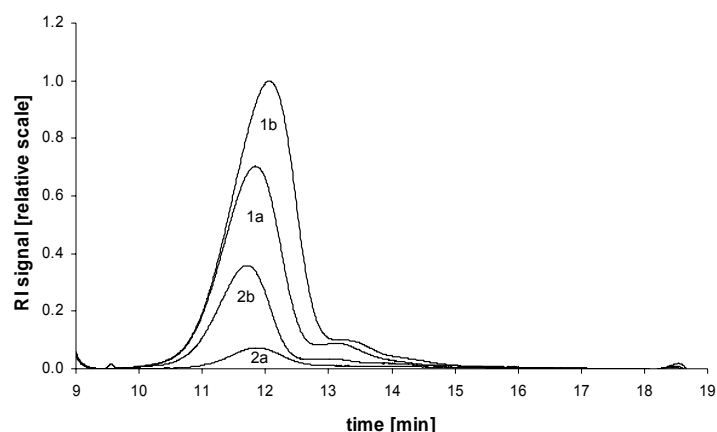


Figure 1.5.6 Fractograms of PEG 5000 before (1b) / (2b) and after (1a) / (2a) the PEGylation of gelatin nanoparticles, the decrease of the particular AUC reflects the degree of the PEGylation; initial PEG concentrations were adjusted to 1 mg/mL (1b) and 0.25 mg/mL (2b)

From the resulting AUCs the particular amounts of PEG bound onto the surface of the nanoparticles were determined. The amount of bound PEG was calculated by the following equation [Zwiorek, 2006]:

$$m_x = (AUC_0 - AUC_x) \times m_0$$

m_0 = initially administered mass of mPEG-NH₂

m_x = mass of mPEG-NH₂ being loaded onto the nanoparticles

AUC_0 = AUC of the RI signal being detected for the amount m_0 of mPEG-NH₂ before incubation

AUC_x = AUC of the RI signal being detected for the amount m_x of residual free mPEG-NH₂ after incubation

Figure 1.5.7 shows the mass of bound PEG plotted against the initially administered PEG. From the hyperbolic shape of the resulting curve it is obvious that the amount of PEG bound onto the surface of a given number of gelatin nanoparticles is limited. We could determine a maximum mass of ~0.350 mg PEG per mg gelatin nanoparticles that can be completely bound. PEG administered in lower concentrations (0.125 mg and 0.25 mg per mg nanoparticles) is almost completely bound, whereas the application of higher amounts of PEG did not lead to a further PEGylation of the nanoparticles. In a comparable context Xu et al. determined an amount of 0.01 to 0.02 mg PEG 5000 monomethyl ether incorporated into 1 mg silica nanoparticles with a FT-IR based quantification method. But, due to

some technical considerations they did not chose optimum conditions that may lead to higher degrees of PEGylation [Xu et al., 2003].

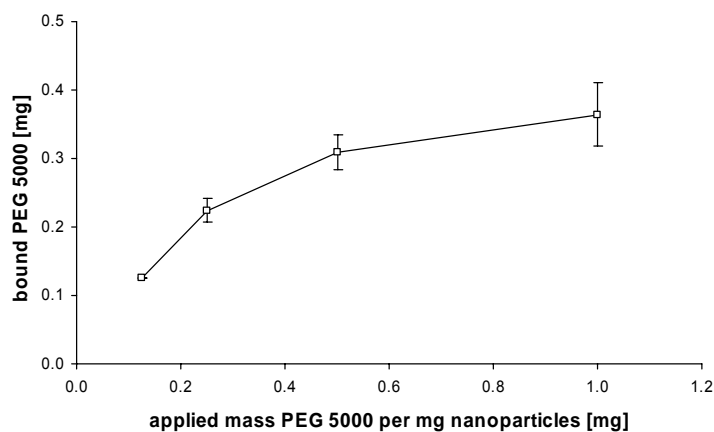


Figure 1.5.7 Mass of PEG 5000 bound onto 1 mg nanoparticles in dependency of the initially applied amount of PEG

Referred to the PEGylation mechanism as it is shown in Figure 1.2.1 a limited number of monofunctionally bound glutaraldehyde is accessible for PEGylation, thus leading to the assumed threshold. Applying a validated process for the manufacturing of the gelatin nanoparticles the number of free aldehyde groups is held constant for each nanoparticle batch.

Finally, we could show the pH dependency of the PEGylation process. As the coupling of aldehydes with primary amino groups demands slightly alkaline conditions we could show a successful PEGylation in borate buffer pH 8.4. When changing the pH towards an acidic value of pH 3.0 the fractograms showed identical peaks for PEG control solutions and PEG derived from the incubation process (data not shown). These data prove the assumed influence of the pH on the coupling reaction and provides at the same time a successful negative control for the described quantification procedure. This could be verified by control studies additionally performed in the absence of gelatin nanoparticles that revealed unchanged detection signals for each applied PEG concentration thus demonstrating the successful PEGylation.

Figure 1.5.6 and Figure 1.5.7 have as well been published by Klaus Zwiorek [Zwiorek, 2006] with permission of the author (Jan Carl Zillies). But, the pertaining data have been produced in the course of this thesis.

Visualization of the PEGylation reaction via AFM

The images derived from AFM analysis of the cationized versions of the non PEGylated and the PEGylated nanoparticles are depicted below (Figure 1.5.8).

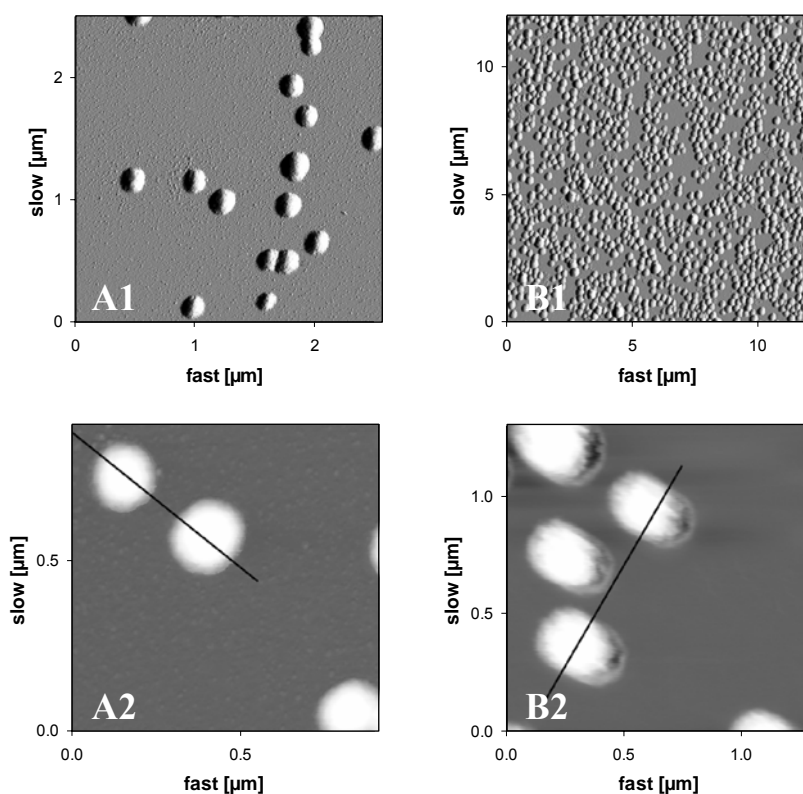


Figure 1.5.8 AFM images of plain (A1/A2) and PEGylated (B1/B2) gelatin nanoparticles; A/B 1: error channel image, A/B 2: height channel image [pictures provided by Christian Löbbe from JPK Instruments, Berlin, Germany]

Overview images being employed in the amplitude mode demonstrated the good homogeneity of the applied samples (Figure 1.5.8 A1 / B1). No significant differences between both batches were seen. So, previous SEM data, where gelatin nanoparticles were assessed as homogeneous smooth spheres, were substantiated (data not shown). But, analyzing height images, PEGylated nanoparticles seemed to possess an indifferent surface (Figure 1.5.8 A2 / B2). Observing the respective cross sections of these height images finally revealed more detailed information (Figure 1.5.9). Converse to the smooth surface of plain gelatin nanoparticles, PEGylated nanoparticles exhibited a cragged surface when analyzing their height profile, which indicates the presence of PEG-chains on the nanoparticles' surface.

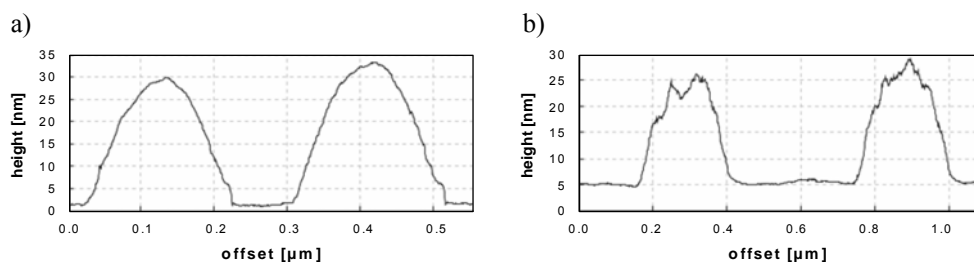


Figure 1.5.9 AFM analysis of a) plain and b) PEGylated gelatin nanoparticles; diagrams represent the respective cross sections of height images displayed in Figure 1.5.8 (cp. black lines) [diagrams provided by Christian Lobbe from JPK Instruments, Berlin, Germany]

The displayed AFM pictures could thus contribute to the proof of a successful PEGylation of gelatin nanoparticles by a direct, independent method.

1.5.3 Summary

After establishing AF4 in the work with gelatin nanoparticles (see chapter 1.4) this method could be used for further analysis of modified gelatin nanoparticles. The quantitative description of the PEGylation process of gelatin nanoparticles via an AF4 separation followed by a direct RI detection was shown. With regard to the broad separation range AF4 spans, an application of the described analytical set-up in other PEGylation (e.g. the PEGylation of proteins) and PEG quantification (e.g. the release from controlled release devices) scenarios seems to be possible.

AFM, as the second analytical tool, completed the set of data and demonstrated its strength by visualizing the presence of PEG chains on the nanoparticles' surface. Especially the combination of both techniques appears to be ideal to track the PEGylation of colloidal carrier systems. The results obtained are of high quality and suggest using both methods as state-of-the-art analysis for various other colloidal systems as the number of existing techniques is rather limited.

1.6 Concluding Remarks

In the beginning of this work research in colloidal drug delivery utilizing gelatin nanoparticles and in investigating aggregation in protein pharmaceuticals via AF4 were separately pursued in our department. Based on the idea to merge these two areas, an AF4 protocol was established that enabled the quantification of single-stranded oligonucleotide-loading onto gelatin nanoparticles. The limits of this quantitative analytical approach were reached while describing the loading of gelatin nanoparticles with a double-stranded oligonucleotide, which could be referred to certain methodical restrictions. Furthermore, insights into the manufacturing process of gelatin nanoparticles were gained as the molecular weight distribution of the gelatin bulk material could be characterized by coupling AF4 and MALS detection. Finally, the knowledge acquired during the quantification of oligonucleotide-loading onto gelatin nanoparticles could be transferred to their PEGylation. Due to the poor spectrophotometrical properties of PEG, quantifying the PEGylation was not accessible via centrifugation and UV-spectroscopy as it was known from oligonucleotide loading. This hindrance was successfully circumvented by employing the combination of AF4 separation and RI detection.

The reported studies prove the outstanding ability of AF4 to separate dissolved from suspended samples during one sample run. And, in the end asymmetrical flow field-flow fractionation can now be stated as well established in the work with gelatin nanoparticles providing the basis for future work in the field of colloidal drug carrier analysis.

The reported work comprises analytical data and results from nanoparticle preparation. The first attempts in analyzing gelatin nanoparticles by AF4 were accomplished by Wolfgang Fraunhofer at this chair. He as well described gelatin bulk material via SE-HPLC/MALS. The quantification of single-stranded oligonucleotide-loading of gelatin nanoparticles was conducted together with him to continue the work with AF4 after he would have had finished his Ph.D. thesis. Klaus Zwioerek in turn contributed to the practical realization of the analytical data from gelatin bulk material investigations by AF4/MALS. He developed the described one-step desolvation procedure for the preparation of gelatin nanoparticles and he

provided PEG-modified gelatin nanoparticles for the quantification of the PEGylation process via AF4/RI. AFM analysis was conducted by Christian Löbbe at JPK Instruments, Berlin, Germany.

1.7 References

- Ahlers, M., Coester, C., Zwioerek, K., and Zillies, J.; Biodegradable gelatin nanoparticles and procedure for their production; Patent Application, DE 102004041340 / WO 2006/021367
- Andersson, M., Fromell, K., Gullberg, E., Artursson, P., and Caldwell, K. D.; Characterization of surface-modified nanoparticles for in vivo biointeraction: a sedimentation field flow fractionation study; *Analytical Chemistry*, 2005, 77(17), 5488-5493
- Arndt, K.-F. and Mueller, G.; *Polymercharakterisierung*; Carl Hanser Verlag GmbH, Munich, 1996
- Augsten, C. and Maeder, K.; Light scattering for the masses: characterization of poly(D,L-lactide-co-glycolide) nanoparticles; *Wyatt Technology Corporation Application Notes*, 2005,
- Babel, W.; Gelatine - Ein vielseitiges Biopolymer; *Chemie in unserer Zeit*, 1996, 30(2), 1-11
- Bajpai, A. K. and Choubey, J.; Release study of sulphamethoxazole controlled by swelling of gelatin nanoparticles and drug-biopolymer interaction; *Journal of Macromolecular Science, Pure and Applied Chemistry*, 2005, A42(3), 253-275
- Bauer, K. H., Froemming, K.-H., and Fuehrer Claus; *Lehrbuch der Pharmazeutischen Technologie*; Wissenschaftliche Verlagsgesellschaft mbH, Stuttgart 2006, 6, 181-182
- Benincasa, M. A. and Caldwell, K. D.; Flow field-flow fractionation of poly(ethylene oxide): effect of carrier ionic strength and composition; *Journal of Chromatography, A*, 2001, 925(1-2), 159-169
- Brinckmann, J.; Collagens at a glance; in *Topics in Current Chemistry: Collagen*; Springer-Verlag GmbH, Berlin, 2005, 247, 1-6
- Caldwell, K. D., Karaiskakis, G., and Giddings, J. C.; Characterization of liposomes by sedimentation field-flow fractionation; *Colloids and Surfaces*, 1981, 3(3), 233-238
- Cascone, M. G., Lazzeri, L., Carmignani, C., and Zhu, Z.; Gelatin nanoparticles produced by a simple W/O emulsion as delivery system for methotrexate; *Journal of Materials Science: Materials in Medicine*, 2002, 13(5), 523-526
- Chamberlain, P. and Mire-sluis, A. R.; An overview of scientific and regulatory issues for the immunogenicity of biological products; *Developments in Biologicals*, 2003, 112 (Immunogenicity of Therapeutic Biological Products), 3-11

- Childs, C. E.; Determination of polyethylene glycol in gamma globulin solutions; *Microchemical Journal*, 1975, 20(2), 190-192
- Coester, C. J., Langer, K., Von Briesen, H., and Kreuter, J.; Gelatin nanoparticles by two step desolvation-a new preparation method, surface modifications and cell uptake; *Journal of Microencapsulation*, 2000, 17(2), 187-193
- Coester, C.; Development of a new carrier system for oligonucleotides and plasmids based on gelatin nanoparticles; *New Drugs*, 2003, (1), 14-17
- Colfen, H. and Antonietti, M.; Field-flow fractionation techniques for polymer and colloid analysis; *Advances in Polymer Science*, 2000, 150 (New Developments in Polymer Analytics I), 67-187
- Crescenzi, C., Di Corcia, A., Marcomini, A., and Samperi, R.; Detection of poly(ethylene glycols) and related acidic forms in environmental waters by liquid chromatography/electrospray/mass spectrometry; *Environmental Science and Technology*, 1997, 31(9), 2679-2685
- Delahunty, T. and Hollander, D.; New liquid-chromatographic method for measuring polyethylene glycol in urine; *Clinical Chemistry*, 1986, 32(2), 351-353
- Dinauer, N., Balthasar, S., Weber, C., Kreuter, J., Langer, K., and von Briesen, H.; Selective targeting of antibody-conjugated nanoparticles to leukemic cells and primary T-lymphocytes; *Biomaterials*, 2005, 26(29), 5898-5906
- Djagny, K. B., Wang, Z., and Xu, S.; Gelatin: A valuable protein for food and pharmaceutical industries: Review; *Critical Reviews in Food Science and Nutrition*, 2001, 41(6), 481-492
- Fakt, C. and Ervik, M.; Determination of low levels of poly(ethylene glycol) 400 in plasma and urine by capillary gas chromatography-selected ion-monitoring mass spectrometry after solid-phase extraction; *Journal of Chromatography, B: Biomedical Sciences and Applications*, 1997, 700(1 + 2), 93-100
- Farrugia, C. A. and Groves, M. J.; Gelatin behaviour in dilute aqueous solution: designing a nanoparticulate formulation; *Journal of Pharmacy and Pharmacology*, 1999, 51(6), 643-649
- Fee, C. J. and Van Alstine, J. M.; PEG-proteins: Reaction engineering and separation issues; *Chemical Engineering Science*, 2005, 61(3), 924-939
- Fraunhofer, W.; Asymmetrical flow-field-fractionation in pharmaceutical Analytics - Investigations in aggregation tendencies of pharmaceutical antibodies, Dissertation, Ludwig-Maximilians-University Munich; 2003
- Fraunhofer, W. and Winter, G.; The use of asymmetrical flow field-flow fractionation in pharmaceutics and biopharmaceutics; *European Journal of Pharmaceutics and Biopharmaceutics*, 2004, 58(2), 369-383

- Fraunhofer, W., Winter, G., and Coester, C.; Asymmetrical flow field-flow fractionation and multiangle light scattering for analysis of gelatin nanoparticle drug carrier systems; *Analytical Chemistry*, 2004, 76(7), 1909-1920
- Friess, W.; Collagen. Biomaterial for drug delivery; *European Journal of Pharmaceutics and Biopharmaceutics*, 1998, 45(2), 113-136
- Garratty, G.; Progress in modulating the RBC membrane to produce transfusable universal/stealth donor RBCs; *Transfusion medicine reviews*, 2004, 18(4), 245-256
- Giddings, C. J.; New separation concept based on a coupling of concentration and flow nonuniformities; *Separation Sciences*, 1966, 1(1), 123-125
- Giddings, J. C.; Field-flow fractionation: analysis of macromolecular, colloidal, and particulate materials; *Science*, 1993, 260(5113), 1456-1465
- Giddings, J. C., Yang, F. J., and Myers, M. N.; Flow field-flow fractionation: new method for separating, purifying, and characterizing the diffusivity of viruses; *Journal of Virology*, 1977, 21(1), 131-138
- Giddings, J. C.; The field-flow fractionation family: underlying principles; in *Field-Flow Fractionation Handbook*, John Wiley & Sons, Inc., New York, 2000, 3-30
- Gimbert, L. J., Andrew, K. N., Haygarth, P. M., and Worsfold, P. J.; Environmental applications of flow field-flow fractionation (FIFFF); *Trends in Analytical Chemistry*, 2003, 22(9), 615-633
- Gupta, A. K., Gupta, M., Yarwood, S. J., and Curtis, A. S. G.; Effect of cellular uptake of gelatin nanoparticles on adhesion, morphology and cytoskeleton organization of human fibroblasts; *Journal of Controlled Release*, 2004, 95(2), 197-207
- Haskell, R. J.; Physical characterization of nanoparticles; *Drugs and the Pharmaceutical Sciences*, 2006, 159 (Nanoparticle Technology for Drug Delivery), 103-138
- Jores, K., Mehnert, W., Drechsler, M., Bunjes, H., Johann, C., and Maeder, K.; Investigations on the structure of solid lipid nanoparticles (SLN) and oil-loaded solid lipid nanoparticles by photon correlation spectroscopy, field-flow fractionation and transmission electron microscopy; *Journal of Controlled Release*, 2004, 95(2), 217-227
- Kaul, G. and Amiji, M.; Long-circulating poly(ethylene glycol)-modified gelatin nanoparticles for intracellular delivery; *Pharmaceutical research*, 2002, 19(7), 1061-1067

- Kaul, G. and Amiji, M.; Tumor-targeted gene delivery using poly(ethylene glycol)-modified gelatin nanoparticles: in vitro and in vivo studies; *Pharmaceutical Research*, 2005, 22(6), 951-961
- Kirkland, J. J. and Dilks, C. H., Jr.; Flow field-flow fractionation of polymers in organic solvents; *Analytical Chemistry*, 1992, 64(22), 2836-2840
- Kirkland, J. J., Dilks, C. H., Jr., and Rementer, S. W.; Molecular weight distributions of water-soluble polymers by flow field-flow fractionation; *Analytical Chemistry*, 1992, 64(11), 1295-1303
- Klein, T. and Niessner, R.; Characterization of heavy-metal-containing seepage water colloids by flow FFF, ultrafiltration, ELISA, and AAS; *Mikrochimica Acta*, 1998, 129(1-2), 47-55
- Kommareddy, S. and Amiji, M.; Preparation and evaluation of thiol-modified gelatin nanoparticles for intracellular DNA delivery in response to glutathione; *Bioconjugate Chemistry*, 2005, 16(6), 1423-1432
- Kowalkowski, T., Buszewski, B., Cantado, C., and Dondi, F.; Field-flow fractionation: theory, techniques, applications and the challenges; *Critical Reviews in Analytical Chemistry*, 2006, 36(2), 129-135
- Kurfurst, M. M.; Detection and molecular weight determination of polyethylene glycol-modified hirudin by staining after sodium dodecyl sulfate-polyacrylamide gel electrophoresis; *Analytical Biochemistry*, 1-2-1992, 200(2), 244-248
- Kwong, E., Baert, L., and Bechard, S.; Gas-liquid chromatographic quantitation of polyethylene glycol 400 in pharmaceutical preparations; *Journal of Pharmaceutical and Biomedical Analysis*, 1995, 13(1), 77-81
- Labhasetwar, V. D. and Dorle, A. K.; Nanoparticles - a colloidal drug delivery system for primaquine and metronidazole; *Journal of Controlled Release*, 1990, 12(2), 113-119
- Lang, R. and Winter, G.; Light scattering for the masses: characterization of virus like particles by asymmetrical flow field-flow fractionation; *Wyatt Technology Corporation Application Notes*, 2006,
- Langer, K., Coester, C., Weber, C., Von Briesen, H., and Kreuter, J.; Preparation of avidin-labeled protein nanoparticles as carriers for biotinylated peptide nucleic acid; *European Journal of Pharmaceutics and Biopharmaceutics*, 2000, 49(3), 303-307
- LaVan, D. A., Lynn, D. M., and Langer, R.; Moving smaller in drug discovery and delivery; *Nature reviews. Drug discovery*, 2002, 1(1), 77-84
- Lee, H., Williams, S. K. R., Allison, S. D., and Anchordoquy, T. J.; Analysis of self-assembled cationic lipid-DNA gene carrier complexes using flow field-flow fractionation and light scattering; *Analytical Chemistry*, 2001, 73(4), 837-843

- Leenheer, J. A., Wershaw, R. L., Brown, P. A., and Noyes, T. I.; Detection of poly(ethylene glycol) residues from nonionic surfactants in surface water by proton and carbon-13 nuclear magnetic resonance spectrometry; *Environmental Science and Technology*, 1991, 25(1), 161-168
- Leo, E., Arletti, R., Forni, F., and Cameroni, R.; General and cardiac toxicity of doxorubicin-loaded gelatin nanoparticles; *Farmaco*, 1997, 52(6-7), 385-388
- Leong, K. W., Mao, H. Q., Truong-Le, V. L., Roy, K., Walsh, S. M., and August, J. T.; DNA-polycation nanospheres as non-viral gene delivery vehicles; *Journal of Controlled Release*, 1998, 53(1-3), 183-193
- Lin, W., Garnett, M. C., Schacht, E., Davis, S. S., and Illum, L.; Preparation and in vitro characterization of HSA-mPEG nanoparticles; *International Journal of Pharmaceutics*, 1999, 189(2), 161-170
- Litzen, A. and Wahlund, K. G.; Zone broadening and dilution in rectangular and trapezoidal asymmetrical flow field-flow fractionation channels; *Analytical Chemistry*, 1991, 63(10), 1001-1007
- Lu, Z., Yeh, T. K., Tsai, M., Au, J. L. S., and Wientjes, M. G.; Paclitaxel-loaded gelatin nanoparticles for intravesical bladder cancer therapy; *Clinical Cancer Research*, 2004, 10(22), 7677-7684
- Marty, J. J., Oppenheim, R. C., and Speiser, P.; Nanoparticles - a new colloidal drug delivery system; *Pharmaceutica Acta Helveticae*, 1978, 53(1), 17-23
- Mazarin, M., Viel, S., Allard-Breton, B., Thevand, A., and Charles, L.; Use of pulsed gradient spin-echo NMR as a tool in MALDI method development for polymer molecular weight determination; *Analytical Chemistry*, 2006, 78(8), 2758-2764
- Meyer, M. and Morgenstern, B.; Characterization of gelatin and acid soluble collagen by size exclusion chromatography coupled with multi angle light scattering (SEC-MALS); *Biomacromolecules*, 2003, 4(6), 1727-1732
- Miller, K. E., Bramanti, E., Prazen, B. J., Prezhdo, M., Skogerboe, K. J., and Synovec, R. E.; Multidimensional analysis of poly(ethylene glycols) by size exclusion chromatography and dynamic surface tension detection; *Analytical Chemistry*, 2000, 72(18), 4372-4380
- Moghimi, S. M. and Szebeni, J.; Stealth liposomes and long circulating nanoparticles: critical issues in pharmacokinetics, opsonization and protein-binding properties; *Progress in Lipid Research*, 2003, 42(6), 463-478
- Moon, M. H. and Giddings, J. C.; Size distribution of liposomes by flow field-flow fractionation; *Journal of Pharmaceutical and Biomedical Analysis*, 1993, 11(10), 911-920

- Murphy, R., Selden, A. C., Fisher, M., Fagan, E. A., and Chadwick, V. S.; High-performance liquid chromatographic analysis of polyethylene glycols; *Journal of Chromatography*, 1981, 211(1), 160-165
- Myers, M. N.; Overview of field-flow fractionation; *Journal of Microcolumn Separations*, 1997, 9(3), 151-162
- Na, D. H., Park, E. J., Youn, Y. S., Moon, B. W., Jo, Y. W., Lee, S. H., Kim, W. B., Sohn, Y., and Lee, K. C.; Sodium dodecyl sulfate-capillary gel electrophoresis of polyethylene glycolylated interferon alpha; *Electrophoresis*, 2004, 25(3), 476-479
- Na, D. H. and Lee, K. C.; Capillary electrophoretic characterization of PEGylated human parathyroid hormone with matrix-assisted laser desorption/ionization time-of-flight mass spectrometry; *Analytical Biochemistry*, 2004, 331(2), 322-328
- Nag, A., Mitra, G., and Ghosh, P. C.; A colorimetric assay for estimation of polyethylene glycol [PEG] and polyethylene glycolated protein using ammonium ferrothiocyanate; *Analytical Biochemistry*, 1996, 237(2), 224-231
- Natarajan, A., Xiong, C., Albrecht, H., DeNardo, G. L., and DeNardo, S. J.; Characterization of site-specific ScFv PEGylation for tumor-targeting pharmaceuticals; *Bioconjugate Chemistry*, 2005, 16(1), 113-121
- Nektar Therapeutics; Nektar Advanced PEGylation, *Catalog 2005-2006*; 2006,
- Nielen, M. W. F. and Buijtenhuijs, F. A.; Polymer analysis by liquid chromatography/electrospray ionization time-of-flight mass spectrometry; *Analytical Chemistry*, 1999, 71(9), 1809-1814
- Ogris, M., Brunner, S., Schuller, S., Kircheis, R., and Wagner, E.; PEGylated DNA/transferrin-PEI complexes: reduced interaction with blood components, extended circulation in blood and potential for systemic gene delivery; *Gene Therapy*, 1999, 6(4), 595-605
- Oliva, A., Armas, H., and Farina, J. B.; HPLC determination of polyethylene glycol 400 in urine: oligomeric profile in healthy and celiac disease subjects; *Clinical Chemistry*, 1994, 40(8), 1571-1574
- Owens, D. E. and Peppas, N. A.; Opsonization, biodistribution, and pharmacokinetics of polymeric nanoparticles; *International Journal of Pharmaceutics*, 2006, 307(1), 93-102
- Peracchia, M. T.; Stealth nanoparticles for intravenous administration; *STP Pharma Sciences*, 2003, 13(3), 155-161
- Peracchia, M. T., Fattal, E., Desmaele, D., Besnard, M., Noel, J. P., Gomis, J. M., Appel, M., d'Angelo, J., and Couvreur, P.; Stealth PEGylated polycyanoacrylate nanoparticles for intravenous administration and splenic targeting; *Journal of Controlled Release*, 1999, 60(1), 121-128

- Ratanathanawongs-Williams, S. K.; Flow field-flow fractionation; in *Field-Flow Fractionation Handbook*, John Wiley & Sons, Inc., New York, 2000, 257-278
- Ratanathanawongs-Williams, S. K. and Lee, D.; Field-flow fractionation of proteins, polysaccharides, synthetic polymers, and supramolecular assemblies; *Journal of Separation Science*, 2006, 29(12), 1720-1732
- Ravi Kumar, M. N., V, Bakowsky, U., and Lehr, C. M.; Preparation and characterization of cationic PLGA nanospheres as DNA carriers; *Biomaterials*, 2004, 25(10), 1771-1777
- Reschiglian, P., Zattoni, A., Roda, B., Michelini, E., and Roda, A.; Field-flow fractionation and biotechnology; *Trends in Biotechnology*, 2005, 23(9), 475-483
- Schimpf, M., Caldwell, K. D., and Giddings, J. C. (eds.); *Field-Flow Fractionation Handbook*, John Wiley & Sons, Inc., New York, 2000
- Skoog, B.; Determination of polyethylene glycols 4000 and 6000 in plasma protein preparations; *Vox sanguinis*, 1979, 37(6), 345-349
- Soppimath, K. S., Aminabhavi, T. M., Kulkarni, A. R., and Rudzinski, W. E.; Biodegradable polymeric nanoparticles as drug delivery devices; *Journal of Controlled Release*, 2001, 70(1-2), 1-20
- Speiser, P. and Pharmaceutical Society of Victoria; Injectable compositions; Australian Patent, 38036/75(1516348), 1974
- Tondelli, L., Ballestri, M., Magnani, L., Vivarelli, D., Fini, A., Cerasi, A., Chiarantini, L., Sparnacci, K., and Laus, M.; Core-shell nanospheres for oligonucleotide delivery V: Adsorption/release behavior of "stealth" nanospheres; *Journal of Biomaterials Science, Polymer Edition*, 2003, 14(11), 1209-1227
- Truong-Le, V. L., Walsh, S. M., Schweibert, E., Mao, H. Q., Guggino, W. B., August, J. T., and Leong, K. W.; Gene transfer by DNA-gelatin nanospheres; *Archives of Biochemistry and Biophysics*, 1999, 361(1), 47-56
- Vandervoort, J. and Ludwig, A.; Preparation and evaluation of drug-loaded gelatin nanoparticles for topical ophthalmic use; *European Journal of Pharmaceutics and Biopharmaceutics*, 2004, 57(2), 251-261
- Verma, A. K., Sachin, K., Saxena, A., and Bohidar, H. B.; Release kinetics from biopolymeric nanoparticles encapsulating protein synthesis inhibitor-cycloheximide, for possible therapeutic applications; *Current Pharmaceutical Biotechnology*, 2005, 6(2), 121-130
- Veronese, F. M.; Peptide and protein PEGylation: a review of problems and solutions; *Biomaterials*, 2001, 22(5), 405-417

- Veronese, F. M. and Pasut, G.; PEGylation, successful approach to drug delivery; *Drug Discovery Today*, 2005, 10(21), 1451-1458
- Wahlund, K. G.; Asymmetrical flow field-flow fractionation; in *Field-Flow Fractionation Handbook*, John Wiley & Sons, Inc., New York, 2000, 279-294
- Wahlund, K. G. and Giddings, J. C.; Properties of an asymmetrical flow field-flow fractionation channel having one permeable wall; *Analytical Chemistry*, 1987, 59(9), 1332-1339
- Walker, G. F., Fella, C., Pelisek, J., Fahrmeir, J., Boeckle, S., Ogris, M., and Wagner, E.; Toward synthetic viruses: endosomal pH-triggered deshielding of targeted polyplexes greatly enhances gene transfer in vitro and in vivo; *Molecular Therapy*, 2005, 11(3), 418-425
- White, R. J.; FFF-MALS - A new tool for the characterization of polymers and particles; *Polymer International*, 1997, 43(4), 373-379
- Wyatt, P. J.; Submicrometer particle sizing by multiangle light scattering following fractionation; *Journal of Colloid and Interface Science*, 1998, 197(1), 9-20
- Xu, H., Yan, F., Monson, E. E., and Kopelman, R.; Room-temperature preparation and characterization of poly (ethylene glycol)-coated silica nanoparticles for biomedical applications; *Journal of Biomedical Materials Research, Part A*, 2003, 66A(4), 870-879
- Yan, X., Scherphof, G., and Kamps, J.; Liposome Opsonization; *Journal of Liposome Research*, 2005, 15(1 & 2), 109-139
- Zhang, G., Wang, X., Wang, Z., Zhang, J., and Suggs, L.; A PEGylated fibrin patch for mesenchymal stem cell delivery; *Tissue engineering*, 2006, 12(1-2), 9-19
- Zillies, J. and Coester, C.; Capillary hydrodynamic fractionation (CHDF) and other semi-chromatographic methods as new analytical tools for the separation and analysis of protein based nanoparticles aside low molecular weight proteins and oligonucleotides; Poster Presentation, Annual Meeting Controlled Release Society Local Chapter Germany, Munich, Germany, April 4, 2003
- Zillies, J. and Coester, C.; Evaluating gelatin based nanoparticles as a carrier system for double stranded oligonucleotides; *Journal of Pharmacy & Pharmaceutical Sciences*, 2004, 7(4), 17-21
- Zwiorek, K.; Gelatin nanoparticles as delivery system for nucleotide-based drugs, Dissertation, Ludwig-Maximilians-University Munich; 2006
- Zwiorek, K., Kloeckner, J., Wagner, E., and Coester, C.; Gelatin nanoparticles as a new and simple gene delivery system; *Journal of Pharmacy & Pharmaceutical Sciences*, 2004, 7(4), 22-28

CHAPTER II

Formulation Development of Freeze-Dried Gelatin Nanoparticles

Abstract

Researching gelatin nanoparticles spans preparation technology as well as application in various *in vitro* and *in vivo* test systems. To provide a convenient nanoparticle formulation for their application either in research or (potentially in future) in clinical studies the freeze-drying properties of gelatin nanoparticles were evaluated. During these studies successful freeze-drying and rehydration of gelatin nanoparticles could be demonstrated. Various freeze-drying excipients and different rehydration volumes were as well investigated as the drying of empty and DNA / RNA oligonucleotide-loaded gelatin nanoparticles. An NF- κ B decoy oligonucleotide-loaded gelatin nanoparticle formulation could be developed and was successfully applied in a drug targeting approach in an animal model. Finally short term storage stability of empty and oligonucleotide-loaded gelatin nanoparticles under accelerated conditions was assessed utilizing sucrose, trehalose, mannitol, as well as mannitol and sucrose in the ratio of 4:1 as freeze-drying excipients. Size, size distribution, residual moisture content, and cake morphology were investigated. Sucrose and trehalose containing formulations provided the best results and mannitol containing formulations showed notable stabilization despite their crystalline nature.

Keywords: freeze-drying, gelatin nanoparticles, colloidal stability, formulation development

2.1 Introduction

The application of nanoparticles in targeted drug delivery has already been reviewed more than 20 years ago [Oppenheim, 1981; Douglas et al., 1987]. Since then enormous progressions have been made in the development of nanoparticulate drug carrier systems, prepared of a broad variety of starting materials, for numerous drugs and therapeutic applications. However, despite intensive research work the current status of colloidal drug delivery still reveals liposomes ahead of nanoparticles in terms of marketed pharmaceuticals [Gruber, 2004; Wagner et al., 2006]. During the step of drug development shelf life and stabilization of the respective products are an important matter of interest. In this context lyophilization was already proposed in 1978 to improve long term stability of liposomes [Van Winden et al., 1997], which finally led to the market authorization for AmbisomeTM as the first freeze-dried liposomal drug formulation in Germany in 1992 (source: homepage of the manufacturer*) and in the USA in 1997 (source: U.S. Food and Drug Administration[#]). Freeze-drying as industrial process is in general known since World War II [Franks, 1998] and is widely applied in stabilizing pharmaceuticals especially labile drugs like proteins [Tang et al., 2004]. Furthermore, freeze-drying of liposomes has been intensively investigated and was recently summarized by Van Winden [Van Winden, 2003]. Nanoparticles in contrast are still part of basic research and only little is reported about their freeze-drying properties in general. Several authors report about freeze-drying in the end of the manufacturing process of their respective systems but did not provide further information about the applied freeze-drying cycle or particle characteristics before and after lyophilization. Others gave some more detailed information about the freeze-drying procedure but only chitosan, poly(lactide) (PLA) / poly(lactide-co-glycolide) (PLGA), and solid lipid nanoparticles (SLN) as well as nanoparticulate lipid- or polycation-DNA complexes (by the group of Anchordoquy) were more precisely investigated for their freeze-drying properties. Table 2.1.1 lists nanoparticle preparations originating from different starting materials that have already been freeze-dried according to literature.

*http://www.gilead-sciences.de/index.php?csrc=http://www.gilead-sciences.de/public/01gilead/c_meilensteine.htm

[#]http://www.accessdata.fda.gov/scripts/cder/drugsatfda/index.cfm?fuseaction=Search.Label_ApprovalHistory#apphist

Table 2.1.1 Freeze-dried nanoparticle preparations that have already been described in literature

Nanoparticle preparation	References
Crosslinked acrylamido-2-desoxy-glucose (AADG) nanoparticles	[Nimesh et al., 2006] ¹
Chitosan-DNA nanoparticles	[Mao et al., 2001] ¹
Core-shell type lecithin / Pluronic [®] nanoparticles	[Oh et al., 2005]
Core-shell type poly(γ -glutamic acid) (γ -PGA) / L-phenylalanineethyl ester (L-PAE) nanoparticles	[Akagi et al., 2005]
Gelatin nanoparticles	[Kaul et al., 2002; 2004; 2005] ¹ [Farrugia et al., 1999] ¹
Glucomannan-coated chitosan nanoparticles	[Cuna et al., 2006]
Lipid-DNA complexes	[Allison et al., 2000] [Molina et al., 2004]
Polyethylenimine (PEI)-DNA complexes (Polyplexes)	[Armstrong et al., 2004] [Anchordoquy et al., 2005] [Brus et al., 2004] [Talsma et al., 1997]
Poly- ϵ -caprolactone nanospheres / nanocapsules	[de Chasteigner et al., 1996] [Abdelwahed et al., 2006b] [Choi et al., 2004]
Poly(isobutylcyanoacrylate) (PIBCA) nanoparticles	[Layre et al., 2006]
Poly(L-lactic acid) (PLA) nanoparticles	[Hirsjarvi et al., 2006] [Bala et al., 2004] ² [De Jaeghere et al., 2000]
Poly(lactide-co-glycolide) (PLGA)	[Avgoustakis, 2004] [Birnbaum et al., 2000] [Jeong et al., 2005]
Poly(methylidene malonate 2.1.2) nanoparticles	[Roy et al., 1997]
Solid lipid nanoparticles (SLN)	[Maeder et al., 2005] ² [Schwarz et al., 1997]

¹Data without further information about the freeze-drying cycle or particle characteristics before and after lyophilization

²Review articles

Based on the (re-)introduction of gelatin nanoparticles into the field of colloidal oligonucleotide and plasmid DNA delivery by Coester [Coester et al., 2000; Coester, 2003] our research group gained comprehensive knowledge and experience in several *in vitro* and *in vivo* applications of gelatin nanoparticles reflected by the dissertation of Klaus Zwioerek [Zwioerek, 2006] and this thesis. As all data obtained from these studies were produced with regard to a later potentially marketed

pharmaceutical product a need for gelatin nanoparticle formulations that are easy to ship, to handle, and to store arose in the meantime. In consequence the aim of the present work was to show the principle applicability of freeze-drying for gelatin nanoparticles and to systematically describe their freeze-drying properties. So, different common freeze-drying excipients namely, sucrose and trehalose as well as mannitol known for their good lyoprotecting and bulking properties respectively [Kim et al., 1998; Wang, 2000] were assessed for their stabilizing potential of empty and oligonucleotide-loaded gelatin nanoparticles. The rehydration volume was varied and the storage stability was intensively studied. In all cases the integrity of size and size distribution of nanoparticles subsequent to freeze-drying are most important and were followed by photon correlation spectroscopy (PCS). In evaluating storage stability residual moisture content and structural changes of the lyophilized products have in addition to be taken into account. Thus, Karl-Fischer titration and differential scanning calorimetry (DSC) were utilized in this context.

Initial freeze-drying experiments took place during a research stay in the labs of Prof. Thomas J. Anchordoquy at the School of Pharmacy of the University of Colorado in Denver, CO, USA. The work was continued in Munich in the labs of Prof. Gerhard Winter at the Department of Pharmacy, Pharmaceutical Technology and Biopharmaceutics of the Ludwig-Maximilians-University Munich, Germany.

2.2 Materials and Methods

Reagents

Reagent	Description	Supplier
Acetone	p.a.	VWR International GmbH (Ismaning, Germany)
Acetone ^d	p.a.	Fischer Scientific L.L.C. (Pittsburgh, PA, USA)
Cholaminechloride hydrochloride	(2-aminoethyl)-trimethyl-ammoniumchloride hydrochloride	Sigma-Aldrich GmbH (Taufkirchen, Germany)
Dextran 3000		Spectrum Chemical Corp (New Brunswick, NJ, USA)
DMF	Dimethylformamide, < 50ppm water	Acros Organics (Morris Plains, NJ, USA)
ds NF- κ B decoy ODN	5'-AGT TGA GGG GAC TTT CCC AGG C-3' phosphorothioate	biomers.net GmbH (Ulm, Germany)
ds scr decoy ODN	5'-CCT TGT ACC ATT GTT AGC C-3' phosphorothioate	biomers.net GmbH (Ulm, Germany)
ds siRNA ODN	5'-CUG GAC UUC CAG AAG AAC A-3' amidate	Sirna Therapeutics, Inc. (Boulder, CO, USA)
EDC	1-ethyl-3-(3-dimethyl-aminopropyl) carbodiimide hydrochloride	Sigma-Aldrich GmbH (Taufkirchen, Germany)
Gelatin type A	175 Bloom	Sigma-Aldrich GmbH (Taufkirchen, Germany)
Glutaraldehyde	25 % aqueous solution	Sigma-Aldrich GmbH (Taufkirchen, Germany)
HCl	2 N	VWR International GmbH (Ismaning, Germany)
HCl ^d	2 N	Fischer Scientific L.L.C. (Pittsburgh, PA, USA)
D-Mannitol	Riedel-de Haën, p.a.	Sigma-Aldrich GmbH (Seelze, Germany)
D-Mannitol ^d		Ferro Pfanstiehl Lab., Inc (Waukegan, IL, USA)
Sucrose		Suedzucker AG (Mannheim, Germany)

Reagent	Description	Supplier
Sucrose ^d		Ferro Pfanstiehl Lab., Inc (Waukegan, IL, USA)
Trehalose	α, α -Dihydrate	Ferro Pfanstiehl Lab., Inc (Waukegan, IL, USA)
Tween [®] 80	Polysorbat 80, Ph. Eur.	Merck KGaA (Darmstadt, Germany)

^dSame excipients from different suppliers utilized during formulation development experiments conducted at the School of Pharmacy of the University of Colorado in Denver, CO, USA and at the Department of Pharmacy, Pharmaceutical Technology and Biopharmaceutics of the Ludwig-Maximilians-University Munich, Germany are listed twice.

Preparation and surface modification of gelatin nanoparticles

Gelatin nanoparticles were manufactured by the two step desolvation method and optionally surface modified (cationized) with cholamine as described in chapter 1.2.

Oligonucleotide-loading of gelatin nanoparticles

NF- κ B decoy, scr decoy and siRNA oligonucleotide-loading was accomplished in highly purified water. 47.3 μ L of an aqueous nanoparticle dispersion containing 1.700 μ g surface modified gelatin nanoparticles were incubated with 85 μ g or rather 170 μ g of the respective oligonucleotide in aqueous solution (i.e., 5 % or 10 % [w/w] oligonucleotide loading) and adjusted with varying freeze-drying excipient containing solutions to a final volume of 1,200 μ L for two 2 h at 22 °C and 800 rpm under constant shaking (Thermomixer Comfort, Eppendorf AG, Hamburg, Germany).

Freeze-drying of empty and oligonucleotide-loaded gelatin nanoparticles

Empty gelatin nanoparticles and gelatin nanoparticle formulations loaded with 5 and 10 % [w/w] oligonucleotide containing 1.4 μ g/mL nanoparticles were prepared in solutions of mannitol, mannitol and sucrose in a ratio of 4:1, sucrose, and trehalose exhibiting varying concentrations related to the oligonucleotide content, even if no oligonucleotide was added. The following excipients to oligonucleotide mass ratios were investigated: 47, 100, 200, 300, 400, 500, 600, 700, 800, 900, and 1000, representing a total amount of 0.3 up to 7 % [w/v]. After preparation aqueous nanoparticle dispersions were transferred to glass vials for freeze-drying. During

initial formulation development experiments 300 μL per vial were filled in 1R glass vials (West Pharmaceutical Services, Inc., Lionville, PA, USA), later samples prepared for storage stability and animal studies contained 300 μL and 1,200 μL per vial respectively in 2R glass vials (Schott AG, Mainz, Germany) prior freeze-drying.

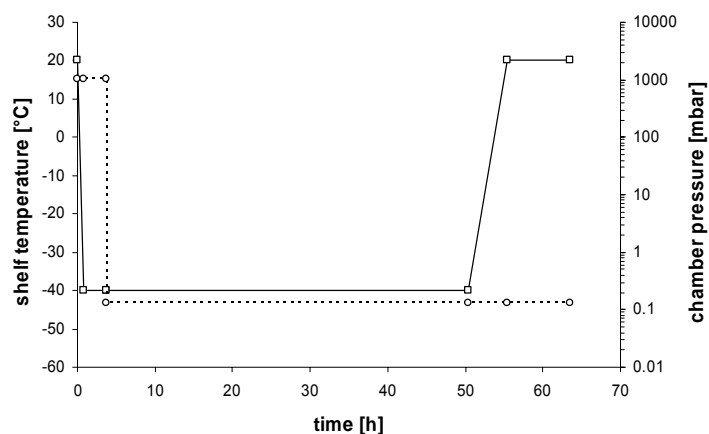


Figure 2.2.1 Freeze-drying cycles with shelf temperature (\square) and chamber pressure (\circ) applied for all samples during formulation development experiments performed at the School of Pharmacy of the University of Colorado in Denver, CO, USA

Freeze-drying during formulation development in the labs of Prof. Thomas J. Anchordoquy at the School of Pharmacy of the University of Colorado in Denver, CO, USA was conducted in a Dura-Stop™ lyophilizer (FTS Systems, Inc., Stone Ridge, NY, USA) following the above stated freeze-drying cycle (Figure 2.2.1). Samples prepared for storage stability and animal studies in the labs of the Department of Pharmacy, Pharmaceutical Technology and Biopharmaceutics of the Ludwig-Maximilians-University Munich, Germany were freeze-dried in an EPSILON 2- 6D pilot scale freeze dryer and an EPSILON 2- 12D freeze dryer respectively (Martin Christ Freeze Dryers GmbH, Osterode, Germany). Nanoparticle formulations containing mannitol-sucrose (4:1), sucrose, and trehalose were dried with the freeze-drying cycle shown in Figure 2.2.2. Mannitol containing samples were dried at increased temperature and pressure as displayed in Figure 2.2.3. Upon completion of the respective cycles the chamber was vented with nitrogen, samples were stoppered under slight vacuum at 800 mbar, and the sealed vials were stored at 20 °C. Rehydration was conducted with different volumes of highly purified water ranging from 1/30th of the original volume to the original volume. All samples were prepared in triplicates. Where used, placebos were accordingly prepared without the addition of gelatin nanoparticles or oligonucleotide.

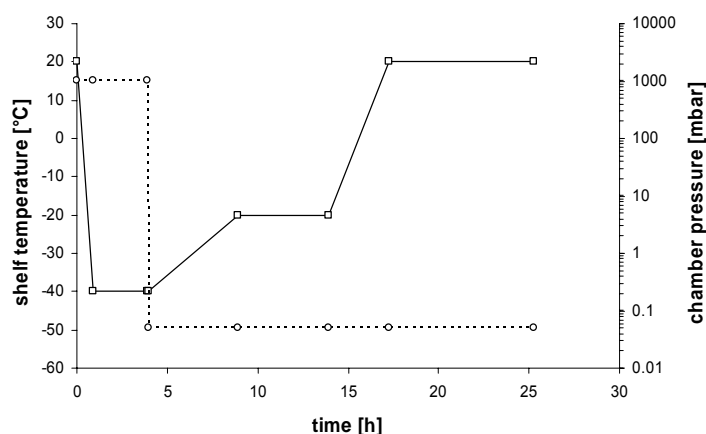


Figure 2.2.2 Freeze-drying cycles with shelf temperature (□) and chamber pressure (○) for lyophilization of mannitol-sucrose (4:1), sucrose, and trehalose containing samples prepared for storage stability and animal studies

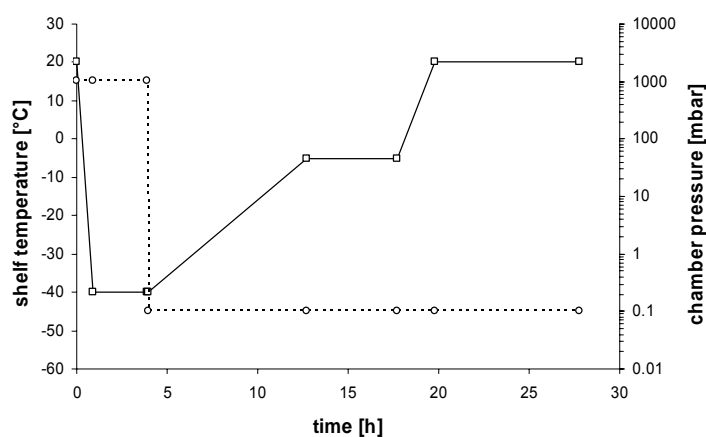


Figure 2.2.3 Freeze-drying cycles with shelf temperature (□) and chamber pressure (○) for lyophilization of mannitol containing samples prepared for storage stability and animal studies

Storage conditions during stability studies

Samples were stored under accelerated conditions in sealed vials at 30 °C and 40 °C as well as open vials at 30 °C / 30 % relative humidity (RH) and 30 °C / 60 % RH. Storage was performed for 4 weeks and 10 weeks in drying chambers, whereas defined relative humidity was adjusted in closed containers by saturated solutions of magnesium chloride (maintaining 30 % RH at 30 °C) and ammonium nitrate (maintaining 60 % RH at 30 °C).

Characterization of gelatin nanoparticles

Size determination of gelatin nanoparticle batches was conducted by dynamic light scattering (DLS) using a Nicomp 380 Particle Sizer (Particle Sizing Systems,

Santa Barbara, CA, USA) and a Nanosizer ZS (Malvern Instruments, Worcestershire, UK). In contrast to the polydispersity index (PDI) calculated by the Malvern software, the Particle Sizing Systems instrument expresses the width of the size distribution by a so called coefficient of variation. As the results of the initial formulation development experiments are acquired with the Nicomp 380 Particle Sizer, their quality is estimated by means of this coefficient. Prior to measurements samples were diluted 10x in highly purified water.

Karl-Fischer titration

Residual moisture content of samples was determined by coulometric Karl-Fischer titration either with a Mettler DL37 Coulometer (Mettler-Toledo, Inc., Columbus, OH, USA) or with an Aqua 40.00 titrator comprising a headspace module (Analytik Jena AG, Halle, Germany). Using the DL37 Coulometer samples were dissolved in anhydrous DMF and sonicated prior to analysis. The exact mass of DMF was determined gravimetrically. Samples were prepared in a dry-nitrogen-purged glove box to avoid hydration resulting from atmosphere. Aliquots were withdrawn with a syringe through the rubber stopper of the instrument to the titration solution (Pyridine Free Vessel Solution, Photovolt Instruments, Inc., St. Louis Park, MN, USA) where the water amount was determined. Blank values of DMF were acquired with every test series. For measurements with the Aqua 40.00 titrator no further sample preparation was necessary. After placing into the headspace module samples were heated up to 80 °C and the evaporated water was transferred to the titration solution (HYDRANAL[®]-Coulomat AG, Riedel-de Haën, Sigma-Aldrich GmbH, Seelze, Germany), where its amount was determined. Blank values were obtained from empty vials identically treated like verum samples throughout preparation and storage.

Differential scanning calorimetry (DSC)

DSC was used to study the glass transition of the maximally freeze-concentrated solution (T_g') of gelatin nanoparticle formulations and depending on the applied freeze-drying excipient glass transition (T_g) or melting temperature (mp) of lyophilized verum and placebo samples. Around 20 mg of liquid samples and with respect to the investigated formulation between 1 and 8 mg of the dried samples, handled in a dry-nitrogen-purged glove box to avoid hydration resulting from

atmosphere, were analyzed in crimped aluminum crucibles. T_g' was determined with a Perkin-Elmer Diamond DSC (PerkinElmer, Inc., Wellesley, MA, USA). T_g and mp respectively were determined with a Netzsch 204 Phoenix[®] DSC (Netzsch-Geraetebau GmbH, Selb, Germany). Applied temperature programs are summarized in Table 2.2.1 a) and b).

Table 2.2.1 a) Temperature programs for determination of T_g' of sucrose containing gelatin nanoparticle formulations and of T_g of sucrose and trehalose containing gelatin nanoparticle (verum) and placebo formulations

T_g' suc		T_g suc		T_g tre	
T[°C]	Scanning rate / Time	T[°C]	Scanning rate / Time	T[°C]	Scanning rate / Time
25	1 min	0	1 min	0	1 min
25 → -50	2.5 K/min	0 → 80	10 K/min	0 → 130	10 K/min
-50	10 min	80	1 min	130	1 min
-50 → 25	10 K/min	80 → -10	10 K/min	130 → -10	10 K/min
		-10	1 min	-10	1 min
		-10 → 150	10 K/min	-10 → 180	10 K/min
		150	1 min	180	1 min
		150 → 20	50 K/min	180 → 20	50 K/min

Table 2.2.1 b) Temperature programs for determination of mp of mannitol and mannitol and sucrose in a ratio of 4:1 containing gelatin nanoparticle (verum) and placebo formulations

mp_{man}		$mp_{man-suc}$	
T[°C]	Scanning rate / Time	T[°C]	Scanning rate / Time
0	1 min	0	1 min
0 → 80	10 K/min	0 → 80	10 K/min
80	1 min	80	1 min
80 → -10	10 K/min	80 → -10	10 K/min
-10	1 min	-10	1 min
-10 → 180	10 K/min	-10 → 180	10 K/min
180	1 min	180	1 min
180 → 20	50 K/min	180 → -10	10 K/min
		-10	1 min
		-10 → 180	10 K/min
		180	1 min
		180 → 20	50 K/min

Glass transition (point of inflection) of the maximally freeze-concentrated solution (T_g'), glass transition (point of inflection) (T_g), and melting temperature (peak) (mp) of the excipients were determined from heating scans.

In vivo hepatic lipopolysaccharide (LPS) (sepsis) rat model

To evaluate, beside the quality, the biological function of nanoparticulate bound NF- κ B decoy oligonucleotide after storage formulations were tested in an *in vivo* LPS rat model established during the work described in chapter 3.4. Experiments were conducted twice for each nanoparticle formulation. During the experiments lipopolysaccharides (LPS) were used as exogenous stimulus for the NF- κ B activation within rat liver. The NF- κ B decoy oligonucleotide delivered on the surface of the gelatin nanoparticles binds to the activated transcription factor which is in the following no longer available for detection during the electrophoretic mobility shift assay (EMSA) conducted after terminating the animal experiment. For the detailed mechanism of the decoy effect it is referred to chapter 3.1.4. A successful inhibition of NF- κ B *in vivo* can be proven by diminished or even erased NF- κ B bands from the electrophoresis gel of the shift assay. For a detailed description of the experiments and the subsequent determination of the NF- κ B activity via EMSA it is referred to the according sections of chapter 3.4.

All animal studies and electrophoretic mobility shift assays were conducted by Florian Hoffmann at the department of pharmaceutical biology of the Ludwig-Maximilians-University Munich, Germany.

2.3 Results and Discussion

2.3.1 Applicability of freeze-drying for gelatin nanoparticle suspensions

Characterization of nanoparticles

During the initial experiments conducted in the labs of the School of Pharmacy of the University of Colorado in Denver a Nicomp 380 Particle Sizer was available for particle size determination. The coefficient of variation calculated by the Nicomp software to describe the quality of the particle size distribution varies within broader ranges than it is known from the polydispersity index determined with particle sizing machines from Malvern Instruments. To compare coefficient of variation data obtained for gelatin nanoparticles manufactured in the Denver labs and polydispersity indices samples were shipped to Munich and analyzed with a Nanosizer ZS. Interestingly, even high coefficients of variation represent homogeneously distributed nanoparticle populations with polydispersity indices clearly below 0.100. These findings are in good accordance to the optical properties of the nanoparticle suspensions macroscopically assessed. All suspensions exhibited the typical opalescent appearance without any visible particulate matter. In addition, particle sizes slightly vary with the emphasis on bigger numbers determined with the Nanosizer ZS. Data from particle size analysis of gelatin nanoparticles applied during freeze-drying experiments are summarized in Table 2.3.1.

Table 2.3.1 Size, coefficient of variation, polydispersity, and surface charge of the nanoparticle formulations applied in the freeze-drying applicability studies

		Gelatin nanoparticles		Surface modified gelatin nanoparticles	
		GNPCO3	GNPCO5	GNPCO3 _{pos}	GNPCO4 _{pos}
size [nm]	Nanosizer ZS	160.9	172.0	185.6	n/a*
	Nicomp 380 Particle Sizer	122.9	174.3	151.7	190,2
PDI	Nanosizer ZS	0.061	0.032	0.087	n/a*
coefficient of variation	Nicomp 380 Particle Sizer	0.343	0.213	0.501	0.641

*As aggregation of gelatin nanoparticles occurred during storage this batch was no longer available for particle sizing after the return to Munich

Initial freeze-drying experiments

Good stabilizing properties of sucrose are well known for freeze-dried protein pharmaceuticals [Wang, 2000]. In addition, successful stabilization of viral and non viral gene delivery systems during freeze-drying by adding sucrose is reported [de Chasteigner et al., 1996; Talsma et al., 1997; Anchordoquy et al., 2005; Jeong et al., 2005]. Thus, sucrose was chosen as lyoprotectant for the first freeze-drying attempts. As the later aim of the experiments was to develop a freeze-dried formulation for oligonucleotide-loaded gelatin nanoparticles, the amount of sucrose was calculated related to the mass of the oligonucleotide present in particular formulations based on a 5 % [w/w] oligonucleotide-loading on gelatin nanoparticles. The sucrose to ODN ratio was adjusted in increments of 100 ranging from 0 to 1000, which at the same time arises the formulation's denomination. At the same time masses of oligonucleotide and nanoparticles were kept constant for all formulations. The resulting sucrose amount and the formulation name were applied over all studies conducted with and without oligonucleotide.

The freeze-drying cycle stated above (Figure 2.2.1) was adopted from the work of Prof. Anchordoquy and his group with liposomes and polyplexes after checking the T_g' of sucrose containing gelatin nanoparticle suspensions to be above the chosen freezing temperature of $-40\text{ }^{\circ}\text{C}$ (Table 2.3.2). T_g' was investigated for pure nanoparticle suspensions (0) and for the lowest (100) and the highest (1000) applied sucrose amount. Values for sucrose containing formulations are confirmed by Liu as well as Her and Nail [Her et al., 1994; Liu, 2006]; they saw as well the slight increase of T_g' as a function of concentration of sucrose as it can be taken from data displayed in Table 2.3.2 [Her et al., 1994].

Table 2.3.2 T_g' (point of inflection) of sucrose containing freeze-drying solutions / suspensions of empty gelatin nanoparticles (GNPCO3)

Formulation	T_g' [$^{\circ}\text{C}$]	Stdv [$^{\circ}\text{C}$]
0	-34.47	0.04
100	-33.40	0.11
1000	-31.69	0.07

The same observation was made by Allison for nanoparticulate lipid-DNA complexes. T_g' ranged from $-37.2\text{ }^{\circ}\text{C}$ to $-31.6\text{ }^{\circ}\text{C}$ with increasing sucrose to DNA ratio [Allison et al., 2000]. For freeze concentrated, pure nanoparticle suspensions the glass transition could be determined slightly below T_g' of sucrose containing formulations. No T_g' was observed for pure poly(D,L-lactic-glycolic) (PLGA) nanoparticle suspensions [Saez et al., 2000] and DOTAP/DOPC liposomes in a comparable set-up (Michael Wiggernhorn, personal communication). Formulated with sucrose T_g' of polycaprolactone (PCL) and PLGA nanoparticle suspensions appeared at $-33\text{ }^{\circ}\text{C}$ [Saez et al., 2000] whereas Ugwu detected a T_g' of $-47.7\text{ }^{\circ}\text{C}$ for cholesterol containing DOPC liposomes at the same sucrose to lipid ratio [w/w] like formulation 100 [Ugwu et al., 2005]. Interestingly, they reported an increase of T_g' of $10\text{ }^{\circ}\text{C}$ by doubling the sucrose to lipid ratio which is in contrast to our results that show T_g' to be risen only for $1.24\text{ }^{\circ}\text{C}$ after increasing the sucrose to nanoparticle ratio by factor 10. In terms of efficient freeze-drying these findings are advantageous as they offer the possibility to optimally dry the different gelatin nanoparticle formulations applying the same freeze-drying cycle.

Results from initial freeze-drying experiments of gelatin nanoparticle formulations 100 to 1000 are displayed in Figure 2.3.1 and Figure 2.3.2. With respect to size and size distribution a successful stabilization can be stated for all investigated formulations. Subsequent to freeze-drying and rehydration none of the formulations showed increasing particle sizes or particle aggregation and the coefficient of variation remains almost unaffected, which reflects the constant quality of the samples (Figure 2.3.1 a) and b). Comparable results from particle sizing could be obtained for all formulations despite sucrose amounts rising from formulation 100 to 1000 by diluting samples prior to PCS analysis, which rules out viscosity derived alteration of PCS data. The slightly reduced particle size obtained after rehydration may possibly be explained with an incomplete recovery of the swollen state of the gelatin nanoparticles present prior to freeze-drying. Nanoparticles are manufactured of gelatin in an aqueous surrounding causing certain water content within the nanoparticle matrix even after stabilizing them by crosslinking. After nearly complete extraction of water during freeze-drying a porous structure of the dried nanoparticles can be assumed according to Kang who could demonstrate the porosity of crosslinked gelatin scaffolds produced by freeze-drying [Kang et al., 1999].

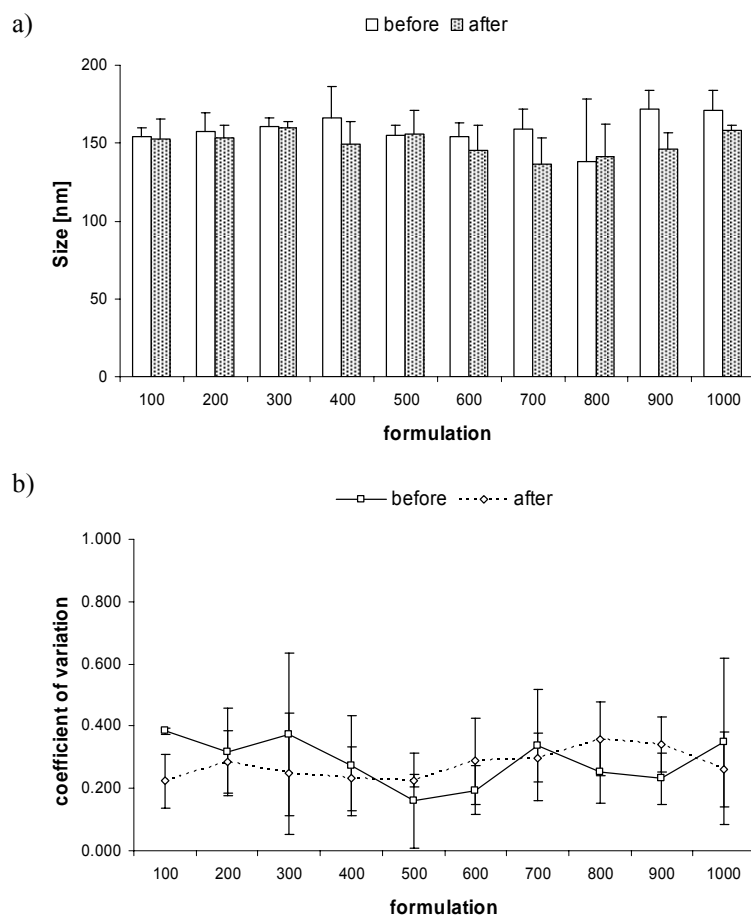


Figure 2.3.1 a) size and b) coefficient of variation of empty gelatin nanoparticles (GNPCO3) formulated with sucrose before freeze-drying and rehydrated right after freeze-drying

Driven by these porous structures certain shrinkage of nanoparticles may occur, which is obviously not completely reversible after rehydration expressed in reduced hydrodynamic diameter. Reduced particle sizes determined via PCS were as well reported by Schwarz for solid lipid nanoparticles dried with trehalose [Schwarz et al., 1997] and by Abdelwahed for PCL nanoparticles dried with sucrose [Abdelwahed et al., 2006a]. PCL nanoparticles dried without further excipients could not sufficiently be stabilized, whereas particle growth was correlated with the freezing rate [Choi et al., 2004]. Drying of pure gelatin nanoparticle suspensions in contrast led to completely aggregated samples where particle size analysis was no longer possible.

The pertaining residual moisture contents [% (w/w)] are displayed in Figure 2.3.2 a). All samples exhibit very low water content between 0.2 and 0.4 %. Interestingly, values pass through a minimum and do not constantly decrease with rising total solid content, as it might be expected for percent declaration. But, with respect to the almost identical very low amounts this seems to be negligible.

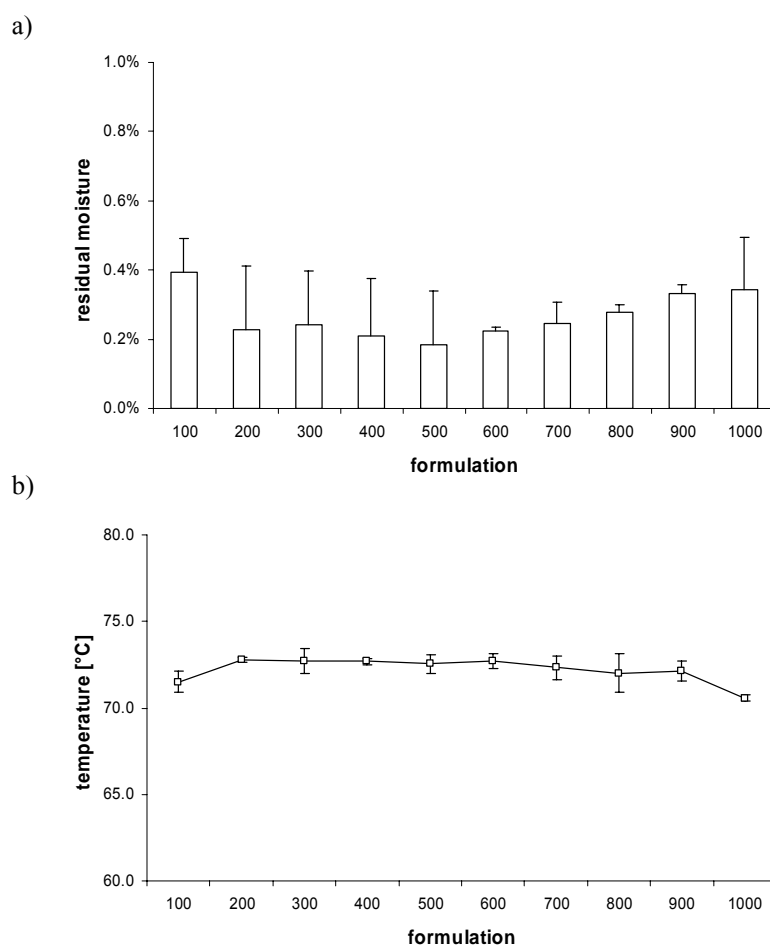


Figure 2.3.2 a) residual moisture content and b) T_g (point of inflection) of sucrose containing formulations of empty gelatin nanoparticles (GNPCO3) right after freeze-drying

The shape of the curve obtained for the glass transition temperatures of the formulations reflects the findings of residual moisture analysis with passing through a flat maximum (Figure 2.3.2 b). This inversely proportional relationship of increased residual moisture and decreased glass transition temperatures of amorphous solids is already described by te Booy and was systematically investigated by Hancock and Zografis [Te Booy et al., 1992; Hancock et al., 1994]. Basically T_g of sucrose is confirmed by literature [Wang, 2000; Liu, 2006].

After demonstrating the successful freeze-drying of empty gelatin nanoparticles oligonucleotide-loaded gelatin nanoparticles were investigated in the next step. Therefore, nanoparticles were loaded with the NF- κ B and the scr decoy oligonucleotide respectively applied during the *in vitro* and *in vivo* studies described in **CHAPTER III**. In addition, siRNA oligonucleotide-loaded gelatin nanoparticles were freeze-dried. Stability of oligonucleotide-loading was checked via UV-spectroscopy before and after freeze-drying and proven to be stable for all

investigated formulations (data not shown). Particle sizes and size distributions of scr decoy ODN-loaded nanoparticle formulations 100 to 1000 are depicted in Figure 2.3.3. Again no particle aggregation could be observed and the coefficient of variation data express the constant quality of the samples. Solely the formulations 100 and 200 show minor but significantly increased particle sizes. However, with respect to their coefficient of variation obtained after freeze-drying and rehydration and their optical properties strong effects on particle quality can be excluded.

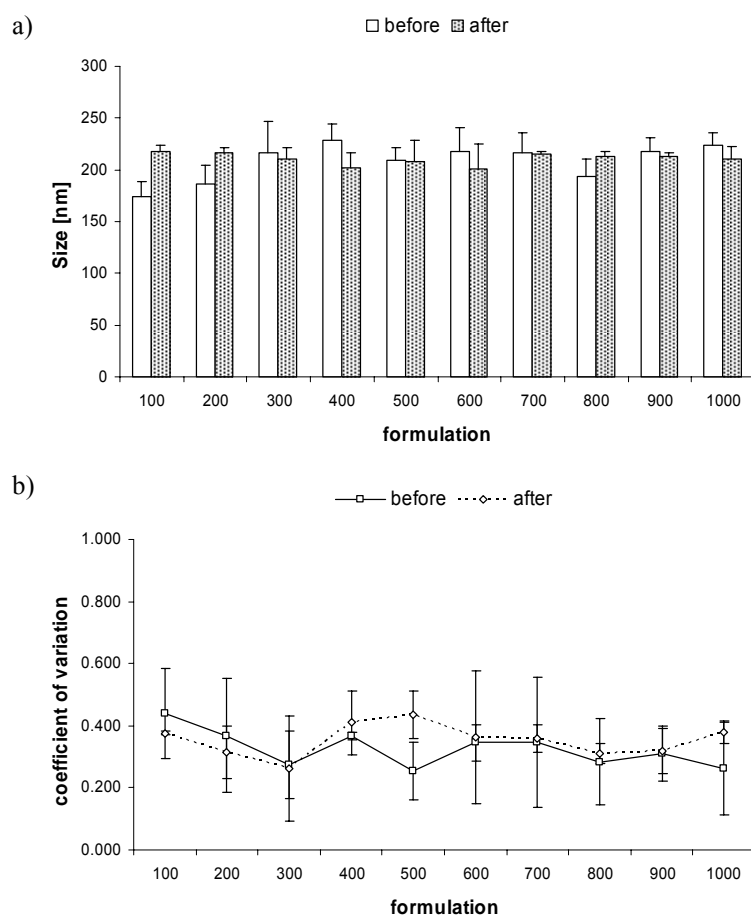


Figure 2.3.3 a) size and b) coefficient of variation of ds scr decoy ODN-loaded gelatin nanoparticles (GNPCO₃_{pos}) formulated with sucrose before freeze-drying and rehydrated right after freeze-drying

At the same time the impact of the applied oligonucleotide seems to be negligible for the outcome of the experiments. According to the manufacturer and to literature freeze-drying properties of 18-25 base pair long phosphorothioate ODNs (PTOs) are exceptional. Even without any excipients drying is easily possible. Aggregation is not induced and the T_g ' as well as the collapsing temperature (T_c) between $-20\text{ }^\circ\text{C}$ and $-8\text{ }^\circ\text{C}$ fit to the applied freeze-drying cycle resulting in a stable amorphous product exhibiting a T_g above $100\text{ }^\circ\text{C}$ [biomers.net GmbH, Ulm, 82

Germany personal communication; Jameel et al., 2001]. Only exposure to repeated freeze/thaw cycles leads to degradation of oligonucleotides depending on their base sequence [Davis et al., 2000].

Comparable results were reported by Brus for the stabilization of oligonucleotide-polyethylenimine (PEI) complexes during freeze-drying [Brus et al., 2004]. For the low sucrose to ODN ratios ranging from 5 to 26, compared to 100 which was the lowest ratio investigated during our work, they saw as well slightly increased particle sizes upon freeze-drying with sucrose. Residual moisture and thermal properties of ODN-loaded formulations were not investigated as there was not enough material, required for a series of triplicate studies of all the investigated formulations.

During the work with NF- κ B decoy oligonucleotide-loaded gelatin nanoparticles in the hepatic ischemia reperfusion (I/R) injury rat model introduced in chapter 3.4, the oligonucleotide amount deliverable per animal study was not high enough to initiate the aspired biological effect. Utilizing the oligonucleotide-loading method explained in **CHAPTER I**, based on electrostatic attraction forces of positively charged nanoparticles and negatively charged oligonucleotide molecules, it was not possible to further increase the concentration [mg/mL] of the oligonucleotide-loaded gelatin nanoparticles. Firstly, this procedure is limited by the given surface charge of the nanoparticles which is compensated by the oligonucleotide during loading. Secondly, increasing the concentration of both led to immediate aggregation during the loading process by formation of inter-nanoparticulate aggregates caused by “bridging” via the oligonucleotide. But, subsequent to oligonucleotide-loading the electrostatic situation with slightly positive charged ODN-loaded nanoparticles provides stable suspensions. It was the idea to concentrate these suspensions by means of freeze-drying i.e., the rehydration of freeze-dried samples with reduced volumes and the combination of a particular number of samples. Basically this method is used for protein pharmaceuticals [Shire et al., 2004] and was described by Anchordoquy for PEI/DNA complexes [Anchordoquy et al., 2005]. Based on his work freeze-dried ODN-loaded gelatin nanoparticles were firstly rehydrated in reduced volumes and secondly dried with dextran 3000 / sucrose blends to obtain isotonic formulations upon rehydration in a reduced volume concurrently maintaining the excipient mass necessary for stabilization of nanoparticles.

5 % and 10 % [w/w] NF- κ B decoy ODN-loaded gelatin nanoparticle formulations were prepared with decreasing amounts of sucrose that provide isotonic solutions (10 % [w/v]) upon rehydration in 1/10th, 1/20th, and 1/30th of the original volume (450 μ L). Particle sizing was conducted after rehydration in the original volume (“after 450”), after rehydration with the accordingly reduced volume (“conc.”), and after rehydration in a reduced volume which was completed to the original volume after waiting for 2 h (“conc. 450”). Besides, additional data were collected for empty nanoparticles. The resulting data are summarized in Figure 2.3.4. Due to the intended isotonicity only formulations containing sucrose to ODN ratios 24, 71, and 141 [w/w] were investigated resulting in particle sizes slightly to moderately ranging above initial values as it was already seen in Figure 2.3.3 for the formulations 100 and 200.

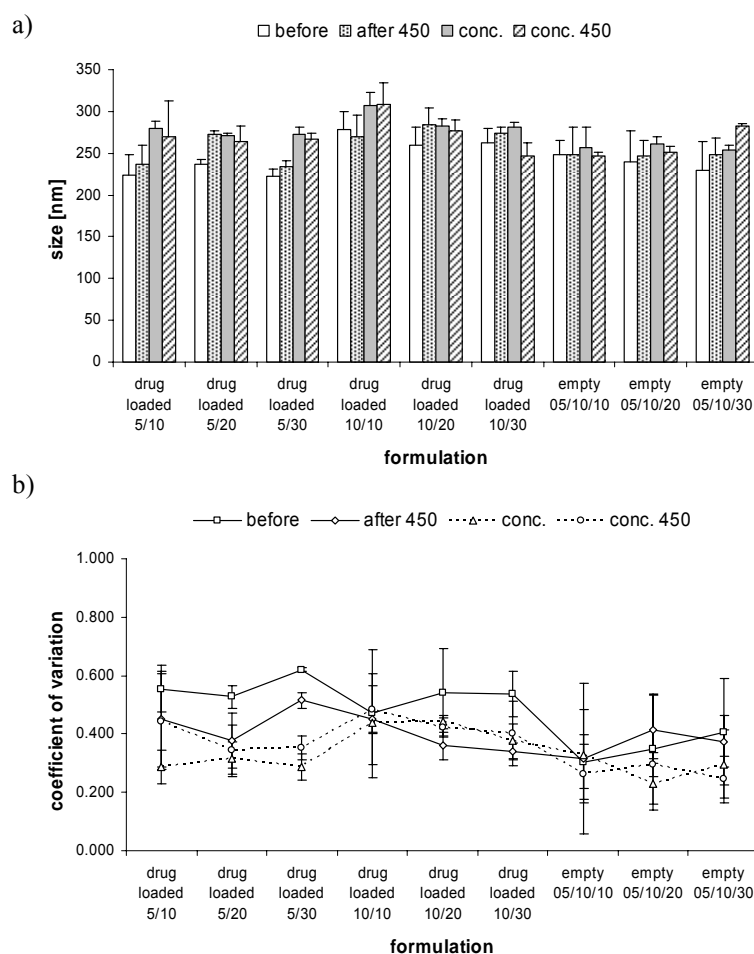


Figure 2.3.4 a) size and b) coefficient of variation of ds NF- κ B decoy ODN-loaded (5 % and 10 % [w/w]) (“5/X” and “10/X”) and empty (“5/10/X”) gelatin nanoparticles (GNPCO_{4, pos}) formulated with sucrose before freeze-drying and rehydrated in the original volume (“after 450”) and in 1/10th, 1/20th, and 1/30th (“X/10”, “X/20”, and “X/30”) of the original volume (“conc.” / “conc. 450”) right after freeze-drying

Regarding the concentrated samples, the same tendency can be observed, whereas reduced particle sizes have to be stated for certain formulations at the same time. However, sizes determined before and after freeze-drying only varied within a small range and with respect to the margins of deviation no significant differences can be attributed to the investigated drug loading amounts and/or the chosen rehydration volume. Taking in addition the respective coefficient of variation into consideration it can be assumed that the concept of concentrating oligonucleotide-loaded gelatin nanoparticles by freeze-drying is feasible. Experiments conducted with siRNA loaded gelatin nanoparticles basically confirmed the findings discussed above (Figure 2.3.5). Except nanoparticles loaded with 10 % (w/w) oligonucleotide, they initially exhibited high coefficients of variation but also clearly reduced particle sizes of formulation 10/10 and 10/30.

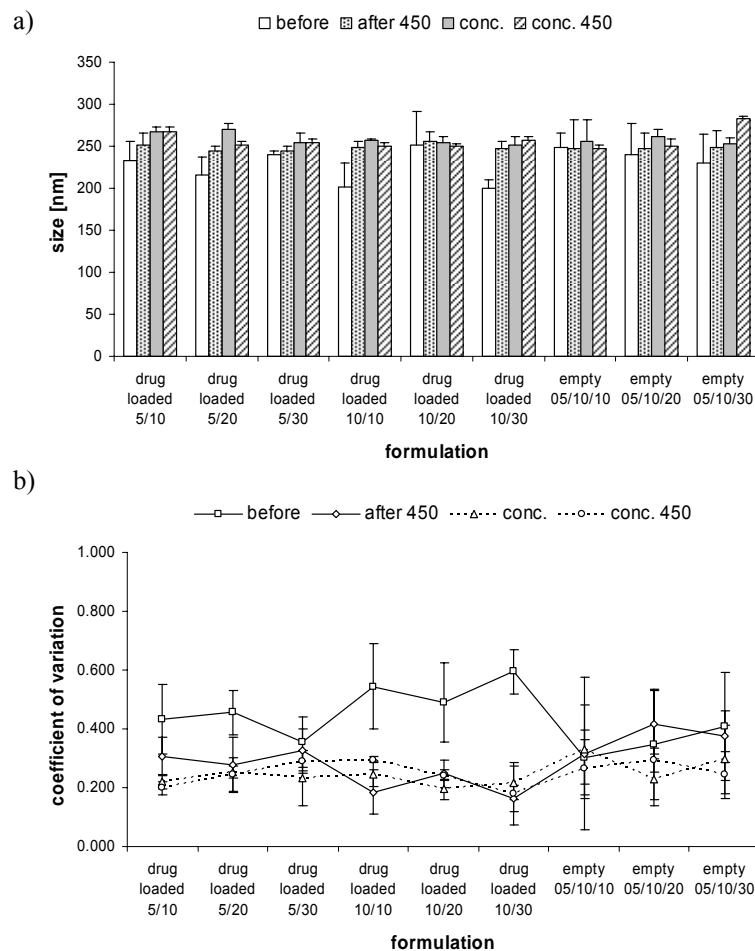


Figure 2.3.5 a) size and b) coefficient of variation of ds siRNA ODN-loaded (5 % and 10 % [w/w]) (“5/X” and “10/X”) and empty (“5/10/X”) gelatin nanoparticles (GNPCO_{4, pos}) formulated with sucrose before freeze-drying and rehydrated in the original volume (“after 450”) and in 1/10th, 1/20th, and 1/30th (“X/10”, “X/20”, and “X/30”) of the original volume (“conc.” / “conc. 450”) right after freeze-drying

If sample aggregation would have been occurred during siRNA loading increased particles sizes would have to be expected. As those were not detectable and as the after freeze-drying measured particle sizes only slightly vary for all formulations, a corrupted sample quality is not likely. These data additionally demonstrate the independence of the outcome of the freeze-drying process from the surface charge i.e., zeta potential of gelatin nanoparticles. Experiments conducted with plain nanoparticles exhibiting a slightly negative zeta potential, ODN-loaded, surface modified nanoparticles exhibiting a slightly positive zeta potential, and empty surface modified nanoparticles exhibiting a clear positive zeta potential all maintained size and equal size distribution properties after freeze-drying and rehydration.

Concurrently with the reduction of the rehydration volume the amount of sucrose required to provide isotonic solutions upon rehydration decreases. Thus, formulations designated to rehydration in $1/30^{\text{th}}$ of the original volume contain only little sucrose i.e., total solid causing flimsy cakes. Substituting sucrose partially or in total by a lyoprotectant of higher molecular weight and with reduced osmotic activity like dextran 3000 could be an approach to improve cake morphology and was therefore investigated in the following. Figure 2.3.6 shows the data of empty nanoparticles formulated with dextran 3000 / sucrose blends (containing 10.0 % / 4.0 %, 11.1 % / 3.3 %, 13.9 % / 1.7 %, and 16.7 % / 0.0 % dextran 3000 and sucrose respectively for both rehydration volumes: $1/20^{\text{th}}$ and $1/30^{\text{th}}$ of the original volume) which are characterized by increased excipient masses building stronger cakes but still providing isotonic solutions upon rehydration with reduced volumes. The resulting data set with slightly increased particle sizes and almost constant size distribution is in accordance with what has been described so far. Interestingly, both formulations merely containing dextran 3000, No. 79 and No. 118, are able to stabilize gelatin nanoparticles at their own, which confirms the findings of Anchordoquy who observed dextran 3000 to be an effective stabilizer for concentrated nanoparticulate PEI/DNA complexes [Anchordoquy et al., 2005].

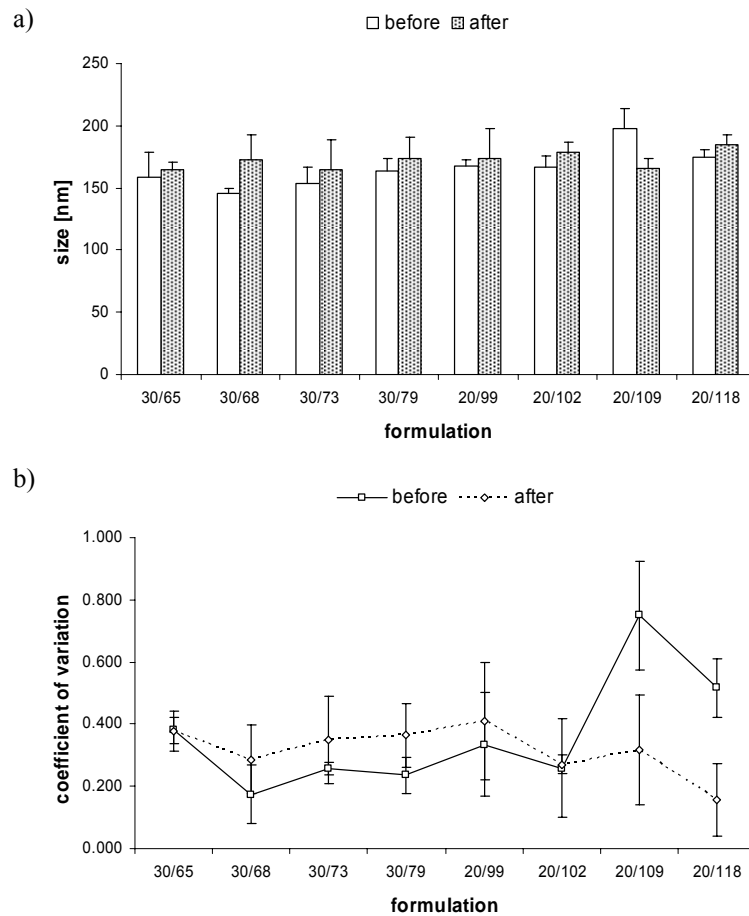


Figure 2.3.6 a) size and b) coefficient of variation of empty gelatin nanoparticles (GNPCO5) formulated with dextran + sucrose containing solutions accounting for varying excipient to ODN ratios (“X/65”-“X/118”) before freeze-drying and rehydrated in 1/30th and 1/20th of the original volume (“30/X” and “20/X”) right after freeze-drying

In sum the results of this first part not only show the general applicability of freeze-drying for gelatin nanoparticle suspensions but also the durability of gelatin nanoparticle populations throughout the process expressed by the good results obtained for different excipient to ODN / gelatin nanoparticle ratios, ODN-loaded gelatin nanoparticles, concentrated formulations, and the application of dextran 3000 / sucrose blends.

Derived from the concentration experiments a formulation was developed to address the failure of NF- κ B decoy ODN-loaded gelatin nanoparticles during the hepatic ischemia reperfusion studies (cp. chapter 3.4). A sucrose to ODN ratio of 200 i.e., formulation 200 was chosen for freeze-drying of 10 % oligonucleotide-loaded gelatin nanoparticles to guarantee best possible stabilization and to enable at the same time rehydration to reduced isotonic volumes. Compared to former studies that utilized 5 % [w/w] oligonucleotide loading, which is the maximum amount

achievable under the ionic conditions of a PBS buffered environment the loading could be doubled to 10 % [w/w] while conducting it in sucrose solution. With the resulting sucrose amount an isotonic nanoparticle suspension was obtained after rehydration in 141.5 μ L highly purified water, originating from an original volume of 1 mL i.e., a concentration by factor 7. Four of these samples were unified, completed with isotonic sucrose solution (10 % [w/v]) to a total volume of 1 mL and applied in the hepatic I/R rat model. Unification of four samples led to a four times increased amount of oligonucleotide deliverable at once, whereas the nanoparticle load per animal study was only doubled due to increased oligonucleotide loading. The addition to a total volume of 1 mL was accomplished for technical reasons and can be abandoned in case of lower volumes required e.g., in mice or in case of demanding higher concentrations of ODN-loaded nanoparticles, obtainable by unification of more than the described four samples.

But, upon exposure to blood plasma formulations were observed to aggregate immediately. This might be explained by the stabilizing repulsion, deriving from the positive surface charge of the ODN-loaded gelatin nanoparticles maintained in sucrose solution that is compensated after changing the environmental conditions towards an ionic milieu like blood plasma with its elevated ionic strength. Thus, further stabilization became crucial. Goetting reported similar results for oligonucleotide-loading of cationic polystyrene nanoparticles. To overcome this problem they successfully demonstrated a surfactant coating with poloxamer 388 that stabilized the ODN-loaded nanoparticles against aggregation [Goetting et al., 1999]. In accordance, we could proof our formulation to be macroscopically stable within blood plasma after incubating ODN-loaded nanoparticles for 1 h with Tween[®] 80. The Tween[®] 80 coating of the nanoparticles was conducted in a 1:1 [w/w] Tween[®] 80:nanoparticle ratio subsequent to rehydration and combination of four samples and before completion to the final volume. The resulting Tween[®] 80 concentration of 0.28 % is considerably high but still clearly below the highest amount of 10 % contained in already FDA-approved drugs for intravenous injection (source: FDA Inactive Ingredients Database of inactive ingredients present in FDA-approved drugs; <http://www.accessdata.fda.gov/scripts/cder/iig/index.cfm>). The according results obtained from animal studies are discussed in detail in chapter 3.4. In the second part storage stability and further freeze-drying excipients are evaluated

for empty and oligonucleotide-loaded gelatin nanoparticles. Furthermore, the maintained biological activity of the NF- κ B decoy oligonucleotide loaded onto gelatin nanoparticles was investigated after storage.

2.3.2 Storage stability tests of freeze-dried empty and oligonucleotide-loaded gelatin nanoparticles

Four different excipient systems were chosen to evaluate their stabilizing capacity for gelatin nanoparticles: sucrose (S), trehalose (T), mannitol (M), and the combination of mannitol and sucrose in the ratio 4:1 (MS); whereas the later combines the good bulking properties of mannitol with the lyoprotection of sucrose as it is reported for protein stabilization [Johnson et al., 2002]. Trehalose was chosen as it is one of the most widely used freeze-drying excipients for biomaterials [Crowe et al., 1996] and is stated to be supposedly superior to sucrose due to its high T_g and temperature of “zero” mobility (T_0) respectively [Yu, 2001]. Mannitol readily crystallizes during freeze-drying and possesses no lyoprotectant activity beneficial in terms of protein stabilization in the crystalline state [Cavatur et al., 2002]. Mannitol lyophilizates were therefore investigated in comparison to amorphous sucrose and trehalose cakes to evaluate whether crystalline structures negatively affect gelatin nanoparticle stabilization during freeze-drying. Based on the initially applied freeze-drying cycle a shortened cycle was developed (Figure 2.2.2). With respect to the vapor pressure curve above ice the applied vacuum of 0.05 mbar maintained a product temperature of $-48\text{ }^\circ\text{C}$ during primary drying. Thus, sucrose and trehalose, exhibiting a T_g' around $-30\text{ }^\circ\text{C}$ [Wang, 2000; Liu, 2006], and mannitol-sucrose (in the ratio of 4:1) containing formulations, exhibiting a T_g' of $-41.8\text{ }^\circ\text{C}$ [Hawe, 2006] could be effectively dried during the same run using this cycle. Mannitol samples could be dried at a higher primary drying shelf temperature of $-5\text{ }^\circ\text{C}$ (Figure 2.2.3) due to the high melting point known for its ice eutectic mixture of $-1.5\text{ }^\circ\text{C}$ [Kim et al., 1998].

Empty nanoparticles were investigated in five formulations: 47, 100, 200, 400, and 800, at the same time only formulation 200 was prepared from ds NF- κ B oligonucleotide-loaded (5 % [w/w]) gelatin nanoparticles. Formulation 47 was already assessed during experiments discussed above and possesses a sucrose amount necessary for isotonic rehydration in $1/30^{\text{th}}$ of the original volume. It was investigated to evaluate the lower limit of the system. Size, size distribution, residual moisture, and thermal properties of empty nanoparticle formulations were as well investigated as size, size distribution, and biological activity of the ds NF- κ B decoy

oligonucleotide-loaded gelatin nanoparticles. Accelerated storage conditions for closed samples (30 °C and 40 °C) and open samples (30 °C / 30 % RH and 30 °C / 60 % RH) were chosen in terms of short term stress testing over a period of 4 and 10 weeks respectively. Studies were conducted in comparison to placebo formulations. All samples were prepared and measured in triplicates except DSC scans which were accomplished in duplicates. Thus, data are presented as mean values with respective standard deviation (stdv). Besides displaying selected data for discussion all values measured for particle size and size distribution, residual moisture, and thermal properties are tabular summarized in the annex of this chapter. Due to the large number of samples required and the limited batch size of gelatin nanoparticles that is obtained from two step desolvation four nanoparticle batches, all exhibiting similar sizes, were utilized for sample preparation. To enable *intra*-excipient comparability of particle sizes one of the four batches was used for all formulations manufactured of sucrose, one for trehalose, one for mannitol, and one for mannitol-sucrose formulations respectively. Determining polydispersity indices allowed evaluation of *intra*- and *inter*-excipient data in terms of size distribution quality and was chosen for explaining stability data. Residual moisture and thermal properties are in any case comparable as they are almost excipient governed and thus independent from particular nanoparticle batches.

Empty gelatin nanoparticles

Particle sizing Data from all prepared gelatin nanoparticle formulations measured before and right after freeze-drying are summarized in Table 2.3.3. For all formulations PDIs below 0.100 were determined prior to freeze-drying reflecting the very good quality of all samples applied for storage stability testing. Freeze-drying of formulations 100 to 800 showed the same outcome as it was already observed during initial applicability studies (Figure 2.3.1), exhibiting slightly reduced particle sizes and maintained sample quality with PDIs still below 0.100. Formulation 47 in turn shows increased PDIs for all freeze-drying excipients. Sucrose and trehalose formulations showed both, increased particle sizes and PDIs, whereas the latter were still acceptable but ranged above 0.100. The highest PDI can be seen for the mannitol-sucrose formulation, remarkably with a decreased particle size at the same

time. Interestingly, only mannitol provides sufficient stabilization resulting in a PDI below 0.100, but also this value has already increased upon freeze-drying.

Table 2.3.3 Size and polydispersity indices of empty gelatin nanoparticles before freeze-drying and rehydrated right after freeze-drying

Formulation	Size [nm]					PDI			
	Before		After		Before		After		
	Mean	Stdv	Mean	Stdv	Mean	Stdv	Mean	Stdv	
Sucrose	47	177.0	2.0	183.7	1.2	0.041	0.016	0.117	0.011
	100	177.0	1.0	174.3	1.2	0.073	0.014	0.048	0.006
	200	176.0	1.0	171.3	1.2	0.050	0.005	0.046	0.006
	400	176.0	1.0	171.7	1.5	0.059	0.016	0.051	0.011
	800	179.0	1.7	171.0	1.0	0.092	0.012	0.035	0.005
Trehalose	47	179.0	1.7	182.0	1.7	0.066	0.019	0.114	0.028
	100	177.0	1.0	172.0	1.0	0.054	0.009	0.055	0.008
	200	177.0	1.0	171.7	0.6	0.051	0.013	0.039	0.009
	400	177.3	0.6	170.3	2.5	0.062	0.002	0.051	0.012
	800	178.3	0.6	172.0	1.0	0.059	0.017	0.061	0.011
Mannitol	47	175.3	0.6	175.7	1.5	0.039	0.008	0.082	0.008
	100	175.3	1.5	170.0	1.7	0.059	0.002	0.082	0.012
	200	173.7	1.2	170.0	1.0	0.063	0.014	0.065	0.011
	400	174.3	2.1	169.7	2.1	0.054	0.006	0.047	0.025
	800	175.0	1.0	174.3	6.8	0.068	0.011	0.051	0.005
Man-Suc	47	208.0	8.7	198.0	1.7	0.085	0.024	0.123	0.019
	100	210.3	2.1	188.0	1.0	0.094	0.006	0.075	0.013
	200	210.0	1.0	187.3	2.5	0.076	0.019	0.069	0.022
	400	203.7	7.6	186.7	1.5	0.080	0.006	0.072	0.009
	800	210.3	0.6	187.3	1.5	0.077	0.016	0.062	0.007

Due to the different nature of the respective lyophilizates it can be assumed that vitrification is not exclusively crucial for the stabilization of gelatin nanoparticles. Even in crystalline (cp. DSC data stated below) mannitol formulations, known to inadequately stabilize most proteins in the dried solid, nanoparticle integrity is preserved. Allison formulated the particle isolation hypothesis to explain these findings [Allison et al., 2000]. Along their hypothesis aggregation of non viral vectors during freezing is prevented by virtually any excipient applied in sufficient amounts by a spatial separation of particles within the unfrozen fraction.

Different storage times and conditions reinforce *intra*- and *inter*-excipient differentiation. Figure 2.3.7 and Figure 2.3.8 show the changes in the quality of the samples indicated by increasing polydispersity occurring after 4 and 10 weeks of closed storage at 30 °C and 40 °C.

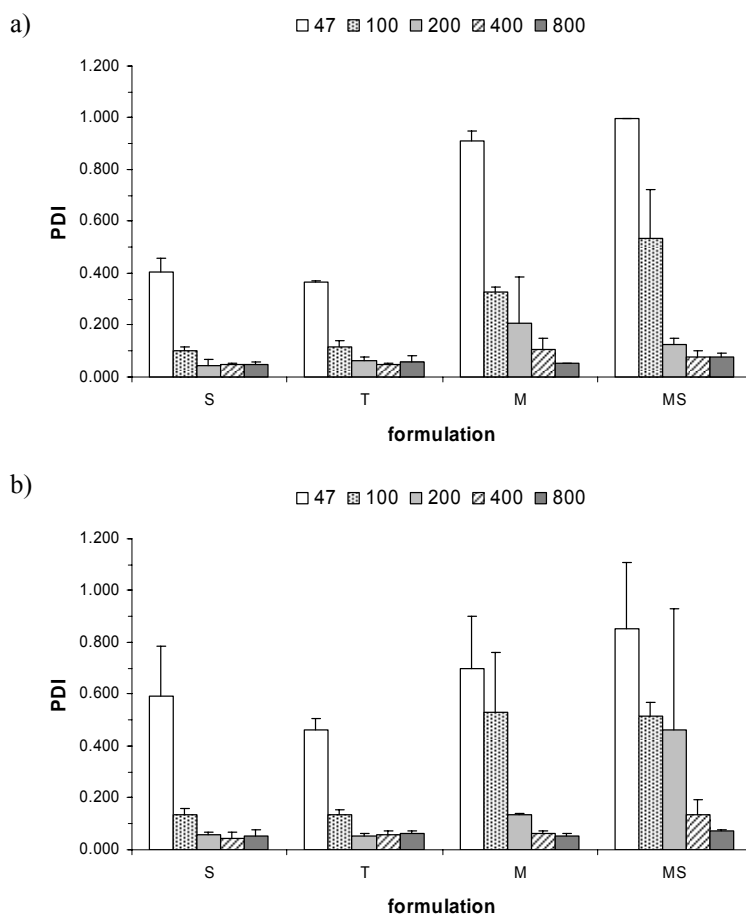


Figure 2.3.7 Polydispersity indices of freeze-dried gelatin nanoparticles rehydrated after a) 4 weeks and b) 10 weeks closed storage at 30 °C

In none of the investigated samples formulation 47 is able to provide sufficient stabilization. With increasing excipient amounts stabilizing properties are improving. Looking at the results after 10 weeks storage at 40 °C (Figure 2.3.8 b) the tendencies already seen after 10 weeks storage at 30 °C (Figure 2.3.7 b) are further pronounced. Only the formulations 400 and 800 containing the highest excipient amounts maintained the nanoparticle quality. The lyoprotectant activity of sucrose, trehalose, and mannitol can be thereby stated as equivalent. Mannitol-sucrose formulations in turn failed to sufficiently stabilize gelatin nanoparticles in all investigated formulations despite combining two excipients both with good stabilizing properties at their own.

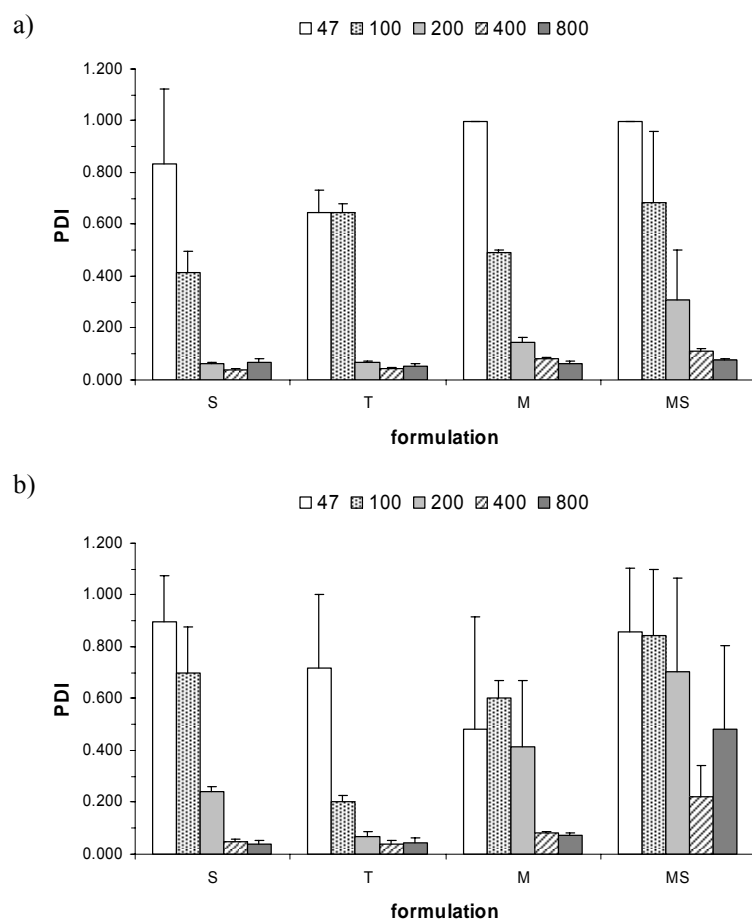


Figure 2.3.8 Polydispersity indices of freeze-dried gelatin nanoparticles rehydrated after a) 4 weeks and b) 10 weeks closed storage at 40 °C

Storage under open conditions at accelerated relative humidity led to nearly entire sample loss, which is almost completed already after 4 weeks (Figure 2.3.9 a and Figure 2.3.10 a). At 30 % RH trehalose formulations 400 and 800 notably reveal good stabilization after 10 weeks though they were already destroyed after 4 weeks. This indicates that the stabilization properties of trehalose under these conditions can not be assumed as undoubtful. Basically, only mannitol formulation 800 withstands the high relative humidity of 30 % and provides certain stabilization. The differences for sucrose and trehalose formulations between closed and open storage (Figure 2.3.7 b and Figure 2.3.9 b) are thereby much more pronounced than for mannitol-sucrose formulations presumably reflecting the low hygroscopicity of mannitol in the crystalline state.

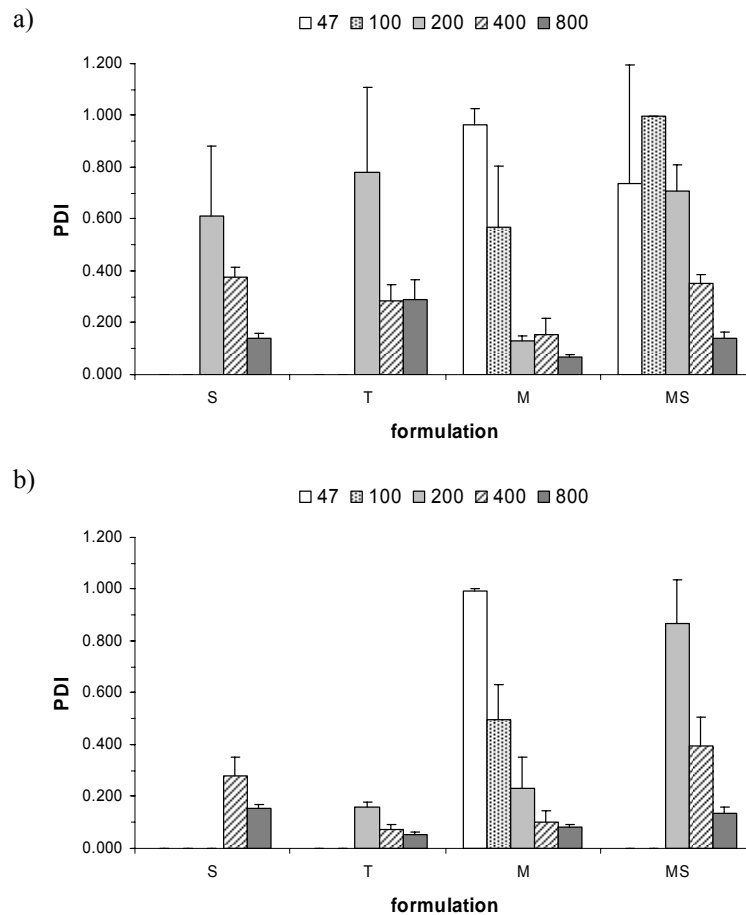


Figure 2.3.9 Polydispersity indices of freeze-dried gelatin nanoparticles rehydrated after a) 4 weeks and b) 10 weeks open storage at 30 °C / 30 % RH

None of the samples were recovered with acceptable sizes or size distribution, neither after 4 weeks nor after 10 weeks storage at 30 °C / 60 % RH. Missing bars in Figure 2.3.9 and Figure 2.3.10 thereby reflect complete sample destruction.

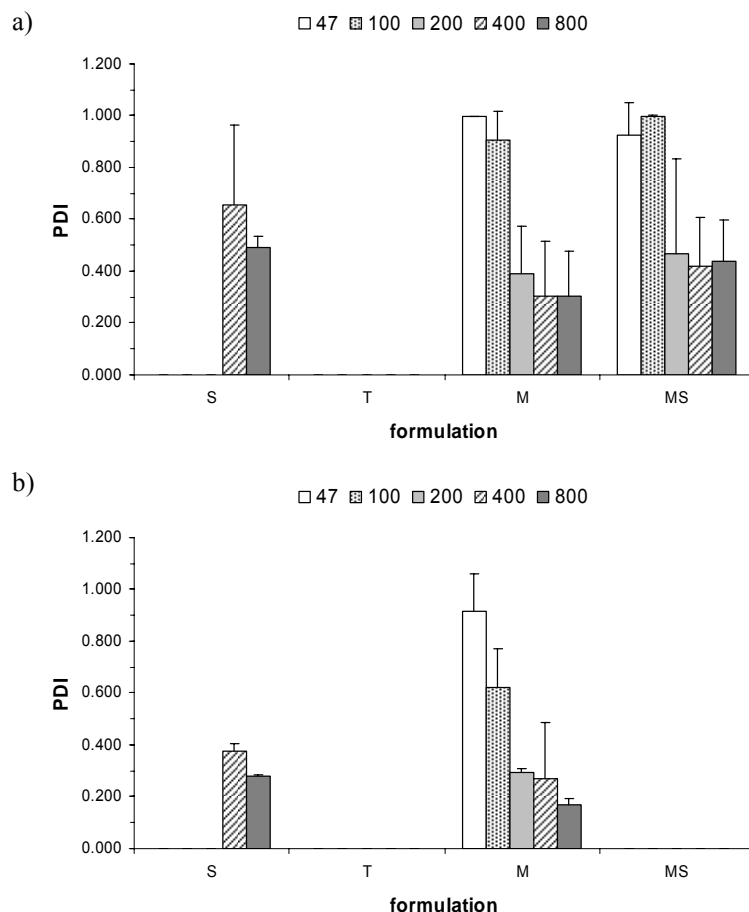


Figure 2.3.10 Polydispersity indices of freeze-dried gelatin nanoparticles rehydrated after a) 4 weeks and b) 10 weeks open storage at 30 °C / 60 % RH

Determination of residual moisture contents Analyzing Karl-Fischer titration data elucidates the findings from particle sizing. According to Shalaev and Zografis increasing water contents contribute to accelerated chemical degradation of small molecules and proteins especially in amorphous solids [Shalaev et al., 1996]. As they expect this to be related to changed molecular mobility it can be assumed that increasing water contents negatively influence nanoparticle stability based on the same mechanism. Thereby, chemical degradation presumably plays a minor role compared to particle aggregation. Derived from particle isolation hypothesis discussed above and the considerations of Shalaev and Zografis an increased molecular mobility may diminish the spatial separation of nanoparticles finally leading to their aggregation when getting once into direct contact.

In the following residual moisture is exemplarily displayed for all formulations after closed storage at 30 °C and for sucrose and trehalose formulations after open storage at 30 °C / 60 % RH. In addition trehalose verum and placebo formulations are compared after closed storage at 30 °C. Complete data sets for all formulations and storage conditions are presented in tables summarized in the annex of this chapter.

Residual moisture was initially determined to be below 1 % except sucrose formulation 47 (Figure 2.3.11 a) and mannitol formulation 200 (Figure 2.3.12 a). Upon 4 weeks closed storage comparable amounts of water were absorbed by sucrose and trehalose formulations, whereas the latter were determined to be slightly more hygroscopic (Figure 2.3.11).

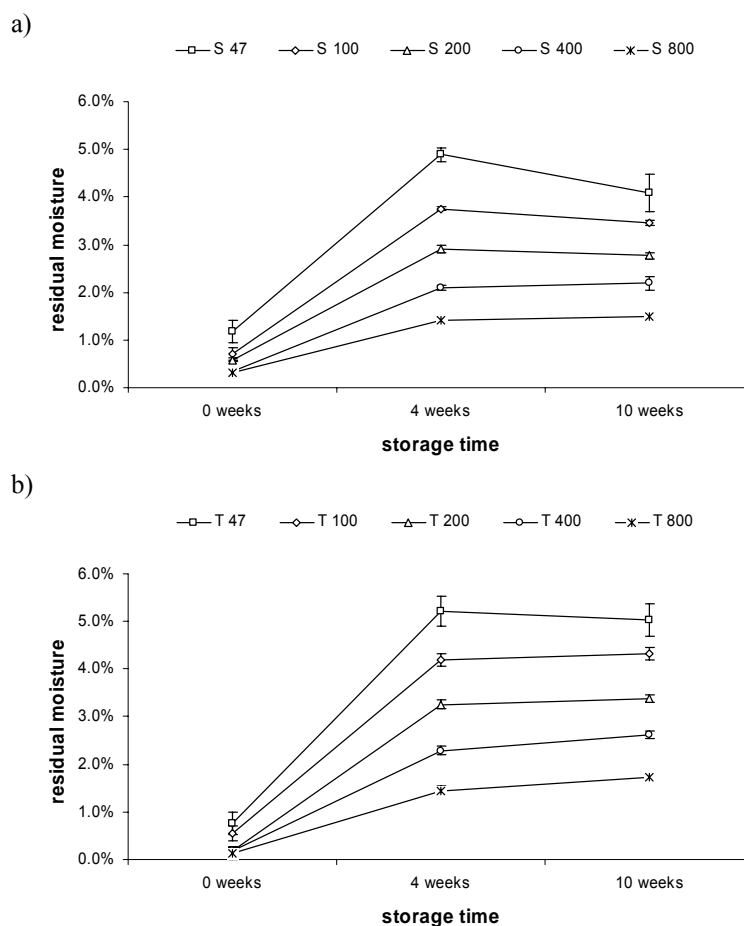


Figure 2.3.11 Residual moisture content of freeze-dried gelatin nanoparticle formulations containing a) sucrose and b) trehalose right after the drying process and after 4 and 10 weeks closed storage at 30 °C

Mannitol and mannitol-sucrose formulations adsorbed clearly less water (Figure 2.3.12). Pure mannitol formulations were almost inert against water sorption and

especially formulations 400 and 800 still possessed residual moisture contents below 1% . These findings are confirmed by Fakes who systematically investigated the sorption behavior of bulking agents used in lyophilized products [Fakes et al., 2000]. Residual moisture contents of mannitol-sucrose formulations ranged between pure sucrose and mannitol formulations as it could be expected.

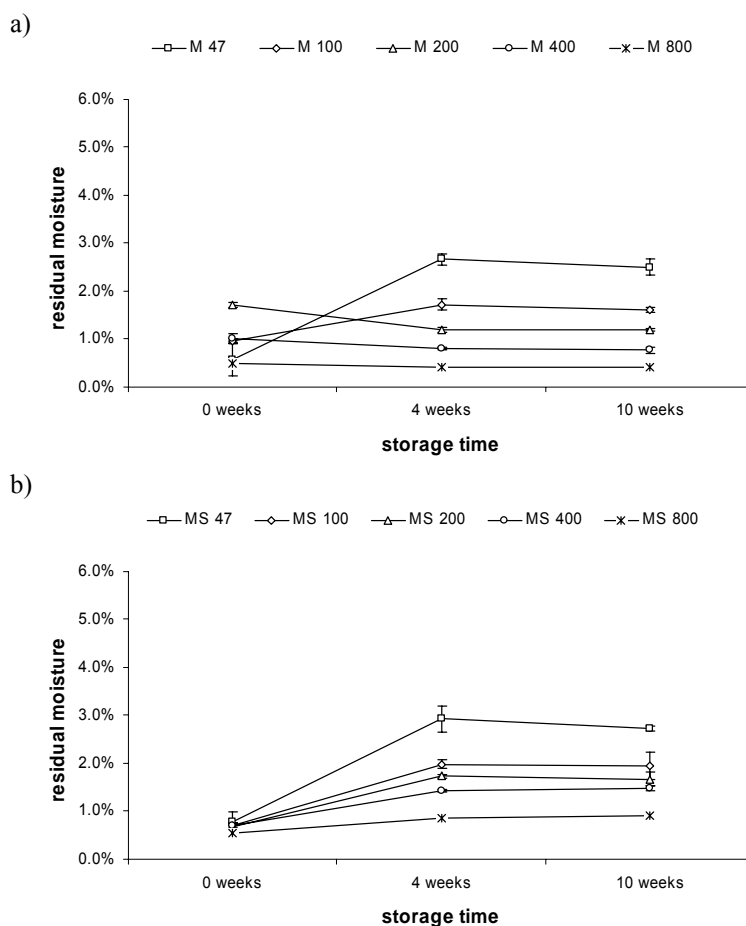


Figure 2.3.12 Residual moisture content of freeze-dried gelatin nanoparticle formulations containing a) mannitol and b) mannitol-sucrose right after the drying process and after 4 and 10 weeks closed storage at 30 °C

During closed storage at 30 °C and 40 °C comparable sorption of water occurred. Further increased amounts were absorbed during open storage at 30 °C / 30 % RH, which were additionally raised at 30 °C / 60 % RH (Annex: Table 2.6.7 and Table 2.6.9). Independent from the investigated excipient formulations 47, 100, and 200 in general exhibited stronger hygroscopicity than the formulations with higher excipient amounts 400 and 800. In sum, highest values were obtained for trehalose followed by sucrose, mannitol-sucrose, and mannitol; only after storage at 30 °C / 60 % RH sucrose adsorbed most water.

Residual moisture data gained after 10 weeks storage revealed no further progression of water sorption compared to 4 weeks storage (Figure 2.3.11 and Figure 2.3.12, Annex: Table 2.6.7 and Table 2.6.9). Mere formulations containing sucrose and trehalose openly stored at 30 °C / 60 % RH absorbed additional water (Figure 2.3.13). Related to particle sizing data it can be stated that the amount of initially absorbed water already present after 4 weeks was enough to enable continued sample destruction monitored after 10 weeks (Figures 2.3.7 to 2.3.10).

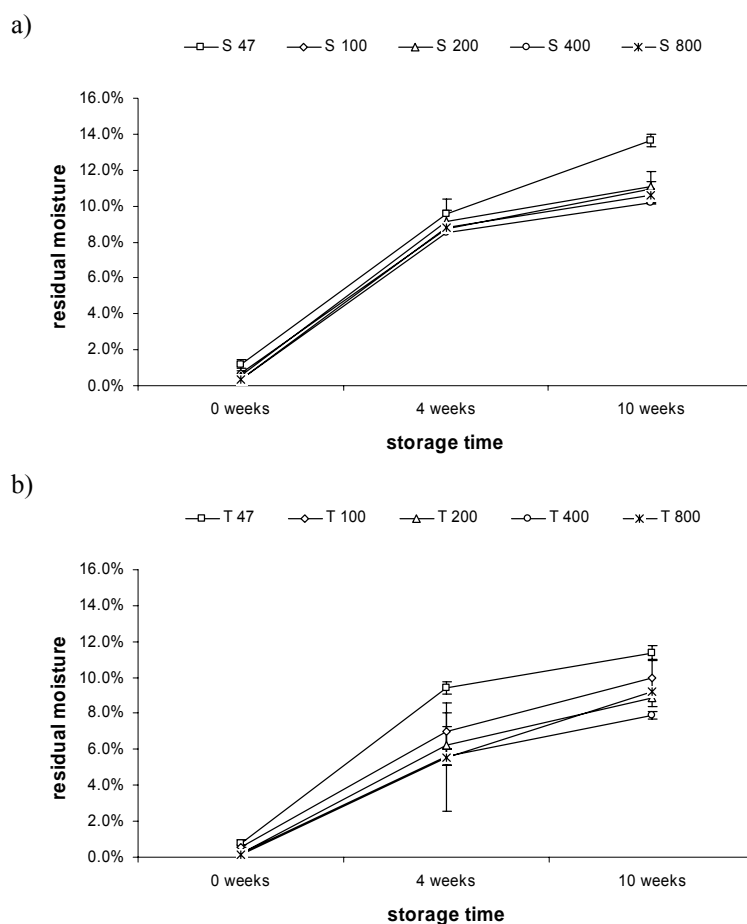


Figure 2.3.13 Residual moisture content of freeze-dried gelatin nanoparticle formulations containing a) sucrose and b) trehalose right after the drying process and after 4 and 10 weeks open storage at 30 °C / 60 % RH

Correlating residual moisture contents and particle sizing data it can in fact be proven for sucrose and trehalose formulations that with increasing water contents increasing nanoparticle aggregation can be followed above an observed threshold of about 3 % water content. For crystalline mannitol formulations a comparable threshold can not be defined as also at minimal water contents below 0.5 % obtained for formulation 800 particle aggregation occurred upon open storage at

30 °C / 60 % RH. Thus, with respect to the particle isolation hypothesis the contribution of vitrification to nanoparticle stabilizing during freeze-drying is not negligible as the glassy structure of sucrose and trehalose seems to be superior in preventing nanoparticle aggregation even at higher residual moisture contents. Mannitol-sucrose formulations obviously suffer from their blended nature. Despite smaller residual moisture values the stabilizing properties of sucrose under closed conditions were not reached, and stored at 30 °C / 30 % RH the beneficial properties of pure mannitol formulations with a PDI still below 0.100 for formulation 800 could not be verified.

The influence of the gelatin nanoparticles themselves on the sorption of water during storage was evaluated by comparing results with placebo data. Interestingly, the obtained values were within the same range for both verum and placebo formulations, why results are only exemplarily shown for closed storage of trehalose formulations at 30 °C in Figure 2.3.14.

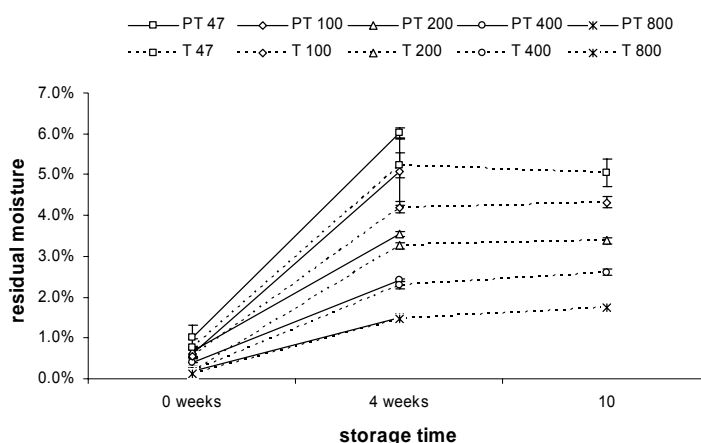


Figure 2.3.14 Residual moisture content of freeze-dried gelatin nanoparticle and placebo formulations containing trehalose right after the drying process and after 4 and 10 weeks closed storage at 30 °C

The placebo control study was terminated after 4 weeks as there were already comparable water contents determined for placebo and verum samples. This was, with respect to verum data being almost unchanged after 10 weeks, expected to be the same for placebo data after 10 weeks.

Differential scanning calorimetry All samples were investigated for their T_g and their melting point (mp) respectively. Due to different thermal properties of the respective freeze-drying excipients results are discussed in distinct sections in the following. In addition to samples available for particle sizing and Karl-Fischer titration there was a set of verum samples stored for 4 weeks at room temperature that was analyzed via DSC. These samples were available due to technical problems with the DSC instrument causing a delay of 4 weeks in exploring samples actually prepared for analysis right after freeze drying. Data right after freeze-drying were then collected from newly prepared samples with the same nanoparticle batches.

Glass transition temperatures monitored for **sucrose** clearly reflect findings from residual moisture content testing. According to Hancock and Zografi there is a clear relation between glass transition temperature and the water content of amorphous pharmaceutical solids [Hancock et al., 1994]. They described a rapid initial reduction of T_g as water is absorbed. This can be followed for sucrose samples (Figure 2.3.15) and is confirmed by literature [Hancock et al., 1994]. As similar water contents were absorbed, all formulations showed a comparable reduction of their glass transition temperatures, which can be recognized at a parallel shift of the respective curves obtained after 4 weeks storage at 30 °C and 40 °C (Figure 2.3.15 a and b). Even samples stored at 20 °C showed depression of T_g s which was stronger pronounced for samples with lower excipient contents (Figure 2.3.15 c). Especially formulation 47 reached values of ~30 °C as well seen for storage at 30 °C and 40 °C. Invariably all samples stored at open conditions with accelerated relative humidity collapsed to rigorous chunks sticking at the bottom of the vials and were thus not applicable for DSC analysis. During closed storage at 40 °C collapse occurred for sucrose containing formulations 100 and 200 after 4 weeks and formulations 100, 200, and 400 after 10 weeks. In accordance to Karl-Fischer data there were no significant differences detectable between data obtained after 4 and 10 weeks; almost unchanged water contents led to equivalent T_g s (Figure 2.3.15 a and b). The same can be stated for verum and placebo data, thus only summarized in Table 2.6.10 and Table 2.6.11 of the Annex. Furthermore, starting values are characterized by T_g s concomitantly decreasing with the excipient amount. Taking the known inverse relation between T_g and residual moisture content discussed above and the corresponding residual moisture curve (Figure 2.3.11 a), which demonstrated increased relative water

contents coming along with declined excipient to nanoparticle ratios, into account, this could be expected to a certain extent.

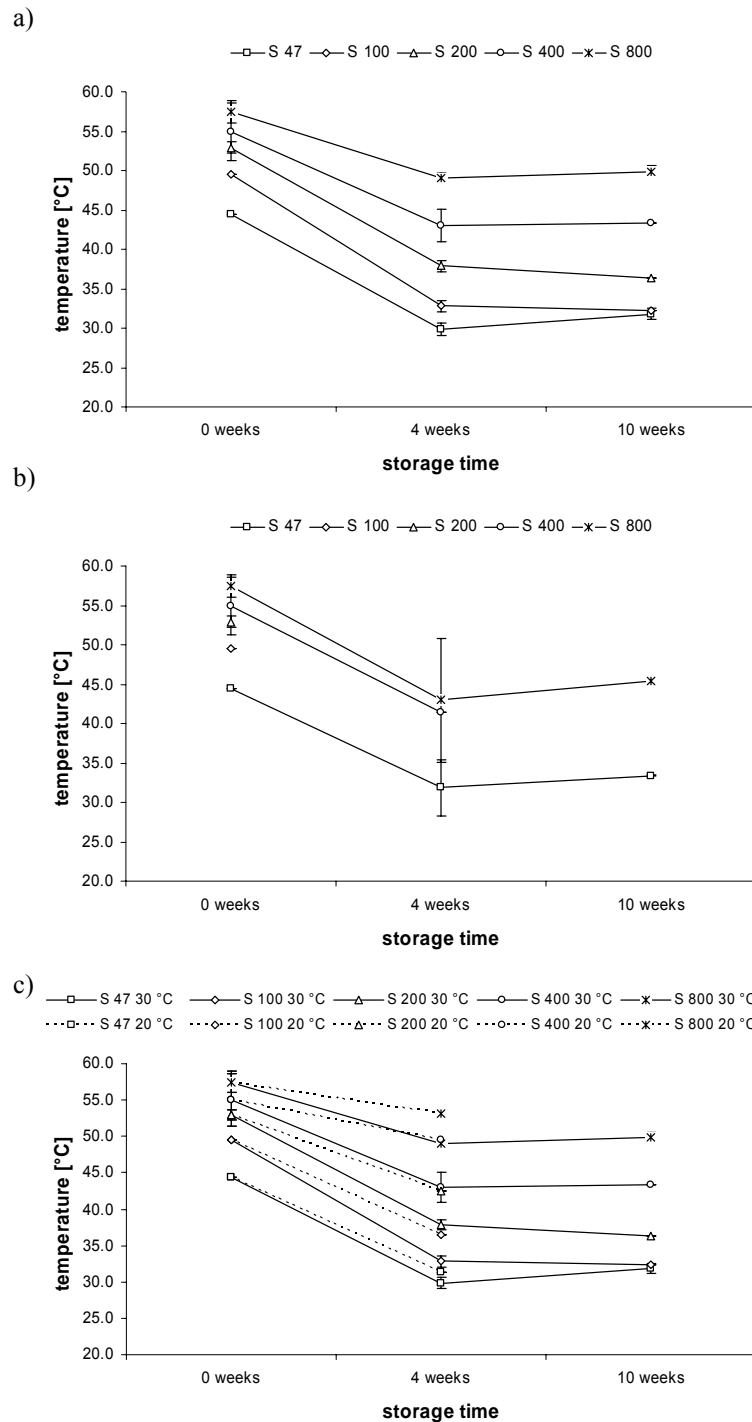


Figure 2.3.15 T_g (point of inflection) of sucrose containing freeze-dried gelatin nanoparticle formulations a) right after freeze-drying and after 4 and 10 weeks closed storage at 30 °C, b) right after freeze-drying and after 4 and 10 weeks closed storage at 40 °C, and c) right after freeze-drying and after 4 and 10 weeks closed storage at 30 °C in comparison to 4 weeks storage at 20 °C

But with respect to the small differences in water contents determined right after freeze-drying the clear response in T_g variation was not assumed. As this phenomenon was also observed for the melting point of mannitol containing formulations (Figure 2.3.17 and Figure 2.3.18), which should be independent from residual moisture content, and as placebo studies ruled out these strong variations possibly driven by gelatin nanoparticles themselves a sample mass dependent mechanism is likely to be assumed as reason for these findings. Due to the aim of the study to develop a freeze-dried oligonucleotide-loaded gelatin nanoparticle formulation the amount of nanoparticles per sample was given and the ratio of excipient to ODN / nanoparticles was varied. This in turn led to varying total solid contents varying from 1.4 mg per vial up to 17 mg per vial. As the optimum sample weight for DSC analysis is stated with 3 mg, this amount was not reached for the smaller formulations and thus increasing masses were transferred into DSC pans.

Sample mass dependent shifts of glass transition temperatures and melting points determined by DSC are described in literature [Hoehne et al., 1989; Mano et al., 2004] and are confirmed by the manufacturer of the applied instrument (Netzsch-Geraetebau GmbH, Selb, Germany). This correlation of thermal events taking place at reduced temperatures and decreasing sample mass can be seen for all investigated samples and has thus to be taken into consideration in assessing storage stability properties of freeze-dried gelatin nanoparticle formulations. Nevertheless, the influence of residual moisture contents in terms of thermally inducible conversions can be easily followed by DSC data.

The DSC analysis of **trehalose** formulations in general revealed residual moisture and sample mass dependent alterations of the glass transition temperature of trehalose similar to those observed for sucrose formulations (Figure 2.3.16). The influence of the residual moisture content on the T_g of trehalose is basically confirmed by literature [Surana et al., 2004]. Upon closed storage for 4 weeks at 30 °C and 40 °C a comparable reduction of T_g s could be followed and the depression of T_g s monitored for 4 weeks closed storage at 20 °C, which was pronounced for samples with lower excipient contents, was confirmed. Open storage as well led to complete sample loss but in contrast to sucrose, trehalose was able to maintain sample integrity during closed storage at 40 °C as collapse did not occur. Again, in

accordance to Karl-Fischer data there were no significant differences detectable between data obtained after 4 and 10 weeks storage (Figure 2.3.16 a and b) as well as data obtained from verum and placebo samples (Annex: Table 2.6.12 and Table 2.6.13).

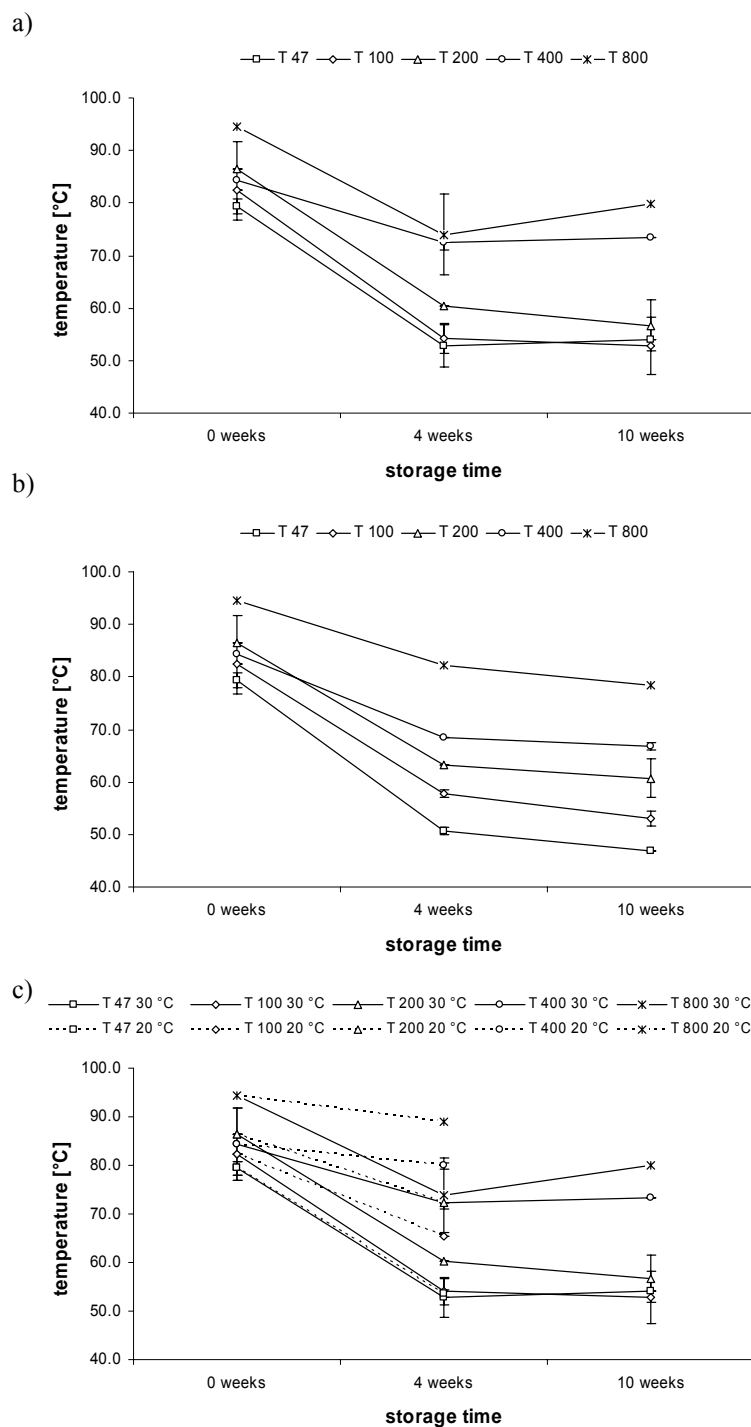


Figure 2.3.16 T_g (point of inflection) of trehalose containing freeze-dried gelatin nanoparticle formulations a) right after freeze-drying and after 4 and 10 weeks closed storage at 30 °C, b) right after freeze-drying and after 4 and 10 weeks closed storage at 40 °C, and c) right after freeze-drying and after 4 and 10 weeks closed storage at 30 °C in comparison to 4 weeks storage at 20 °C

Absolute numbers initially determined for the T_g s of gelatin nanoparticle formulations 800 containing **sucrose** or **trehalose** ranged with just under 60 °C or 94 °C respectively within values known from literature [Te Booy et al., 1992; Wang, 2000; Imamura et al., 2003] and were verified by placebo data (Annex: Table 2.6.11 and Table 2.6.13). In comparison T_g values determined during initial applicability studies in the first part of this chapter (Figure 2.3.2 b) ranged higher and did not show a sample mass dependent behavior. As these former investigations were accomplished using a Perkin-Elmer Diamond differential scanning calorimeter a different sensitivity of these two systems could presumably be the reason for this discrepancy.

In contrast to sucrose and trehalose formulations, **mannitol** formulations exhibited maintained thermal properties for verum and placebo formulations right after freeze-drying and over all tested storage conditions. Hence, just one part of mannitol data is exemplarily summarized in Figure 2.3.17. The melting point was constantly calculated around 164 °C for formulation 800 (Annex: Table 2.6.14 to Table 2.6.16) as described in literature for α and β modification of D-mannitol respectively [Burger et al., 2000]. No further exotherms or endotherms were detected during heating indicating the complete crystallization of mannitol in α or β modification and concomitantly the absence of mannitol hemihydrate or the δ polymorph of mannitol [Nunes et al., 2004].

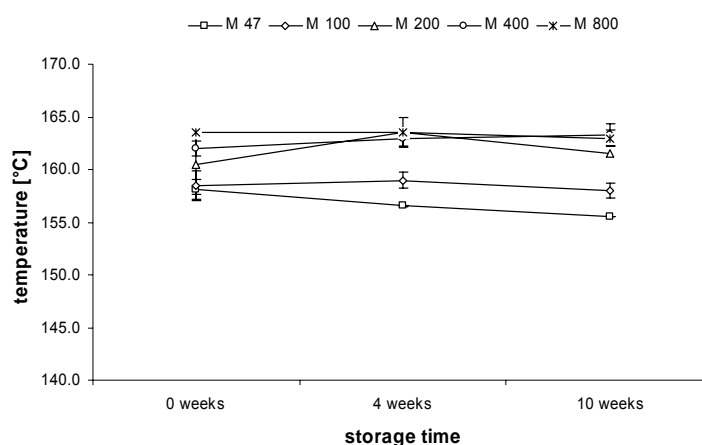


Figure 2.3.17 Melting point (peak) of mannitol containing freeze-dried gelatin nanoparticle formulations right after freeze-drying and after 4 and 10 weeks open storage at 30 °C / 30 % RH

The parallel shifted course of the resulting curves was related to sample mass effects as already discussed above, which lead to melting points decreasing with reduced mannitol to gelatin nanoparticle ratios.

Basically observations made for mannitol formulations correspond to those of **mannitol-sucrose** formulations. An unaffected melting point was obtained for all verum and placebo formulations regardless of storage time and conditions. Again the influence of the sample mass could be derived from respective data exemplarily displayed in Figure 2.3.18.

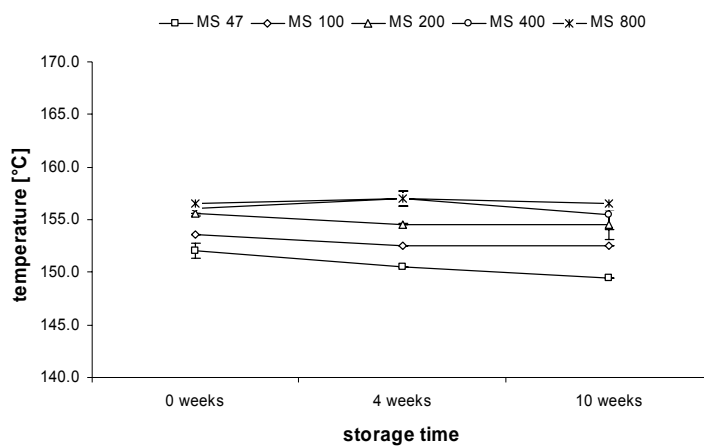


Figure 2.3.18 Melting point (peak) of mannitol-sucrose containing freeze-dried gelatin nanoparticle formulations right after freeze-drying and after 4 and 10 weeks open storage at 30 °C / 30 % RH

Compared to pure formulations the melting point of mannitol itself is reduced and was calculated around 156 °C for formulation 800 (Annex: Table 2.6.17 to Table 2.6.19). This reduced melting temperature may be addressed to the presence of sucrose potentially disturbing crystallization of mannitol. Telang reported a melting point depression of mannitol of 15 °C for the mixture with NaCl (10 % [w/w]) [Telang et al., 2003]. Complete crystallization of the second excipient sucrose can be thereby excluded. According to Johnson we observed an exotherm just before the melting endotherm of mannitol (Figure 2.3.19), which they attributed to crystallization of sucrose [Johnson et al., 2002]. The displayed crystallization signal seems to be as well mass dependent as it finally disappears with the decreasing sample mass from formulation 800 down to formulation 47. Furthermore, along the dashed line the proportionality of sample mass and melting point can be followed, with increasing sample mass the melting point further approaches this mark. In

addition, glass transition of sucrose could be determined for the formulations 200 - 800 (data not shown), whereas the signal intensity was only weak and the values ranged below 30 °C. As only 1/5th of the whole excipient amount was sucrose, it was assumed that the resulting low amount of sucrose was the reason for both.

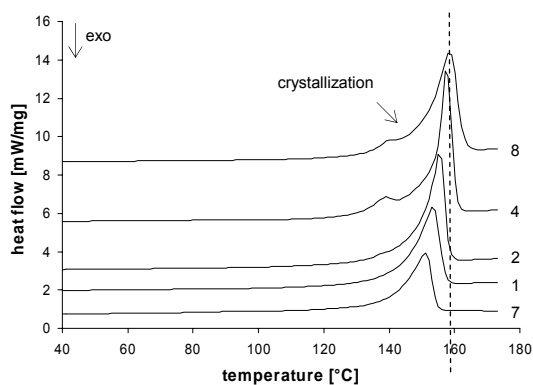


Figure 2.3.19 DSC (2nd) heating scans of mannitol-sucrose containing freeze-dried gelatin nanoparticle formulations 47 (7), 100 (1), 200 (2), 400 (4), and 800 (8) after 4 weeks closed storage at 40 °C

A reduced T_g for mannitol and sucrose containing lyophilizates is already described by Lueckel [Lueckel et al., 1998] and has to be taken into consideration in terms of microcollapse of sucrose within a mannitol matrix [Chatterjee et al., 2005] and its outcome for storage conditions and stability of lyophilized gelatin nanoparticles. Finally an assumption could be deduced from DSC scans that could explain the bad stabilizing properties of mannitol-sucrose containing formulations for gelatin nanoparticles identified during storage stability tests. Samples investigated right after freeze-drying clearly showed crystallization during the first DSC scan (Figure 2.3.20) indicating the presence of at least partially amorphous mannitol emerged during freeze-drying.

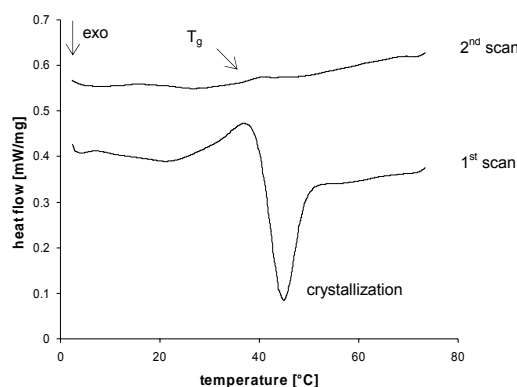


Figure 2.3.20 DSC heating scans of mannitol-sucrose containing freeze-dried gelatin nanoparticle formulation 47 right after freeze-drying

This can possibly be attributed to the presence of sucrose, generally recovered in its amorphous state upon freeze-drying. In contrast after cooling and reheating up to 180 °C the weak T_g of Sucrose, afore masked by the crystallization exotherm of mannitol, appeared (Figure 2.3.20, 2nd scan) and the melting of the α or β polymorph of mannitol respectively [Burger et al., 2000] could be followed. None of the samples analyzed after storage neither after 4 weeks nor after 10 weeks showed comparable thermograms. Taking additionally the low T_g of amorphous mannitol of 13.7 °C into consideration [Cavatur et al., 2002] it can be therefore concluded that mannitol crystallization occurred during storage at all storage conditions and led to the reported poor stability data of gelatin nanoparticles. Interestingly, the crystalline state at its own did not negatively affect storage stability as it is described above for pure mannitol formulations, but the conversion from the amorphous to the crystalline state obviously had a clear negative effect. Similar findings are described by Hawe, she could demonstrate the development of partial amorphous mannitol within lyophilized mixtures of mannitol and sucrose in the ratios 1:1 and 3:1, but not in the ratio 4:1 [Hawe, 2006]. Including an annealing step into the freeze-drying cycle fosters crystallization of mannitol and can be used to circumvent this problem [Hawe, 2006]. Concomitantly increasing amounts of mannitol hydrate which in turn may as well negatively affect storage stability due to the release of water can be prevented by conducting secondary drying at higher temperatures [Johnson et al., 2002].

The described observations were made for verum as well as placebo formulations, thus ruling out a direct correlation between gelatin nanoparticles and amorphous emerging mannitol during freeze-drying.

Oligonucleotide-loaded gelatin nanoparticles

Storage stability of oligonucleotide-loaded gelatin nanoparticles was investigated with the major emphasis laid on the assessment of maintained ODN function within an LPS (sepsis) rat model (cp. chapter 3.4). In addition, particle sizing data were gained to estimate the respective formulation's quality prior to animal studies. Besides, the influence of the oligonucleotide on the storage stability of gelatin nanoparticles could be evaluated based on PCS data. As four samples had to be combined for application *in vivo* and lyophilizates for two experiments were prepared for every excipient high amounts of oligonucleotide were required. Therefore the study was restricted to 4 weeks storage and only formulation 200 which was developed for the use in the hepatic ischemia reperfusion injury rat model (cp. chapter 2.3.1 and chapter 3.4) was studied.

Figure 2.3.21 shows the particle sizes and polydispersity indices of all employed gelatin nanoparticles batches loaded with the NF- κ B decoy oligonucleotide. Nanoparticle sizes varied for the different excipient formulations as four different batches were utilized. In contrast to the as well successful oligonucleotide-loading studies described in chapter 2.3.1 and in accordance to freeze-drying of empty nanoparticles (Figure 2.3.1 and Table 2.3.3) freeze-drying caused a decrease in particles sizes. Together with respective PDIs the introduced good freeze-drying properties of oligonucleotide-loaded and empty gelatin nanoparticles were again confirmed. Compared to empty nanoparticles higher PDI values were measured for ODN-loaded nanoparticles prior to freeze-drying what was already known from former work. However, PCS raw data revealed a broader but still monomodal size distribution curve indicating the absence of bigger aggregates, which could be macroscopically confirmed. Here interestingly, the PDI of all investigated nanoparticle excipient combinations significantly decreased as a result of freeze-drying. Taking the already discussed particle isolation hypothesis of Allison into consideration [Allison et al., 2000] this concept seems to be beneficial even for improving nanoparticle size distribution slightly disturbed by oligonucleotide loading.

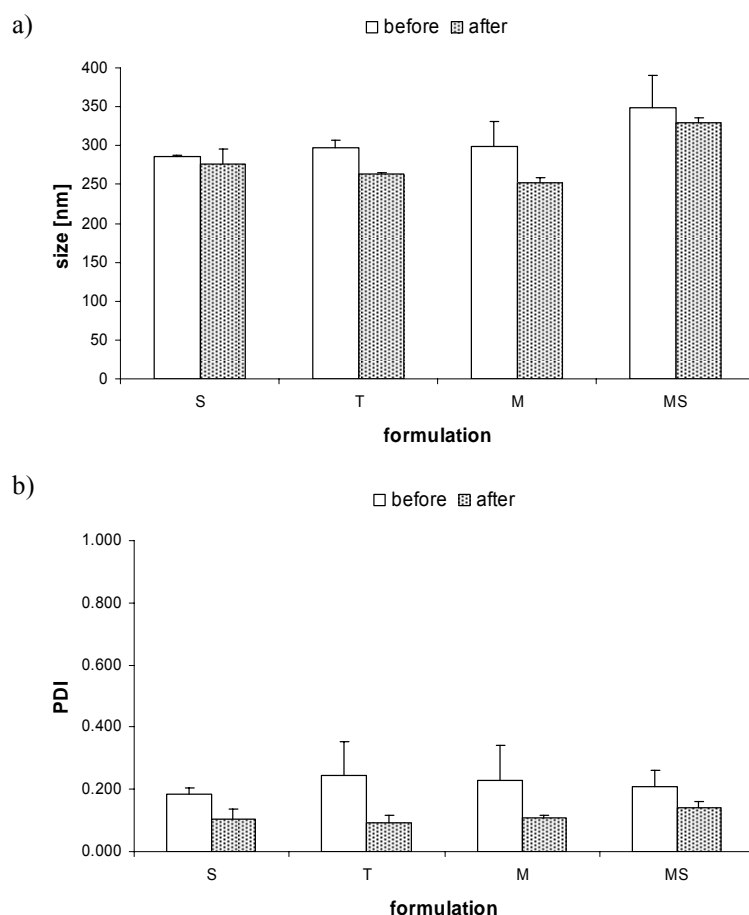


Figure 2.3.21 a) size and b) polydispersity indices of NF- κ B decoy ODN-loaded gelatin nanoparticles formulated with sucrose (S), trehalose (T), mannitol (M), and mannitol-sucrose (MS) before freeze-drying and rehydrated right after freeze-drying

Subsequent to storage the resulting particle sizes and PDIs are in good accordance to data obtained for empty nanoparticles (Figure 2.3.22). Sucrose and trehalose provided good stabilizing properties after closed storage, whereas mannitol and mannitol-sucrose failed to sufficiently stabilize the ODN-loaded gelatin nanoparticles at all storage conditions. None of the samples stored at 30 °C / 60 % RH were recovered with acceptable size or size distribution (data not shown). Surprisingly nanoparticles formulated with trehalose exhibited almost retained polydispersity after storage at 30 °C / 30 % RH. This was not expected from empty nanoparticle investigations, so no trehalose containing samples were prepared for *in vivo* testing after storage at 30 °C / 30 % RH. Prior to the storage stability study, all formulations were examined for their ODN effect i.e., the NF- κ B inhibition in the LPS rat model right after freeze-drying. Therefore, samples were firstly rehydrated according to the procedure described in chapter 2.3.1 for the newly developed sucrose based NF- κ B decoy loaded gelatin nanoparticle formulation.

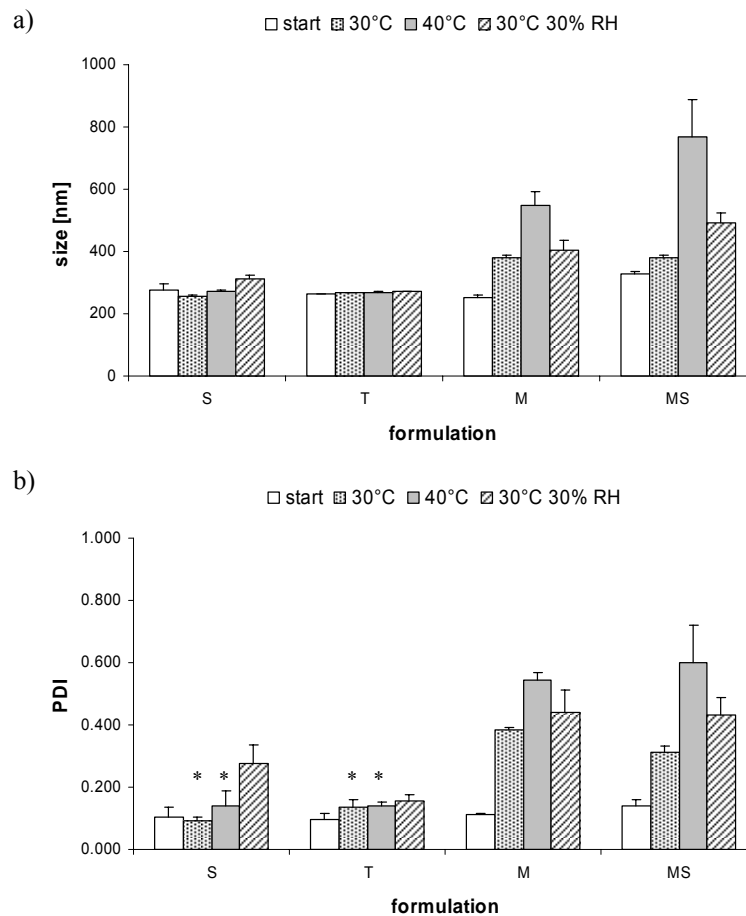


Figure 2.3.22 a) size and b) polydispersity indices of NF-κB decoy ODN-loaded gelatin nanoparticles formulated with sucrose (S), trehalose (T), mannitol (M), and mannitol-sucrose (MS) rehydrated right after freeze-drying, after 4 weeks closed storage at 30 °C and 40 °C, and after 4 weeks open storage at 30 °C / 30 % RH

*formulations that were further investigated *in vivo* within the LPS rat model

Independent from the contained excipient samples were rehydrated with the same amount of water leading to an excipient concentration of 10 % [w/v] and after unification of four of them adjusted with isotonic sucrose solution to the final volume of 1 mL. This procedure provided isotonic sucrose and trehalose solutions ($c = 0.292$ osmol/L) as they exhibit the same osmotic activity and slightly hypertonic mannitol and mannitol-sucrose solutions with concentrations of 0.437 osmol/L and 0.408 osmol/L respectively. Due to formulations prepared with identical excipient masses and the smaller molecular weight a higher number of mannitol molecules was contained thus leading to accordingly increased osmolarity. However, as the intravenous administration performed over a period of 5 min was slow enough to allow dilution within blood, isotonicity of the applied solutions became less important [DeLuca et al., 1984]. Samples investigated after storage stability tests were treated the same way.

Particle sizing data obtained from sucrose and trehalose formulations stored for 4 weeks in closed vials at 30 °C and 40 °C revealed maintained sample quality. Thus, these formulations were investigated for the biological activity of the NF- κ B decoy oligonucleotide loaded onto the gelatin nanoparticles in an LPS rat model. For optimum comparison EMSA was accomplished with samples from all animal studies conducted with samples of the respective excipient and of the respective storage condition at once. The resulting electrophoresis gel demonstrates the excipient independent maintained ODN function upon freeze-drying and underlines the good storage stability properties of gelatin nanoparticles under closed conditions at 30 °C and 40 °C respectively even for their oligonucleotide-loaded state (Figure 2.3.23). In all cases the NF- κ B band is clearly diminished or almost completely erased compared to the control.

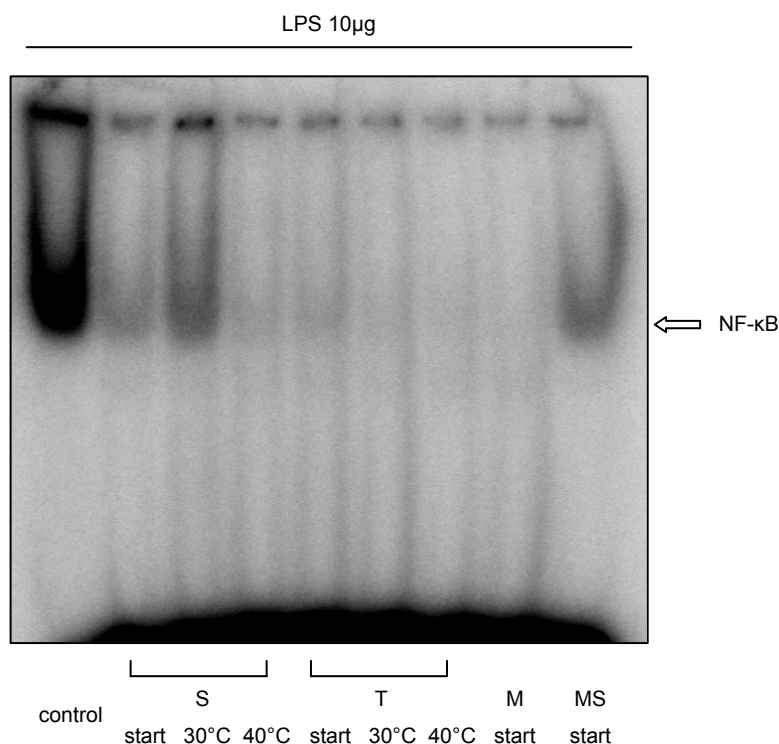


Figure 2.3.23 Hepatic NF- κ B activation after stimulation with 10 μ g LPS of animals treated with 20 nmol NF- κ B decoy oligonucleotide-loaded gelatin nanoparticles and of untreated animals; nanoparticle formulations containing sucrose (S) and trehalose (T) were investigated right after freeze-drying and after 4 weeks closed storage at 30 °C and 40 °C, mannitol (M) and mannitol-sucrose (MS) containing formulations are only investigated right after freeze-drying; one band represents one animal study

Derived from sucrose experiments inter individual variability typically seen during animal studies can be stated to cause unequal NF- κ B band intensities. Regarding initial (Figure 2.3.23: “start”) experiments the nature of the cake emerging

from lyophilization either amorphous for sucrose and trehalose or crystalline for mannitol and mannitol-sucrose formulations did not differentiate the *in vivo* results in terms of altered ODN activity upon freeze-drying. Thus, data are congruent with those of empty gelatin nanoparticles discussed above. In addition, it can be assumed that good particle size and size distribution properties preserved during storage guarantee a maintained function of the investigated NF- κ B decoy oligonucleotide bound onto the surface of gelatin nanoparticles. All animal studies and subsequent EMSA were conducted twice, to confirm the described results.

Molina and co-workers evaluated the stabilizing properties of lipid/DNA complexes formulated with glucose, sucrose, and trehalose for plasmid DNA in a long term stability study over 2 years without further stress factors at -20 °C, 4 °C, and 22 °C [Molina et al., 2004]. Their results reveal particle size independent reduced transfection rates of the applied plasmid already after 10 weeks further progressing during the investigated 2 years period. They propose the formation of reactive oxygen species (ROS) in the dried solid to be responsible. Due to the respective molecular size the requirements for oligonucleotide and plasmid DNA stabilization may not be the same but these findings have to be taken into consideration in future long term stability studies of oligonucleotide-loaded gelatin nanoparticles.

2.4 Summary

During the present work the applicability of freeze-drying for the stabilization of gelatin nanoparticles was demonstrated. Formulations of gelatin nanoparticles containing sucrose, trehalose, mannitol, as well as mannitol and sucrose in the ratio of 4:1 were prepared with total excipient amounts ranging from 0.3 to 7.0 % [w/v]. With exception of formulations possessing the lowest excipient contents size and size distribution of gelatin nanoparticles were preserved over the drying process, whereas a tendency to slightly reduced particle sizes resulting from freeze-drying could be observed. Interestingly, no differences were observed with respect to amorphous or crystalline emerging cakes. In accordance to the particle isolation hypothesis of Allison this led to the assumption that the spatial separation of nanoparticles during freeze-drying is even more decisive than vitrification of the utilized excipient [Allison et al., 2000].

Furthermore, experiments were conducted with NF- κ B and scr decoy oligonucleotide as well as siRNA oligonucleotide-loaded gelatin nanoparticles. The good results from empty nanoparticles were verified and in addition, rehydration in, compared to freeze-drying suspensions / solutions, reduced volumes down to 1/30th of the original volume could successfully be accomplished. Prior to drying sucrose was thereby added as freeze-drying excipient in amounts accounting for isotonic concentrations after rehydration in reduced volumes. Low excipient contents could be circumvented at concomitantly maintained osmotic activity by substituting portions of sucrose by dextran 3000. At the same time surface modified but unloaded gelatin nanoparticles were evaluated as controls. As they were recovered from freeze-drying with unaffected size and size distribution independence of the process from the nanoparticles' zeta potential was proven. Based on the results obtained with oligonucleotide-loaded gelatin nanoparticles and reduced rehydration volumes isotonic samples with increased ODN concentration could be prepared. Compared to the regular oligonucleotide-loading process a four times higher ODN concentration was achieved. In the following these samples were successfully applied in the hepatic ischemia reperfusion rat model established during the cooperation work described in chapter 3.4, where they contributed to the breakthrough in terms of a selective NF- κ B inhibition in the Kupffer cells of the liver.

Finally a storage stability study was performed which differentiated the stabilization properties of the respective freeze-drying excipients. In sum sucrose and trehalose showed a comparable performance whereas the higher T_g of trehalose caused better stabilization during storage at 40 °C while some of the sucrose formulations collapsed. A threshold of 3 % water content could be determined above which nanoparticle aggregation occurred. Thus, storage at accelerated relative humidity leading to clearly elevated residual moisture contents revealed the failure of both to sufficiently stabilize gelatin nanoparticles. Higher excipient masses can be stated as superior as for the sorption of identical amounts of water the described threshold is reached later. Mannitol and mannitol-sucrose containing formulations in turn are characterized by a certain resistance against water sorption even at open storage at 30 % and 60 % RH. Despite these findings both excipients were unable to provide nanoparticle stabilization after storage at 60 % RH. On the other hand the formulation containing the highest amount of mannitol was the only one that kept size and size distribution almost constant after storage at 30 %RH. According to sucrose and trehalose, mannitol containing formulations demanded higher excipient amounts to provide comparable stabilization. With respect to the newly developed concentrated and isotonic samples this has to be assessed as disadvantageous. Otherwise, under special geographical circumstances when handling or storage of lyophilized gelatin nanoparticles occurs under extreme climatic conditions the marginal water sorption of mannitol would become vital. Mannitol-sucrose containing formulations provided worst stabilization properties of all applied excipients which were not expected especially regarding the good results obtained for pure mannitol formulations. In this context DSC analysis could prove the conversion of partially amorphous mannitol present upon freeze drying into its crystalline state during storage. This led to the conclusion that crystallizing mannitol contributed to the observed nanoparticle aggregation in mannitol-sucrose formulations. Including an annealing step into the freeze-drying cycle could foster complete mannitol crystallization throughout drying which presumably improves stabilization properties of mannitol-sucrose formulations for gelatin nanoparticles. In the end storage stability data were completed by evaluating oligonucleotide-loaded gelatin nanoparticles. Results confirmed the observations made so far demonstrating that only sucrose and trehalose provided sufficient stabilization of the selected

formulations of ODN-loaded gelatin nanoparticles. The oligonucleotide itself did not disturb the drying process or negatively affected the stability of gelatin nanoparticles. It could rather be proven to function *in vivo* upon freeze-drying on the surface of gelatin nanoparticles and storage.

In conclusion freeze drying of gelatin nanoparticles could be successfully demonstrated and based on the presented results it can be characterized as a convenient and robust method that provides excellent stabilization. At least it should be mentioned that every application of gelatin nanoparticles requires specific characteristics which can not be covered with a general freeze-dried product, but based on the acquired results respective adaptation might be feasible. The newly developed NF- κ B decoy oligonucleotide-loaded gelatin nanoparticle formulation for example could be further customized by adding Tween[®] 80 already to the freeze-drying solution, by adjusting the sucrose content to enable rehydration only with water to the desired final isotonic volume, and by increasing the sample volume dried per vial by factor 4 to avoid the sample unification step prior to use. Furthermore, long term stability testing of gelatin nanoparticles in general has to be accomplished in future to step forward towards a well defined product applicable for manifold research projects.

2.5 References

- Abdelwahed, W., Degobert, G., and Fessi, H.; Freeze-drying of nanocapsules: Impact of annealing on the drying process; *International Journal of Pharmaceutics*, 2006, 324(1), 74-82
- Abdelwahed, W., Degobert, G., and Fessi, H.; Investigation of nanocapsules stabilization by amorphous excipients during freeze-drying and storage; *European Journal of Pharmaceutics and Biopharmaceutics* 2006, 63(2), 87-94
- Akagi, T., Kaneko, T., Kida, T., and Akashi, M.; Preparation and characterization of biodegradable nanoparticles based on poly(g-glutamic acid) with L-phenylalanine as a protein carrier; *Journal of Controlled Release*, 2005, 108(2-3), 226-236
- Allison, S. D., Molina, M., and Anchordoquy, T. J.; Stabilization of lipid/DNA complexes during the freezing step of the lyophilization process: the particle isolation hypothesis; *Biochimica et Biophysica Acta, Biomembranes*, 2000, 1468(1-2), 127-138
- Anchordoquy, T. J., Armstrong, T. K., and Molina, M. D. C.; Low molecular weight dextrans stabilize nonviral vectors during lyophilization at low osmolalities: Concentrating suspensions by rehydration to reduced volumes; *Journal of Pharmaceutical Sciences*, 2005, 94(6), 1226-1236
- Armstrong, T. K. and Anchordoquy, T. J.; Immobilization of nonviral vectors during the freezing step of lyophilization; *Journal of Pharmaceutical Sciences*, 2004, 93(11), 2698-2709
- Avgoustakis, K.; Pegylated poly(Lactide) and poly(Lactide-Co-Glycolide) nanoparticles: Preparation, properties and possible applications in drug delivery; *Current Drug Delivery*, 2004, 1(4), 321-333
- Bala, I., Hariharan, S., and Kumar, M. N. V. R.; PLGA nanoparticles in drug delivery: The state of the art; *Critical Reviews in Therapeutic Drug Carrier Systems*, 2004, 21(5), 387-422
- Birnbaum, D. T., Kosmala, J. D., and Brannon-Peppas, L.; Optimization of preparation techniques for poly(lactic acid-co-glycolic acid) nanoparticles; *Journal of Nanoparticle Research*, 2000, 2(2), 173-181
- Brus, C., Kleemann, E., Aigner, A., Czubayko, F., and Kissel, T.; Stabilization of oligonucleotide-polyethylenimine complexes by freeze-drying: physicochemical and biological characterization; *Journal of Controlled Release*, 2004, 95(1), 119-131

- Burger, A., Henck, J. O., Hetz, S., Rollinger, J. M., Weissnicht, A. A., and Stottner, H.; Energy/temperature diagram and compression behavior of the polymorphs of D-mannitol; *Journal of Pharmaceutical Sciences*, 2000, 89(4), 457-468
- Cavatur, R. K., Vemuri, N. M., Pyne, A., Chrzan, Z., Toledo-Velasquez, D., and Suryanarayanan, R.; Crystallization behavior of mannitol in frozen aqueous solutions; *Pharmaceutical Research*, 2002, 19(6), 894-900
- Chatterjee, K., Shalaev, E. Y., and Suryanarayanan, R.; Partially crystalline systems in lyophilization: II. Withstanding collapse at high primary drying temperatures and impact on protein activity recovery; *Journal of Pharmaceutical Sciences*, 2005, 94(4), 809-820
- Choi, M. J., Briancon, S., Andrieu, J., Min, S. G., and Fessi, H.; Effect of freeze-drying process conditions on the stability of nanoparticles; *Drying Technology*, 2004, 22(1&2), 335-346
- Coester, C. J., Langer, K., Von Briesen, H., and Kreuter, J.; Gelatin nanoparticles by two step desolvation-a new preparation method, surface modifications and cell uptake; *Journal of Microencapsulation*, 2000, 17(2), 187-193
- Coester, C.; Development of a new carrier system for oligonucleotides and plasmids based on gelatin nanoparticles; *New Drugs*, 2003, (1), 14-17
- Crowe, L. M., Reid, D. S., and Crowe, J. H.; Is trehalose special for preserving dry biomaterials?; *Biophysical Journal*, 1996, 71(4), 2087-2093
- Cuna, M., onso-Sande, M., Remunan-Lopez, C., Pivel, J. P., onso-Lebrero, J. L., and Alonso, M. J.; Development of phosphorylated glucomannan-coated chitosan nanoparticles as nanocarriers for protein delivery; *Journal of Nanoscience and Nanotechnology*, 2006, 6(9/10), 2887-2895
- Davis, D. L., O'Brien, E. P., and Bentzley, C. M.; Analysis of the degradation of oligonucleotide strands during the freezing/thawing processes using MALDI-MS; *Analytical Chemistry*, 2000, 72(20), 5092-5096
- de Chasteigner, S., Cave, G., Fessi, H., Devissaguet, J. P., and Puisieux, F.; Freeze-drying of itraconazole-loaded nanosphere suspensions: a feasibility study; *Drug Development Research*, 1996, 38(2), 116-124
- De Jaeghere, F., Allemann, E., Feijen, J., Kissel, T., Doelker, E., and Gurny, R.; Freeze-drying and lyopreservation of diblock and triblock poly(lactic acid)-poly(ethylene oxide) (PLA-PEO) copolymer nanoparticles; *Pharmaceutical Development and Technology*, 2000, 5(4), 473-483
- DeLuca, P. P. and Boylan, J. C.; Formulation of small volume parenterals; in *Pharmaceutical Dosage Forms: Parenteral Medications Volume 1*; Marcel Dekker, Inc., New York 1984, 139-202

- Douglas, S. J., Davis, S. S., and Illum, L.; Nanoparticles in drug delivery; *Critical Reviews in Therapeutic Drug Carrier Systems*, 1987, 3(3), 233-261
- Fakes, M. G., Dali, M. V., Haby, T. A., Morris, K. R., Varia, S. A., and Serajuddin, A. T. M.; Moisture sorption behavior of selected bulking agents used in lyophilized products; *PDA Journal of Pharmaceutical Science and Technology*, 2000, 54(2), 144-149
- Farrugia, C. A. and Groves, M. J.; Gelatin behaviour in dilute aqueous solution: designing a nanoparticulate formulation; *Journal of Pharmacy and Pharmacology*, 1999, 51(6), 643-649
- Franks, F.; Freeze-drying of bioproducts: putting principles into practice; *European Journal of Pharmaceutics and Biopharmaceutics*, 1998, 45(3), 221-229
- Goetting, N., Fritz, H., Maier, M., Von Stamm, J., Schoofs, T., and Bayer, E.; Effects of oligonucleotide adsorption on the physicochemical characteristics of a nanoparticle-based model delivery system for antisense drugs; *Colloid and Polymer Science*, 1999, 277(2-3), 145-152
- Gruber, F.; Untersuchungen zur Encapsulierung von Paclitaxel in kationische Liposomen, Dissertation, Ludwig-Maximilians-University Munich; 2004
- Hancock, B. C. and Zografi, G.; The relationship between the glass transition temperature and the water content of amorphous pharmaceutical solids; *Pharmaceutical Research*, 1994, 11(4), 471-477
- Hawe, A.; Studies on stable formulations for a hydrophobic cytokine, Dissertation, Ludwig-Maximilians-University Munich; 2006
- Her, L. M. and Nail, S. L.; Measurement of glass transition temperatures of freeze-concentrated solutes by differential scanning calorimetry; *Pharmaceutical Research*, 1994, 11(1), 54-59
- Hirsjarvi, S., Peltonen, L., Kainu, L., and Hirvonen, J.; Freeze-drying of low molecular weight poly(L-lactic acid) nanoparticles: effect of cryo- and lyoprotectants; *Journal of Nanoscience and Nanotechnology*, 2006, 6(9/10), 3110-3117
- Hoehne, G. W. H. and Gloeggler, E.; Some peculiarities of the DSC-2/-7 (Perkin-Elmer) and their influence on accuracy and precision of the measurements; *Thermochimica Acta*, 1989, 151, 295-304
- Imamura, K., Ogawa, T., Sakiyama, T., and Nakanishi, K.; Effects of types of sugar on the stabilization of protein in the dried state; *Journal of Pharmaceutical Sciences*, 92(2), 266-274
- Jameel, F., Amsberry, K. L., and Pikal, M. J.; Freeze drying properties of some oligonucleotides; *Pharmaceutical Development and Technology*, 2001, 6(2), 151-157

- Jeong, Y. I., Shim, Y. H., Kim, C., Lim, G. T., Choi, K. C., and Yoon, C.; Effect of cryoprotectants on the reconstitution of surfactant-free nanoparticles of poly(lactide-co-glycolide); *Journal of Microencapsulation*, 2005, 22(6), 593-601
- Johnson, R. E., Kirchhoff, C. F., and Gaud, H. T.; Mannitol-sucrose mixtures-versatile formulations for protein lyophilization; *Journal of Pharmaceutical Sciences*, 2002, 91(4), 914-922
- Kang, H. W., Tabata, Y., and Ikada, Y.; Fabrication of porous gelatin scaffolds for tissue engineering; *Biomaterials*, 1999, 20(14), 1339-1344
- Kaul, G. and Amiji, M.; Long-circulating poly(ethylene glycol)-modified gelatin nanoparticles for intracellular delivery; *Pharmaceutical Research*, 2002, 19(7), 1061-1067
- Kaul, G. and Amiji, M.; Biodistribution and targeting potential of poly(ethylene glycol)-modified gelatin nanoparticles in subcutaneous murine tumor model; *Journal of Drug Targeting*, 2004, 12(9-10), 585-591
- Kaul, G. and Amiji, M.; Tumor-targeted gene delivery using poly(ethylene glycol)-modified gelatin nanoparticles: in vitro and in vivo studies; *Pharmaceutical Research*, 2005, 22(6), 951-961
- Kim, A. I., Akers, M. J., and Nail, S. L.; The physical state of mannitol after freeze-drying: effects of mannitol concentration, freezing rate, and a noncrystallizing cosolute; *Journal of Pharmaceutical Sciences*, 1998, 87(8), 931-935
- Layre, A. M., Couvreur, P., Richard, J., Requier, D., Ghermani, N. E., and Gref, R.; Freeze-drying of composite core-shell nanoparticles; *Drug Development and Industrial Pharmacy*, 2006, 32(7), 839-846
- Liu, J.; Physical characterization of pharmaceutical formulations in frozen and freeze-dried solid states: techniques and applications in freeze-drying development; *Pharmaceutical Development and Technology*, 2006, 11(1), 3-28
- Lueckel, B., Bodmer, D., Helk, B., and Leuenberger, H.; Formulations of sugars with amino acids or mannitol-influence of concentration ratio on the properties of the freeze-concentrate and the lyophilizate; *Pharmaceutical Development and Technology*, 1998, 3(3), 325-336
- Maeder, K. and Mehnert, W.; Solid lipid nanoparticles - concepts, procedures, and physicochemical aspects; in *Lipospheres in Drug Targets and Delivery*, CRC Press, LLC., Boca Raton, FL, 2005, 1-22
- Mano, J. F. and Gomez Ribelles, J. L.; Influence of the sample mass on the study of the glass transition and the structural relaxation by differential scanning calorimetry; *Journal of Non-Crystalline Solids*, 2004, 337(1), 68-77

- Mao, H. Q., Roy, K., Troung-Le, V. L., Janes, K. A., Lin, K. Y., Wang, Y., August, J. T., and Leong, K. W.; Chitosan-DNA nanoparticles as gene carriers: synthesis, characterization and transfection efficiency; *Journal of Controlled Release*, 2001, 70(3), 399-421
- Molina, M., Armstrong, T. K., Zhang, Y., Patel, M. M., Lentz, Y. K., and Anchordoquy, T. J.; The stability of lyophilized lipid/DNA complexes during prolonged storage; *Journal of Pharmaceutical Sciences*, 2004, 93(9), 2259-2273
- Nimesh, S., Manchanda, R., Kumar, R., Saxena, A., Chaudhary, P., Yadav, V., Mozumdar, S., and Chandra, R.; Preparation, characterization and in vitro drug release studies of novel polymeric nanoparticles; *International Journal of Pharmaceutics*, 2006, 323(1-2), 146-152
- Nunes, C., Suryanarayanan, R., Botez, C. E., and Stephens, P. W.; Characterization and crystal structure of D-mannitol hemihydrate; *Journal of Pharmaceutical Sciences*, 2004, 93(11), 2800-2809
- Oh, K. S., Lee, K. E., Han, S. S., Cho, S. H., Kim, D., and Yuk, S. H.; Formation of core/shell nanoparticles with a lipid core and their application as a drug delivery system; *Biomacromolecules*, 2005, 6(2), 1062-1067
- Oppenheim, R. C.; Solid colloidal drug delivery systems: nanoparticles; *International Journal of Pharmaceutics*, 1981, 8(3), 217-234
- Roy, D., Guillon, X., Lescure, F., Couvreur, P., Bru, N., and Breton, P.; On shelf stability of freeze-dried poly(methylidene malonate, 2.1.2) nanoparticles; *International Journal of Pharmaceutics*, 1997, 148(2), 165-175
- Saez, A., Guzman, M., Molpeceres, J., and Aberturas, M. R.; Freeze-drying of polycaprolactone and poly(d,l-lactic-glycolic) nanoparticles induce minor particle size changes affecting the oral pharmacokinetics of loaded drugs; *European Journal of Pharmaceutics and Biopharmaceutics*, 2000, 50(3), 379-387
- Schwarz, C. and Mehnert, W.; Freeze-drying of drug-free and drug-loaded solid lipid nanoparticles (SLN); *International Journal of Pharmaceutics*, 1997, 157(2), 171-179
- Shalaev, E. Y. and Zografí, G.; How does residual water affect the solid-state degradation of drugs in the amorphous state?; *Journal of Pharmaceutical Sciences*, 1996, 85(11), 1137-1141
- Shire, S. J., Shahrokh, Z., and Liu, J.; Challenges in the development of high protein concentration formulations; *Journal of Pharmaceutical Sciences*, 2004, 93(6), 1390-1402
- Surana, R., Pyne, A., and Suryanarayanan, R.; Effect of aging on the physical properties of amorphous trehalose; *Pharmaceutical Research*, 2004, 21(5), 867-874

- Talsma, H., Cherng, J. Y., Lehrmann, H., Kursa, M., Ogris, M., Hennink, W. E., Cotten, M., and Wagner, E.; Stabilization of gene-delivery systems by freeze-drying; *International Journal of Pharmaceutics*, 1997, 157(2), 233-238
- Tang, X. and Pikal, M. J.; Design of freeze-drying processes for pharmaceuticals: practical advice; *Pharmaceutical Research*, 2004, 21(2), 191-200
- Te Booy, M. P. W. M., De Ruiter, R. A., and De Meere, A. L. J.; Evaluation of the physical stability of freeze-dried sucrose-containing formulations by differential scanning calorimetry; *Pharmaceutical Research*, 1992, 9(1), 109-114
- Telang, C., Suryanarayanan, R., and Yu, L.; Crystallization of D-mannitol in binary mixtures with NaCl: phase diagram and polymorphism; *Pharmaceutical Research*, 2003, 20(12), 1939-1945
- Ugwu, S., Zhang, A., Parmar, M., Miller, B., Sardone, T., Peikov, V., and Ahmad, I.; Preparation, characterization, and stability of liposome-based formulations of mitoxantrone; *Drug Development and Industrial Pharmacy*, 2005, 31(2), 223-229
- Van Winden, E. C. A. and Crommelin, D. J. A.; Long term stability of freeze-dried, lyoprotected doxorubicin liposomes; *European Journal of Pharmaceutics and Biopharmaceutics*, 1997, 43(3), 295-307
- Van Winden, E. C. A.; Freeze-drying of liposomes: theory and practice; *Methods in Enzymology*, 2003, 367(Liposomes, Part A), 99-110
- Wagner, V., Dullaart, A., Bock, A. K., and Zweck, A.; The emerging nanomedicine landscape; *Nature Biotechnology*, 2006, 24(10), 1211-1217
- Wang, W.; Lyophilization and development of solid protein pharmaceuticals; *International Journal of Pharmaceutics*, 2000, 203(1-2), 1-60
- Yu, L.; Amorphous pharmaceutical solids: preparation, characterization and stabilization; *Advanced Drug Delivery Reviews*, 2001, 48(1), 27-42
- Zwiorek, K.; Gelatin nanoparticles as delivery system for nucleotide-based drugs, Dissertation, Ludwig-Maximilians-University Munich; 2006

2.6 Annex

2.6.1 Stability data of empty gelatin nanoparticles

Photon correlation spectroscopy (PCS) data

Table 2.6.1 Size of freeze-dried gelatin nanoparticles rehydrated after 4 weeks closed storage at 30 °C and 40 °C and open storage at 30 °C / 30 % RH and 30 °C / 60 % RH

Formulation		Size [nm]							
		4w 30 °C		4w 40 °C		4w 30 °C / 30 % RH		4w 30 °C / 60 % RH	
		Mean	Stdv	Mean	Stdv	Mean	Stdv	Mean	Stdv
Sucrose	47	289.0	16.7	4990.0	833.5	n/a	n/a	n/a	n/a
	100	185.7	2.5	249.7	17.6	n/a	n/a	n/a	n/a
	200	178.7	0.6	172.7	0.6	761.5	393.9	n/a	n/a
	400	177.0	2.0	172.0	1.0	262.0	29.8	1130.7	953.8
	800	177.0	3.6	171.0	1.7	197.7	3.1	400.7	59.8
Trehalose	47	233.7	1.5	336.7	29.2	n/a	n/a	n/a	n/a
	100	184.7	3.2	186.7	4.0	n/a	n/a	n/a	n/a
	200	176.3	2.3	170.7	0.6	1445.3	1153.0	n/a	n/a
	400	173.7	1.2	170.0	1.7	239.7	22.1	n/a	n/a
	800	173.7	2.1	168.7	2.1	273.0	54.0	n/a	n/a
Mannitol	47	1303.3	66.6	4743.3	950.0	1696.7	330.8	8563.3	1385.5
	100	235.3	2.5	362.7	25.9	614.3	464.1	1573.3	433.6
	200	217.7	50.6	197.7	1.5	192.0	2.6	555.0	532.7
	400	188.7	11.9	183.7	1.2	209.7	21.0	377.0	266.0
	800	179.7	0.6	182.3	1.5	190.3	5.1	689.0	771.6
Man-Suc	47	2300.0	636.6	4243.3	1525.7	10290.0	1391.2	15833.3	11938.4
	100	546.7	410.0	1076.3	964.5	6213.3	1866.3	8023.3	805.3
	200	215.3	2.5	313.3	122.7	1138.7	480.7	6260.0	4380.4
	400	206.0	2.0	216.3	2.3	277.7	5.0	2082.0	1446.9
	800	203.3	0.6	208.3	1.5	225.7	5.9	4073.3	1123.2

Table 2.6.2 Polydispersity indices of freeze-dried gelatin nanoparticles rehydrated after 4 weeks closed storage at 30 °C and 40 °C and open storage at 30 °C / 30 % RH and 30 °C / 60 % RH

Formulation		PDI							
		4w 30 °C		4w 40 °C		4w 30 °C / 30 % RH		4w 30 °C / 60 % RH	
		Mean	Stdv	Mean	Stdv	Mean	Stdv	Mean	Stdv
Sucrose	47	0.406	0.050	0.832	0.291	n/a	n/a	n/a	n/a
	100	0.100	0.014	0.414	0.082	n/a	n/a	n/a	n/a
	200	0.044	0.022	0.062	0.007	0.611	0.271	n/a	n/a
	400	0.046	0.006	0.038	0.007	0.374	0.040	0.655	0.310
	800	0.048	0.012	0.066	0.014	0.139	0.020	0.492	0.042
Trehalose	47	0.364	0.008	0.647	0.086	n/a	n/a	n/a	n/a
	100	0.118	0.020	0.145	0.034	n/a	n/a	n/a	n/a
	200	0.063	0.013	0.068	0.004	0.780	0.328	n/a	n/a
	400	0.046	0.006	0.042	0.008	0.285	0.063	n/a	n/a
	800	0.057	0.023	0.055	0.005	0.289	0.079	n/a	n/a
Mannitol	47	0.910	0.038	1.000	0.000	0.964	0.062	1.000	0.000
	100	0.329	0.019	0.490	0.011	0.570	0.235	0.906	0.109
	200	0.207	0.178	0.145	0.017	0.131	0.018	0.390	0.182
	400	0.105	0.046	0.082	0.007	0.154	0.063	0.302	0.213
	800	0.051	0.004	0.062	0.012	0.066	0.012	0.303	0.174
Man-Suc	47	1.000	0.000	1.000	0.000	0.736	0.457	0.928	0.125
	100	0.534	0.187	0.685	0.273	1.000	0.000	0.997	0.005
	200	0.127	0.021	0.310	0.193	0.707	0.101	0.466	0.365
	400	0.077	0.022	0.109	0.011	0.351	0.034	0.419	0.187
	800	0.077	0.013	0.078	0.003	0.139	0.023	0.437	0.161

Table 2.6.3 Size of freeze-dried gelatin nanoparticles rehydrated after 10 weeks closed storage at 30 °C and 40 °C and open storage at 30 °C / 30 % RH and 30 °C / 60 % RH

Formulation		Size [nm]							
		10w 30 °C		10w 40 °C		10w 30 °C / 30 % RH		10w 30 °C / 60 % RH	
		Mean	Stdv	Mean	Stdv	Mean	Stdv	Mean	Stdv
Sucrose	47	463.3	127.6	5596.7	4746.5	n/a	n/a	n/a	n/a
	100	179.0	0.0	765.0	268.7	n/a	n/a	n/a	n/a
	200	170.3	0.6	200.7	3.2	n/a	n/a	n/a	n/a
	400	168.0	1.0	169.3	1.2	222.0	11.1	274.3	14.8
	800	170.0	1.0	169.3	4.2	188.0	6.9	207.7	6.7
Trehalose	47	264.7	8.0	614.0	180.3	n/a	n/a	n/a	n/a
	100	188.0	3.6	201.0	6.2	n/a	n/a	n/a	n/a
	200	177.3	0.6	176.0	1.0	201.3	4.5	n/a	n/a
	400	175.7	1.5	174.3	1.5	177.3	2.1	n/a	n/a
	800	176.0	1.0	173.7	1.5	174.7	1.2	n/a	n/a
Mannitol	47	3251.0	2112.7	6823.3	755.1	3916.7	2761.6	4630.0	2592.8
	100	568.0	315.7	565.7	204.6	335.7	135.4	2685.0	3128.3
	200	187.3	1.5	371.0	264.2	212.7	33.5	220.3	7.5
	400	178.7	4.7	174.0	1.0	192.3	10.7	434.0	421.8
	800	179.7	3.2	172.3	1.2	185.7	5.7	212.3	14.8
Man-Suc	47	4413.3	2992.2	3056.7	2674.2	n/a	n/a	n/a	n/a
	100	1337.7	1605.1	2263.3	1204.3	n/a	n/a	n/a	n/a
	200	1162.7	1574.0	1677.3	1274.5	1096.7	580.3	n/a	n/a
	400	233.0	31.4	265.3	69.1	283.7	31.5	n/a	n/a
	800	210.0	17.8	820.7	511.8	216.3	0.6	n/a	n/a

Table 2.6.4 Polydispersity indices of freeze-dried gelatin nanoparticles rehydrated after 10 weeks closed storage at 30 °C and 40 °C and open storage at 30 °C / 30 % RH and 30 °C / 60 % RH

Formulation		PDI							
		10w 30 °C		10w 40 °C		10w 30 °C / 30 % RH		10w 30 °C / 60 % RH	
		Mean	Stdv	Mean	Stdv	Mean	Stdv	Mean	Stdv
Sucrose	47	0.592	0.193	0.895	0.182	n/a	n/a	n/a	n/a
	100	0.136	0.023	0.697	0.180	n/a	n/a	n/a	n/a
	200	0.057	0.010	0.242	0.020	n/a	n/a	n/a	n/a
	400	0.044	0.021	0.047	0.011	0.281	0.071	0.377	0.029
	800	0.055	0.023	0.038	0.016	0.156	0.013	0.279	0.007
Trehalose	47	0.464	0.043	0.717	0.285	n/a	n/a	n/a	n/a
	100	0.136	0.020	0.204	0.021	n/a	n/a	n/a	n/a
	200	0.051	0.013	0.069	0.019	0.159	0.019	n/a	n/a
	400	0.058	0.013	0.037	0.014	0.074	0.018	n/a	n/a
	800	0.063	0.008	0.045	0.019	0.054	0.008	n/a	n/a
Mannitol	47	0.699	0.203	0.481	0.432	0.994	0.010	0.917	0.144
	100	0.530	0.231	0.600	0.068	0.495	0.136	0.623	0.145
	200	0.136	0.006	0.416	0.252	0.229	0.122	0.293	0.016
	400	0.062	0.012	0.080	0.009	0.103	0.043	0.269	0.220
	800	0.051	0.013	0.072	0.009	0.081	0.009	0.170	0.023
Man-Suc	47	0.855	0.251	0.856	0.247	n/a	n/a	n/a	n/a
	100	0.517	0.053	0.844	0.253	n/a	n/a	n/a	n/a
	200	0.461	0.467	0.704	0.364	0.868	0.167	n/a	n/a
	400	0.135	0.060	0.221	0.121	0.395	0.110	n/a	n/a
	800	0.072	0.006	0.484	0.320	0.136	0.025	n/a	n/a

*Karl-Fischer titration data***Table 2.6.5** Residual moisture content of freeze-dried gelatin nanoparticle (verum) formulations right after the drying process

Formulation	Residual moisture [%]							
	Sucrose _v		Trehalose _v		Mannitol _v		Man-Suc _v	
	Mean	Stdv	Mean	Stdv	Mean	Stdv	Mean	Stdv
47	1.2	0.2	0.8	0.2	0.6	0.3	0.8	0.2
100	0.7	0.1	0.6	0.2	1.0	0.0	0.7	0.1
200	0.6	0.0	0.2	0.1	1.7	0.1	0.7	0.1
400	0.3	0.0	0.2	0.0	1.0	0.1	0.7	0.1
800	0.3	0.0	0.1	0.1	0.5	0.0	0.5	0.1

Table 2.6.6 Residual moisture content of freeze-dried placebo formulations right after the drying process

Formulation	Residual moisture [%]							
	Sucrose _p		Trehalose _p		Mannitol _p		Man-Suc _p	
	Mean	Stdv	Mean	Stdv	Mean	Stdv	Mean	Stdv
47	0.9	0.2	1.0	0.3	1.4	n/a	0.8	0.1
100	0.3	0.1	0.6	0.1	0.8	n/a	0.7	0.1
200	0.6	0.0	0.2	0.0	2.9	1.0	0.7	0.7
400	0.4	0.1	0.4	0.1	0.7	0.2	0.6	0.4
800	0.4	0.1	0.7	0.1	0.7	0.3	0.5	0.2

Table 2.6.7 Residual moisture content of freeze-dried gelatin nanoparticle (verum) formulations after 4 weeks closed storage at 30 °C and 40 °C and open storage at 30 °C / 30 % RH and 30 °C / 60 % RH

Formulation	Residual moisture [%]								
	Sucrose _v		Trehalose _v		Mannitol _v		Man-Suc _v		
	Mean	Stdv	Mean	Stdv	Mean	Stdv	Mean	Stdv	
47	30 °C	4.9	0.1	5.2	0.3	2.7	0.1	2.9	0.3
	40 °C	5.4	0.3	5.8	0.2	2.9	0.2	3.5	0.1
	30 °C / 30 % RH	6.8	0.5	8.6	0.3	2.9	0.3	4.0	0.5
	30 °C / 60 % RH	9.6	0.8	9.4	0.4	3.6	1.4	6.6	0.0
100	30 °C	3.8	0.0	4.2	0.1	1.7	0.1	2.0	0.1
	40 °C	3.9	0.2	4.7	0.2	1.8	0.0	2.4	0.2
	30 °C / 30 % RH	3.8	0.6	7.6	0.4	1.7	0.1	3.3	0.1
	30 °C / 60 % RH	8.8	0.1	7.0	1.0	2.5	0.1	5.1	0.2
200	30 °C	2.9	0.1	3.3	0.1	1.2	0.1	1.7	0.1
	40 °C	2.3	0.8	3.5	0.2	1.3	0.0	1.7	0.1
	30 °C / 30 % RH	3.7	0.4	6.2	0.2	0.9	0.1	2.8	0.1
	30 °C / 60 % RH	9.1	0.6	6.2	1.1	1.4	0.0	4.6	0.0
400	30 °C	2.1	0.0	2.3	0.1	0.8	0.0	1.4	0.0
	40 °C	2.5	0.1	2.7	0.0	0.8	0.0	1.3	0.0
	30 °C / 30 % RH	2.9	0.0	5.5	0.1	0.6	0.0	2.2	0.2
	30 °C / 60 % RH	8.5	0.0	5.6	0.4	0.9	0.0	4.0	0.1
800	30 °C	1.4	0.1	1.5	0.1	0.4	0.0	0.9	0.0
	40 °C	1.8	0.1	1.8	0.0	0.4	0.0	1.0	0.0
	30 °C / 30 % RH	2.6	0.1	5.3	0.1	0.3	0.0	2.1	0.0
	30 °C / 60 % RH	8.8	0.0	5.6	3.0	0.4	0.0	2.8	1.4

Table 2.6.8 Residual moisture content of freeze-dried placebo formulations after 4 weeks closed storage at 30 °C and 40 °C and open storage at 30 °C / 30 % RH and 30 °C / 60 % RH

Formulation	Residual moisture [%]								
	Sucrose _p		Trehalose _p		Mannitol _p		Man-Suc _p		
	Mean	Stdv	Mean	Stdv	Mean	Stdv	Mean	Stdv	
47	30 °C	4.0	0.4	6.0	0.1	3.1	0.1	3.3	0.3
	40 °C	3.3	0.3	7.0	0.2	2.4	0.0	3.2	1.2
	30 °C / 30 % RH	5.5	0.2	4.4	0.1	4.9	n/a	1.6	0.1
	30 °C / 60 % RH	11.1	0.4	9.5	0.7	2.4	0.3	5.2	1.0
100	30 °C	3.5	0.7	5.1	0.8	2.0	0.3	2.7	0.1
	40 °C	2.9	0.2	5.7	1.1	1.3	0.9	2.6	1.0
	30 °C / 30 % RH	3.4	0.5	3.2	0.4	1.5	n/a	1.6	0.2
	30 °C / 60 % RH	11.3	0.7	6.6	1.8	1.0	1.9	4.1	1.2
200	30 °C	3.1	0.1	3.6	0.1	1.2	0.0	2.5	0.4
	40 °C	2.5	0.1	4.0	0.0	0.9	0.4	2.2	1.3
	30 °C / 30 % RH	3.3	0.1	1.8	0.4	1.3	0.2	1.6	0.0
	30 °C / 60 % RH	10.9	0.3	4.9	2.0	0.2	0.0	3.9	0.3
400	30 °C	2.0	0.1	2.4	0.0	1.0	0.2	2.2	0.1
	40 °C	2.1	0.6	2.8	0.1	0.5	0.3	1.2	0.4
	30 °C / 30 % RH	2.4	0.3	1.2	0.1	0.3	0.0	1.4	0.0
	30 °C / 60 % RH	6.0	3.6	4.2	0.9	0.2	0.1	2.7	0.0
800	30 °C	1.5	0.1	1.5	0.0	0.6	0.2	1.1	0.1
	40 °C	1.6	0.1	1.9	0.1	0.3	0.1	1.0	0.3
	30 °C / 30 % RH	2.4	0.2	1.1	0.1	0.2	0.3	1.4	0.2
	30 °C / 60 % RH	6.8	0.6	4.2	2.9	0.1	0.0	3.2	0.1

Table 2.6.9 Residual moisture content of freeze-dried gelatin nanoparticle (verum) formulations after 10 weeks closed storage at 30 °C and 40 °C and open storage at 30 °C / 30 % RH and 30 °C / 60 % RH

Formulation	Residual moisture [%]								
	Sucrose _v		Sucrose _v		Sucrose _v		Sucrose _v		
	Mean	Mean	Mean	Mean	Mean	Mean	Mean	Mean	
47	30 °C	4.1	0.4	5.0	0.3	2.5	0.2	2.7	0.0
	40 °C	3.7	0.6	2.0	0.0	2.6	0.3	3.7	0.2
	30 °C / 30 % RH	4.3	1.3	6.1	0.5	4.0	0.9	4.4	0.5
	30 °C / 60 % RH	13.6	0.4	11.3	0.4	5.2	0.1	5.2	0.1
100	30 °C	3.5	0.0	4.3	0.1	1.6	0.0	2.0	0.3
	40 °C	2.0	0.1	2.8	0.1	1.7	0.0	2.3	0.2
	30 °C / 30 % RH	1.7	0.5	5.3	0.1	1.9	0.1	2.6	0.1
	30 °C / 60 % RH	10.9	0.4	10.0	1.0	3.0	0.1	4.0	0.2
200	30 °C	2.8	0.1	3.4	0.1	1.2	0.0	1.7	0.1
	40 °C	2.7	0.1	3.6	0.1	1.1	0.1	1.7	0.1
	30 °C / 30 % RH	2.1	0.3	4.7	0.3	1.0	0.0	2.0	0.1
	30 °C / 60 % RH	11.1	0.8	8.9	0.5	1.5	0.0	3.6	0.1
400	30 °C	2.2	0.1	2.6	0.1	0.8	0.1	1.5	0.0
	40 °C	2.3	0.1	4.4	0.2	0.8	0.1	0.8	0.2
	30 °C / 30 % RH	2.0	0.0	3.7	0.2	0.7	0.0	1.7	0.1
	30 °C / 60 % RH	10.2	0.0	7.9	0.2	1.0	0.0	3.6	n/a
800	30 °C	1.5	0.1	1.7	0.1	0.4	0.0	0.9	0.1
	40 °C	1.8	0.0	5.3	0.3	0.5	0.1	0.9	0.0
	30 °C / 30 % RH	1.6	0.0	3.2	0.0	0.4	0.0	1.5	0.1
	30 °C / 60 % RH	10.6	0.0	9.2	0.2	0.4	0.0	3.2	0.0

*Differential scanning calorimetry (DSC) data***Table 2.6.10** T_g (point of inflection) of freeze-dried sucrose containing gelatin nanoparticle (verum) formulations right after the drying process and after 4 weeks closed storage at 20 °C, 30 °C, and 40 °C and open storage at 30 °C / 30 % RH and 30 °C / 60 % RH

Formulation	Start	T _g [°C]											
		20 °C				4w 30 °C				10w 40 °C			
		Mean	Stdv	Mean	Stdv	Mean	Stdv	Mean	Stdv	Mean	Stdv	Mean	Stdv
47	44.4	n/a	31.4	0.00	29.9	0.78	31.9	3.61	31.8	0.71	33.4	0.05	
100	49.5	0.00	36.4	0.00	32.8	0.71	n/a	n/a	32.3	0.00	n/a	n/a	
200	52.9	0.71	42.5	0.00	37.9	0.71	n/a	n/a	36.3	0.00	n/a	n/a	
400	55.0	3.61	49.5	0.00	43.0	2.12	41.4	0.00	43.4	0.00	n/a	n/a	
800	57.5	1.41	53.1	0.71	49.0	0.71	43.0	7.85	49.9	0.71	45.4	0.00	

Table 2.6.11 T_g (point of inflection) of freeze-dried sucrose containing placebo formulations right after the drying process and after 4 weeks closed storage at 30 °C and 40 °C and open storage at 30 °C / 30 % RH and 30 °C / 60 % RH

Formulation	Start	T _g [°C]					
		30 °C		4w 30 °C		40 °C	
		Mean	Stdv	Mean	Stdv	Mean	Stdv
47	41.9	0.71	n/a	n/a	n/a	n/a	
100	49.5	0.07	n/a	n/a	n/a	n/a	
200	54.5	n/a	34.7	0.78	n/a	n/a	
400	57.5	0.07	43.8	0.71	38.8	0.78	
800	58.5	1.41	50.8	0.71	46.3	1.41	

Table 2.6.12 T_g (point of inflection) of freeze-dried trehalose containing gelatin nanoparticle (verum) formulations right after the drying process and after 4 weeks closed storage at 20 °C, 30 °C, and 40 °C and open storage at 30 °C / 30 % RH and 30 °C / 60 % RH

Formulation	T_g [°C]											
	Start		4w						10w			
	Mean	Stdv	20 °C		30 °C		40 °C		30 °C		40 °C	
47	79.4	1.4	53.6	0.7	52.8	4.0	50.6	0.7	54.1	n/a	46.9	0.0
100	82.4	n/a	65.4	0.0	54.2	2.8	57.7	0.7	52.8	5.4	53.1	1.4
200	86.4	n/a	72.4	0.0	60.3	n/a	63.3	0.0	56.7	4.9	60.7	3.7
400	84.3	7.4	79.9	0.7	72.4	1.4	68.4	0.0	73.4	0.0	66.8	0.7
800	94.5	0.1	89.0	0.7	74.0	7.7	82.1	0.6	79.9	0.7	66.3	17.2

Table 2.6.13 T_g (point of inflection) of freeze-dried trehalose containing placebo formulations right after the drying process and after 4 weeks closed storage at 30 °C and 40 °C and open storage at 30 °C / 30 % RH and 30 °C / 60 % RH

Formulation	T_g [°C]						
	Start		4w				
	Mean	Stdv	30 °C		40 °C		
47	69.2	0.2	48.2	0.1	45.3	0.7	
100	80.4	0.0	56.7	0.0	54.6	0.8	
200	86.4	0.0	64.1	3.0	63.6	0.6	
400	88.2	0.4	75.6	1.5	68.3	0.0	
800	94.0	0.7	84.3	0.8	82.9	0.7	

Table 2.6.14 Melting point (peak) of freeze-dried mannitol containing gelatin nanoparticle (verum) formulations right after the drying process and after 4 weeks closed storage at 20 °C, 30 °C, and 40 °C and open storage at 30 °C / 30 % RH and 30 °C / 60 % RH

Formulation	Melting point (peak) [°C]											
	Start		4w									
	Mean	Stdv	20 °C		30 °C		40 °C		30 °C / 30 % RH		30 °C / 60 % RH	
47	158.2	0.9	157.6	0.1	156.6	0.1	157.5	0.0	156.6	0.1	155.0	0.7
100	158.5	1.4	160.5	1.4	159.1	0.7	161.1	2.2	159.0	0.7	157.5	0.0
200	160.5	2.8	163.1	2.1	164.5	2.8	164.1	0.6	163.5	1.4	161.5	0.0
400	162.0	0.7	165.0	0.7	164.5	0.0	163.1	0.7	163.0	0.7	163.5	0.0
800	163.5	0.0	163.5	0.0	165.0	2.1	163.6	0.1	163.5	0.0	163.5	1.4

Table 2.6.15 Melting point (peak) of freeze-dried mannitol containing placebo formulations right after the drying process and after 4 weeks closed storage at 30 °C and 40 °C and open storage at 30 °C / 30 % RH and 30 °C / 60 % RH

Formulation	Melting point (peak) [°C]										
	Start		4w								
	Mean	Stdv	30 °C		40 °C		30 °C / 30 % RH		30 °C / 60 % RH		
47	160.0	0.6	160.9	0.7	161.5	0.0	161.4	n/a	161.5	n/a	
100	161.4	0.1	162.4	0.0	163.0	0.6	163.4	0.0	163.4	0.0	
200	163.5	6.4	163.4	0.0	164.4	0.0	164.4	0.0	163.9	0.7	
400	165.0	0.7	162.4	0.0	163.9	0.7	163.4	0.0	164.4	0.1	
800	165.5	0.0	164.8	0.7	164.4	0.0	165.4	0.1	163.9	0.7	

Table 2.6.16 Melting point (peak) of freeze-dried mannitol containing gelatin nanoparticle (verum) formulations after 10 weeks closed storage at 30 °C and 40 °C and open storage at 30 °C / 30 % RH and 30 °C / 60 % RH

Formulation	Melting point (peak) [°C]							
	10w							
	30 °C		40 °C		30 °C / 30 % RH		30 °C / 60 % RH	
Mean	Stdv	Mean	Stdv	Mean	Stdv	Mean	Stdv	
47	155.5	0.0	157.1	0.6	155.5	0.0	155.5	n/a
100	158.5	0.0	158.5	0.0	158.0	0.7	157.5	n/a
200	164.5	1.4	164.0	2.1	161.5	n/a	161.5	0.0
400	163.0	0.7	163.0	0.7	163.3	1.1	162.5	0.0
800	164.0	0.7	161.5	0.1	163.0	0.7	164.5	0.0

Table 2.6.17 Melting point (peak) of freeze-dried mannitol-sucrose containing gelatin nanoparticle (verum) formulations right after the drying process and after 4 weeks closed storage at 20 °C, 30 °C, and 40 °C and open storage at 30 °C / 30 % RH and 30 °C / 60 % RH

Formulation	Start	Melting point (peak) [°C]											
		4w											
		20 °C		30 °C		40 °C		30 °C / 30 % RH		30 °C / 60 % RH			
Mean	Stdv	Mean	Stdv	Mean	Stdv	Mean	Stdv	Mean	Stdv	Mean	Stdv		
47	153.6	0.1	152.1	0.7	153.1	3.5	150.8	0.2	150.5	0.0	149.6	0.0	
100	154.1	0.8	153.6	0.0	153.6	0.0	153.6	0.0	152.5	0.0	151.6	0.1	
200	153.1	0.8	155.6	0.0	155.1	0.7	155.6	0.0	154.6	0.1	153.6	0.0	
400	153.5	1.4	156.1	0.7	156.6	0.1	157.1	0.7	157.0	0.7	157.6	1.3	
800	153.5	0.0	156.6	0.1	156.6	0.1	158.1	0.7	157.0	0.7	155.1	0.7	

Table 2.6.18 Melting point (peak) of freeze-dried mannitol-sucrose containing placebo formulations right after the drying process and after 4 weeks closed storage at 30 °C and 40 °C and open storage at 30 °C / 30 % RH and 30 °C / 60 % RH

Formulation	Start	Melting point (peak) [°C]									
		4w									
		30 °C		40 °C		30 °C / 30 % RH		30 °C / 60 % RH			
Mean	Stdv	Mean	Stdv	Mean	Stdv	Mean	Stdv	Mean	Stdv		
47	153.5	0.0	155.0	0.8	156.4	0.0	155.4	0.0	156.5	0.1	
100	151.0	0.7	154.5	0.0	157.5	0.1	156.4	0.0	156.5	0.1	
200	151.1	2.2	157.5	0.0	158.5	0.1	157.5	0.0	156.4	0.0	
400	154.1	0.8	155.0	0.7	158.5	0.1	157.9	2.1	156.5	0.1	
800	155.5	2.8	156.9	0.7	157.0	0.7	157.4	0.0	157.4	1.4	

Table 2.6.19 Melting point (peak) of freeze-dried mannitol-sucrose containing gelatin nanoparticle (verum) formulations after 10 weeks closed storage at 30 °C and 40 °C and open storage at 30 °C / 30 % RH and 30 °C / 60 % RH

Formulation	Melting point (peak) [°C]							
	10w							
	30 °C		40 °C		30 °C / 30 % RH		30 °C / 60 % RH	
Mean	Stdv	Mean	Stdv	Mean	Stdv	Mean	Stdv	
47	150.5	0.0	150.6	0.0	149.5	0.0	149.5	0.0
100	152.6	0.1	152.6	0.1	152.5	0.0	152.5	0.0
200	155.0	0.7	155.1	0.6	154.5	1.4	153.5	0.0
400	156.6	0.1	158.1	0.8	155.5	1.4	156.0	0.7
800	156.6	0.1	156.1	0.6	156.5	0.0	155.0	0.7

2.6.2 Stability data of oligonucleotide-loaded gelatin nanoparticles

Photon correlation spectroscopy (PCS) data

Table 2.6.20 Size and polydispersity indices of oligonucleotide-loaded gelatin nanoparticles before freeze-drying and rehydrated right after freeze-drying

Formulation	Size [nm]				PDI				
	Before		After		Before		After		
	Mean	Stdv	Mean	Stdv	Mean	Stdv	Mean	Stdv	
200	Sucrose	286.3	1.5	276.0	19.8	0.184	0.022	0.103	0.033
	Trehalose	297.7	9.0	263.3	1.5	0.245	0.110	0.094	0.023
	Mannitol	298.7	32.5	253.0	6.2	0.227	0.112	0.110	0.006
	Man-Suc	349.0	41.1	329.0	6.0	0.210	0.051	0.140	0.020

Table 2.6.21 Size of freeze-dried oligonucleotide-loaded gelatin nanoparticles rehydrated after 4 weeks closed storage at 30 °C and 40 °C and open storage at 30 °C / 30 % RH and 30 °C / 60 % RH

Formulation	Size [nm]								
	4w 30 °C		4w 40 °C		4w 30 °C / 30 % RH		4w 30 °C / 60 % RH		
	Mean	Stdv	Mean	Stdv	Mean	Stdv	Mean	Stdv	
200	Sucrose	257.3	1.5	273.0	4.9	312.3	12.9	456.0	86.3
	Trehalose	267.7	2.1	270.0	1.7	270.7	3.1	n/a	n/a
	Mannitol	378.7	9.1	548.3	42.6	404.7	33.0	962.7	124.3
	Man-Suc	380.7	7.5	769.7	116.4	493.3	29.4	1800.0	631.0

Table 2.6.22 Polydispersity indices of freeze-dried oligonucleotide-loaded gelatin nanoparticles rehydrated after 4 weeks closed storage at 30 °C and 40 °C and open storage at 30 °C / 30 % RH and 30 °C / 60 % RH

Formulation	PDI								
	4w 30 °C		4w 40 °C		4w 30 °C / 30 % RH		4w 30 °C / 60 % RH		
	Mean	Stdv	Mean	Stdv	Mean	Stdv	Mean	Stdv	
200	Sucrose	0.090	0.012	0.142	0.048	0.277	0.061	0.604	0.028
	Trehalose	0.136	0.025	0.140	0.011	0.158	0.018	n/a	n/a
	Mannitol	0.384	0.009	0.546	0.022	0.439	0.074	0.834	0.022
	Man-Suc	0.311	0.022	0.602	0.118	0.433	0.055	0.950	0.087

CHAPTER III

Gelatin Nanoparticles for Targeted Oligonucleotide Delivery to Kupffer Cells During Hepatic Ischemia Reperfusion (I/R) Injury

Abstract

Hepatic ischemia reperfusion injury is a common and severe adverse reaction in several clinical situations. Basic understanding of the mechanisms behind led to the assumption of the transcription factor NF- κ B released in Kupffer cells playing a central role in the inflammatory cascade finally causing loss of liver tissue. The aim of the present work was to provide the basis for further elucidation of the processes related to NF- κ B activation. Therefore a selective Kupffer cell targeting of an NF- κ B inhibiting decoy oligonucleotide was proposed as pharmacological intervention facilitated by a nanoparticulate drug carrier system based on gelatin in a warm hepatic I/R injury rat model. During initial studies the exclusive Kupffer cell uptake of NF- κ B decoy oligonucleotide-loaded gelatin nanoparticles within liver was proven. The evaluation of plasma protein adsorption patterns conducted in comparison to solid lipid nanoparticles via 2D-PAGE analysis could contribute to the explanation of these data and compared to liposomes a superior Kupffer cell selectivity can be stated for gelatin nanoparticles. In the following the successful inhibition of NF- κ B with NF- κ B decoy oligonucleotide-loaded gelatin nanoparticles in the rat model could be demonstrated in a concentration dependent manner. Based on the established model future work can now be accomplished in terms of clarifying the role of NF- κ B in the course of hepatic ischemia reperfusion injury.

Keywords: Hepatic I/R injury, NF- κ B, drug targeting, gelatin nanoparticles, decoy

3.1 Introduction

Interruption of blood flow to an organ or tissue (ischemia) and subsequent reperfusion lead to an acute inflammatory response that may cause significant cellular damage and organ dysfunction. This phenomenon is named as ischemia reperfusion (IR) injury.

The clinical relevance of this disease for the liver and liver transplantation respectively was already described in 1975. But the term “Hepatic Ischemia Reperfusion Injury” became widely accepted among experts not until the 1980s. Depending on external circumstances two types of hepatic IR injury are differentiated. Together with surgical interventions, liver transplantations, hemorrhagic shock, toxic or vein occlusive events, and the Budd-Chiari syndrome the so called warm hepatic ischemia reperfusion injury (warm I/R) occurs. Resulting from preservation conditions during transport of the removed organ or storage during transplantation, the occurrence of the so called cold hepatic ischemia reperfusion injury (cold I/R) is also possible during liver transplantation. Both share the basic pathophysiological mechanism but there are as well clear differences [Teoh et al., 2003a]. Consequences of hepatic ischemia reperfusion injury include liver failure and in more severe cases liver failure in association with remote organ failure, both with significant rates of morbidity and mortality [Lentsch et al., 2000].

The aim of the presented work was to establish an animal model enabling the demonstration of an effective interruption of the inflammatory cascade during hepatic I/R injury. In terms of a drug targeting approach the application of a nanoparticulate drug delivery system should be the therapeutical basis. To keep the long term perspective of investigating the newly developed system in a clinical trial, it was decided to focus on a model based on warm ischemia reperfusion injury. Mechanisms on cellular and subcellular stage leading to ischemia reperfusion injury are very complex and there is still a need to better understand the pathophysiology [Jaeschke, 2003]. In the following these processes are therefore only explained in brief, while the pathophysiological quintessences and the resulting targets are elucidated in detail.

The work was part of a DFG funded cooperation (subproject C, research group FOR 440) between the chairs of pharmaceutical biology (Prof. A. Vollmar / PD Dr.

S. Zahler / Ph.D. student Florian Hoffmann) and pharmaceutical technology (Prof. G. Winter / Dr. C. Coester / Ph.D. student Jan C. Zillies) of the Ludwig-Maximilians-University Munich, Germany. The obtained data are a result of the close collaboration between the author and Florian Hoffmann and are accordingly denoted.

3.1.1 Anatomic fundamentals

The liver is composed of two major groups of cells, the parenchymal and the non-parenchymal cells. The parenchymal cells are the so called hepatocytes that maintain the metabolic function of the liver. They account for 65% of all liver cells and above 90% of the entire liver mass. Kupffer cells, endothelial cells, and Ito cells (fat storing cells) form the non-parenchymal part of the liver tissue. The Kupffer cells are part of the mononuclear phagocytosis system (MPS) and are the largest single population of macrophages in body. They originate from stem cells of the bone marrow and are embedded into the capillaries (sinusoids) of the liver after transformation into tissue macrophages. The Kupffer Cells account for 15% of all liver cells but only for 3% of the entire liver mass [Ponnappa et al., 2002; Löffler et al., 2003b].

Liver blood supply is sustained by Arteria hepatica (liver artery), feeding oxygen rich blood and Vena portae (portal vein) feeding venous blood carrying the metabolic products from stomach and intestine. Despite this twofold blood supply and the possibility of an anaerobic metabolism hypoxic damage of the liver may occur [Ponnappa et al., 2002; Mutschler, 2003; Teoh et al., 2003a].

The macroscopic view shows the four different sized lobes of the liver: two big ones, the larger right lobe (Lobus dexter) and the smaller left lobe (Lobus sinister) separated by the peritoneal duplication and two minor lobes (Lobus caudatus and Lobus quadratus). In addition the liver is divided in “Partes” and Divisiones”. This classification derives from the branching of A. hepatica, V. portae, and Ductus hepaticus. They are separated by externally invisible fissures [Sobotta, 1999].

The hepatic lobules are the units the liver is made of on the microscopic stage. The human liver consists of approximately 500,000 of these hexagonal appearing 1-2 mm in diameter sized lobules. The above mentioned parenchymal and non-parenchymal cells are the basic modules of this system. The hepatocytes within the particular lobules are radially arranged around a central vein (Vena centralis) and

build a three dimensional network (liver parenchyma) permeated by an as well radially arranged capillary network (sinusoids). The non-parenchymal cell types are preferentially located along the sinusoids being in close anatomical and functional relationship with the parenchymal cells. The endothelial cells cover the sinusoids at the inner wall and form an open work endothelium, the endothelial fenestrae measuring 150 – 175 nm in diameter [Braet et al., 2002]. The Kupffer cells adhere at the walls of the sinusoid too. But they are able to detach from the united cell structure after a rounding and circulate afterwards with the blood stream. The Ito cells are tightly associated with the hepatocytes, in addition they form cytoplasmic extensions wrapped around the endothelium of the sinusoids. They are located in the Disse's space, a small fissure that separates the walls of the endothelium from the hepatocytes. The hepatocytes bear so called microvilli at their surface extending into the Disse's space. This layout allows an intensive exchange between the capillaries of the lobules and the hepatocytes [Löffler et al., 2003b]. According to their function the hepatocytes contain many mitochondria with a broad spectrum of metabolic enzymes [Thews et al., 1999].

3.1.2 Pathophysiological mechanisms

Consequences of ischemia and reperfusion can not be definitely attributed to one of these two events; in fact the changes caused by the hypoxic state during ischemia predispose to the later reoxygenation injury [Li et al., 2002].

Hypoxia alters enzyme activities and mitochondrial functions and affects the structure of the cytoskeleton, the membrane transport and antioxidant defenses. Thus the activity of the mitochondrial cytochrome oxidase is reduced, whereby an electron acceptor is missing that leads to enhanced production of reactive oxygen species (ROS). ROS in turn cause the oxidative inhibition of the Na⁺-K⁺-ATPase which is among other things responsible for swelling and subsequent cytolysis during reoxygenation [Li et al., 2002]. The processes taking place during ischemia are thus not the direct reason for I/R injury but part of the triggering of the pathophysiological mechanisms that are activated with reperfusion. There are two distinct phases of liver injury after warm I/R. The initial or early phase (< 2 h after reperfusion) is characterized by the production of ROS, the late phase (6-48 h after reperfusion) by inflammatory events mediated by neutrophils [Lentsch et al., 2000; Teoh et al.,

2003a]. Figure 3.1.1 shows the cascade of early and late phase of liver injury. By reperfusion endothelial cells and Kupffer cells as well as complement are activated (1). Within the Kupffer cells ROS are produced in the following in a mainly NADPH-Oxidase mediated process (2). This again activates endothelial cells (5) and leads to the release of several cytokines (7, 10) and chemokines (8) via the transcription factor NF- κ B (4). Besides inducible nitric oxide synthase (iNOS) is expressed in the different liver cell types (9). It is discussed whether this disturbs via the increased nitric oxide (NO) production the equilibrium between the vasodilator NO and the, at the same time released, vasoconstrictor endothelin (ET). This imbalance would lead to a failure of the microcirculation (9a) and finally contribute to I/R injury [Teoh et al., 2003a]. As the vasodilatory properties of NO and its influence on neutrophils can positively affect the course of I/R, amount and origin of released NO have to be taken into consideration.

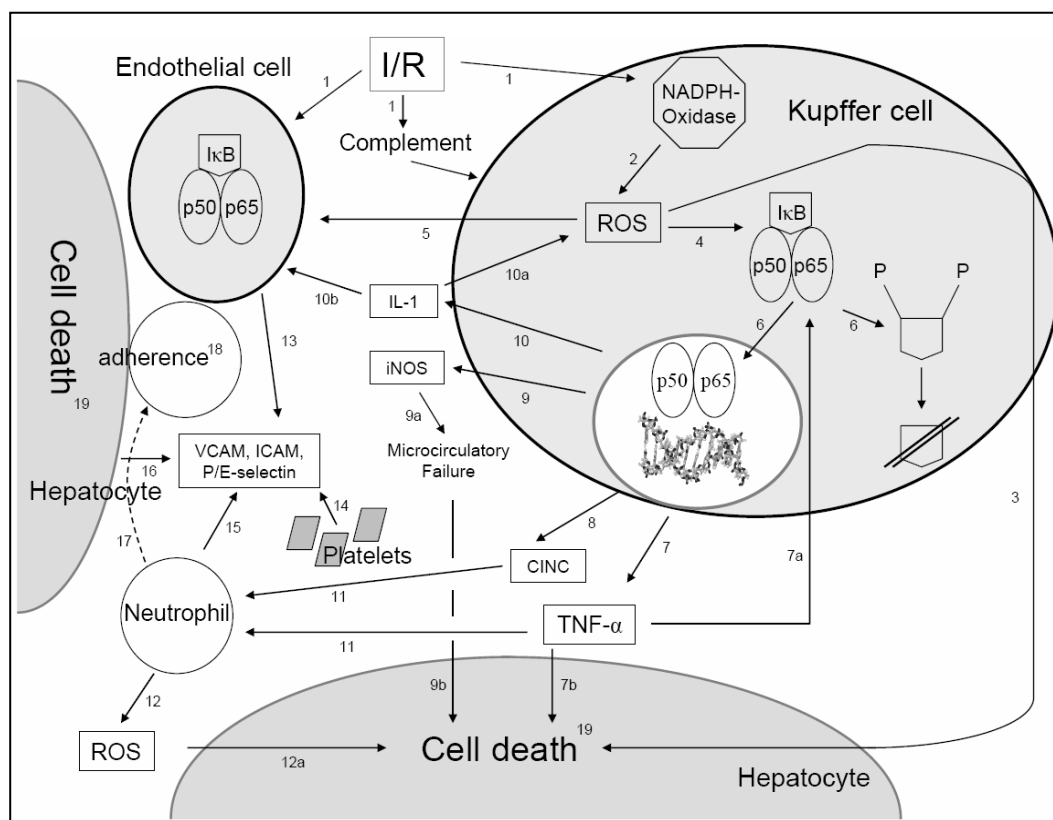


Figure 3.1.1 Pathophysiological mechanism of early and late phase of hepatic I/R injury [modified after Lentsch et al., 2000; Jaeschke, 2003; Teoh et al., 2003a]

NO produced by the constitutive present endothelial NO-synthase (eNOS) has a positive influence while guaranteeing the blood circulation of the liver whereas an

exaggerated iNOS mediated NO production has a negative effect caused by the enhanced formation of peroxynitrite [Jaeschke, 2003]. NF- κ B is an inducible transcription factor, located in its inactivated state in the cytosol while being complexed with inhibitory κ B (I κ B). The NF- κ B transcription factor family comprises the proteins p50, p52, p65 (RelA), c-Rel, and RelB. The activated state of NF- κ B is in general a heterodimer of the subunits p50 and p65 [Zwacka et al., 1998]. But depending on the particular cell type homodimers and further heterodimers are known. In general driven by prime pathogenous stimuli like physical or chemical stress as well as viruses and bacteria or cytokines I κ B is rapidly phosphorylated at serine residues 32 and 36. Afterwards it is ubiquitinated and ultimately degraded by proteolytic cleavage (6). At the same time NF- κ B is released and binds after translocation into the nucleus (6) to its recognition (consensus) sequence within the genome where it regulates the transcription of various genes. Different consensus sequences are thereby described in literature followed from the composition of the NF- κ B dimers [Chen et al., 1999; Löffler et al., 2003a]. Additionally, during I/R NF- κ B activation independent from I κ B degradation based on a tyrosine phosphorylation is known to be a likely pathway [Zwacka et al., 1998].

The release of cyto- and chemokines marks the change from early to late phase of liver injury. Interleukin 1 (IL-1) fosters further production of ROS in terms of a positive feedback (10a) and contributes to the activation of endothelial cells (10b). The activation of neutrophils results from TNF α and CINC (cytokine induced neutrophil chemoattractant) (11), a very potent chemotactic chemokine [Teoh et al., 2003a]. TNF α itself is as well part of a positive feedback loop (7a) and neutrophils also induce ROS production (12). Endothelial cells, hepatocytes, platelets, and neutrophils express adhesion molecules and selectins (13-16) that initially mediate the adsorption (17) and later the transmigration (18) of neutrophils at the endothelium and into the liver parenchyma respectively. P- and E-selectin are surface glycoproteins that are responsible for interception and adhesion of circulation neutrophils. The adhesion molecules VCAM (vascular cell adhesion molecule) and ICAM (intracellular adhesion molecule) are members of the immunoglobulin superfamily. They are expressed on the surface of endothelial cells and provide a firm binding of at first slightly adhered neutrophils at the endothelium. Thus they

allow a subsequent immigration of neutrophils to the site of inflammation [Jaeschke, 2003; Teoh et al., 2003a].

In sum the coaction of the various described mechanisms, the formation of ROS (3, 12a) and TNF α , the microcirculatory failure (9b) as well as the neutrophil mediated inflammatory processes finally cause the destruction of liver tissue (19). Attributing cell death to the mode of apoptosis or necrosis is thereby still controversially discussed in literature [Gujral et al., 2001; Kim et al., 2003; Meguro et al., 2003; Vilatoba et al., 2005].

3.1.3 Therapeutic options

To minimize the loss of blood during surgical interventions at the liver e.g., after severe traumata or during liver transplantation, it is necessary to interrupt the blood supply of parts of the organ or the organ in total for a certain period of time. The concurrent clamping of Arteria hepatica and Vena portae, known as Pringle maneuver, is still widely used to completely interrupt the blood flow through the liver. The main disadvantage is the often appearing warm I/R injury followed from the transient hypoxia.

To reduce or to exclude the post surgical liver injury one tries to improve the surgical options on the one hand and to selectively interact with the above described pathophysiological cascade on the other hand.

Surgical options

Aim of the surgical options is the increasing abdication of the Pringle maneuver with its long lasting organ wide ischemic period. This is feasible by clamping single arterial branches, prevention of bleeding by coagulating injured blood vessels with an argon laser, or the application of supersonic assisted tissue sections [Lentsch et al., 2000; Teoh et al., 2003a].

Interruption of pathophysiological signal transduction pathways

Hepatic preconditioning The concept of ischemic preconditioning is based on the biological principle that tissue primed by various types of sublethal stress develops tolerance to subsequent lethal injury [Kang, 2002].

During ischemic preconditioning liver is exposed to short intervals (5-10 min) of ischemia and reperfusion, whereby negative consequences of warm I/R can be clearly reduced. The underlying mechanisms of the protective effect are so far not completely understood, altered TNF α release, involvement of adenosine A₂ receptors and NO, maintenance of the microcirculation as well as an enhanced cytoprotection mediated by an accelerated entrance into cell cycle are discussed in literature [Lentsch et al., 2000; Kang, 2002; Koti et al., 2003; Teoh et al., 2003a; Teoh et al., 2003b].

Aside it is reported about positive effects towards oxidative stress caused by Kupffer cells that were activated by hormonal preconditioning with atrial natriuretic peptide (ANP) [Bilzer et al., 2000; Kang, 2002].

Pharmacological interventions There are certain clinical situations e.g., acute liver traumata, where a time frame for preventive strategies as described above is not given. In these cases pharmacotherapeutic approaches are necessary to attenuate or to avoid hepatic I/R injury. The application of particular pharmaceuticals may be carried out before or during ischemia and reperfusion. The first is described as pharmacological preconditioning [Kang, 2002].

Arising from the numerous illustrated factors leading to liver injury (chapter 3.1.2) several points of attack are imaginable based on antioxidative strategies, genterapeutical approaches, receptor blockade, and anti-inflammatory or immunosuppressive mediators.

In the beginning ROS formation plays the main role in the pathological events [Teoh et al., 2003a]. Thus different antioxidative strategies that should diminish the outcome of the excessive ROS production are described in this context. Apart from the application of antioxidative active low molecular weight substances like vitamin E [Serracino-Inglott et al., 2001; Jaeschke, 2002] or the endogenous glutathione [Bilzer et al., 2000; Kang, 2002], the reduction of ROS is aimed for by the administration of enzymes. From initially built peroxides superoxide anions are produced within hepatocyte mitochondria which in turn are degraded by the superoxide dismutase (SOD). This rapidly proceeding reaction circumvents the oxidation of NO to peroxynitrite explaining the cytoprotective effect of SOD [Jaeschke, 2002]. Beside the direct administration of the modified enzyme [Yabe et

al., 2001] a combined gene therapeutic and antioxidative approach is described. To amplify the enzymatic potency its gene is transferred into hepatocytes via an adenoviral vector where it is subsequently expressed [Jaeschke, 2002]. A further adenoviral mediated gene expression is utilized for the application of hemoxygenase (HO). As oxidative events foster the natural transcription of HO an advanced protection from ischemia induced oxidative stress by an enhanced HO expression is suggested which could already be proven in several models [Fondevila et al., 2003].

Within the inflammatory cascade activation of Kupffer cells play the main role. In an animal model it could be shown that a gadolinium chloride induced suppression of Kupffer cell activity lead to an attenuated hepatic I/R injury [Mosher et al., 2001; Giakoustidis et al., 2003]. Augmentation of Kupffer cell activity by latex beads in comparison worsens the state of the liver after ischemia and reperfusion [Shiratori et al., 1994]. Modulation of Kupffer cell activity and therefore the impact on numerous released inflammatory mediators is thus a potential target for pharmacotherapeutical interventions [Mosher et al., 2001]. So it could be shown that blocking TNF α and IL-1 as well as subsequent mediators like VCAM or certain chemokines clearly reduce hepatic I/R injury [Lentsch et al., 2000]. Most of the mentioned proinflammatory mediators have the regulation of their transcription via the inducible transcription factor NF- κ B in common [Morishita et al., 1998; Serracino-Inglott et al., 2001]. This is crucial for the inflammatory processes followed from Kupffer cell activation and has to be taken into consideration as potential target during anti-inflammatory therapy [Banafsche et al., 2001].

A further point of attack within the pathophysiological mechanism of I/R injury is the maintenance of the microcirculation. Microcirculation is controlled by the interaction of the functional antagonists' nitric oxide and endothelin as described in chapter 3.1.2. The administration of exogenous nitric oxide via an NO donor (FK 409) improves the hepatic microcirculation, suppresses the production of endogenous NO and therewith the formation of peroxynitrite as well as the activation of neutrophils [Nozaki et al., 2003]. On the other hand endothelin receptor antagonists and inhibitors of the endothelin converting enzyme also contribute to an improved microcirculation after ischemia and reperfusion [Ricciardi et al., 2001; Uhlmann et al., 2001; Witzigmann et al., 2002].

Further more it was reported about hepatoprotective effects against ischemia and reperfusion for the immunosuppressive substances azathioprine and cyclosporine as well as tacrolimus (FK 506) proved in transplantation-medicine [Kawano et al., 1993; Baron et al., 2002].

3.1.4 Therapeutic strategy – Gelatin nanoparticles for targeted delivery of an NF- κ B decoy oligonucleotide to Kupffer cells

Due to the central function NF- κ B takes within the mechanisms leading to hepatic I/R injury, the inhibition of the NF- κ B controlled proinflammatory mediator release in Kupffer cells was chosen as target. But, the role NF- κ B plays in the liver is ambivalent. Besides the described contribution to hepatic I/R injury there is a protective effect known. Subsequent to liver transplantation it helps to regenerate liver tissue and leads to a reduced apoptosis of hepatocytes. Thus if NF- κ B activation is unselectively eliminated in each of the liver cell types an increased rate of apoptosis would be the outcome, finally damaging liver tissue [Lentsch et al., 2000]. This double role causes the need for the intended inhibition of NF- κ B to be limited to the Kupffer cells [Banafsche et al., 2001]. Kupffer cells are the resident macrophages of the liver and part of the MPS (chapter 3.1.1). Due to their strategic position inside the sinusoids Kupffer cells are the first within the group of macrophages that encounter foreign material entering the circulation via the portal vein [Ponnappa et al., 2002]. Thus they strongly influence bioavailability and biodistribution of colloidal drug carrier systems [Kreuter, 1983; Kreuter, 1992; Thews et al., 1999] as they recognize and phagocyte colloidal structures like liposomes and nanoparticles due to the rapid opsonization immediately occurring after application [Yan et al., 2005; Owens et al., 2006]. To invert this drawback of resulting low plasma half lives that minimizes most therapeutic effects to a selective Kupffer cell targeting is the basic idea behind the therapeutical approach it is aimed at. A successful Kupffer cell targeting was already shown for oligonucleotides incorporated in anionic and cationic (HVJ-) liposomes [Ponnappa et al., 2002; Yoshida et al., 2002] as well as poly(isobutylcyanoacrylate) nanoparticles and low density lipoprotein (LDL) bound oligonucleotides [Nakada et al., 1996; Bijsterbosch et al., 2001]. Here, gelatin nanoparticles were chosen as vehicle for the targeted delivery to the Kupffer cells of the liver.

Active principle of the therapeutical approach is to inhibit the NF- κ B controlled release of proinflammatory mediators using a decoy strategy. Decoys are single- or doublestranded DNA oligonucleotides (ODNs) whose base sequences are identical with the consensus sequence of a particular transcription factor. To circumvent fast enzymatic degradation by nucleases *in vivo* these oligonucleotides can be substituted by so called phosphorothioates, DNA analogues comprising sulphur instead of non-bridging oxygen in the phosphodiester backbone [Agrawal et al., 2000]. Figure 3.1.2 shows the mechanism of the decoy induced transcription factor blockade.

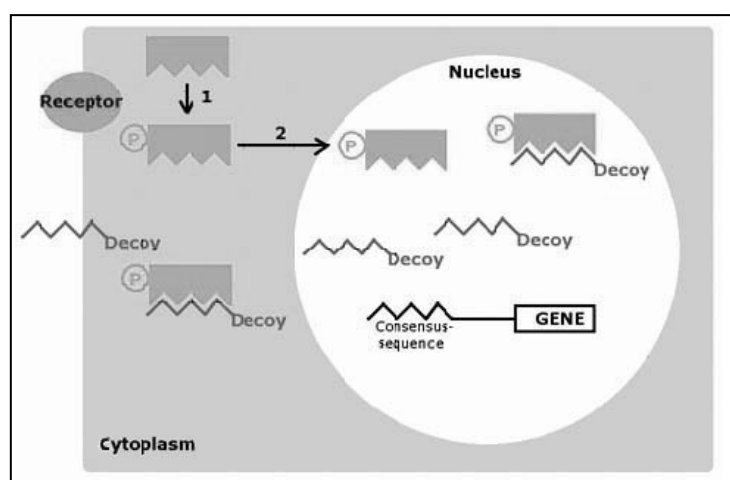


Figure 3.1.2 Mechanism of the decoy effect

Triggered by an exogenous stimulus receptor mediated transcription factor activation (1) is followed from its translocation into the nucleus (2). But, in the presence of a decoy the subsequent transcription factor binding to its respective consensus sequence is stopped. Instead a bonding is formed between the transcription factor and the consensus sequence within the decoy oligonucleotide, whereby the transcription factor is not able to maintain its regulatory function for gene expression. The described reaction between decoy oligonucleotide and transcription factor already occurs in the cytoplasm directly after activation of the transcription factor (1) and without the necessity of a previous translocation into the nucleus. A successful inhibition of an NF- κ B induced mediator release could be proven for single stranded [Tan et al., 2002] as well as double stranded [Ogushi et al., 2003] decoy oligonucleotides. Since the utilized consensus sequences clearly vary and there are several NF- κ B consensus sequences described in literature as already indicated in chapter 3.1.2 it makes it difficult to focus on “the one” sequence.

Based on promising results obtained during former experiments of some members of our research group [Kupatt et al., 1999] it was decided to apply a double stranded phosphorothioate (PTO) oligonucleotide bearing the following NF- κ B consensus sequence for the present work:

5'-AGT TGA GGG GAC TTT CCC AGG C-3'

A phosphorothioate oligonucleotide was chosen as those ODNs exhibit an improved stability against enzymatic degradation, which is due to substitution of a non-bridging oxygen atom with a sulphur atom in the nucleic acid backbone [Ciafre et al., 1995].

3.2 Proof of Principle – Kupffer Cell Targeting

Before any effect, induced by delivery of the NF- κ B decoy oligonucleotide, could be interpreted it had to be ensured that this effect is related to the selective inhibition of NF- κ B within Kupffer cells. For this reason the solely Kupffer cell targeting of gelatin nanoparticles had to be proven at first. For this purpose biodistribution studies in rats were accomplished with fluorescent-labeled gelatin nanoparticles. Rats were chosen for the later establishing of the hepatic I/R model as there was already certain experience existing in the work with them and as the size of liver and other organs offer a simplified handling esp. in comparison with mice. Thus biodistribution data were as well acquired from studies conducted in rats.

3.2.1 Materials and methods

Reagents

Reagent	Description	Supplier
Acetone	p.a.	VWR International GmbH (Ismaning, Germany)
Cholaminechloride hydrochloride	(2-aminoethyl)-trimethyl-ammoniumchloride hydrochloride	Sigma-Aldrich GmbH (Taufkirchen, Germany)
EDC	1-ethyl-3-(3-dimethyl-aminopropyl) carbodiimide hydrochloride	Sigma-Aldrich GmbH (Taufkirchen, Germany)
Gelatin type A	175 Bloom	Sigma-Aldrich GmbH (Taufkirchen, Germany)
Glutaraldehyde	25 % aqueous solution	Sigma-Aldrich GmbH (Taufkirchen, Germany)
HCl	2 N	VWR International GmbH (Ismaning, Germany)
PBS	Dulbecco's phosphate buffered saline pH 7.4 (1x concentrate)	PAA Laboratories GmbH (Linz, Austria)

Cell culture

Reagent	Description	Supplier
Collagenase H		Roche Diagnostics (Mannheim, Germany)
DMEM	Dulbecco's modified eagle medium pH 7.0-7.5	Cambrex Profarmaco Landen Landen, Belgium
FBS	fetal bovine serum	PAA Laboratories GmbH (Linz, Austria)
Formalin solution	neutral buffered, 10 %	Sigma-Aldrich GmbH (Taufkirchen, Germany)
L-Glutamine solution	200 mM	Cambrex Profarmaco Landen Landen, Belgium
Penicillin/Streptomycin (Pen/Strep) solution	100x concentrate	PAA Laboratories GmbH (Linz, Austria)
Trypsin solution	1x concentrate	PAA Laboratories GmbH (Linz, Austria)

Fluorescent staining

Reagent	Description	Supplier
Alexa Fluor [®] 488 goat- anti-mouse IgG ₁ (γ_1)	λ_{em} 519 nm	Invitrogen GmbH (Karlsruhe, Germany)
BSA	bovine serum albumin, Cohn Fraction V	Sigma-Aldrich GmbH (Taufkirchen, Germany)
ds NF- κ B decoy ODN ₄₈₈	5'-AGT TGA GGG GAC TTT CCC AGG C-3' 5' Alexa Fluor [®] 488 labeled, λ_{em} 519 nm, phosphorothioate	biomers.net GmbH (Ulm, Germany)
Hoechst 33342	trihydrochloride, trihydrate, λ_{em} 461 nm	Invitrogen GmbH (Karlsruhe, Germany)
Mouse-anti-rat CD163 IgG ₁		AbD Serotec GmbH (Duesseldorf, Germany)
Permafluor	aqueous mounting medium	Beckmann Coulter GmbH (Krefeld, Germany)

Reagent	Description	Supplier
Texas Red [®] sulfonyl chloride	mixed isomers, λ_{em} 615 nm	Invitrogen GmbH (Karlsruhe, Germany)
Triton [®] X-100		Sigma-Aldrich GmbH (Taufkirchen, Germany)
Vybrant [™] DiD cell labeling solution	λ_{em} 665 nm	Invitrogen GmbH (Karlsruhe, Germany)

Solutions

Solution	Components*	Concentration
Buffer A (pH 7.35)	NaCl	115 mM
	NaHCO ₃	25 mM
	KCl	5.9 mM
	MgCl ₂	1.18 mM
	NaH ₂ PO ₄	1.23 mM
	Na ₂ SO ₄	1.2 mM
	CaCl ₂	2.5 mM
	Hepes	20 mM
Medium A	DMEM	83 % [v/v]
	FBS	15 % [v/v]
	Glutamin sol.	1 % [v/v]
	Pen/Strep sol.	1 % [v/v]
Medium B	DMEM	84 % [v/v]
	FBS	15 % [v/v]
	Glutamin sol.	1 % [v/v]

*All buffer salts were purchased from Sigma-Aldrich GmbH (Taufkirchen, Germany)

Preparation and surface modification of gelatin nanoparticles

Gelatin nanoparticles were manufactured by the two step desolvation method and surface modified (cationized) with cholamine as described in chapter 1.2.

Preparation of fluorescent cationic gelatin nanoparticles

Fluorescent-labeled gelatin nanoparticles were prepared by covalent coupling of the gelatin base material with an amino reactive fluorescent dye. After the first desolvation step the remaining gelatine sediment was dissolved in 25 mL of water under constant stirring (500 U/min) and heating up to 50 °C. 1 mg of the fluorescent dye (Texas Red[®]) was added to this solution after dissolving in acetone and the mixture was constantly stirred for 1 h (500 U/min) at 50 °C. After this incubation period the regular gelatin nanoparticle manufacturing process was continued with the second desolvation step. Subsequent to purification cationization was conducted as usual (chapter 1.2).

Oligonucleotide-loading of gelatin nanoparticles

540 µL of an aqueous nanoparticle dispersion containing 3.6 mg surface modified fluorescent gelatin nanoparticles was incubated with 120 µL of an aqueous oligonucleotide solution containing 6 nmol NF-κB decoy ODN₄₈₈ (i.e., 2.5 % [w/w] drug loading) in PBS adjusted to a final volume of 1,200 µL for 2 h at 22 °C and 800 rpm under constant shaking (Thermomixer Comfort, Eppendorf AG, Hamburg, Germany).

Characterization of nanoparticles

Size and zeta potential of the gelatin nanoparticle batches were determined by dynamic light scattering (DLS) using a Zetasizer 3000 HSA (Malvern Instruments, Worcestershire, UK). Zeta potential measurements were conducted under standardized ionic conditions in 10 mM NaCl at pH 7.0.

Isolation and purification of Kupffer cells

Initially rat livers were digested by rinsing with 80 mg of Collagenase in 100 mL buffer A. Subsequently, livers were resected and stored in 100 mL ice cold PBS (1x). After gentle mincing and filtration (150 µm mesh) hepatocytes were separated from non parenchymal cells (cp. chapter 3.1.1) by centrifugation for 5 min at 50 g and 4 °C. Remaining supernatant was centrifuged for 10 min at 500 g and the pellet was resuspended in 40 mL medium A. The resulting suspension was transferred to a cell culture vessel to allow cells to adhere for 1 h at 37 °C in an incubator. Afterwards endothelial cells were removed by adding 7 mL of trypsin solution. Remaining

Kupffer cells were washed with medium A, suspended by scraping and centrifuged for 10 min at 500 g. Finally 15 mL of medium were added; cells were resuspended and cultivated in cell culture vessels.

Kupffer cell uptake studies

At first cover slips were placed in each well of 24-well plates. Subsequent 1 mL of a Kupffer cell suspension acquired from isolation process ($\sim 0.3 \times 10^6$ cells/mL) was plated to each well of the prepared well plates. After 1 h of adherence to the cover slips, cells were washed with medium B once and 450 μ L medium B were added. Cells were then incubated with 50 μ L of an NF- κ B decoy ODN₄₈₈ loaded fluorescent gelatin nanoparticle suspension. The final decoy ODN concentration per well was adjusted to 0.5 μ mol/L i.e., 3.7 μ g ODN per well. The according nanoparticle concentration resulting from 2.5 % [m/m] drug loading accounted for 148.4 μ g gelatin nanoparticles per well. After 15 min and 1 h respectively of incubation cells were fixed with 3 % formalin in PBS for 10 min and washed thrice with PBS.

In vivo biodistribution experiments

Experiments were conducted in male Sprague-Dawley rats. Fluorescent-labeled gelatin nanoparticle formulations were prepared in PBS (1 mg/mL) and injected (1 mL) into rat either via the crural vein or directly into the portal vein. Prior to injection rats were anesthetized by i.p. injection of 0.005 mg/kg Fentanyl and 2.0 mg/kg Midazolam. Anesthesia was maintained over the whole experiment with 1.5 % Isofluran continuously applied using a vaporizer with Carbogen (5 % CO₂ / 95 % O₂) as carrier gas. To monitor blood pressure and control anesthesia the jugular artery was cannulated with a 16 gauge PE catheter and connected to a blood-pressure gauge. For intraportal injection the abdomen was opened by midline-laparotomy and the portal triad was prepared. The body temperature was kept between 36.0 °C and 37.0 °C with a warming lamp.

After 1h rats were sacrificed and blood was rinsed out. Brain, heart, kidneys, liver, lungs, parts of femoral muscle, and spleen were resected, frozen with liquid nitrogen and stored at -80 °C. The distribution of nanoparticles into the different organs was determined via confocal laser scanning microscopy (CLSM).

CLSM imaging

Isolated Kupffer cells Subsequent to fixing and washing Kupffer cells were permeabilized for 2 min with 0.2 % Triton[®] X in PBS and washed three times with PBS. Afterwards cells were blocked with 0.2 % BSA in PBS for 10 min and washed another three times with PBS. Nuclear staining was then performed by incubating cells with 10 μ L Hoechst solution (50 μ g/mL) in 500 μ L PBS for 10 min. After washing thrice with PBS cells were incubated with 2.5 μ L Vybrant[™] DiD cell labeling solution in 500 μ L PBS for 10 min to accomplish endosomal membrane staining. Following finally washing for three times with PBS cover slips were taken from well plates and were fixed with Permafluor on a microscopic slide. After storing over night the Kupffer cell preparations were analyzed with a Zeiss LSM 510 Meta confocal laser scanning microscope (Carl Zeiss Microscope Systems, Jena, Germany).

Tissue samples from biodistribution studies 10 μ m thin slices of the frozen organs from the *in vivo* biodistribution experiments were prepared using a HM 500 Kryostat (Microm International AG, Volketswil, Switzerland) and transferred to microscopic slides. After thawing samples were mounted in Permafluor with a cover slip. In addition liver tissue slices were further stained for Kupffer cells prior to mounting. Right after thawing preparations were fixed with 3 % formalin in PBS for 3 min and stored in PBS until staining. For the staining procedure microscopic slides were adjusted in a staining trough. Preparations were initially washed three times for 3 min with PBS, and blocked with 1.0 % BSA in PBS (100 μ L) for 20 min. Subsequent incubation with the primary antibody (mouse-anti-rat CD 163 IgG₁, 1:100) was conducted for 40 min in 100 μ L of 0.2 % BSA in PBS. After a washing step (3x 3 min with PBS) the staining procedure was completed applying a secondary antibody (Alexa Fluor[®] 488 goat-anti-mouse IgG₁, 1:400) in 100 μ L of 0.2 % BSA in PBS for another 40 min. Finally preparations were washed twice for 3 min with PBS and tissue slices were sealed in Permafluor with a cover slip. CLSM imaging was performed with a Zeiss LSM 510 Meta confocal laser scanning microscope (Carl Zeiss Microscope Systems, Jena, Germany).

Kupffer cell isolation, *in vitro* uptake studies, *in vivo* biodistribution studies and fluorescent staining of the obtained cell and tissue samples were conducted together

with Florian Hoffmann at the department of pharmaceutical biology of the Ludwig-Maximilians-University Munich, Germany. So, the present data are a result from the cooperation between the chairs of Pharmaceutical Technology and Pharmaceutical Biology of the Ludwig-Maximilians-University described at the beginning of this chapter and will be discussed under further aspects in the thesis of Florian Hoffmann [Hoffmann, 2007].

3.2.2 Results and discussion

Characterization of nanoparticles

Both fluorescent-labeled nanoparticle formulations applied during biodistribution and cell culture experiments had almost the same size (~270 nm) and the same homogenous size distribution with a PDI around 0.060. Zetapotential values differed due to the conducted surface modification of G-NP_{Tex} 04-024 pos, which was required for oligonucleotide loading. Initially conducted biodistribution experiments focused on the *in vivo* distribution and the selective Kupffer cell uptake of empty and *not* surface-modified gelatin nanoparticles in general. Whether surface modification and oligonucleotide-loading i.e., different surface charges affect biodistribution and phagocytotic uptake by macrophages is discussed in detail in chapter 3.3. The experiments performed with isolated Kupffer cells in turn addressed the intracellular distribution of NF- κ B decoy oligonucleotide loaded gelatin nanoparticles and the intracellular release of the oligonucleotide. The selective Kupffer cell uptake of oligonucleotide loaded gelatin nanoparticles is reviewed in chapter 3.4.

Table 3.2.1 Size, polydispersity, and surface charge of the fluorescent-labeled nanoparticle formulations applied for biodistribution[#] and cell culture experiments[§]

	[#] Fluorescent gelatin nanoparticles (G-NP _{Tex} 04-002)	[§] Surface modified and fluorescent gelatin nanoparticles (G-NP _{Tex} 04-024 pos)
size [nm]	269,8	268.1
PDI	0.056	0.066
ZP [mV]	-3.4	+17.2

Biodistribution of intravenously and intraportally applied gelatin nanoparticles

Based on the knowledge of a suppressed Kupffer cell activity reducing hepatic ischemia reperfusion injury [Mosher et al., 2001; Giakoustidis et al., 2003] and of the role of NF- κ B in the hepatic inflammatory response [Lentsch et al., 2000], we proposed a Kupffer cell targeted delivery of an NF- κ B decoy to positively affect hepatic I/R injury. Thus, it was at first crucial to demonstrate that the chosen drug delivery vehicle i.e., gelatin nanoparticles is selectively taken up by Kupffer cells

after intraportal application, as it can be assumed from former biodistribution studies with colloidal drug delivery systems [Kreuter, 1983]. Therefore slices from deep-frozen organs were prepared for CSLM analysis subsequent to biodistribution studies conducted with fluorescent-labeled gelatin nanoparticles in rat. At first, the impact of the route of administration was explored. Thereby, compared to systemic application a clear liver accumulation of gelatin nanoparticles could be demonstrated after intraportal injection. Figure 3.2.1 shows the nanoparticle distribution after systemic application to the organs of the MPS, liver (A), spleen (B), and lung (C), typically involved in the clearance of particulate matter (cp. chapter 3.3). In addition, none of the gelatin nanoparticles could be detected in kidney.

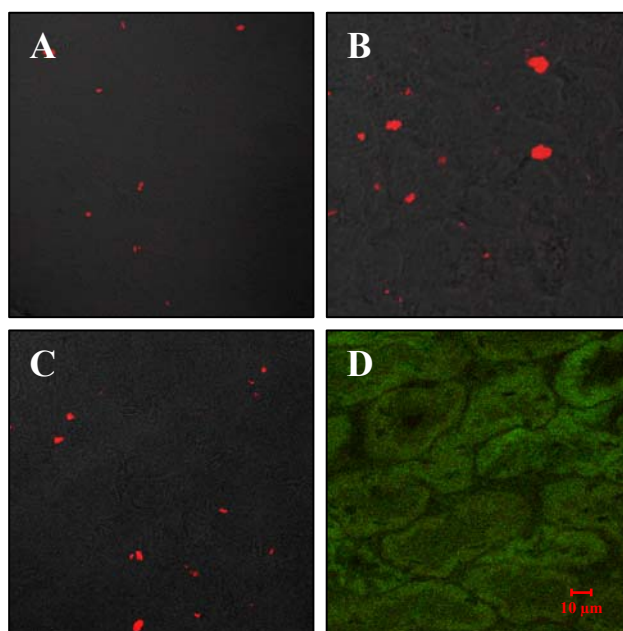


Figure 3.2.1 CLSM pictures of (A) liver, (B) spleen, (C) lung, and (D) kidney taken from organs resected 1 h after injection of G-NP_{Tex} 04-002 (red dots) into the *crural* vein

The resulting pronounced liver accumulation after intraportal application is displayed in Figure 3.2.2. Liver (A) uptake is increased and at the same time fewer nanoparticles could be detected in spleen (B) and lung (C). In kidney, again no nanoparticles were observed. Presumably liver macrophages i.e., Kupffer cells were not able to phagocyte the complete amount of nanoparticles applied as their total amount exceeded the phagocytotic capacity of the Kupffer cells.

As each CLSM image only covers small sections of whole preparations these findings were confirmed by taking a series of pictures both from the same and from different liver tissue slices.

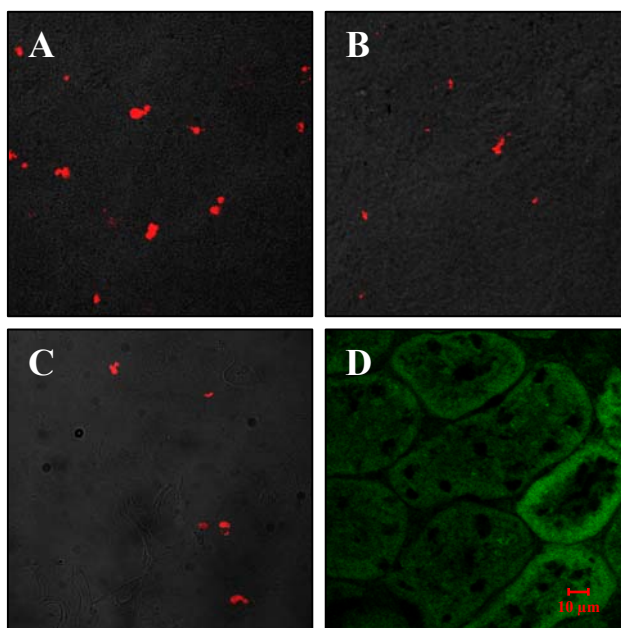


Figure 3.2.2 CLSM pictures of (A) liver, (B) spleen, (C) lung, and (D) kidney taken from organs resected 1 h after injection of G-NP_{Tex} 04-002 (red dots) into the *portal* vein

However, within liver the selective Kupffer cell uptake of gelatin nanoparticles is much more important for the proposed NF- κ B decoy strategy than an exclusive organ distribution to the liver. To prove the intraorgan distribution a Kupffer cell selective fluorescent secondary antibody staining of liver tissue slices was performed for CLSM analysis. The successful staining is shown in Figure 3.2.3 B. The overlay of Kupffer cell (B) and nanoparticle (A) images demonstrates the distinct colocalization of both (Figure 3.2.3 C), which indicates the distribution of gelatin nanoparticles within the liver being confined to Kupffer cells.

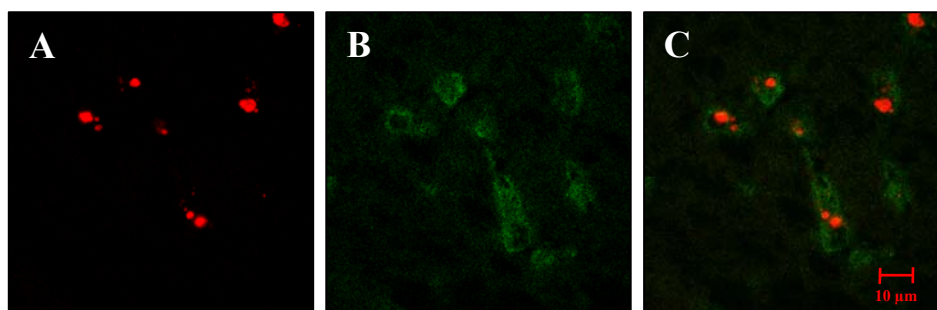


Figure 3.2.3 CLSM pictures of liver tissue taken from liver resected 1 h after injection of G-NP_{Tex} 04-002 into the *portal* vein; pictures show (A) gelatin nanoparticles (red), (B) fluorescently stained Kupffer cells (green), and (C) the overlay of both

Again data were confirmed by taking a series of pictures from the same and from different liver preparations.

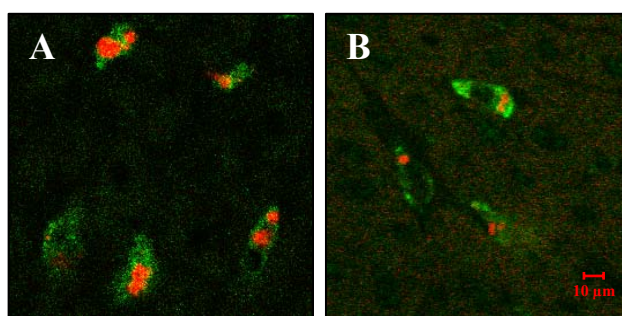


Figure 3.2.4 CLSM pictures of liver tissue taken from liver resected 1 h after injection of G-NP_{Tex} 04-002 into (A) portal vein and (B) crural vein; both pictures show gelatin nanoparticles (red) and fluorescent stained Kupffer cells (green)

Figure 3.2.4 reveals the Kupffer cell accumulation of gelatin nanoparticles after intraportal application in an overlay of nanoparticle and Kupffer cell images. Administering the same amount of nanoparticles either intraportally or systemically, the intensity of the emitted fluorescence of gelatin nanoparticles seen per Kupffer cell is much stronger after intraportal application. In addition to Figure 3.2.1 and Figure 3.2.2 this further clarifies the aspired selective Kupffer cell targeting of gelatin nanoparticles to be feasible.

Intracellular distribution of gelatin nanoparticles in Kupffer cells

Besides the discussed targeting issues the uptake of gelatin nanoparticles loaded with NF- κ B decoy oligonucleotide into Kupffer cells was closer looked at. Thus, Kupffer cells isolated from rat liver were incubated with fluorescent-labeled gelatin nanoparticles loaded with fluorescent-labeled NF- κ B decoy ODN. Loading of G-NP_{Tex} 04-024 pos with the Alexa Fluor[®] 488 labeled ds NF- κ B decoy ODN was successfully conducted in PBS. The applied 2.5 % [w/w] ODN were completely attached onto the surface of the nanoparticles, which could be proven via UV-spectroscopy.

To further describe the intracellular distribution, endosomal membranes were as well stained with a fluorescent dye as the nucleus. In Figure 3.2.5 the single stained elements are summarized (A-D). Pictures E and F show an isolated Kupffer cell and an overly of all taken pictures respectively. From the overlay colocalization of single elements revealing e.g., endosomal uptake or ODN loaded nanoparticles can be derived.

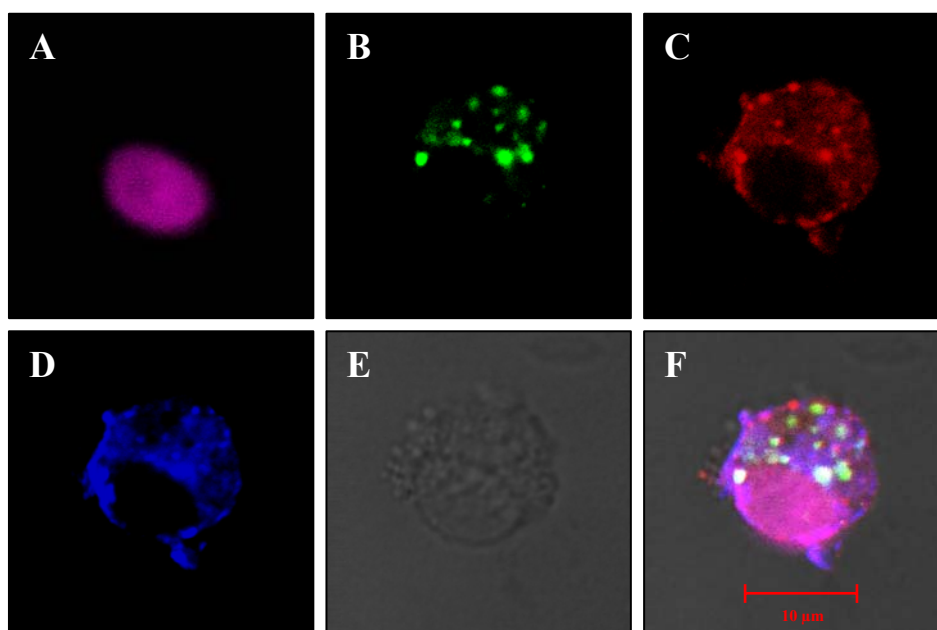


Figure 3.2.5 CLSM pictures of a Kupffer cell taken after 15 min of incubation with ds NF- κ B decoy ODN₄₈₈ loaded G-NP_{Tex} 04-024 pos; pictures show different fluorescent stained structures (A) nucleus (violet), (B) decoy ODN (green), (C) gelatin nanoparticles (red), and (D) endosomal membranes (blue) as well as (E) the isolated Kupffer cell and (F) an overlay of all

To achieve improved visualization and interpretation of these colocalizations selected pictures are chosen for different overlay diagrams in Figure 3.2.6. Picture F_i demonstrates the endosomal uptake of gelatin nanoparticles as the pronounced pink combination color results from the blue endosomal membrane staining and the red nanoparticle staining located at the same position. An endosomal uptake of gelatin nanoparticles is all well described by Zwiorek who successfully addressed the endosomal standing Toll Like Receptor 9 (TLR9) [Zwiorek, 2006]. Basically the cellular uptake of most of the nonviral gene or drug delivery systems follows, according to the current state of knowledge, endocytosis [Wattiaux et al., 2000; Maitra, 2005].

At the same time few extra endosomal appearing nanoparticles can be detected. In picture F_{ii} NF- κ B decoy ODN loaded onto gelatin nanoparticles expressed by the yellow combination color are displayed. Additionally, ODN release from nanoparticles could be observed already after 15 min of incubation with free nanoparticles (red dots) as well as free decoy ODN (green dots) within the cells, which is furthermore substantiated by literature. Arnedo described an immediate release of a single stranded oligonucleotide electrostatically bound onto the surface of albumin nanoparticles under *in vitro* conditions in different buffered release media

[Arnedo et al., 2002]. Under similar conditions the complete release of plasmid DNA from gelatin nanoparticles within 8 h was reported by Kaul [Kaul et al., 2005].

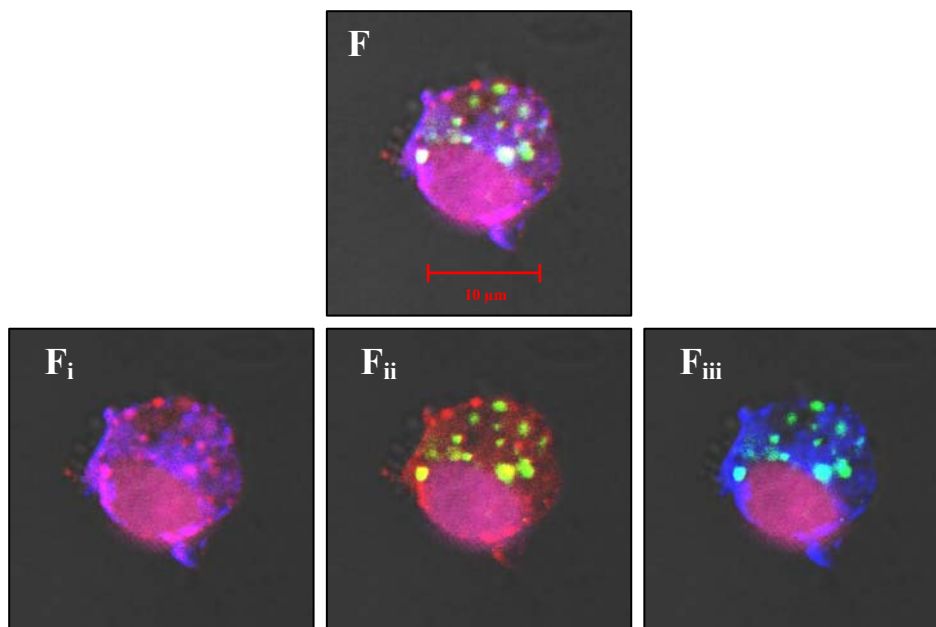


Figure 3.2.6 CLSM pictures of a Kupffer cells taken after 15 min of incubation with ds NF- κ B decoy ODN₄₈₈ loaded G-NP_{Tex} 04-024 pos; pictures show different fluorescent stained structures: (F) nucleus (violet), decoy ODN (green), gelatin nanoparticles (red), and endosomal membranes (blue) (cp. Figure 3.2.5); (F_i) nucleus (violet), gelatin nanoparticles (red), and endosomal membranes (blue); (F_{ii}) nucleus (violet), decoy ODN (green), and endosomal membranes (blue); (F_{iii}) nucleus (violet), decoy ODN (green), and gelatin nanoparticles (red)

In contrast ODN release from complexed protamine oligonucleotide nanoparticles started not until 24 h post administration [Dinauer et al., 2004]. As these data were obtained in a comparable approach applying CLSM analysis of macrophages incubated with fluorescent-labeled protamine and ODN respectively, it reveals general differences in drug release between the delivery of ODN adsorbed onto the surface of nanoparticles or incorporated in a nanoparticulate matrix.

Derived from the pink combination color seen in Figure 3.2.6 F_i nanoparticles were proven to be almost located within endosomes. Thus, decoy oligonucleotide loaded onto their surface is certainly as well colocalized with endosomal structures revealed by an azure combination color in picture F_{iii}. Likewise appearing green dots indicate the presence of some free oligonucleotide outside endosomes. Finally neither nanoparticles nor decoy ODN could be detected in the nucleus, which changes after 2 h of incubating Kupffer cells with oligonucleotide loaded gelatin nanoparticles. Figure 3.2.7 F clearly shows a progression of ODN release, which is

expressed in wider areas of green fluorescence in comparison to the yellow combination color caused by colocalized nanoparticles and oligonucleotide.

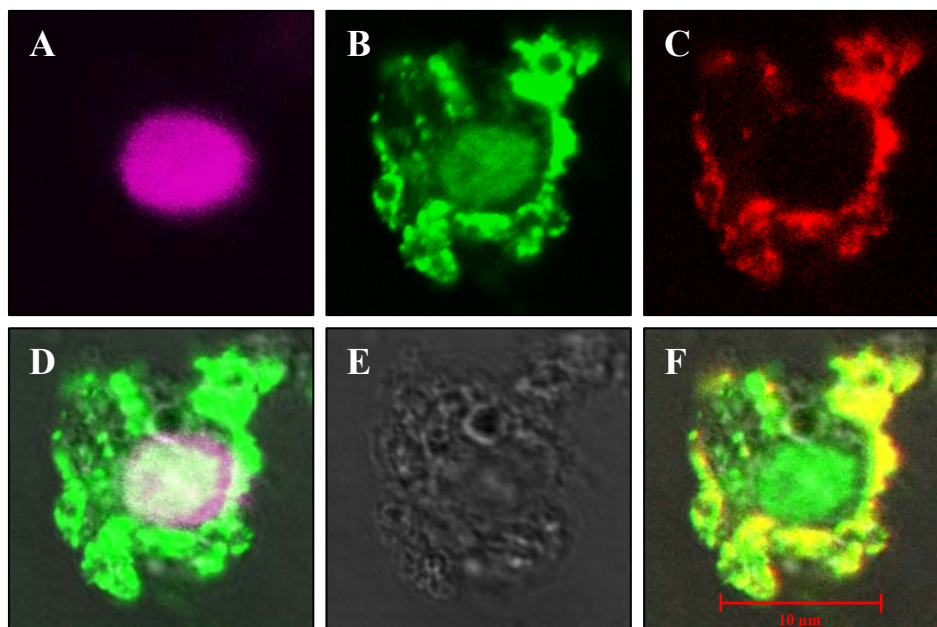


Figure 3.2.7 CLSM pictures of a Kupffer cell taken after 2 h of incubation with ds NF- κ B decoy ODN₄₈₈ loaded G-NP_{Tex} 04-024 pos; pictures show different fluorescent stained structures (A) nucleus (violet), (B) decoy ODN (green), and (C) gelatin nanoparticles (red), as well as (E) an isolated Kupffer cell and overlay of pictures of (D) nucleus and oligonucleotide and (F) gelatin nanoparticles and oligonucleotide

Free oligonucleotide is now detectable in the nucleus (Figure 3.2.7 D) and the fluorescence appears more diffusive than before, further indicating ODN release from particulate structures i.e., gelatin nanoparticles. The appearance of oligonucleotide in the nucleus has thereby not to be considered as decisive for the mode of action of the NF- κ B decoy, as it functions within cytoplasm as well as in the nucleus and does not necessarily require a transfer to the nucleus (Figure 3.1.2).

3.2.3 Summary

CLSM data demonstrated biodistribution of gelatin nanoparticles to be limited to the organs of the MPS after systemical administration. Changing the route of administration towards the portal vein led to a clearly pronounced uptake of gelatin nanoparticles into the liver, whereas the basic biodistribution into the MPS organs was maintained. Within liver the exclusive distribution of gelatin nanoparticles to Kupffer cells could be proven by accomplishing selective immunostaining and following a perfect colocalization of Kupffer cells and gelatin nanoparticles in CLSM imaging. In addition intracellular CLSM analysis showed the oligonucleotide

loaded nanoparticles to be almost completely located in endosomes and an ODN release from nanoparticles already being visible after 15 min, which further advanced over 2 hours leading to a certain transfer to the nucleus.

As the proven Kupffer cell uptake is prerequisite for the proposed NF- κ B decoy strategy in the context of hepatic ischemia reperfusion injury, these data provided the basis to further progress with decoy ODN loaded gelatin nanoparticles in an hepatic I/R animal model.

3.3 Excursus – Comparing Plasma Protein Adsorption Pattern and Biodistribution of Gelatin Nanoparticles and Solid Lipid Nanoparticles (SLN)

3.3.1 Introduction

In vivo fate of colloidal drug carrier systems

In terms of drug delivery most target sites within the body are accessible through either microcirculation by blood capillaries or pores present at various surfaces and membranes. As the majority of apertures, openings, and gates on cellular and subcellular levels are of nanometer size and the diameter of the narrowest capillaries is about 2,000 nm nanoparticulate drug carrier systems are most suitable in reaching this dimension [Gupta, 2006]. But, it is well known since the early days of colloidal or nanoparticulate drug delivery that the *in vivo* fate of such systems is predominately determined by a rapid clearance from circulation after intravenous injection by the cells of the Mononuclear Phagocytic System (MPS) [Wilkins et al., 1966; Kreuter, 1983]. This leads to a typical body distribution pattern comprising the macrophage possessing organs of the MPS, namely liver, spleen, lungs, and bone marrow [Mueller et al., 1990; Kreuter, 1992]. The mechanisms behind this observation are related to endogenous processes that clear the body from foreign substances and particulate matter. Recognition of such material e.g., nanoparticles by phagocytic cells is mediated by so called opsonins (from the Greek “opson” = condiment) [Patel, 1992], proteins circulating with the plasma that interact with foreign material immediately after application [Goepfert et al., 2005]. Thus, finally triggering phagocytosis opsonization is decisive for the plasma half life of nanoparticulate drug carriers [Moghimi et al., 2003; Owens et al., 2006], whereas three physicochemical properties surface hydrophobicity / hydrophilicity, charge, and size determine the pattern of the adsorbed proteins [Moghimi et al., 2001; Passirani et al., 2005; Vonarbourg et al., 2006]. Basically hydrophobic surfaces are stronger prone to opsonization than hydrophilic surfaces because of hydrophobic interactions with proteins [Patel, 1992; Stolnik et al., 1995]. But, it has to be stated that hydrophilic surfaces do not necessarily protected from phagocytosis [Stolnik et al., 1995]. Referred to surface charges, findings are ambivalent. On the one hand it is

generally accepted that nanoparticles with negatively charged surfaces showed reduced circulation times compared to those with positively charged, and neutral surfaces [Patel, 1992; Stolnik et al., 1995]. On the other hand there was no difference in the circulation time of negatively charged, positively charged, or neutral albumin nanoparticles [Roser et al., 1998]. At the same time protein adsorption seems to be size dependent to a certain extent with liposomes larger than 100 nm being preferably opsonized [Moghimi et al., 2001].

Main opsonins are immunoglobulins (IgG and IgM) and components of the complement system (C3 and C4 fragments) [Patel, 1992; Passirani et al., 2005; Vonarbourg et al., 2006]. Due to the interaction between its Fc portion and an Fc receptor present on macrophages IgG exhibits a direct opsonic activity [Patel, 1992]. In addition, IgG is assumed to concomitantly increase the surface hydrophobicity of the opsonized particle [Patel, 1992; Allemann et al., 1997] as it is known for bacteria, whereas increased hydrophobicity is attributed to the Fc portion [Van Oss, 1978]. IgM, as well as IgG, activates the classical complement pathway leading to complement opsonization by forming an IgM/IgG – C3b complex. Whereas following the alternative complement pathway results in a direct C3b opsonization of exogenous surfaces. In both cases C3b initiates rapid phagocytosis via its macrophage receptor. The opsonic activity of C4 or C4b respectively is based on the same mechanism but less pronounced compared to C3 [Patel, 1992; Passirani et al., 2005]. Further plasma proteins exhibiting a receptor on MPS cells are fibronectin [Patel, 1992; Vonarbourg et al., 2006], fibrinogen [Altieri et al., 1986], transferrin [Vogel et al., 1987], and α 2-macroglobuline [Van Leuven et al., 1986].

Besides these proteins there is a group of so called dysopsonins described. Their adsorption leads to a certain protection from phagocytosis [Absolom, 1986]. Well known dysopsonins are Albumin and IgA [Stolnik et al., 1995; Thiele et al., 2003; Ogawara et al., 2004], both decreasing surface hydrophobicity [Stolnik et al., 1995; Ogawara et al., 2004].

Based on the basic understanding of surface opsonization and phagocytotic uptake of colloidal drug carriers Müller and Heinemann formulated already in 1989 the concept of differential opsonization [Mueller et al., 1990]. The concept makes the assumption that macrophages of different subpopulations recognize different opsonization patterns, which in turn could be used for a directed distribution of

accordingly surface modified nanoparticles by adsorbing only certain opsonins. However, despite the knowledge about opsonins and their governing properties today there is still a lack of the possibility to directly predict biodistribution patterns of colloidal drug carriers systems from their physicochemical properties. But, the look onto nanoparticulate opsonization patterns contributes to the understanding of related biodistribution data. In this context it was the aim of this study to correlate plasma protein adsorption patterns of gelatin nanoparticles with their respective biodistribution data in comparison to solid lipid nanoparticles (SLN).

Two dimensional polyacrylamide gel electrophoresis (2D-PAGE or 2-DE) was applied as method of choice for the description of the plasma protein adsorption patterns. Biodistribution experiments with fluorescent-labeled gelatin and solid lipid nanoparticles were performed in rats and the results were visualized by confocal laser scanning microscopy (CLSM) as well as fluorescence assorted cell sorting (FACS).

Two dimensional polyacrylamide gel electrophoresis (2D-PAGE)

For the detailed qualitative and quantitative description of a protein collectivity 2D-PAGE is the state of the art analytical tool [Goerg et al., 2004]. During analysis proteins are separated by two independent physicochemical properties. After an isoelectric focusing in the first dimension a molecular weight related differentiation in the second dimension takes place. Both underlying methods isoelectric focusing (IEF) and sodium dodecyl sulfate polyacrylamide gel electrophoresis (SDS-PAGE) were developed during the 1960ies [Righetti, 2004]. But it lasted until the mid 1970s till the potential of the (orthogonal) combination of these two techniques was recognized when three groups independently published their first 2-DE approaches [Klose, 1975; O'Farrell, 1975; Scheele, 1975]. Since these early days two major drawbacks of the method had to be overcome. At first the application of soluble carrier ampholytes for the generation of the pH gradient during IEF suffered from variability between different brands and even batches of the ampholytes due to their manufacturing by "chaotic" synthesis [Righetti, 2004]. This led to a cathodic drift of the analytes and finally to not reproducible results [Righetti et al., 1973]. The introduction of immobilized pH gradients (IPGs), gained by covalent linkage of buffering groups to the polyacrylamid matrix, described by Bjellqvist could solve

this problem [Bjellqvist et al., 1982]. Second the complete identification of thousands of protein spots remained almost impossible limiting the wide spread application of 2-DE [Beranova-Giorgianni, 2003; Righetti, 2004]. Coupling 2-DE with mass spectrometry (MS) nowadays allows the accurate profiling and quantification of complex protein mixtures. This finally led to a number of 10,000 proteins to be highly reproducibly separated and identified on one gel, compared to 300 in the very beginning [Sperling, 2001; Goerg et al., 2004].

Besides addressing the current challenges in proteomics [Sperling, 2001; Beranova-Giorgianni, 2003; Goerg et al., 2004] 2D-PAGE is applied in clinics [Young et al., 1995] and was established for the work with colloidal drug carrier systems by the groups of Rainer H. Müller [Blunk et al., 1993; Luck et al., 1998; Goeppert et al., 2003] and Robert Gurny [Leroux et al., 1994; Allemann et al., 1997].

In sum the basic steps of a 2D-PAGE analysis with IPGs and MS identification comprises [Goerg et al., 2004]:

- a) sample preparation and protein solubilization
- b) protein separation by 2-DE
- c) protein detection and quantification
- d) computer assisted analysis of 2-DE patterns
- e) protein identification and characterization, and
- f) 2-D protein database construction.

The presented data emerged from cooperation between the chairs of pharmaceutical technology of the Free University of Berlin, Germany (Prof. R. H. Müller / Ph.D. student Torsten Göppert) and of the Ludwig-Maximilians-University Munich, Germany (Prof. G. Winter / Dr. C. Coester / Ph.D. student Jan C. Zillies). Animal studies were conducted by Florian Hoffmann (Chair of pharmaceutical biology, Prof. A. Vollmar, Ludwig-Maximilians-University Munich, Germany). The contributions of our cooperation partners are accordingly denoted in the text.

3.3.2 Materials and methods

Reagents

Reagent	Description	Supplier
Acetone		VWR International GmbH (Ismaning, Germany)
Cetylpalmitate	Cutina® CP	Henkel KGaA (Düsseldorf, Germany)
Cholamine chloride hydrochloride	(2-aminoethyl)-trimethyl-ammoniumchloride hydrochloride	Sigma-Aldrich GmbH (Taufkirchen, Germany)
ds NF-κB decoy ODN	5'-AGT TGA GGG GAC TTT CCC AGG C-3' phosphorothioate	biomers.net GmbH (Ulm, Germany)
Dulbecco's Phosphate Buffered Saline	pH 7.4	PAA Laboratories GmbH (Linz, Austria)
EDC	1-ethyl-3-(3-dimethyl-aminopropyl) carbodiimide hydrochloride	Sigma-Aldrich GmbH (Taufkirchen, Germany)
BD PharmLyse™	FACS Lysis Buffer (10x concentrate)	Becton Dickinson GmbH (Heidelberg, Germany)
Gelatin type A	175 Bloom	Sigma-Aldrich GmbH (Taufkirchen, Germany)
Glutaraldehyde	25 % aqueous solution	Sigma-Aldrich GmbH (Taufkirchen, Germany)
HCl	2 N	VWR International GmbH (Ismaning, Germany)
Lutrol® F68	Poloxamer 188	BASF AG (Ludwigshafen, Germany)
PBS	Dulbecco's phosphate buffered saline pH 7.4 (1x concentrate)	PAA Laboratories GmbH (Linz, Austria)
Permafluor	aqueous mounting medium	Beckmann Coulter GmbH (Krefeld, Germany)

Fluorescent dyes

Reagent	Description	Supplier
Coumarin 6	laser grade, 98 %, λ_{em} 497 nm	Acros Organics (Geel, Belgium)
FluoProbes [®] 488	NHS, λ_{em} 517 nm	FluoProbes (Interchim) (Montluçon Cedex, France)

2D-PAGE analysis

Reagent*	Description	Supplier
Acrylamide		SERVA Electrophoresis GmbH (Heidelberg, Germany)
Acrylamide / Bis Solution	(37.5:1), 30 % (w/v)	SERVA Electrophoresis GmbH (Heidelberg, Germany)
Agarose		Bio-Rad Laboratories GmbH (München, Germany)
Acetic acid	99 %	Merck KGaA (Darmstadt, Germany)
Bromphenol blue		Merck KGaA (Darmstadt, Germany)
CHAPS	3-[(3-Cholamidopropyl)dimethylammonio]-1-propanesulfonate	Sigma-Aldrich Co. (St. Louis, USA)
DTE	1,4-dithioerythritol	Merck KGaA (Darmstadt, Germany)
Ethanol	undenaturated, 96 %	Branntwein-Monopolstelle (Berlin, Germany)
Human plasma	citrate stabilized	German Red Cross (Berlin, Germany)
Iodoacetamide		Sigma-Aldrich GmbH (Taufkirchen, Germany)
N,N'-Methylene bisacrylamide		SERVA Electrophoresis GmbH (Heidelberg, Germany)
Rat plasma	citrate stabilized from Wistar rats	Institute for Infection Medicine, Free University (Berlin, Germany)

Reagent*	Description	Supplier
SDS	Sodium dodecyl sulfate	Merck KGaA (Darmstadt, Germany)
Silver nitrate		Merck KGaA (Darmstadt, Germany)
Sodium phosphate dibasic dodecahydrate		Merck KGaA (Darmstadt, Germany)
Sodium phosphate monobasic dihydrate		Merck KGaA (Darmstadt, Germany)
TRIS	Tris(hydroxymethyl)aminomethane	Merck KGaA (Darmstadt, Germany)
Urea		Merck KGaA (Darmstadt, Germany)

*For detailed composition of the applied solutions during 2D-PAGE experiments see Goeppert 2005: Plasma protein adsorption patterns on intravenously injectable colloidal drug carriers for drug delivery across the blood-brain barrier, Ph.D. thesis

Preparation and surface modification of gelatin nanoparticles

Gelatin nanoparticles were manufactured by the two step desolvation method and optionally surface modified (cationized) with cholamine as described in chapter 1.2.

Preparation of fluorescent cationic gelatin nanoparticles

Fluorescent-labeled gelatin nanoparticles were prepared by covalent coupling of the gelatin base material with FluoProbes[®] 488 NHS (cp. chapter 3.2.1). FluoProbes[®] 488 was chosen instead of TexasRed[®] to visualize the nanoparticles in a FACScalibur flow cytometer (Becton Dickinson, Franklin Lakes, NJ, USA) equipped with a laser unit emitting the according excitation wavelength.

Oligonucleotide-loading of gelatin nanoparticles

113.5 μ L of an aqueous nanoparticle dispersion containing 1.2 mg surface modified and fluorescent-labeled gelatin nanoparticles was incubated with 84.4 μ L of an aqueous oligonucleotide solution containing 4.22 nmol NF- κ B decoy ODN (i.e., 5 % [w/w] drug loading) in PBS adjusted to a final volume of 1,200 μ L for 2 h

at 22 °C and 800 rpm under constant shaking (Thermomixer Comfort, Eppendorf AG, Hamburg, Germany).

Manufacturing of SLN

SLN were prepared by hot high pressure homogenization according to literature [Mehnert et al., 2001; Goeppert, 2005] using a Micron LAB 40 lab scale high pressure homogenizer (APV Systems, Unna, Germany). The batch size was 40 g comprising 10 % cetylpalmitate, 1.2 % Poloxamer 188, and water. Lipid and aqueous phase were heated up to 70 °C, whereas the emulsifier was dissolved in the aqueous phase. Subsequent the lipid phase was dispersed in the aqueous surfactant solution with an Ultra-Turrax TP 18-10 (Janke and Kunkel, Staufen, Germany) for 1 min at 20,000 rpm in a vessel at 70 °C. The obtained pre-emulsion was then passed through the homogenizer three times with a pressure of 500 bar per cycle. Due to the lack of a temperature control jacket the product touching parts of the homogenizer were tempered in a drying oven to 80 °C over night to guarantee a working temperature above the melting point of the lipid. Finally the resulting hot nanoemulsion was cooled down under constant stirring (500 rpm) whereby nanoparticles are formed by recrystallization of the lipid matrix.

Manufacturing of fluorescent-labeled SLN

Fluorescent labeling of SLN was conducted by incorporating a fluorescent dye into the lipid phase: 5 mg of Coumarin 6 were dissolved in the cetylpalmitate melt under stirring prior to emulsification. The manufacturing process was afterwards continued as described above.

Characterization of nanoparticles

Size and zeta potential (ZP) of the applied gelatin nanoparticle batches were determined by dynamic light scattering (DLS) using a Zetasizer 3000 HSA and a Nanosizer ZS respectively (both from Malvern Instruments, Worcestershire, UK). Zeta potential measurements were conducted under standardized ionic conditions in 10 mM NaCl at pH 7.0.

In vivo biodistribution experiments

Experiments were conducted in male Sprague-Dawley rats. Fluorescent-labeled gelatin and solid lipid nanoparticle formulations were prepared in PBS (1 mg/mL) and injected (1 mL) into rat via the jugular vein. Prior to injection rats were anesthetized by i.p. injection of 0.005 mg/kg Fentanyl and 2.0 mg/kg Midazolam. Anesthesia was maintained over the whole experiment with 1.5 % Isofluran continuously applied using a vaporizer with Carbogen (5 % CO₂ / 95 % O₂) as carrier gas. To monitor blood pressure and control anesthesia the jugular artery was cannulated with a 16 gauge PE catheter and connected to a blood-pressure gauge.

After 1h rats were sacrificed and blood was rinsed out. Brain, heart, kidneys, liver, lungs, parts of femoral muscle, and spleen were resected, frozen with liquid nitrogen and stored at -80 °C. The distribution of nanoparticles into the different organs was determined via confocal laser scanning microscopy (CLSM).

All animal studies were conducted by Florian Hoffmann at the department of pharmaceutical biology of the Ludwig-Maximilians-University Munich, Germany.

CLSM imaging

10 µm thin slices of the frozen organs from the *in vivo* biodistribution experiments were prepared using a HM 500 Kryostat (Microm International AG, Volketswil, Switzerland) and transferred to microscopic slides. After thawing samples were mounted in Permafluor with a cover slip. Preparations were not further stained for specific cell types or organelles as it was the intention to just check the qualitative nanoparticle distribution into single organs. CLSM imaging was performed with a Zeiss LSM 510 Meta confocal laser scanning microscope (Carl Zeiss Microscope Systems, Jena, Germany).

FACS analysis of rat whole blood and plasma

600 µL of rat blood were taken during the *in vivo* biodistribution experiments at the following time points: 0, 15, 30, and 60 min. 100 µL whole blood were diluted with FACS lysis buffer in a FACS sample tube (1:10) and directly analyzed by flow cytometry in a FACScalibur (Becton Dickinson, Franklin Lakes, NJ, USA). 500 µL whole blood were centrifuged (10 min / 5,000 rpm) and the obtained plasma

supernatant was diluted with PBS pH 7.4 in the ratio 1:3. This solution was as well analyzed by flow cytometry.

FACS analysis was conducted under assistance of Dr. Stefan Zahler at the department of pharmaceutical biology of the Ludwig-Maximilians-University Munich, Germany.

2D-PAGE experiments

Sample preparation Nanoparticle suspensions (0.5 mL) were incubated with 1.5 mL of citrate stabilized plasma (human or rat) for 5 min at 37 °C. Following incubation particles were separated from bulk medium by centrifugation (22,940 g, 60 min) and redispersed in 20 mM sodium phosphate buffer pH 7.4. This washing step was repeated another two times. Desorption of adsorbed plasmaproteins was conducted using a solubilizing solution containing 10 % (w/v) SDS and 2.32 % (w/v) DTE (5 min at 95 °C). After cooling, 190 µL of a solution containing DTE, CHAPS, urea, TRIS, and bromphenol blue were added. The mixture was vortexed and centrifuged (22,940 g, 15 min), 100 µL were transferred to Isoelectric focusing (IEF).

Isoelectric focusing (IEF) IEF was performed within immobilized pH gradient (IPG) stripes (Immobiline DryStripes, pH 3-10, non linear) using a Multiphore II both from Amersham Pharmacia Biotech and an E 752 power supply from Consort (Turnhout, Belgium) with a total volt hour product of 20,375 Vh.

Equilibration and SDS-PAGE IPG stripes were equilibrated with two SDS containing solutions: solution I additionally containing DTE (15 min residence time) and solution II additionally containing iodoacetamide (20 min residence time). Subsequent to equilibration IPG stripes were attached to the SDS-PAGE polyacrylamide gels and fixed with an agarose gel (0.5 %). SDS-PAGE was carried out in Protean II Multi Cells with a PowerPac 1000 power supply (Bio-Rad Laboratories, Munich, Germany). Gels had a size of 16x16 cm and a gradient ranging from 9 % T (total acrylamide concentration) to 16 % T using 2.67 % (related to the acrylamide content) N,N'-methylenebisacrylamide as cross-linking agent.

Qualitative and quantitative analysis For qualitative and quantitative analysis proteins within the gels were initially fixed in a precipitation bath with undenaturated ethanol and acetic acid and visualized with a silver staining. Protein spots were

identified by comparison with 2-D-PAGE reference maps published for human and rat plasma [Anderson et al., 1991; Haynes et al., 1998]. In addition the ExPASy (**Expert Protein Analysis System**) proteomics server of the University of Geneva offers online access to reference maps of several organisms (<http://www.expasy.ch/ch2d/>). After scanning the gels (ImageScanner, Amersham Pharmacia Biotech) data were processed with the MELANIE III (**M**edical **E**lectrophoresis **A**nalysis **I**nteractive **E**xpert **S**ystem) software (Bio-Rad Laboratories, Munich, Germany) allowing the quantitative analysis of the obtained proteins spots among different gels.

All 2D-PAGE experiments were conducted by Torsten Göppert at the department of pharmaceutical technology of the Free University of Berlin, Germany. The described procedure is derived from literature [Hochstrasser et al., 1988; Blunk, 1994] and is the standard protocol that was applied in our cooperation project and is published in his Ph.D. thesis [Goeppert, 2005]. For more detailed information about the conduction of the 2D-PAGE experiments it is referred to this thesis.

3.3.3 Results and discussion

Characterization of nanoparticles

All nanoparticle formulations applied during 2D-PAGE experiments (Table 3.3.1) had a similar size (140 to 260 nm) and a homogenous size distribution with a PDI below 0.100. Due to surface modification and drug loading the surface charge of the single gelatin nanoparticles batches is different expressed in a zetapotential ranging from slightly negative values up to +15 mV. The negative zetapotential of P188-SLN results from acidic components always contained in the cetylpalmitate phase to a certain extent. At physiological pH values their carboxyl groups appear deprotonated and thus negatively charged.

Table 3.3.1 Size, polydispersity, and surface charge of the nanoparticle formulations applied in 2D-PAGE investigations

	Gelatin nanoparticles (G-NP)	Surface modified gelatin nanoparticles (G-NP pos)	Surfacemodified and oligonucleotide loaded gelatin nanoparticles (G-NP pos + O)	Cetylpalmitate 10% Poloxamer 188 1.2% Aqua purificata ad 100% P188-SLN
size [nm]	139	164	166	259
PDI	0.073	0.043	0.054	0.078
ZP [mV]	-2.5	+14.6	+3.6	-45.7

The nanoparticle formulations applied for biodistribution experiments (Table 3.3.2) had as well a similar size (200 to 300 nm) and a homogenous size distribution with a PDI around 0.100. The surface charge properties meet the dimensions described above for the not fluorescent-labeled nanoparticle batches.

A comparable size for all nanoparticle batches > 100 nm is important as this threshold is assumed to be critical in determining the degree of opsonization (see chapter 3.3.1). The modification of gelatin with a fluorescent dye and the variability of the manufacturing process thereby caused the increased particle size observed for the gelatin nanoparticle batches applied during biodistribution experiments

Table 3.3.2 Size, polydispersity, and surface charge of the fluorescent-labeled nanoparticle formulations applied for biodistribution experiments

	Fluorescent gelatin nanoparticles (G-NP₄₈₈)	Surface modified fluorescent gelatin nanoparticles (G-NP₄₈₈ pos)	Surface modified and oligonucleotide loaded fluorescent gelatin nanoparticles (G-NP₄₈₈ pos + O)	Cetylpalmitate 10% Poloxamer 188 1.2% Coumarin 6 0.013 % Aqua purificata ad 100% P188-SLN_{C6}
size [nm]	223	310	305	205
PDI	0.067	0.123	0.105	0.112
ZP [mV]	-10.7	+15.5	+4.0	-43.6

Drug loading of G-NP pos and G-NP₄₈₈ pos respectively with the ds NF- κ B decoy oligonucleotide was successfully conducted in PBS. The applied 5 % [w/w] ODN were completely attached onto the surface of the nanoparticles, which could be proven via UV-spectroscopy.

Plasma protein adsorption patterns – gelatin nanoparticles vs. SLN

Figure 3.3.1 shows the resulting 2-DE gels of G-NP, G-NP pos, and G-NP pos + O incubated with human plasma. Interestingly the different gelatin nanoparticle formulations possess a similar protein adsorption pattern, consisting of a distinct adsorption of albumin, fibrinogen, the opsonic immunoglobulins IgG and IgM, and α 2-macroglobulin.

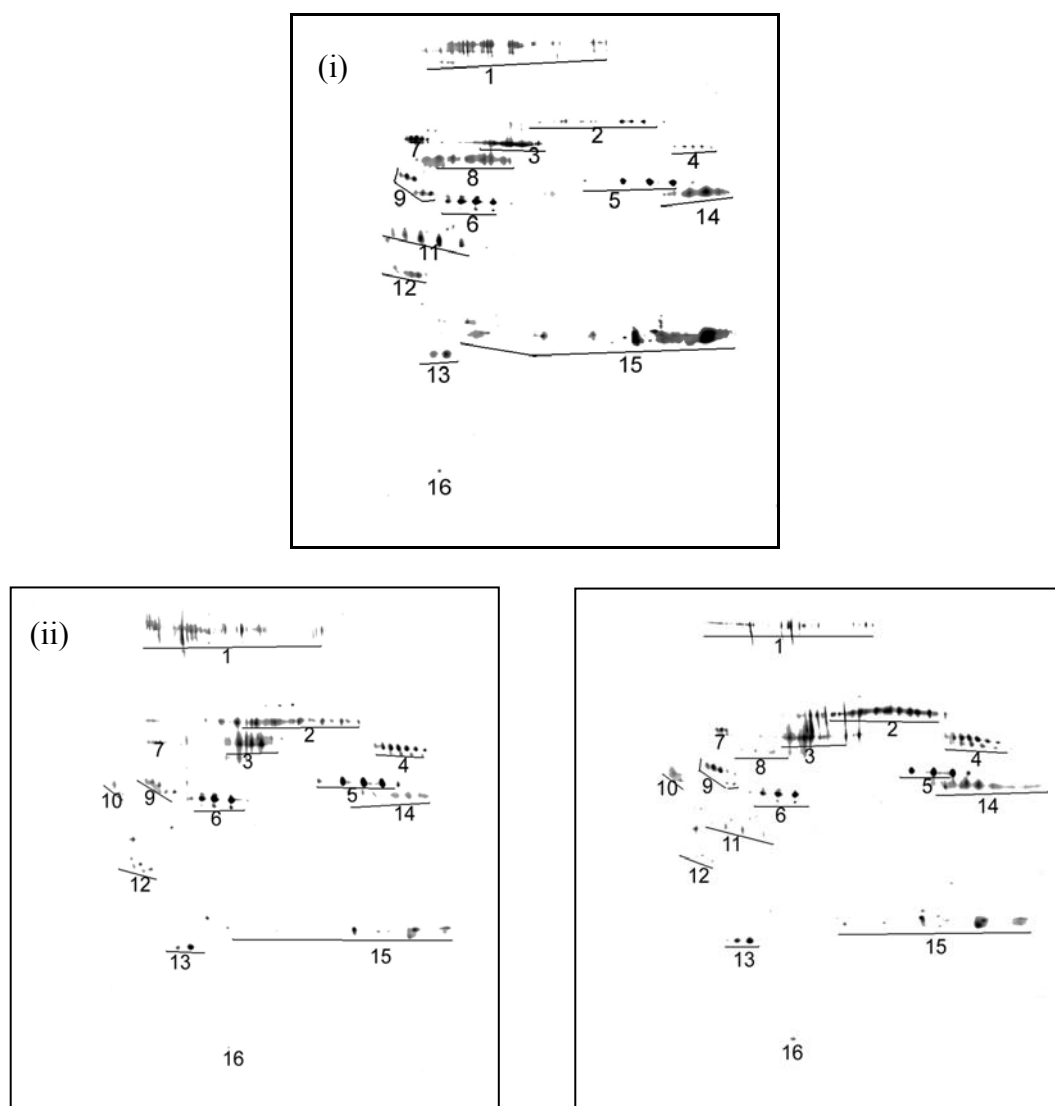


Figure 3.3.1 Plasma protein adsorption pattern on gelatin nanoparticles after incubation with human plasma: (i) G-NP, (ii) G-NPpos, (iii) G-NPpos + O, *Abscissa*: pH 4-9 (from left to right), *Ordinate*: MW 250 kDa-6 kDa (from top to bottom); *Proteinspots*: (1) α 2-macroglobulin, (2) IgM μ chain, (3) albumin, (4) fibrinogen α chain, (5) fibrinogen β chain, (6) fibrinogen γ chain, (7) α 1-b-glycoprotein, (8) IgA, (9) α 1-antitrypsin, (10) α 2-hs-glycoprotein, (11) haptoglobin β chain, (12) ApoJ, (13) ApoA-I, (14) IgG γ chain, (15) Ig light chains, (16) transthyretin

Assuming a given surface hydrophilicity related to the gelatin base material for all formulations, which is not basically altered by the oligonucleotide loading, the varying surface charge does not direct the adsorption pattern towards any qualitative changes. Thus, the surface hydrophilicity seems to determine the qualitative composition of the adsorbed protein spectrum. A semi quantitative summary of the identified proteins is given in Figure 3.3.2. Beside the described similarities regarding the kind of proteins the congruent masses of single proteins being adsorbed especially for G-NPpos and G-NPpos + O attracts attention as it further indicates that the drug loading process does not differentiate plasma protein adsorption. In fact, the surface charge seems to play a certain role in this context. On the surface of slightly negative G-NP the adsorption of immunoglobulins varied compared to G-NPpos and G-NPpos + O. The increased adsorption of Ig light chains is thereby accompanied by a diminished adsorption of IgM. In general, it can be stated that adsorption on the positively charged formulations G-NPpos and G-NPpos + O was almost identical and exhibited a pattern different from the one of negatively charged G-NP.

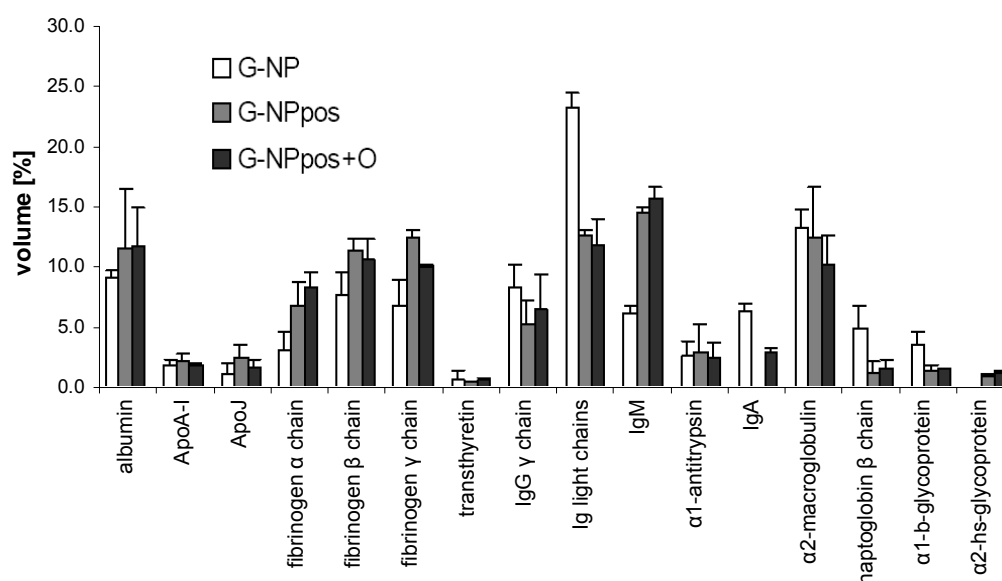


Figure 3.3.2 Portion of single proteins of the totally detected protein patterns on gelatin nanoparticles after incubation with human plasma (n = 2)

However, differences are subtle and the predominant adsorption of strong opsonins leads to the assumption of all formulations being rapidly cleared from circulation by the phagocytosing cells of the MPS. Furthermore α 2-macroglobulin strengthens opsonization. Besides its macrophage receptor [Van Leuven et al., 1986] opsonic properties for α 2-macroglobulin are described by Molnar [Molnar et al.,

1977]. An adsorption of $\alpha 2$ -macroglobulin has already been reported from Bucke for gelatin modified liposomes [Bucke et al., 1998]. As poloxamer and polysorbate modified liposomes did not show any adsorption, a certain gelatin affinity of $\alpha 2$ -macroglobulin can be derived from their findings. Interestingly the portion of 10-13 % (Figure 3.3.2) of all adsorbed proteins matches the data of Bucke who detected a portion of 12 % [Bucke et al., 1998].

In Figure 3.3.3 plasma protein adsorption patterns of gelatin nanoparticles (G-NPpos + O) and solid lipid nanoparticles (P188-SLN) are opposed. Proteins adsorbed onto P188-SLN are basically apolipoproteins, at the same time immunoglobulins and albumin are only adsorbed to a very little extent. The subclasses of these apolipoproteins vary depending on the lipid matrix and the emulsifier the SLN are manufactured of. But, the high amount of apolipoproteins adsorbed onto the SLN's surface remains constant [Goepfert, 2005].

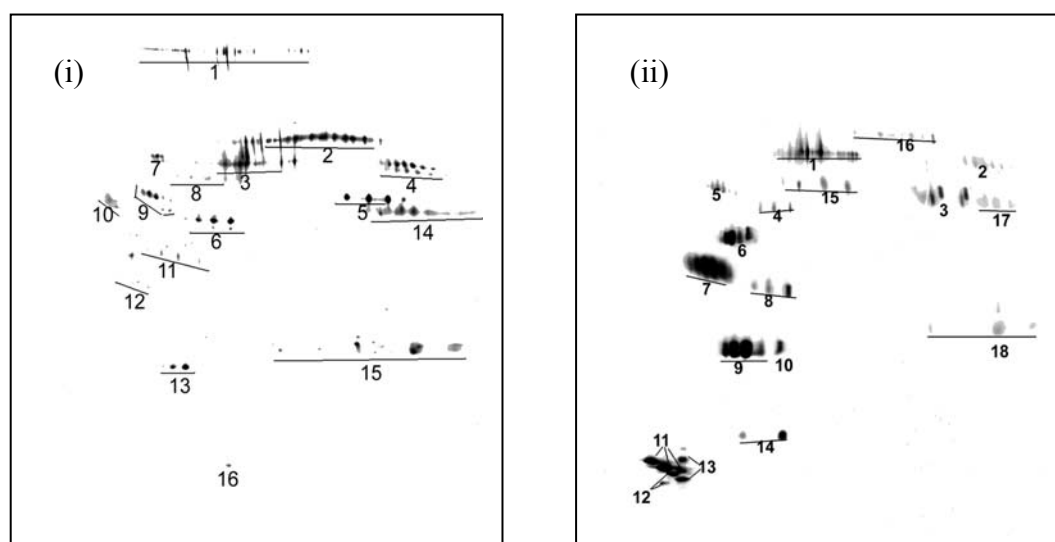


Figure 3.3.3 Plasma protein adsorption pattern on (i) gelatin nanoparticles (G-NPpos + O) and (ii) SLN (P188-SLN) after incubation with human plasma, *Abscissa*: pH 4-9 (from left to right), *Ordinate*: MW 250 kDa-6 kDa (from top to bottom);

Proteinspots (G-NPpos + O): (1) $\alpha 2$ -macroglobulin, (2) IgM μ chain, (3) albumin, (4) fibrinogen α chain, (5) fibrinogen β chain, (6) fibrinogen γ chain, (7) $\alpha 1$ -b-glycoprotein, (8) IgA, (9) $\alpha 1$ -antitrypsin, (10) $\alpha 2$ -hs-glycoprotein, (11) haptoglobin β chain, (12) ApoJ, (13) ApoA-I, (14) IgG γ chain, (15) Ig light chains, (16) transthyretin;

Proteinspots (P188-SLN): (1) albumin, (2) fibrinogen α chain, (3) fibrinogen β chain, (4) fibrinogen γ chain, (5) $\alpha 1$ -antitrypsin, (6) ApoA-IV, (7) ApoJ, (8) ApoE, (9) ApoA-I, (10) ProapoA-I, (11) ApoC-III, (12) ApoC-II, (13) ApoA-II, (14) transthyretin, (15) ApoH, (16) IgM μ chain, (17) IgG γ chain, (18) Ig light chains

The enormous differences between gelatin and solid lipid nanoparticles are summarized in the histogram in Figure 3.3.4. 80 % adsorbed apolipoproteins on P188-SLN front only 3 % apolipoproteins adsorbed on G-NPpos + O. On the other hand about 50 % immunoglobulins dominate the adsorption pattern on G-NPpos + O.

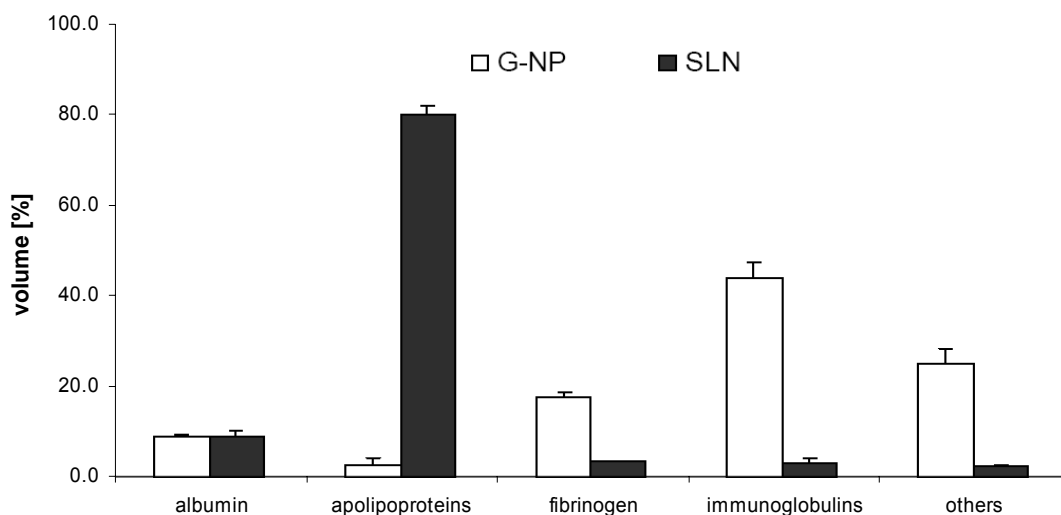


Figure 3.3.4 Plasma protein adsorption patterns on gelatin nanoparticles (G-NPpos + O) compared with SLN (P188-SLN) (n = 2)

Related to these data a clear difference in circulation time and biodistribution has to be expected for gelatin and solid lipid nanoparticles. As biodistribution studies were conducted in rats to verify this hypothesis, 2D-PAGE analysis of plasma protein adsorption patterns obtained from incubation of gelatin nanoparticles with rat plasma were at first accomplished. These investigations should clarify whether the different adsorption patterns observed for gelatin and solid lipid nanoparticles after incubation with human plasma are maintained after the incubation with rat plasma and whether the assumed differences in circulation time and biodistribution could be expected to be the same in rats. The 2-DE gels of G-NP, G-NP pos, and G-NP pos + O after incubation with rat plasma are depicted in Figure 3.3.5. Again the adsorption patterns of the three investigated formulations are qualitatively identical.

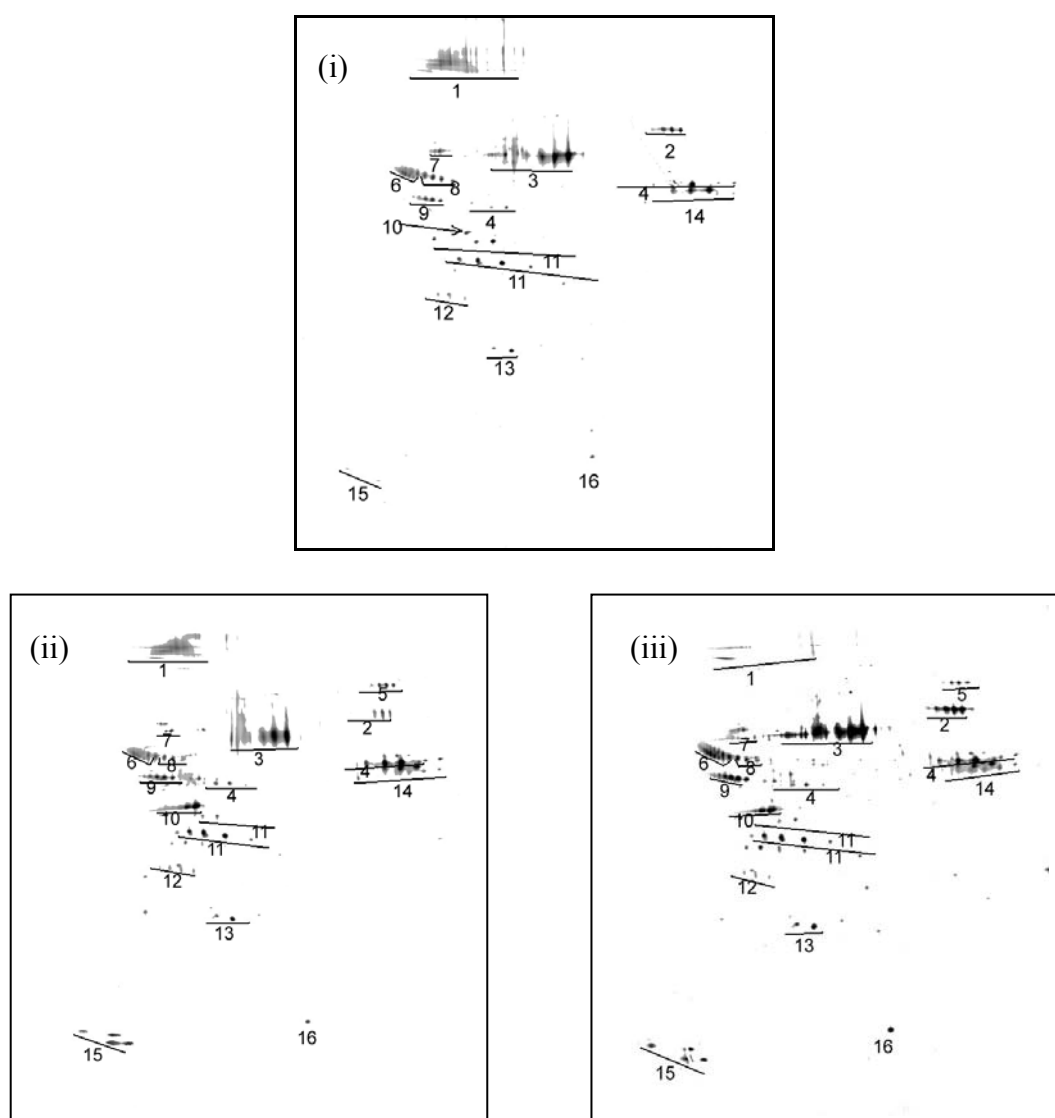


Figure 3.3.5 Plasma protein adsorption pattern on gelatin nanoparticles after incubation with rat plasma: (i) G-NP, (ii) G-NPpos, (iii) G-NPpos + O, *Abscissa*: pH 4-9 (from left to right), *Ordinate*: MW 250 kDa-6 kDa (from top to bottom);

Proteinspots: (1) α 2-macroglobulin, (2) IgM μ chain, (3) albumin, (4) fibrinogen, (5) transferrin, (6) kallikrein-binding protein, (7) α 1-b-glycoprotein, (8) α 2-hs-glycoprotein, (9) α 1-antitrypsin, (10) ApoA-IV, (11) haptoglobin β chain, (12) ApoJ, (13) ApoA-I, (14) IgG γ chain, (15) ApoC, (16) transthyretin

The semi quantitative view reveals albumin, fibrinogen, the opsonic immunoglobulins IgG and IgM, and α 2-macroglobulin to be the main proteins, whereas the similarities between G-NP pos and G-NP pos + O are likewise remarkable and the opsonization of G-NP is in comparison to those pronounced (Figure 3.3.6). Certainly some species specific differences were detected. The albumin portion accounts for more than 20 % and the apolipoproteins were stronger represented in total after incubation in rat plasma. But, the results obtained from

incubation with human plasma could be confirmed in general, thus leading to the expectations formulated above to be proven *in vivo*.

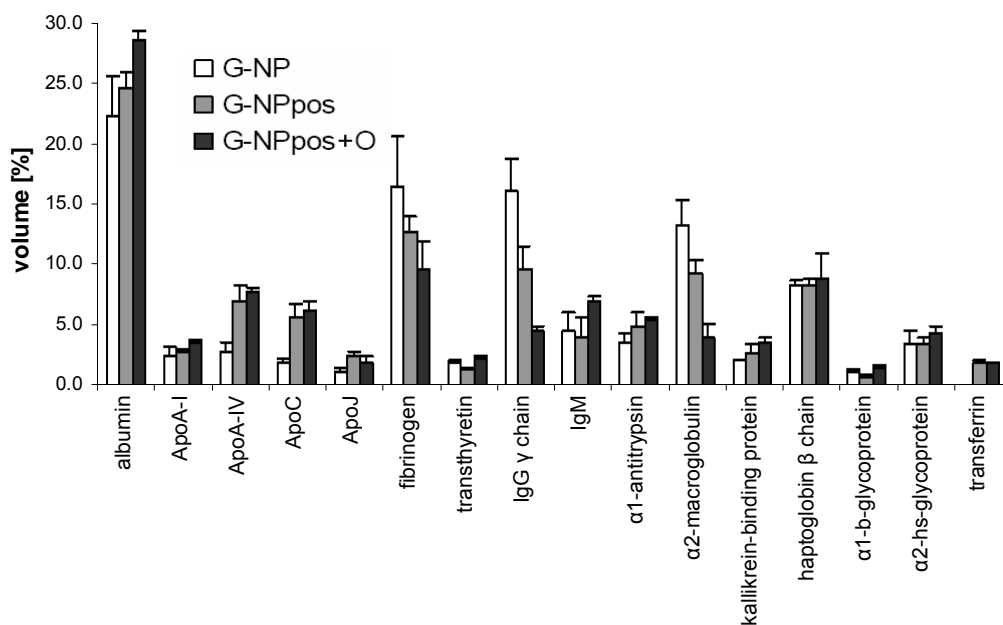


Figure 3.3.6 Portion of single proteins of the totally detected protein patterns on gelatin nanoparticles after incubation with rat plasma (n = 2)

Biodistribution

Basic idea behind the biodistribution experiments was to monitor the organ distribution of different nanoparticle formulations and to follow the kinetics of their clearance from circulation. The organ distribution was ascertained in an endpoint procedure via CLSM analysis of single organs, resected subsequent to termination of the animal study after 1 h of circulation. By contrast sampling of whole blood and plasma for FACS analysis was concurrently conducted during the animal studies at 0, 15, 30, and 60 min. Figures 4.3.7 to 4.3.9 show the CLSM images taken of slices from liver, spleen, lung, kidney, and femoral muscle revealing the qualitative organ distribution of gelatin nanoparticles. As the emphasis lies on the qualitative description of the nanoparticle distribution into single organs no further fluorescent staining of different cell types or compartments was conducted. For all three investigated formulations the same biodistribution could be observed with nanoparticles accumulated in liver, spleen, and lung. Due to the opsonin dominated plasma protein adsorption monitored in 2D-PAGE analysis this was expected and is in accordance to basic considerations of nanoparticle biodistribution discussed in literature [Kreuter, 1983].

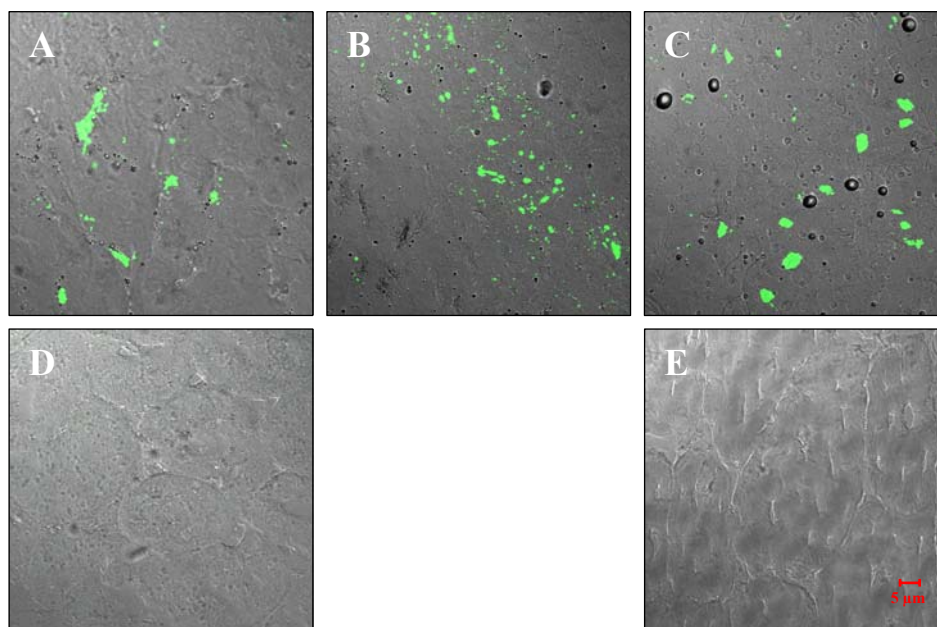


Figure 3.3.7 CLSM pictures of (A) liver, (B) spleen, (C) lung, (D) kidney, and (E) femoral muscle taken from organs resected 1 h after injection of G-NP₄₈₈ (green) into the jugular vein

Comparing the distribution into single organs among each other an equal distribution is observed in liver and lung, whereas the distribution within the spleen shows distinct heterogeneity. Caused by just displaying limited sections CLSM only reflects that to a certain extent (Figure 3.3.7 B and Figure 3.3.9 B).

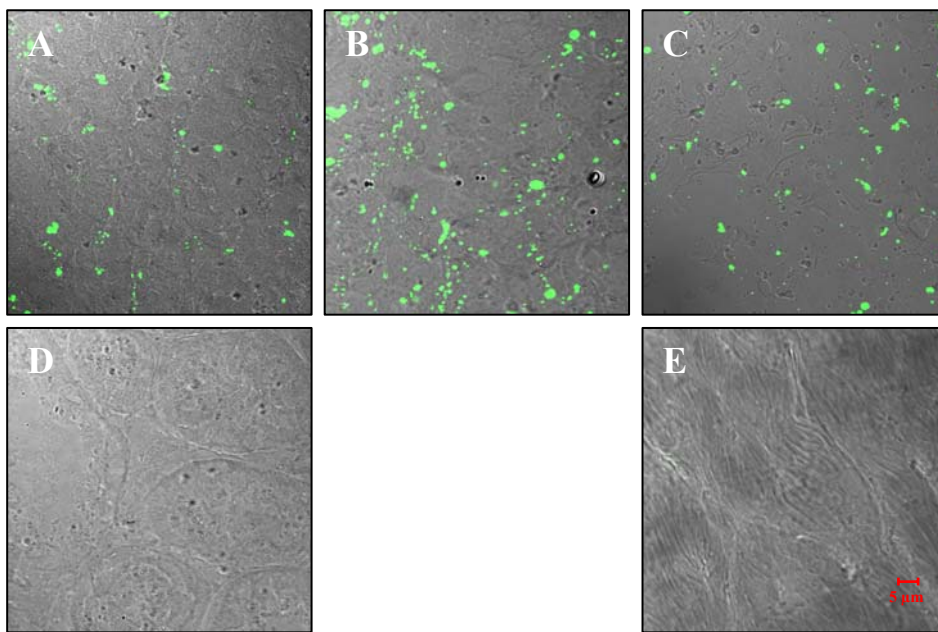


Figure 3.3.8 CLSM pictures of (A) liver, (B) spleen, (C) lung, (D) kidney, and (E) femoral muscle taken from organs resected 1 h after injection of G-NP₄₈₈ pos (green) into the jugular vein

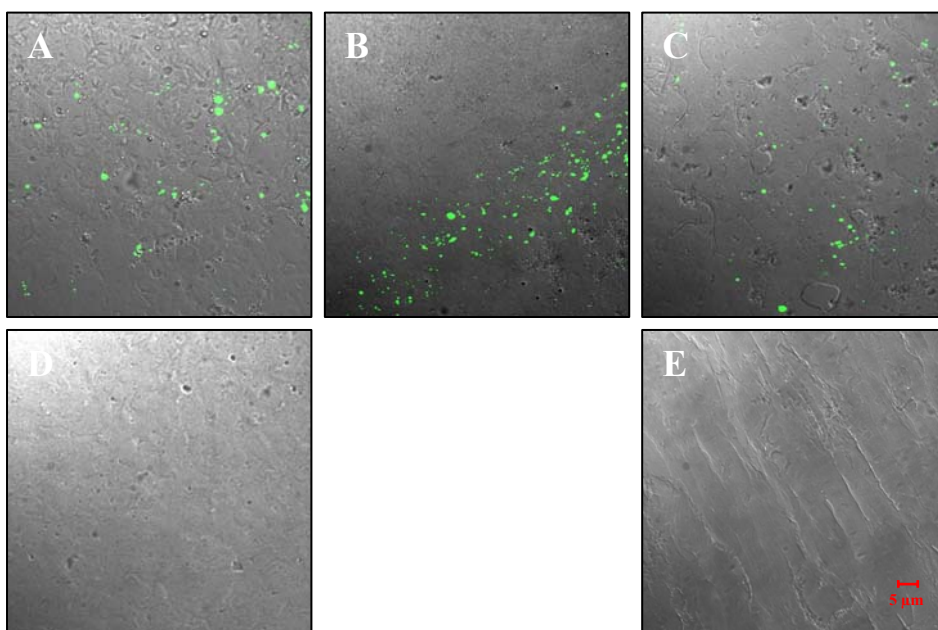


Figure 3.3.9 CLSM pictures of (A) liver, (B) spleen, (C) lung, (D) kidney, and (E) femoral muscle taken from organs resected 1 h after injection of G-NP₄₈₈ pos + O (green) into the jugular vein

But the view through the ocular of the microscope covering whole slices makes this impression obvious. Assuming a selective macrophage uptake the anatomy of the spleen might help to explain the described findings. Splenic macrophages are not evenly spread within the organ, in fact they are attributed to the regions of the red pulp and the zones enclosing the white pulp, but not to the white pulp itself, which is anatomically separated from the other regions [Mebius et al., 2005].

The kinetic data indicated the clearance from circulation to be completed within the first 15 min of the experiments. FACS analysis showed no freely circulating nanoparticles within plasma, neither after 15 min nor after 30 or 60 min. Formulation dependent differences did not occur like expected from CLSM data. Thus FACS results are in the following exemplarily shown for G-NP₄₈₈. The histogram plots of rat plasma sampled before the application of nanoparticles and after 15 min of circulation are displayed in Figure 3.3.10.

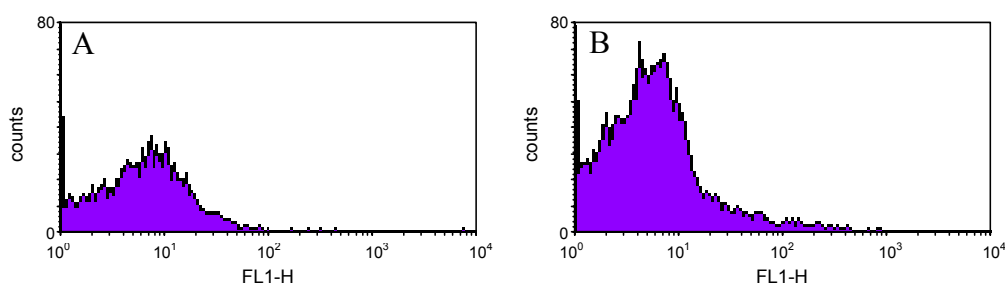


Figure 3.3.10 Histogram plots of rat plasma analyzed before (A) and 15 min after (B) the application of G-NP₄₈₈

Both plots exhibit almost the same shape, whereas a shift to the right i.e., towards a higher number of fluorescent events could not be detected (Figure 3.3.10 B), indicating the rapid clearance of nanoparticles from circulation. The difference in total counts is related to sample preparation as it is very difficult to collect an identical sample volume at each sampling point.

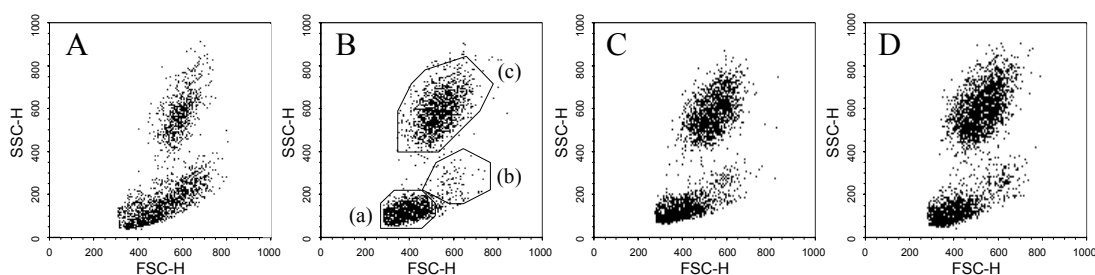


Figure 3.3.11 Dot plots of rat whole blood analyzed before (A) and 15 min (B), 30 min (C), and 60 min (D) after the application of G-NP₄₈₈; displayed cell types exemplarily highlighted in dot plot B are lymphocytes (a), monocytes (b), and neutrophil granulocytes (c)

Analyzing whole blood at every sampling point the typical pattern of leucocytes with lymphocytes, monocytes, and neutrophil granulocytes could be observed (Figure 3.3.11 B (a)-(c)). But, additional peripheral phagocytosis into blood monocytes was not detectable at any time as none of the detected cell populations was associated with fluorescence expressed by the black dot plots (Figure 3.3.11 A-D). Figure 3.3.12 further confirms this finding by a missing shift of the according histogram plot towards increased fluorescence.

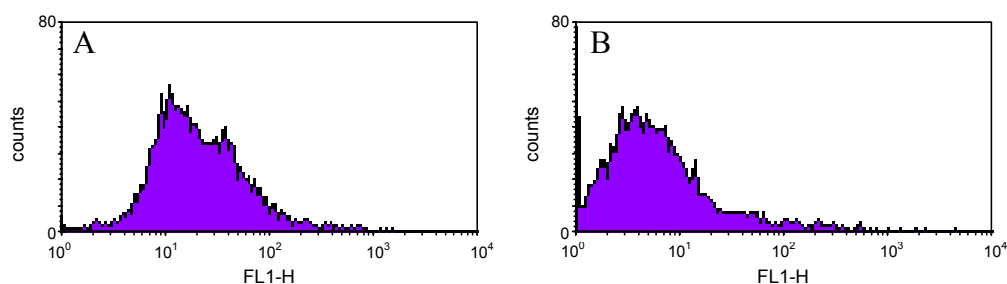


Figure 3.3.12 Histogram plots of rat whole blood analyzed before (A) and 15 min after (B) the application of G-NP₄₈₈

The observation of a very rapid accumulation within the MPS organs independently from surface charge made for the three tested gelatin nanoparticle formulations is confirmed by the findings of Roser who worked with albumin nanoparticles and described comparable results [Roser et al., 1998].

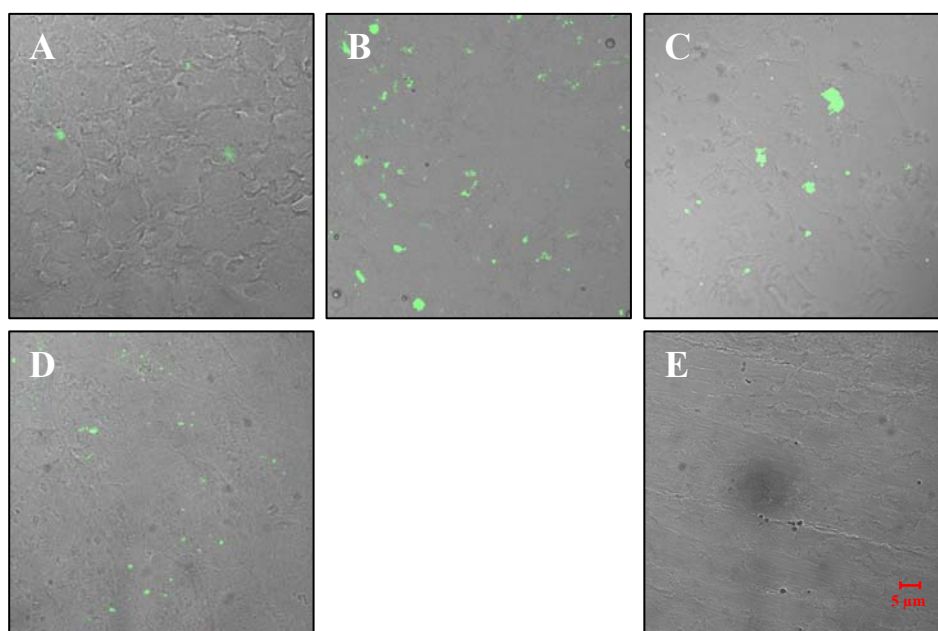


Figure 3.3.13 CLSM pictures of (A) liver, (B) spleen, (C) lung, (D) kidney, and (E) femoral muscle taken from organs resected 1 h after injection of P188-SLNC₆ (green) into the jugular vein

The organ distribution of solid lipid nanoparticles is shown in Figure 3.3.13. In contrast to gelatin nanoparticle formulations a certain amount was detected in the spleen and only small amounts were detected in liver, lung, and interestingly as well in kidney. The lower extent accumulated in single organs and the appearance of SLN in the kidney reflect the differences already found during 2D-PAGE analysis for gelatin and solid lipid nanoparticle formulations. The main differences obtained from organ distribution studies are opposed in Figure 3.3.14.

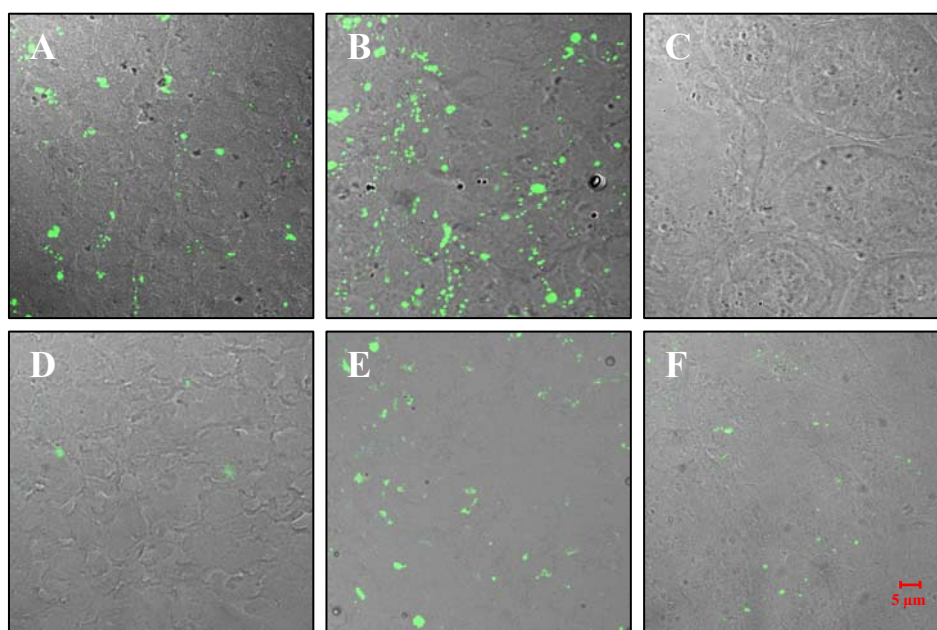


Figure 3.3.14 CLSM pictures of (A/D) liver, (B/E) spleen, and (C/F) kidney taken from organs resected 1 h after injection of G-NP₄₈₈ pos (A/B/C) (green) and P188-SLN_{C6} (D/E/F) (green) respectively into the jugular vein

The lack of opsonin adsorption on SLN seems to prevent an extensive phagocytosis by the MPS and presumably prolongs circulation. Though kinetic data from FACS analysis of P188-SLN_{C6} distribution studies revealed at first complete clearance from circulation as well after 15 min, which was contradictory considering the low organ accumulation demonstrated via CLSM. There were not any nanoparticles detectable in plasma or in association with blood monocytes and thus, with lacking fluorescence the histogram plots again look almost identical (Figure 3.3.15).

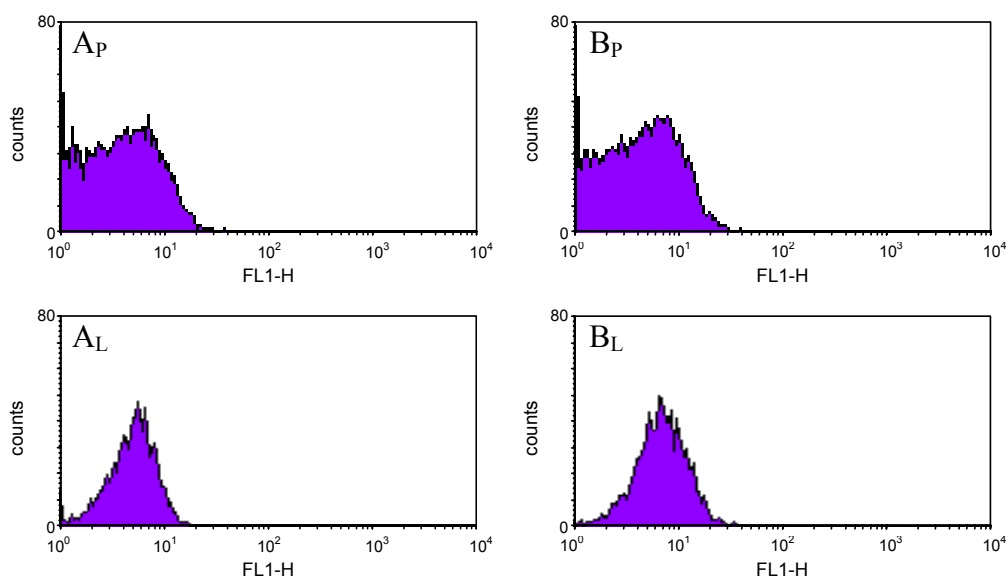


Figure 3.3.15 Histogram plots of rat plasma (A_P/B_P) and whole blood (A_L/B_L) analyzed before (A_P/A_L) and 15 min after (B_P/B_L) the application of P188-SLN_{C6}

Increasing the applied SLN concentration by factor 20 suggested a dilution effect to be responsible for these findings. Monitoring the organ distribution pattern to be qualitatively and (semi-) quantitatively constant, SLN could be detected circulating with plasma (Figure 3.3.16) and associated with white blood cells (Figure 3.3.17). In both series of histogram plots a pronounced shift of counted events towards increased fluorescence intensity can be found for all three – after application of SLN – investigated sampling points.

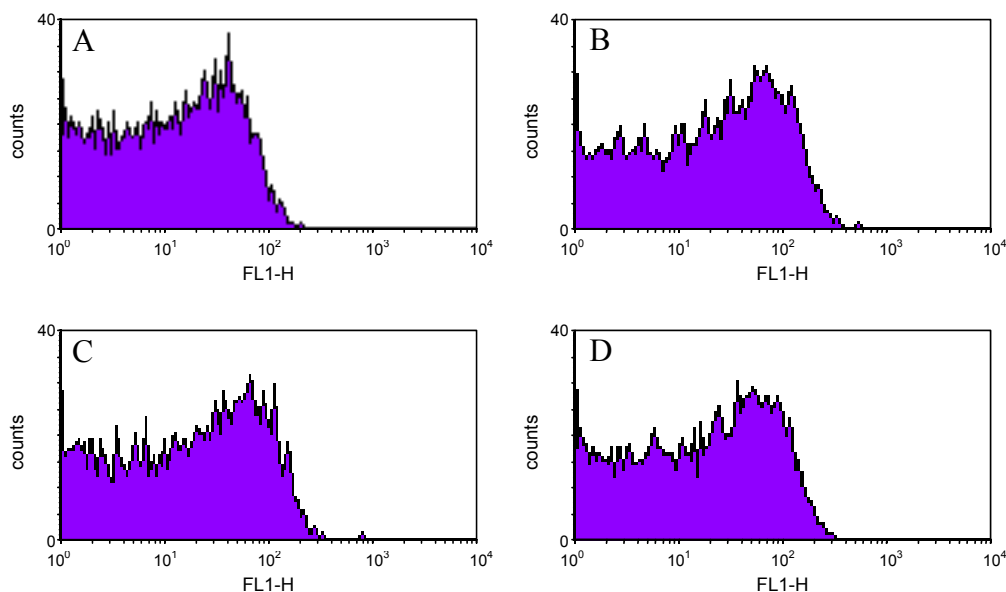


Figure 3.3.16 Histogram plots of rat plasma analyzed before (A) and 15 min (B), 30 min (C), and 60 min (D) after application of a 20x increased amount of P188-SLN_{C6}

It has to be mentioned that it can not be differentiated from these data between phagocytosis and adsorption to blood cells. But with respect to the low rate of phagocytosis reported for tissue macrophages an adsorptive process seems to be more likely.

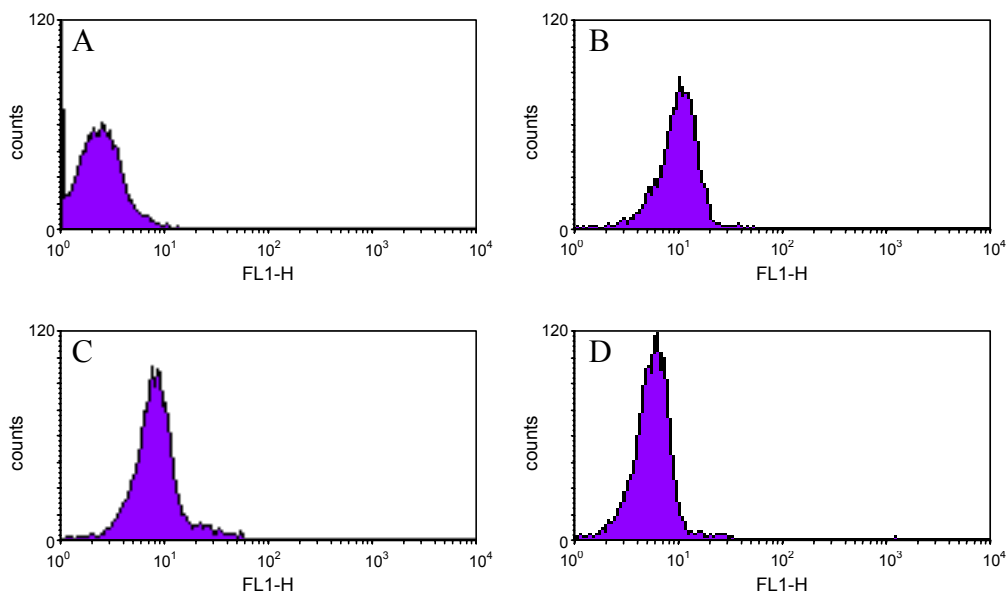


Figure 3.3.17 Histogram plots of rat whole blood analyzed before (A) and 15 min (B), 30 min (C), and 60 min (D) after application of a 20x increased amount of P188-SLN_{C6}

The increase in fluorescence intensity determined in plasma is summarized in Figure 3.3.18. Interestingly comparable intensities were observed over the complete experiment duration, which denotes clearly prolonged circulation of solid lipid nanoparticles compared to gelatin nanoparticles. But it has to be confined, that the dramatic increase in SLN concentration causes live threatening conditions for the test animal and that data from these experiment mainly contributes to elucidating the dilution effect seen for SLN applied in standard concentrations. Thus data should not be overestimated in terms of interpreting biodistribution and circulation time.

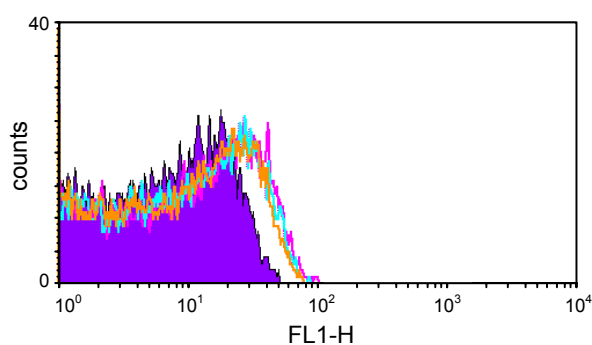


Figure 3.3.18 Histogram plots of rat plasma analyzed before (violet) and 15 min (pink), 30 min (light blue), and 60 min (orange) after application of a 20x increased amount of P188-SLN_{C6}

3.3.4 Summary

Plasma protein adsorption patterns of all investigated gelatin nanoparticle formulations were proven to be comparable. The introduction of the positively charged cholamin onto the surface of the nanoparticles caused thereby slight quantitative changes in the observed adsorption patterns compared to not surface-modified gelatin nanoparticles. This was not further pronounced by loading the nanoparticles with a double-stranded DNA oligonucleotide. All plasma protein adsorption patterns are dominated by opsonic proteins, which is in strong contrast to solid lipid nanoparticles mainly adsorbing apolipoproteins. Species specific differences could be detected after incubating gelatin nanoparticles with human or rat plasma but still revealing an adsorption pattern dominated by opsonic proteins.

In addition to 2D-PAGE data *in vivo* results showed a differentiated behavior for gelatin and solid lipid nanoparticles and confirmed the knowledge about the plasma protein adsorption pattern to be decisive for the *in vivo* fate of colloidal drug carrier systems. Slight formulation dependent differences in between gelatin nanoparticles revealed by 2-DE were leveled by the *in vivo* conditions, which is reflected by rapid clearance from circulation and almost identical biodistribution observed for all gelatin nanoparticle formulations. In contrast SLN exhibited a reduced and unspecific organ distribution accompanying with a prolonged plasma half life.

Thus our data could contribute to the intended correlation of plasma protein adsorption patterns with the respective biodistribution data of nanoparticulate drug delivery systems in terms of a better understanding of *in vivo* findings. In this context it has to be stated that gelatin nanoparticles exhibit only poor circulating properties and are thus not applicable for effective drug delivery except macrophage targeting without further modifications extending their plasma half life like PEGylation (cp. chapter 1.5).

Finally, the missing organ specific accumulation and the described dilution of solid lipid nanoparticles within the blood stream led - compared to gelatin nanoparticles - to a low recovery rate of the SLN in the sum of CLSM and FACS analysis.

3.4 NF- κ B Inhibition During Hepatic Ischemia Reperfusion Injury

With respect to the proposed selective inhibition of NF- κ B in Kupffer cells positively affecting hepatic I/R injury the exclusive Kupffer cell uptake of gelatin nanoparticles could be proven (chapter 3.2). In the second step it was thereafter the challenge to develop an NF- κ B decoy oligonucleotide loaded gelatin nanoparticle formulation which is stable under physiological conditions and that delivers adequate amounts of the NF- κ B decoy ODN for the inhibition of NF- κ B in Kupffer cells and that does not further pronounce liver injury occurring from ischemia and reperfusion.

3.4.1 Materials and methods

Reagents

Reagent	Description	Supplier
Acetone	p.a.	VWR International GmbH (Ismaning, Germany)
Cholaminechloride hydrochloride	(2-aminoethyl)-trimethyl-ammoniumchloride hydrochloride	Sigma-Aldrich GmbH (Taufkirchen, Germany)
DOPC	1,2-dioleoyl-sn-glycero-3-phosphocholine	Avanti Polar Lipids, Inc. (Alabaster, AL, USA)
DOTAP-Cl	1,2-dioleoyl-3-trimethylammonium-propane (chloride salt)	Avanti Polar Lipids, Inc. (Alabaster, AL, USA)
ds NF- κ B decoy ODN	5'-AGT TGA GGG GAC TTT CCC AGG C-3' phosphorothioate	biomers.net GmbH (Ulm, Germany)
ds scr decoy ODN	5'-CCT TGT ACC ATT GTT AGC C-3' phosphorothioate	biomers.net GmbH (Ulm, Germany)
EDC	1-ethyl-3-(3-dimethyl-aminopropyl) carbodiimide hydrochloride	Sigma-Aldrich GmbH (Taufkirchen, Germany)
Ethanol	96 %	Merck KGaA (Darmstadt, Germany)
Gelatin type A	175 Bloom	Sigma-Aldrich GmbH (Taufkirchen, Germany)
Glutaraldehyde	25 % aqueous solution	Sigma-Aldrich GmbH (Taufkirchen, Germany)

Reagent	Description	Supplier
HCl	2 N	VWR International GmbH (Ismaning, Germany)
PBS	Dulbecco's phosphate buffered saline pH 7.4 (1x concentrate)	PAA Laboratories GmbH (Linz, Austria)
Sucrose		Suedzucker AG (Mannheim, Germany)
Tween® 80	Polysorbat 80, Ph. Eur.	Merck KGaA (Darmstadt, Germany)

Fluorescent staining

Reagent	Description	Supplier
Alexa Fluor® 633 goat- anti-mouse IgG ₁ (γ ₁)	λ _{em} 647 nm	Invitrogen GmbH (Karlsruhe, Germany)
BSA	bovine serum albumin, Cohn Fraction V	Sigma-Aldrich GmbH (Taufkirchen, Germany)
ds NF-κB decoy ODN ₄₈₈	5'-AGT TGA GGG GAC TTT CCC AGG C-3' 5' Alexa Fluor® 488 labeled, λ _{em} 519 nm, phosphorothioate	biomers.net GmbH (Ulm, Germany)
Hoechst 33342	trihydrochloride, trihydrate, λ _{em} 461 nm	Invitrogen GmbH (Karlsruhe, Germany)
Mouse-anti-rat CD163 IgG ₁		AbD Serotec GmbH (Duesseldorf, Germany)
Permafluor	aqueous mounting medium	Beckmann Coulter GmbH (Krefeld, Germany)
Triton® X-100		Sigma-Aldrich GmbH (Taufkirchen, Germany)

Electrophoretic Mobility Shift Assay (EMSA)

Solution	Components*	Concentration
Buffer A	Hepes pH 7.9	10 mM
	KCl	10 mM
	EDTA	0.1 mM
	EGTA	0.1 mM
	DTT [#]	1 mM
	PMSF [#]	0.5 mM

Solution	Components*	Concentration
Buffer B	Hepes pH 7.9	20 mM
	NaCl	400 mM
	EDTA	1 mM
	EGTA	0.5 mM
	Glycerol	25 %
	DTT [#]	1 mM
	PMSF [#]	1 mM
STE buffer pH 7.5	Tris-HCl	10 mM
	NaCl	100 mM
	EDTA	1 mM
	Glycerol	20 %
5x binding buffer pH 7.5	MgCl ₂	5 mM
	EDTA	2.5 mM
	NaCl	250 mM
	Tris-HCl	50 mM
	Glycerol	20 %
Gel loading buffer pH 7.5	Tris-HCl	250 mM
	Bromphenolblue	0.2 %
	Glycerol	40 %
Reaction buffer	DTT	2.6 mM
	5x binding buffer	90 %
	Gel loading buffer	10 %
10x TBE pH 8.3	Tris	0.89 M
	Boric acid	0.89 M
	EDTA	0.02 M
Non-denaturing polyacrylamid gel (4.5 %)	10x TBE	5.3 %
	PAA solution (30 %)	15.8 %
	Glycerol	2.6 %
	TEMED	0.05 %
	APS	0.08 %

*All buffer salts were purchased from Sigma-Aldrich GmbH (Taufkirchen, Germany)

[#]DTT and PMSF were added to the buffer stock solution (A and B) directly before use

Preparation and surface modification of gelatin nanoparticles

Gelatin nanoparticles were manufactured by the two step desolvation method and surface modified (cationized) with cholamine as described in chapter 1.2.

Oligonucleotide-loading of gelatin nanoparticles

80.9 μL of an aqueous nanoparticle dispersion containing 1.7 mg surface modified gelatin nanoparticles was incubated with 120 μL of an aqueous oligonucleotide solution containing 6 nmol NF- κB decoy ODN (i.e., 5 % [w/w] drug loading) in PBS adjusted to a final volume of 1,200 μL for 2 h at 22 °C and 800 rpm under constant shaking (Thermomixer Comfort, Eppendorf AG, Hamburg, Germany).

Freeze dried formulation of empty and oligonucleotide loaded gelatin nanoparticles

40.5 μL and 34.8 μL of aqueous nanoparticle dispersions containing 0.85 mg and 0.73 mg surface modified gelatin nanoparticles were incubated with 120 μL aqueous oligonucleotide solution containing 6 nmol NF- κB decoy ODN and 6 nmol scr decoy ODN respectively (i.e., 10 % [w/w] drug loading) in 1,030.2 μL and 1,053.7 μL highly purified water for 2 h at 22 °C and 800 rpm under constant shaking (Thermomixer Comfort, Eppendorf AG, Hamburg, Germany). For the formulation of freeze dried empty nanoparticles 0.73 mg surface modified gelatin nanoparticles were diluted in highly purified water to a volume of 1,053.7 μL . Afterwards 169.8 μL and 146.3 μL respectively of a sucrose solution (10 % [w/v] dissolved in highly purified water) were added to a total volume of 1,200 μL . The amount of sucrose added accounted for an excipient to oligonucleotide ratio of 200 (cp. chapter 2.3.1). Subsequent suspensions were transferred to 2R glass vials (Schott AG, Mainz, Germany) and dried in an EPSILON 2- 6D pilot scale freeze dryer from Martin Christ Freeze Dryers GmbH, Osterode, Germany with the below stated freeze drying cycle (Figure 3.4.1). Upon completion of this cycle the chamber was vented with nitrogen, samples were stoppered under slight vacuum, and the sealed vials were stored at 20 °C. Rehydration was conducted directly before use in 169.8 μL and 146.3 μL respectively of highly purified water under adding a Tween[®] 80 solution (100 $\mu\text{g}/\mu\text{L}$) in a 1:1 ratio to the mass of gelatin nanoparticles leading to a concentration of 10 % sucrose [w/v], which is almost isoosmotic. Finally, samples were completed with a 10 % [w/v] sucrose solution to a total volume of 300 μL . Four samples were combined per animal study, in sum containing 24 nmol of the respective oligonucleotide in 1.2 mL. For liver distribution studies the described

procedure was conducted with identical amounts of fluorescent-labeled NF- κ B decoy ODN₄₈₈.

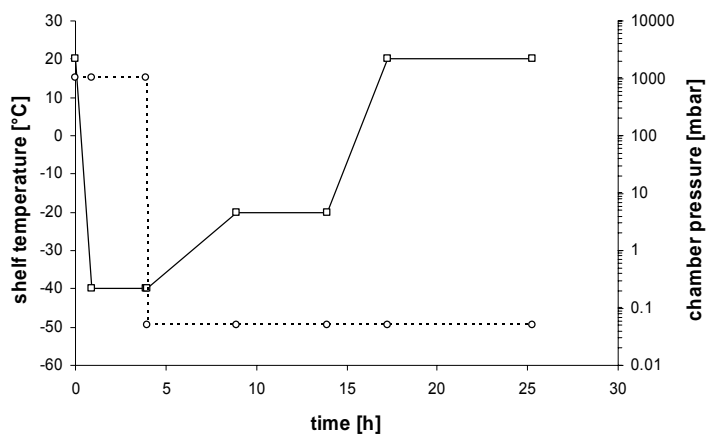


Figure 3.4.1 Freeze drying cycles with shelf temperature (□) and chamber pressure (○)

Preparation of NF- κ B decoy oligonucleotide loaded liposomes

Drug loaded liposomes were prepared by ethanol injection with the oligonucleotide already present in the water phase. The drug loading is driven by opposing electrostatic attractive forces as they are as well utilized for the drug loading process of gelatin nanoparticles. Thereby the positively charged lipid headgroups interact with the negatively charged phosphodiester backbone of the oligonucleotide. The chosen ODN lipid ratio is geared to the work of Ogushi who applied an NF- κ B decoy oligonucleotide in a fatal liver failure murine model [Ogushi et al., 2003]. 28.74 μ L lipid ethanol stock solution (1.7932 g DOTAP-Cl and 1.6961 g DOPC in 10.0 g EtOH), were dropwise added into 1.5 mL ice cooled aqueous oligonucleotide solution containing 15 nmol NF- κ B decoy ODN (i.e., 2 % [w/w] drug loading) under constant stirring. The mixture was then 10x passed through a 0.22 μ m sterile filter. Caused by the extrusion process there is a certain sample loss, thus leading to a final volume around 1.2 mL containing 12 nmol/mL NF- κ B decoy ODN applicable for animal studies, equivalent to the sample volume of gelatin nanoparticle formulations. For liver distribution studies fluorescent-labeled NF- κ B decoy ODN₄₈₈ was incorporated into liposomes in reduced concentration, according to biodistribution studies conducted with ODN loaded gelatin nanoparticles. 150 μ L of ODN stock solution were diluted with PBS to a final volume of 1.5 mL, which was utilized for liposome preparation.

Characterization of liposomes and nanoparticles

Size and zeta potential of the applied liposome and gelatin nanoparticle batches were determined by dynamic light scattering (DLS) using a Nanosizer ZS (Malvern Instruments, Worcestershire, UK). Zeta potential measurements were conducted under standardized ionic conditions in 10 mM NaCl at pH 7.0.

In vivo biodistribution experiments

Experiments were conducted in male Sprague-Dawley rats. 1 mL of liposomal and gelatin nanoparticle formulations either loaded with fluorescent-labeled NF- κ B decoy ODN were directly injected into the portal vein. Prior to injection rats were anesthetized by i.p. injection of 0.005 mg/kg Fentanyl and 2.0 mg/kg Midazolam. Anesthesia was maintained over the whole experiment with 1.5 % Isofluran continuously applied using a vaporizer with Carbogen (5 % CO₂ / 95 % O₂) as carrier gas. To monitor blood pressure and control anesthesia the jugular artery was cannulated with a 16 gauge PE catheter and connected to a blood-pressure gauge. The abdomen was opened by midline-laparotomy and the portal triad was prepared. The body temperature was kept between 36.0 °C and 37.0 °C with a warming lamp.

After 15 min rats were sacrificed and blood was rinsed out. Liver was resected, frozen with liquid nitrogen and stored at -80 °C. The distribution of NF- κ B decoy ODN within the liver was determined via confocal laser scanning microscopy (CLSM).

CLSM imaging

Preparation of tissue samples from biodistribution studies was conducted as described in chapter 3.2.1. Compared to those studies Alexa Fluor[®] 488 labeling was used for the NF- κ B decoy ODN. Thus secondary antibody staining of Kupffer cells had to be achieved with an Alexa Fluor[®] 633 labeled IgG₁, whereas the staining protocol itself remained unaltered. In addition a nuclear staining was conducted following the protocol for the Kupffer cell staining as well explained in chapter 3.2.1. CLSM imaging was performed with a Zeiss LSM 510 Meta confocal laser scanning microscope (Carl Zeiss Microscope Systems, Jena, Germany).

In vivo Hepatic Ischemia Reperfusion rat model

Experiments were conducted in male Sprague-Dawley rats. Rats were anesthetized, the abdomen opened, and the portal triad prepared as described above.

Arterial and portal blood flow to the left lateral and median lobe of the liver was interrupted by applying an atraumatic clip, resulting in a 70 % liver ischemia. After 60 min of ischemia blood supply was restored by removal of the clip.

15 min prior to ischemia 1.0 mL of the accordingly prepared NF- κ B decoy ODN loaded, scr decoy ODN loaded, and empty gelatin nanoparticle suspension respectively was injected into the portal vein with a 1.0 mL syringe over a period of 5 min. Control experiments were conducted with nanoparticle free solvent.

Subsequent to collection of blood samples into heparinized tubes, animals were sacrificed after 120 minutes of reperfusion by bleeding. Liver was rinsed from blood by perfusing with PBS through the portal vein via a peristaltic pump at a flow of 55 mL/min for 2 min. The median lobe was excised and the remaining lobes were perfused with 3 % formalin in PBS for protein fixation. All tissues were cut in 3 mm cubes, immediately snap frozen in liquid nitrogen and kept at -80 °C until further examination. After centrifugation of blood samples at 5000 rpm for 8 min obtained plasma was stored in aliquots at -80 °C.

All animal studies were conducted thrice for each nanoparticle formulation.

In vivo hepatic LPS (sepsis) rat model

Experiments were conducted in male Sprague-Dawley rats. Rats were anesthetized, the abdomen opened, and the portal triad prepared as described above.

1.0 mL of the accordingly prepared NF- κ B decoy ODN loaded, scr decoy ODN loaded, and empty gelatin nanoparticle suspension as well as the liposomal formulation was respectively injected into the portal vein with a 1.0 mL syringe over a period of 5 min. Control experiments were conducted with nanoparticle / liposome free solvent. 15 min thereafter 10 μ g LPS (c = 50 μ g/mL in PBS, E. coli serotype 055:B05, Sigma-Aldrich GmbH, Taufkirchen, Germany) were injected into the portal vein, leading to sublethal sepsis. After waiting for another 30 min experiments were terminated and blood and tissue samples were collected as described above.

All animal studies were conducted thrice for both nanoparticle and liposomal formulations.

Electrophoretic Mobility Shift Assay (EMSA)

Extraction of nuclear protein 60 mg of liver tissue were homogenized in 0.6 mL of ice cooled Buffer A till a homogenous suspension was obtained. Samples were centrifuged at 1,000 rpm at 4 °C for 10 min. The pellet was resuspended in 300 µL Buffer A, followed by addition of 18 µL non ionic detergent (Nonidet) P-40 (USB Corp., Cleveland, Ohio, USA) and careful mixing. After 10 min of incubation under ice cooling, samples were centrifuged for 1 min at 14,000 rpm and 4 °C and the pellet was resuspended in 40 µL Buffer B. Finally samples were incubated by shaking for 30 min at 4 °C. After centrifugation (14,000 rpm, 10 min, 4 °C) undiluted supernatants were transferred to EMSA, and a dilution of 1:20 was used for determination of protein concentrations.

Measurement of protein concentration with Bradford-assay Protein concentration in isolated nuclear fractions was determined as described by Bradford [Bradford, 1976].

Radioactive labeling of consensus oligonucleotides Double stranded oligonucleotides, containing the NF-κB consensus sequence (5'-AGT TGA GGG GAC TTT CCC AGG C-3', Promega GmbH, Mannheim, Germany), were labeled with [γ^{32} P] adenosine triphosphate (3,000 Ci/mmol) by using the T4 polynucleotide kinase (PNK) (USB Corp., Cleveland, Ohio, USA), which catalyzes the transfer of the terminal phosphate of ATP to the 5'-hydroxyl terminus of the ODNs. Oligonucleotides were incubated with PNK for 10 min at 37 °C. The reaction was stopped by adding a 0.5 M EDTA solution. Subsequent radioactive labeled ODN was separated from unlabeled ODN by using NucTrap probe purification columns (Stratagene Inc., La Jolla, California, USA), whereas radiolabeled DNA was eluted from the column with 70 µL of STE buffer and frozen at -20 °C until use for EMSA.

Binding reaction and electrophoretic separation Equal amounts of nuclear protein (approximately 30 µg) were incubated in a total volume of 14 µL containing 2 µg poly(dIdC) and 3 µL reaction buffer for 10 min at room temperature. Afterwards 1 µL of the labeled oligonucleotide solution (approximately 300,000 cpm) was added and incubated with nuclear protein for 30 min at room temperature. The resulting nucleoprotein-oligonucleotide complexes were then separated by gel electrophoresis (Mini-Protean 3, Bio-Rad Laboratories GmbH, 198

Munich, Germany) at 110 V for 60 min on non-denaturing polyacrylamide gels (cp. table “EMSA”; Rotiphorese™ Gel 30, Carl Roth GmbH + Co. KG, Karlsruhe, Germany). Bands were detected by exposure of the gels to Cyclone Storage Phosphor Screens (Canberra-Packard GmbH, Dreieich, Germany) for about 24 h (time of exposure depended on radioactivity of the labeled oligonucleotides), followed by analysis with a phosphorimager station (Cyclone Storage Phosphor System, Canberra-Packard GmbH, Dreieich, Germany).

In vivo studies and electrophoretic mobility shift assays were conducted together with Florian Hoffmann at the department of pharmaceutical biology of the Ludwig-Maximilians-University Munich, Germany. So, the present data are a result from the cooperation between the chairs of Pharmaceutical Technology and Pharmaceutical Biology of the Ludwig-Maximilians-University Munich described at the beginning of this chapter and will be discussed under further aspects in the thesis of Florian Hoffmann [Hoffmann, 2007].

3.4.2 Results and discussion

Characterization of gelatin nanoparticles and liposomes

All applied nanoparticle and liposome formulations had similar sizes between 230 and 280 nm. Compared to gelatin nanoparticles liposomes exhibit a higher polydispersity with a PDI above 0.200 typically seen for liposomes. During manufacturing of liposomes large fluidic structures are broken down; this degrading kind of manufacturing does not provide ideally i.e., homogenously distributed sizes, which is expressed in the depicted polydispersity. In addition due to the positively charged headgroups of the applied lipids, DOTAP/DOPC liposomes are characterized by a very high zetapotential around +45.0 mV (determined in 10 mM NaCl at pH 7.0). Thus the zetapotential after oligonucleotide-loading remains higher than for oligonucleotide loaded gelatin nanoparticles (cp. chapter 3.3.3).

Table 3.4.1 Size, polydispersity, and surface charge of gelatin nanoparticle and liposome formulations applied for biodistribution and *in vivo* ischemia reperfusion and LPS models

	Gelatin nanoparticles (empty) (G-NP 06-028 pos)	DOTAP/DOPC liposomes loaded with NF- κ B decoy ODN ₄₈₈ (Lip + O ₄₈₈)	DOTAP/DOPC liposomes loaded with NF- κ B decoy ODN (Lip + O)
size [nm]	261.0	228.5	279.0
PDI	0.069	0.244	0.269
ZP [mV]	+16.6	+11.3	+12.6

Hepatic Ischemia Reperfusion model in rat

Even though liver injury caused by hepatic I/R injury takes place 6-48 h after reperfusion [Teoh et al., 2003a] the described duration of the animal study with 1 h of ischemia and 2 h of reperfusion is adequate as I κ B phosphorylation, initial step of the NF- κ B activation, already starts after 30 min. After 1 h NF- κ B activation reaches its maximum and both I κ B phosphorylation and NF- κ B activation approximate basal amounts after 3 h of reperfusion [Zwacka et al., 1998]. Thus targeting the NF- κ B activation during the stated experimental period is feasible. In addition, considering the removed abdominal wall, keeping the test animal over a period of 6-48 h alive is even under anesthesia hardly possible. Partial ischemia was chosen to facilitate the

survival of the test animal until the end of the 2 h reperfusion period. Technical reasons led to adjusting the volume of nanoparticle and liposome formulations prepared for the animal studies to 1.2 mL. To guarantee a reproducible injection of 1 mL i.e., a reproducible amount of NF- κ B decoy oligonucleotide applied per attempt is only possible if not the whole formulation has to be injected and a certain excess volume remains within the infusion system.

The first experiments were conducted with 5 nmol NF- κ B decoy oligonucleotide applied per animal study. The amount of 5 nmol represents the maximum pay load of 5 % [w/w] on gelatin nanoparticles achievable under PBS buffered conditions and was proven to be complete via UV-spectroscopy. By further increasing the amount of the NF- κ B decoy ODN for a drug loading above 5 % [w/w] aggregation of the nanoparticles occurred. Similar findings were reported by Goetting who investigated the effect of a 16mer PTO oligonucleotide-loading on the stability of polystyrene nanoparticles investigated as model delivery system for antisense drugs [Goetting et al., 1999]. Presumably this is caused by missing electrostatic repulsion forces between nanoparticles, which are compensated by an elevated drug loading process and are in general necessary to stabilize nanoparticle suspensions [Mueller, 1996]. The, compared to empty surface-modified nanoparticles, reduced zeta potential already referred for 5 % [w/w] oligonucleotide loaded gelatin nanoparticles in chapter 3.3.3 demonstrates the influence of the loading process to the nanoparticles' surface charge and strengthens this assumption. Furthermore, the ionic strength of the PBS buffered environment leads to diminished surface charges and therefore reduced zeta potential values of the nanoparticles. High concentrations of the nanoparticle suspensions may additionally foster interparticulate bridging of oligonucleotide molecules and are thus a possible explanation for the observed nanoparticle aggregation as well. In addition the total suspension volume injected per rat could not be further increased to avoid undesired side effects from a strongly expanded plasma volume. Therefore 5 nmol NF- κ B decoy oligonucleotide were the maximum amount applicable under the chosen conditions.

The presence of NF- κ B within livers obtained from animal studies was followed by an electrophoretic mobility shift assay (EMSA). During this assay NF- κ B extracted from liver tissue is visualized via coupling with a radioactive labeled oligonucleotide bearing the NF- κ B consensus sequence. Built

protein-oligonucleotide complexes are separated from unbound oligonucleotide during gel electrophoresis and can be quantified by their radioactive intensity within the gel. Thus, if NF- κ B amounts are lowered a reduced number of protein-oligonucleotide complexes is formed, which results in fewer radiation intensities detectable. This in turn is expected for the assumed *in vivo* interaction between nanoparticulate delivered NF- κ B decoy oligonucleotides and NF- κ B. Figure 3.4.2 displays the bands of protein-oligonucleotide complexes derived from hepatic I/R animal studies conducted with and without NF- κ B decoy ODN treatment. As the intensities of all bands are almost identical an inhibitory effect of the NF- κ B decoy oligonucleotide can not be stated.

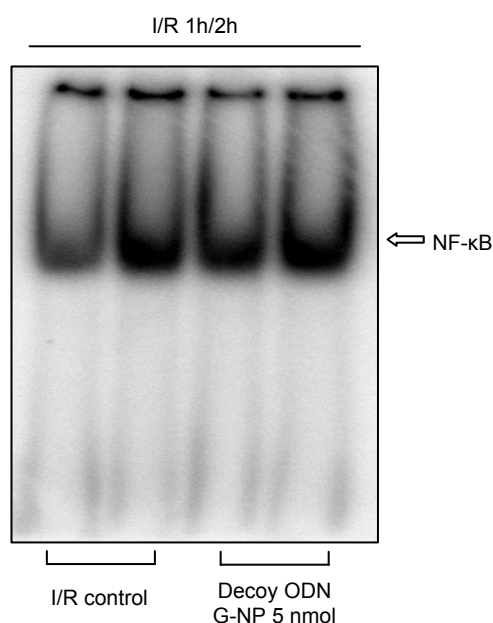


Figure 3.4.2 Hepatic NF- κ B activation caused by 1 h of ischemia and 2 h of reperfusion of animals treated with 5 nmol NF- κ B decoy oligonucleotide and of untreated animals; one band represents one animal study

These results were verified several times and also changing the experimental setup towards a reduced reperfusion time of 1 h did not reveal any detectable NF- κ B inhibition. As the amount of NF- κ B decoy ODN applicable per animal study could not be increased for the above explained reasons, increasing the concentration of the stable 5 % [w/w] oligonucleotide loaded gelatin nanoparticle formulations became crucial. Addressing this need Anchordoquy described a freeze drying based procedure for the production of concentrated suspensions of polyethylenimine (PEI) DNA complexes possessing isoosmotic amounts of freeze drying excipients [Anchordoquy et al., 2005]. Based on their work an analog procedure could be

developed, which allows the preparation of stable 20 nmol NF- κ B decoy oligonucleotide containing drug loaded gelatin nanoparticle suspensions (chapter 2.3.1). The drug loading could thereby be increased to 10 % [w/w] so that the fourfold amount of oligonucleotide comes along with 2x higher amounts of gelatin nanoparticles. Exposure of these newly developed samples to blood plasma with its elevated ionic strength led to the same aggregation tendencies already reported for loading attempts with increased amounts of oligonucleotide and nanoparticles. According to Goetting who worked with poloxamer 388 to overcome this problem [Goetting et al., 1999], concentrated ODN-loaded nanoparticles were coated with Tween[®] 80 in a 1:1 [w/w] Tween[®] 80:nanoparticle ratio as described in chapter 2.3.1. Empty nanoparticle formulations as well as NF- κ B decoy or scr decoy oligonucleotide-loaded nanoparticle formulations were all treated the same way.

To determine the influence of the nanoparticle formulations on the progression of liver injury after ischemia and reperfusion, transaminases were determined in rat plasma samples taken after terminating the animal studies. The plasma concentration of transaminases is the standard clinical parameter that is utilized for evaluating the current liver status as their release is enhanced from damaged hepatocytes, whereas alaninaminotransferase (ALT) and aspartataminotransferase (AST) are the routinely monitored enzymes. Their concentrations after I/R animal studies conducted with and without decoy ODN loaded and empty nanoparticles are summarized in Figure 3.4.3.

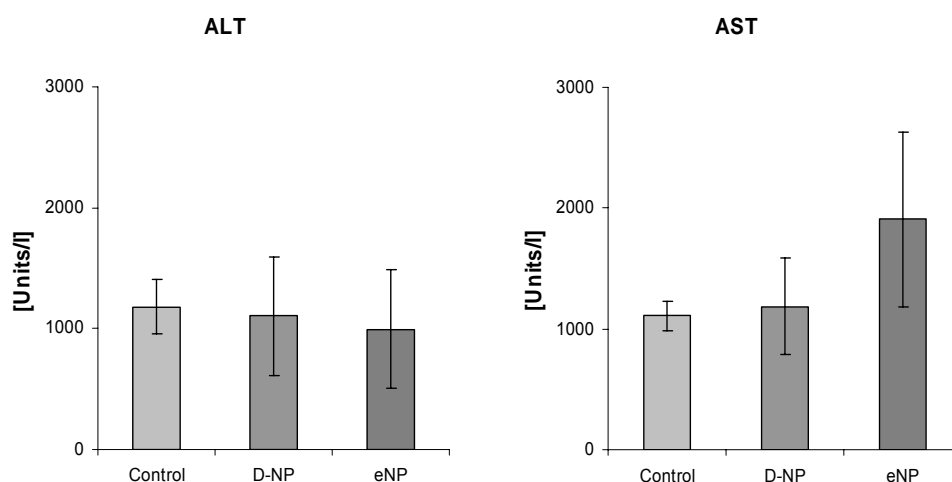


Figure 3.4.3 Transaminases determined in rat plasma after 1 h of ischemia and 2 h of reperfusion of animals treated with 20 nmol NF- κ B decoy oligonucleotide loaded gelatin nanoparticles (D-NP) and empty nanoparticles (eNP) and of untreated animals (Control); each animal study was performed three times represented by the error bars

With respect to the great margins of deviation typically seen for animal studies nearly all displayed transaminase concentrations account for almost identical values. Despite the high concentration of nanoparticle suspensions injected there was no further statistical significant increase in transaminases concentration detectable, which underlines the exceptional physiological tolerability of gelatin nanoparticles already reported by Zwiorek during comparative *in vitro* studies with PEI polyplexes and liposomes [Zwiorek, 2006]. In addition, data indirectly show the successful stabilization of the nanoparticles by Tween[®] 80.

In the following empty nanoparticles as well as scr decoy ODN and NF- κ B decoy ODN loaded gelatin nanoparticles were investigated for their NF- κ B inhibiting properties in hepatic I/R animal studies. Reference experiments were identically performed except the injection of any nanoparticle formulation. The resulting EMSA electrophoresis gel shows a clear attenuation of the NF- κ B band for all three animal studies performed with NF- κ B decoy ODN loaded gelatin nanoparticles (Figure 3.4.4).

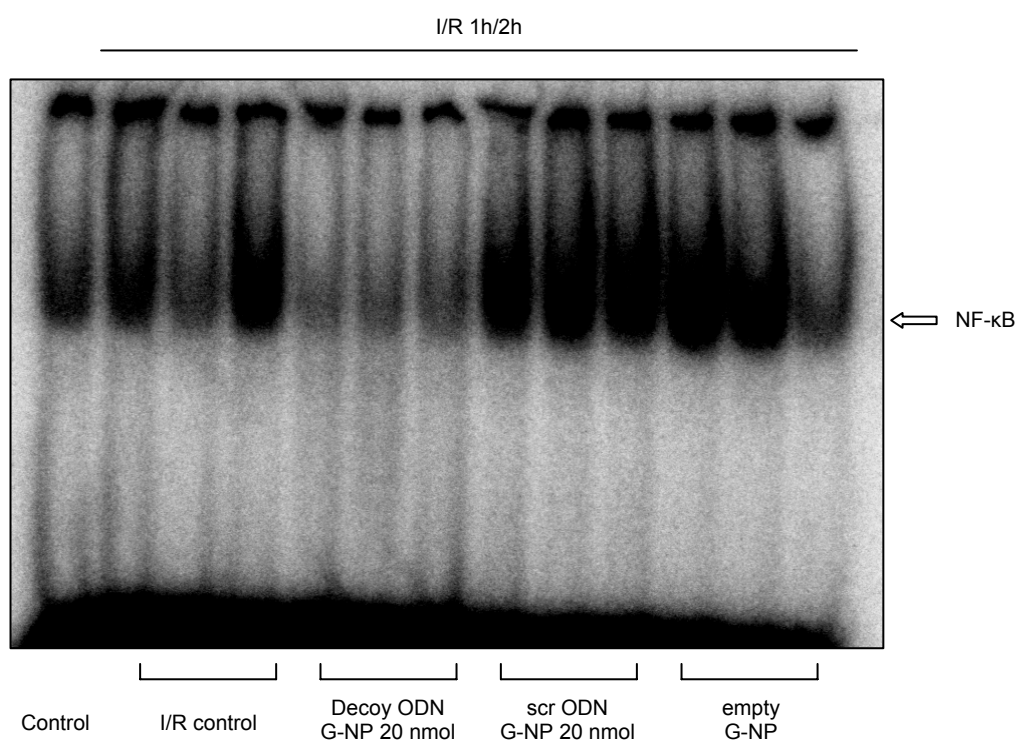


Figure 3.4.4 Hepatic NF- κ B activation caused by 1 h of ischemia and 2 h of reperfusion of animals treated with 20 nmol NF- κ B decoy oligonucleotide and 20 nmol scr decoy oligonucleotide loaded gelatin nanoparticles as well as empty nanoparticles and of untreated animals; one band represents one animal study

Related to the former experiments conducted with 5 nmol NF- κ B decoy ODN a concentration dependent mechanism can be assumed, which illustrates the quantitative principle of action of a decoy oligonucleotide. At the same time scr decoy ODN loaded and empty gelatin nanoparticles only slightly alter the appearance of the detected NF- κ B bands. The exhibited respective radiation intensities are rather comparable to those of the reference (I/R control) experiments than to the experiments applying the NF- κ B decoy ODN. The findings additionally prove the selectivity of the NF- κ B decoy oligonucleotide for NF- κ B especially in comparison to the chosen scr decoy oligonucleotide.

However, phagocytotic uptake through Kupffer cells stands for their activation with its according signaling pathways [Aderem et al., 1999]. In addition to the outcome of I/R injury and the inhibition of NF- κ B, this is a third factor influencing signal transduction and expression of involved proteins. Thus, investigations on the molecular stage might reveal differences for liver tissue derived from animals treated with empty gelatin nanoparticles and from control animals being only exposed to ischemia and reperfusion. These parameters and the outcome of the NF- κ B inhibition within Kupffer cells are further discussed in the work of Florian Hoffmann [Hoffmann, 2007].

Lipopolysaccharide (LPS) induced hepatic NF- κ B response in rat

Subsequent to intraportal injection LPS induces NF- κ B activation in liver. This activation can be as well used for evaluating the NF- κ B inhibitory potential of NF- κ B oligonucleotide loaded gelatin nanoparticles. Compared to the hepatic I/R model the LPS setup is less elaborative and thus provides a faster approach to gain insight into mechanisms attributed to NF- κ B blockade in Kupffer cells. So, LPS was utilized in a second experimental setup to stimulate NF- κ B activation. Interestingly the resulting strong activation of NF- κ B could be as well completely inhibited by the application of 20 nmol nanoparticulate-bound NF- κ B decoy oligonucleotide. In addition neither scr decoy ODN loaded nor empty gelatin nanoparticles had any diminishing influence on the detected NF- κ B bands. Figure 3.4.5 exemplarily displays the described outcome of the shift assays for one series of animal studies.

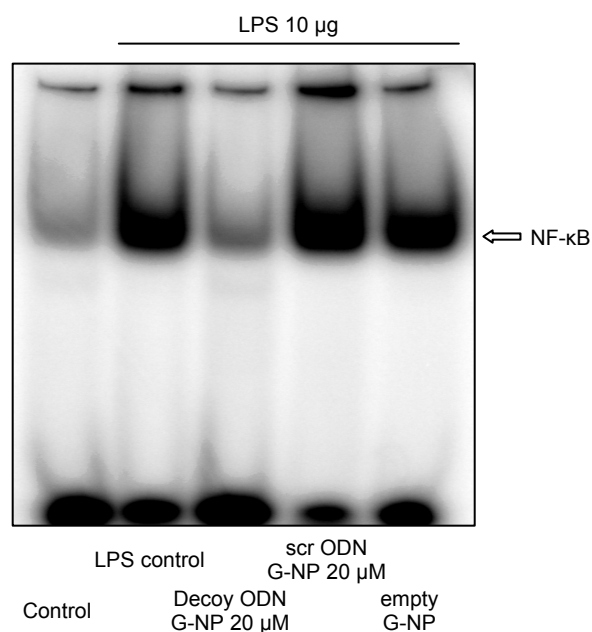


Figure 3.4.5 Hepatic NF- κ B activation after stimulation with 10 μ g LPS of animals treated with 20 nmol NF- κ B decoy oligonucleotide and 20 nmol scr decoy oligonucleotide loaded gelatin nanoparticles as well as empty nanoparticles and of untreated animals; one band represents one animal study

Again, downstream processes related to NF- κ B activation and NF- κ B inhibition respectively are investigated and discussed by Florian Hoffmann [Hoffmann, 2007].

Liposomal vs. gelatin nanoparticulate delivery of the NF- κ B decoy oligonucleotide to Kupffer cells

The so far presented results demonstrate the ability of gelatin nanoparticles to selectively address Kupffer cells and at the same time to deliver an oligonucleotide drug substance to its designated target where it finally could deploy its function. In a further step emphasis was laid on ranking these results. As the liposomal delivery of NF- κ B decoy oligonucleotides to liver was just recently described in literature [Ogushi et al., 2003; Higuchi et al., 2006; Higuchi et al., 2007] liposomes were chosen for comparative studies. Therefore liposomal formulations loaded with the known NF- κ B decoy oligonucleotide were prepared and applied in the established *in vivo* biodistribution and hepatic LPS animal test systems. At first biodistribution studies with liposomes as well as gelatin nanoparticles each loaded with fluorescent-labeled NF- κ B decoy ODN₄₈₈ were conducted, whereas liver distribution after intraportal injection was focused on. The resulting distribution pattern of nanoparticulate delivered NF- κ B decoy ODN₄₈₈ corresponds to the biodistribution

data obtained from fluorescent-labeled gelatin nanoparticles (chapter 3.2.2). CLSM pictures exhibit a yellow combination color expressing the colocalization of fluorescent-labeled Kupffer cells (green) and NF- κ B decoy ODN₄₈₈ (red) (Figure 3.4.6 B, C, and E). No oligonucleotide derived fluorescence could be detected in areas without the green fluorescence from Kupffer cell staining.

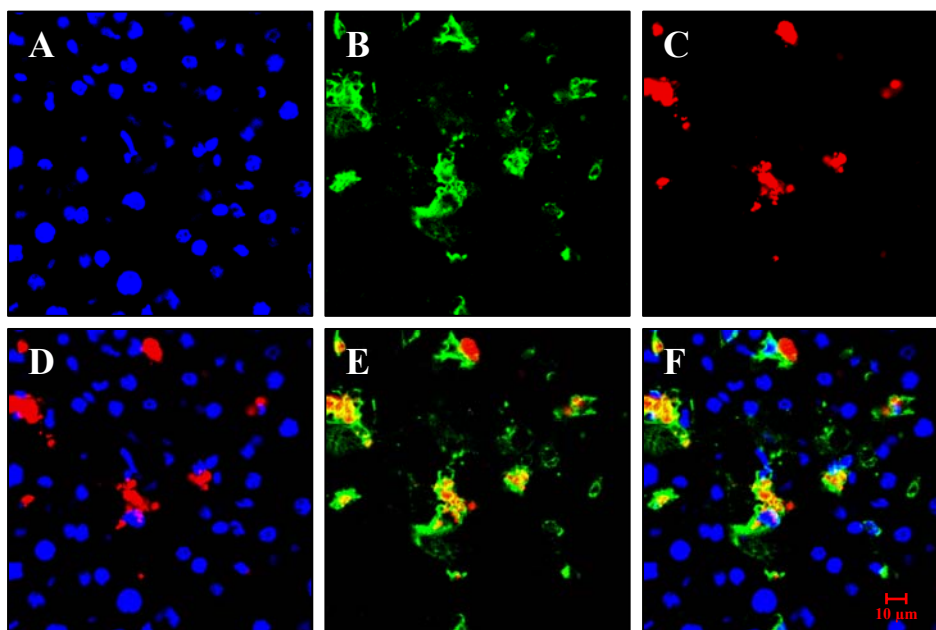


Figure 3.4.6 CLSM pictures of liver tissue taken from liver resected 15 min after injection of gelatin nanoparticulate (G-NP 06-028 pos) loaded ds NF- κ B decoy ODN₄₈₈ into the portal vein; pictures show different fluorescent stained structures (A) nuclei (blue), (B) Kupffer cells (green), (C) decoy ODN (red), and the overlay of (D) nuclei and decoy ODN, (E) Kupffer cells and decoy ODN, and (F) nuclei, Kupffer cells and decoy ODN

Looking at the according CLSM pictures from liposomal ODN delivery a comparable distribution pattern for the NF- κ B decoy ODN₄₈₈ is revealed on the first view (Figure 3.4.7). Again the overlay pictures E and F show the yellow combination color resulting from colocalization of fluorescent-labeled Kupffer cells (green) and NF- κ B decoy ODN₄₈₈ (red). In addition nuclear and ODN colocalization expressed in the pink combination color of picture D can be as well followed in picture F. It is indeed mainly superimposed by the described yellow combination color attributed to the same cells, but there are a couple of pink appearing nuclei (white arrows), which in contrast to nanoparticulate applied NF- κ B decoy ODN₄₈₈ clearly indicate a distribution beyond Kupffer cells. These findings of a preferable uptake into Kupffer cells accompanied by distinct extra Kupffer cell distribution are confirmed by the data of Higuchi. Despite a targeting ligand on the liposomal surface addressing the

fructose receptor uniquely expressed on Kupffer cells he describes liposomal uptake mainly into non parenchymal cells i.e., Kupffer cells but at the same time to certain extent into parenchymal cells i.e., hepatocytes [Higuchi et al., 2007]. According to Romero the uptake of liposomes into hepatocytes can be explained by the fluidic structure that enables their extrusion through the endothelial fenestrae of liver sinusoids despite exhibiting a bigger diameter than those [Romero et al., 1999].

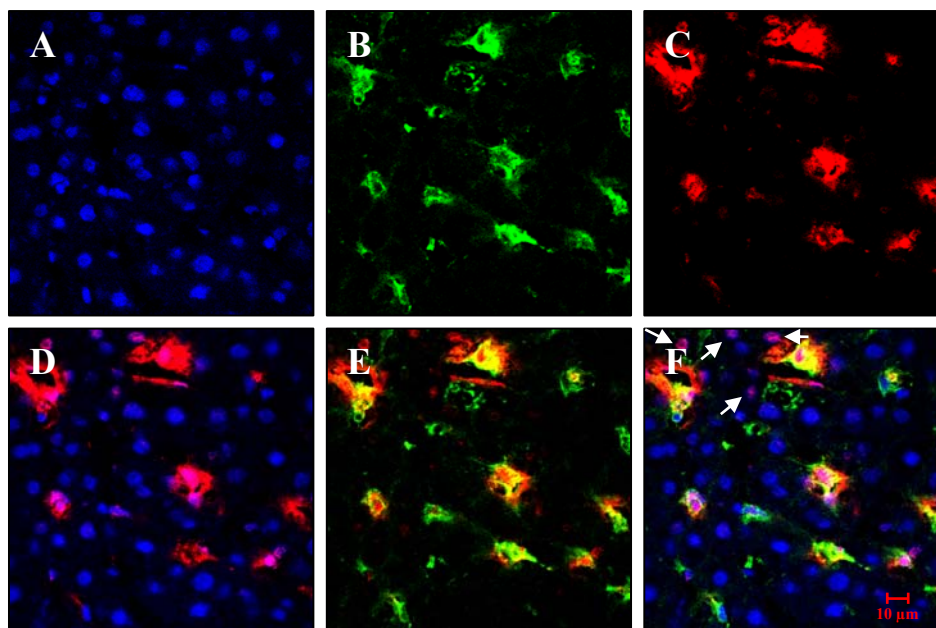


Figure 3.4.7 CLSM pictures of liver tissue taken from liver resected 15 min after injection of liposomal (Lip + O₄₈₈) loaded ds NF- κ B decoy ODN₄₈₈ into the portal vein; pictures show different fluorescent stained structures (A) nuclei (blue), (B) Kupffer cells (green), (C) decoy ODN (red), and the overlay of (D) nuclei and decoy ODN, (E) Kupffer cells and decoy ODN, and (F) nuclei, Kupffer cells and decoy ODN

Thus due to the colloidal nature of the applied drug delivery systems expected similarities in the distribution pattern could be observed, but a compared to liposomes higher Kupffer cell selectivity of gelatin nanoparticles potentially based on their solid nature could be highlighted.

As this study was conducted with the newly developed freeze dried nanoparticle formulation some additional conclusions can be drawn from these data. The increased nanoparticle (2x) and decoy ODN (4x) amount and the stabilizing Tween[®] 80 coating did not negatively affect the biodistribution. A perfect colocalization of Kupffer cells and NF- κ B decoy oligonucleotide could still be observed. To reduce nanoparticle load per test animal by increasing the drug loading up to 10 % [w/w] the freeze dried formulation was developed under reduced ionic strength in sucrose solution. Interestingly the transfer into the *in vivo* situation with

its increased ionic strength did not affect the drug loading in way that a diffusive ODN distribution over the whole organ could be seen which may have been caused by partial unloading of the nanoparticles as it is known for siRNA from former *in vitro* experiments conducted in PBS [Zillies et al., 2004].

In the following studies with 10 nmol NF- κ B decoy oligonucleotide bound to liposomes were accomplished in the LPS rat model. When the liposome experiments were conducted the freeze dried gelatin nanoparticle formulation with its higher amounts of decoy ODN was not yet available. Thus the 10 nmol drug loading was chosen to investigate a compared to gelatin nanoparticles twofold ODN amount per animal study, which finally led to a partial inhibition of NF- κ B (Figure 3.4.8).

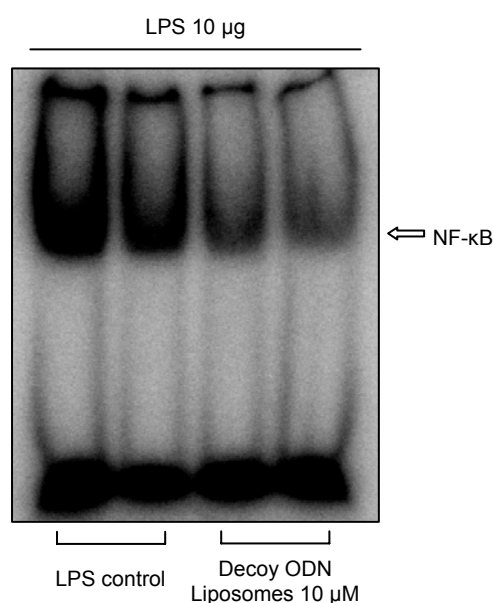


Figure 3.4.8 Hepatic NF- κ B activation after stimulation with 10 μ g LPS of animals treated with 10 nmol NF- κ B decoy oligonucleotide loaded liposomes and of untreated animals; one band represents one animal study

After completing experiments with the freeze dried nanoparticle formulation, samples from the different animal studies were combined in one EMSA to oppose results (Figure 2.3.23). The results substantiate the concentration dependent mechanism discussed above. After the application of 10 nmol liposomal delivered NF- κ B decoy ODN in two of three cases compared to LPS control animals decreased radiation intensity can be observed (Figure 2.3.23).

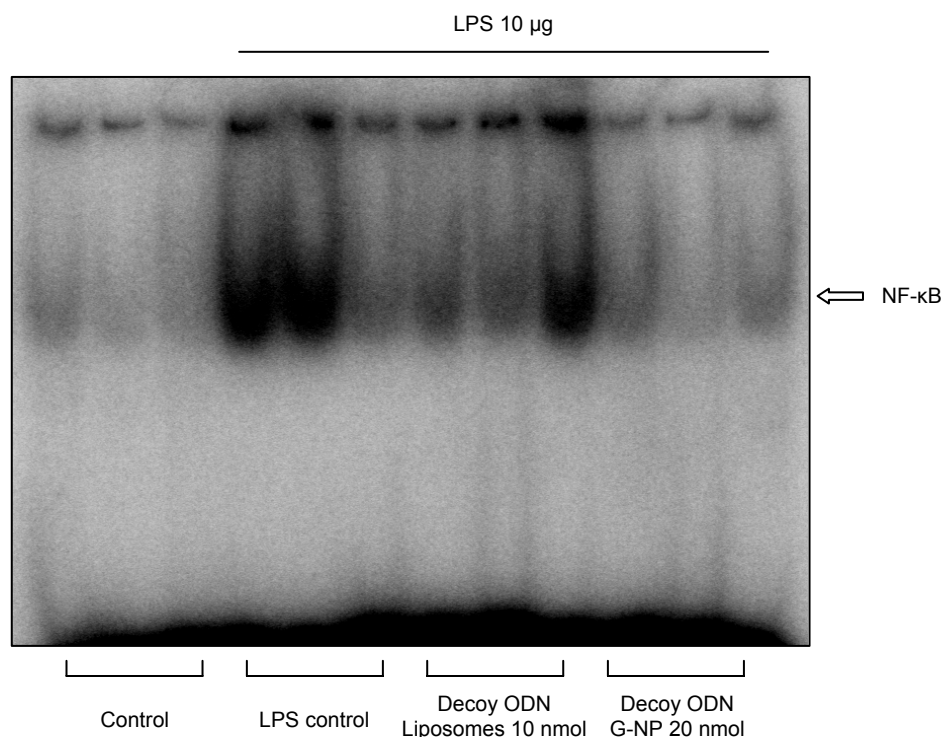


Figure 3.4.9 Hepatic NF- κ B activation after stimulation with 10 μ g LPS of animals treated with 10 nmol NF- κ B decoy oligonucleotide loaded liposomes and 20 nmol NF- κ B decoy oligonucleotide loaded gelatin nanoparticles and of untreated animals; one band represents one animal study

At the same time the difference to the – related to control animals – almost erased bands after application of 20 nmol gelatin nanoparticulate-bound NF- κ B becomes obvious. However, most important in this context is the unspecific distribution of liposomal delivered decoy ODN beyond Kupffer cells, which restricts the correlation between the inhibition of NF- κ B in Kupffer cells and the outcomes to be described in relation to this inhibition.

3.4.3 Summary

The hepatic NF- κ B activation in rats either caused by hepatic ischemia and reperfusion or by LPS stimulation could be nearly completely inhibited with an NF- κ B decoy oligonucleotide selectively delivered to Kupffer cells by gelatin nanoparticles. Scrambled decoy oligonucleotides and empty nanoparticles did not interfere with the mechanisms behind and left the NF- κ B activation unaffected. Based on the decoy mechanism of action a quantitative capture of all activated NF- κ B protein molecules is a prerequisite for the complete blockade of NF- κ B. This concentration dependent relation could be verified by administering different amounts of the decoy oligonucleotide. As samples from liver tissue were transferred

to EMSA in total and not extracted for Kupffer cells prior to analysis the demonstrated NF- κ B activation may possibly stated to be limited to Kupffer cells, which could explain the complete disappearing of NF- κ B bands from electrophoresis gels. Furthermore transaminases data from test animals revealed hepatic I/R injury to be not pronounced by the application of gelatin nanoparticles. To further assess the obtained results comparative data were gained from studies with liposomal delivered NF- κ B decoy oligonucleotide. These data confirmed the concentration dependent NF- κ B inhibition and demonstrated gelatin nanoparticles to be superior compared to liposomes for a selective Kupffer cell targeted drug delivery.

3.5 Concluding Remarks

In the beginning of the cooperate work of the chairs pharmaceutical biology and pharmaceutical technology of the Ludwig-Maximilians-University Munich there was an animal model combined with a drug targeting approach aimed at that enables the interruption of the inflammatory cascade during hepatic I/R injury on the stage of NF- κ B by delivery of a gelatin nanoparticulate-bound NF- κ B decoy oligonucleotide. Basic idea behind this project was to investigate the signaling pathways leading to hepatic ischemia reperfusion injury.

At this point of time the hepatic ischemia reperfusion rat model is established and the proposed selective Kupffer cell delivery of the NF- κ B decoy oligonucleotide, based on a gelatin nanoparticle drug delivery system, was proven. The adoption of 2D-PAGE for the analysis of plasma protein adsorption patterns on gelatin nanoparticles could contribute to the explanation of the observed *in vivo* biodistribution data. Finally a successful inhibition of NF- κ B followed from the administration of NF- κ B decoy oligonucleotide loaded gelatin nanoparticles prior to ischemia and reperfusion could be demonstrated. Regarding the gelatin nanoparticles applied in the hepatic ischemia reperfusion rat model for NF- κ B decoy oligonucleotide delivery modified plasma protein adsorption may occur due to the Tween[®] 80 stabilization of the nanoparticles. As the 2D-PAGE technique was no longer available after the completion of the thesis of Torsten Göppert this issue could not be investigated so far.

The impact of the NF- κ B blockade on the downstream processes of the inflammatory cascade is now particularly interesting and will be addressed in future studies.

During the preparation of NF- κ B decoy ODN loaded nanoparticles a convenient freeze dried formulation could be developed, which is now available and can be easily applied in the future of this cooperation project.

3.6 References

- Absolom, D. R.; Opsonins and dysopsonins: an overview; *Methods in Enzymology*, 1986, 132, 281-318
- Aderem, A. and Underhill, D. M.; Mechanisms of phagocytosis in macrophages; *Annual Review of Immunology*, 1999, 17, 593-623
- Agrawal, S. and Kandimalla, E. R.; Antisense therapeutics: is it as simple as complementary base recognition?; *Molecular Medicine Today*, 2000, 6(2), 72-81
- Allemann, E., Gravel, P., Leroux, J. C., Balant, L., and Gurny, R.; Kinetics of blood component adsorption on poly(DL-lactic acid) nanoparticles: evidence of complement C3 component involvement; *Journal of Biomedical Materials Research*, 1997, 37(2), 229-234
- Altieri, D. C., Mannucci, P. M., and Capitanio, A. M.; Binding of fibrinogen to human monocytes; *The Journal of clinical investigation*, 1986, 78(4), 968-976
- Anchordoquy, T. J., Armstrong, T. K., and Molina, M. D. C.; Low molecular weight dextrans stabilize nonviral vectors during lyophilization at low osmolalities: Concentrating suspensions by rehydration to reduced volumes; *Journal of Pharmaceutical Sciences*, 2005, 94(6), 1226-1236
- Anderson, N. L. and Anderson, N. G.; A two-dimensional gel database of human plasma proteins; *Electrophoresis*, 1991, 12(11), 883-906
- Arnedo, A., Espuelas, S., and Irache, J. M.; Albumin nanoparticles as carriers for a phosphodiester oligonucleotide; *International Journal of Pharmaceutics*, 2002, 244(1-2), 59-72
- Banafsche, R., Gunther, L., Nefflen, J. U., Moutsiou, S., Knolle, P. A., Herfarth, C., and Klar, E.; NF-kB antisense oligonucleotides reduce leukocyte-endothelial interaction in hepatic ischemia-reperfusion; *Transplantation Proceedings*, 2001, 33(7-8), 3726-3727
- Baron, A., Bilzer, M., and Gerbes, A. L.; Short-term treatment with mycophenolic acid increases bile flow in continuously perfused and cold-preserved rat livers and does not affect hepatic ischemia-reperfusion injury; *Transplant International*, 2002, 15(6), 265-271
- Beranova-Giorgianni, S.; Proteome analysis by two-dimensional gel electrophoresis and mass spectrometry: strengths and limitations; *Trends in Analytical Chemistry*, 2003, 22(5), 273-281

- Bijsterbosch, M. K., Manoharan, M., Dorland, R., Waarlo, I. H. E., Biessen, E. A. L., and van Berkel, T. J. C.; Delivery of cholesteryl-conjugated phosphorothioate oligodeoxynucleotides to Kupffer cells by lactosylated low-density lipoprotein; *Biochemical Pharmacology*, 2001, 62(5), 627-633
- Bilzer, M. and Gerbes, A. L.; Preservation injury of the liver: mechanisms and novel therapeutic strategies; *Journal of Hepatology*, 2000, 32(3), 508-515
- Bjellqvist, B., Ek, K., Righetti, P. G., Gianazza, E., Gorg, A., Westermeier, R., and Postel, W.; Isoelectric focusing in immobilized pH gradients: principle, methodology and some applications; *Journal of Biochemical and Biophysical Methods*, 1982, 6(4), 317-339
- Blunk, T.; Plasmaproteinadsorption on colloidal drug carriers; Dissertation, Christian-Albrechts-University Kiel, 1994
- Blunk, T., Hochstrasser, D. F., Sanchez, J. C., Mueller, B. W., and Mueller, R. H.; Colloidal carriers for intravenous drug targeting: plasma protein adsorption patterns on surface-modified latex particles evaluated by two-dimensional polyacrylamide gel electrophoresis; *Electrophoresis*, 1993, 14(12), 1382-1387
- Bradford, M. M.; A rapid and sensitive method for the quantitation of microgram quantities of protein utilizing the principle of protein-dye binding; *Analytical Biochemistry*, 1976, 72(1-2), 248-254
- Braet, F. and Wisse, E.; Structural and functional aspects of liver sinusoidal endothelial cell fenestrae: A review; *Comparative Hepatology*, 2002, 1(1), 1-17
- Bucke, W. E., Leitzke, S., Diederichs, J. E., Borner, K., Hahn, H., Ehlers, S., and Mueller, R. H.; Surface-modified amikacin-liposomes. Organ distribution and interaction with plasma proteins; *Journal of Drug Targeting*, 1998, 5(2), 99-108
- Chen, F. E. and Ghosh, G.; Regulation of DNA binding by Rel/NF-kappaB transcription factors: structural views; *Oncogene*, 1999, 18(49), 6845-6852
- Ciafre, S. A., Rinaldi, M., Gasparini, P., Seripa, D., Bisceglia, L., Zelante, L., Farace, M. G., and Fazio, V. M.; Stability and functional effectiveness of phosphorothioate-modified duplex DNA and synthetic 'mini-genes'; *Nucleic Acids Research*, 1995, 23(20), 4134-4142
- Dinauer, N., Lochmann, D., Demirhan, I., Bouazzaoui, A., Zimmer, A., Chandra, A., Kreuter, J., and von Briesen, H.; Intracellular tracking of protamine/antisense oligonucleotide nanoparticles and their inhibitory effect on HIV-1 transactivation; *Journal of Controlled Release*, 2004, 96(3), 497-507
- Fondevila, C., Busuttil, R. W., and Kupiec-Weglinski, J. W.; Hepatic ischemia/reperfusion injury-a fresh look; *Experimental and Molecular Pathology*, 2003, 74(2), 86-93

- Giakoustidis, D. E., Iliadis, S., Tsantilas, D., Papageorgiou, G., Kontos, N., Kostopoulou, E., Botsoglou, N. A., Gerasimidis, T., and Dimitriadou, A.; Blockade of Kupffer cells by gadolinium chloride reduces lipid peroxidation and protects liver from ischemia/reperfusion injury; *Hepato-Gastroenterology*, 2003, 50(53), 1587-1592
- Goeppert, T.; Plasma protein adsorption patterns on intravenously injectable colloidal drug carriers for drug delivery across the blood-brain barrier, Dissertation, Free University of Berlin; 2005
- Goeppert, T. M. and Mueller, R. H.; Polysorbate-stabilized solid lipid nanoparticles as colloidal carriers for intravenous targeting of drugs to the brain: Comparison of plasma protein adsorption patterns; *Journal of Drug Targeting*, 2005, 13(3), 179-187
- Goeppert, T. M. and Mueller, R. H.; Plasma protein adsorption of Tween 80- and Poloxamer 188-stabilized solid lipid nanoparticles; *Journal of Drug Targeting*, 2003, 11(4), 225-231
- Goerg, A., Weiss, W., and Dunn, M. J.; Current two-dimensional electrophoresis technology for proteomics; *Proteomics*, 2004, 4(12), 3665-3685
- Goetting, N., Fritz, H., Maier, M., Von Stamm, J., Schoofs, T., and Bayer, E.; Effects of oligonucleotide adsorption on the physicochemical characteristics of a nanoparticle-based model delivery system for antisense drugs; *Colloid and Polymer Science*, 1999, 277(2-3), 145-152
- Gujral, J. S., Bucci, T. J., Farhood, A., and Jaeschke, H.; Mechanism of cell death during warm hepatic ischemia-reperfusion in rats: apoptosis or necrosis?; *Hepatology*, 2001, 33(2), 397-405
- Gupta, R. B.; Fundamentals of drug nanoparticles; *Drugs and the Pharmaceutical Sciences*, 2006, 159 (Nanoparticle Technology for Drug Delivery), 1-19
- Haynes, P., Miller, I., Aebersold, R., Gemeiner, M., Eberini, I., Lovati, M. R., Manzoni, C., Vignati, M., and Gianazza, E.; Proteins of rat serum: I. Establishing a reference two-dimensional electrophoresis map by immunodetection and microbore high performance liquid chromatography-electrospray mass spectrometry; *Electrophoresis*, 1998, 19(8-9), 1484-1492
- Higuchi, Y., Kawakami, S., Oka, M., Yamashita, F., and Hashida, M.; Suppression of TNF α production in LPS induced liver failure in mice after intravenous injection of cationic liposomes/NF κ B decoy complex; *Pharmazie*, 2006, 61(2), 144-147
- Higuchi, Y., Kawakami, S., Yamashita, F., and Hashida, M.; The potential role of fucosylated cationic liposome/NF κ B decoy complexes in the treatment of cytokine-related liver disease; *Biomaterials*, 2007, 28(3), 532-539

- Hochstrasser, D. F., Harrington, M. G., Hochstrasser, A. C., Miller, M. J., and Merril, C. R.; Methods for increasing the resolution of two-dimensional protein electrophoresis; *Analytical Biochemistry*, 1988, 173(2), 424-435
- Hoffmann, F.; Dissertation in preparation, Ludwig-Maximilians-University Munich; 2007
- Jaeschke, H.; Molecular mechanisms of hepatic ischemia-reperfusion injury and preconditioning; *American Journal of Physiology*, 2003, 284(1, Pt. 1), G15-G26
- Jaeschke, H.; Antioxidant gene therapy and hepatic ischemia-reperfusion injury; *Hepatology*, 2002, 36(1), 243-245
- Kang, K. J.; Mechanism of hepatic ischemia/reperfusion injury and protection against reperfusion injury; *Transplantation Proceedings*, 2002, 34(7), 2659-2661
- Kaul, G. and Amiji, M.; Cellular interactions and in vitro DNA transfection studies with poly(ethylene glycol)-modified gelatin nanoparticles; *Journal of Pharmaceutical Sciences*, 2005, 94(1), 184-198
- Kawano, K., Kim, Y., I, Ono, M., Goto, S., Kai, T., and Kobayashi, M.; Evidence that both cyclosporin and azathioprine prevent warm ischemia reperfusion injury to the rat liver; *Transplant International*, 1993, 6(6), 330-336
- Kim, J. S., Qian, T., and Lemasters, J. J.; Mitochondrial permeability transition in the switch from necrotic to apoptotic cell death in ischemic rat hepatocytes; *Gastroenterology*, 2003, 124(2), 494-503
- Klose, J.; Protein mapping by combined isoelectric focusing and electrophoresis of mouse tissues. A novel approach to testing for induced point mutations in mammals; *Humangenetik*, 1975, 26(3), 231-243
- Koti, R. S., Seifalian, A. M., and Davidson, B. R.; Protection of the liver by ischemic preconditioning: a review of mechanisms and clinical applications; *Digestive Surgery*, 2003, 20(5), 383-396
- Kreuter, J.; Evaluation of nanoparticles as drug-delivery systems. II: Comparison of the body distribution of nanoparticles with the body distribution of microspheres (diameter greater than 1 micron), liposomes, and emulsions; *Pharmaceutica Acta Helvetiae*, 1983, 58(8), 217-226
- Kreuter, J.; Nanoparticles - preparation and applications; in *Microcapsules and Nanoparticles in Medicine and Pharmacy*, CRC Press, Inc., Boca Raton, FL, 1992, 125-148
- Kupatt, C., Habazettl, H., Goedecke, A., Wolf, D. A., Zahler, S., Boekstegers, P., Kelly, R. A., and Becker, B. F.; Tumor necrosis factor- α contributes to ischemia- and reperfusion-induced endothelial activation in isolated hearts; *Circulation Research*, 1999, 84(4), 392-400

- Lentsch, A. B., Kato, A., Yoshidome, H., McMasters, K. M., and Edwards, M. J.; Inflammatory mechanisms and therapeutic strategies for warm hepatic ischemia/reperfusion injury; *Hepatology*, 2000, 32(2), 169-173
- Leroux, J. C., Gravel, P., Balant, L., Volet, B., Anner, B. M., Allemann, E., Doelker, E., and Gurny, R.; Internalization of poly(DL-lactic acid) nanoparticles by isolated human leukocytes and analysis of plasma proteins adsorbed onto the particles; *Journal of Biomedical Materials Research*, 1994, 28(4), 471-481
- Li, C. and Jackson, R. M.; Reactive species mechanisms of cellular hypoxia-reoxygenation injury; *American Journal of Physiology*, 2002, 282(2, Pt. 1), C227-C241
- Löffler, G. and Petrides, P. E.; *Biochemie & Pathobiochemie*; Springer-Verlag GmbH, Berlin, 2003a, 7, 262-263
- Löffler, G. and Petrides, P. E.; *Biochemie & Pathobiochemie*; Springer-Verlag GmbH, Berlin, 2003b, 7, 1104-1105
- Luck, M., Paulke, B. R., Schroder, W., Blunk, T., and Muller, R. H.; Analysis of plasma protein adsorption on polymeric nanoparticles with different surface characteristics; *Journal of Biomedical Materials Research*, 1998, 39(3), 478-485
- Maitra, A.; Calcium phosphate nanoparticles: second-generation nonviral vectors in gene therapy; *Expert Review of Molecular Diagnostics*, 2005, 5(6), 893-905
- Mebius, R. E. and Kraal, G.; Structure and function of the spleen; *Nature Reviews Immunology*, 2005, 5(8), 606-616
- Meguro, M., Katsuramaki, T., Kimura, H., Isobe, M., Nagayama, M., Kukita, K., Nui, A., and Hirata, K.; Apoptosis and necrosis after warm ischemia-reperfusion injury of the pig liver and their inhibition by ONO-1714; *Transplantation*, 2003, 75(5), 703-710
- Mehnert, W. and Mader, K.; Solid lipid nanoparticles. Production, characterization and applications; *Advanced Drug Delivery Reviews*, 2001, 47(2-3), 165-196
- Moghimi, S. M. and Szebeni, J.; Stealth liposomes and long circulating nanoparticles: critical issues in pharmacokinetics, opsonization and protein-binding properties; *Progress in Lipid Research*, 2003, 42(6), 463-478
- Moghimi, S. M., Hunter, A. C., and Murray, J. C.; Long-circulating and target-specific nanoparticles: Theory to practice; *Pharmacological Reviews*, 2001, 53(2), 283-318
- Molnar, J., McLain, S., Allen, C., Laga, H., Gara, A., and Gelder, F.; The role of an α 2-macroglobulin of rat serum in the phagocytosis of colloidal particles; *Biochimica et Biophysica Acta, Protein Structure*, 1977, 493(1), 37-54

- Morishita, R., Higaki, J., Tomita, N., and Ogihara, T.; Application of transcription factor "decoy" strategy as means of gene therapy and study of gene expression in cardiovascular disease; *Circulation Research*, 1998, 82(10), 1023-1028
- Mosher, B., Dean, R., Harkema, J., Remick, D., Palma, J., and Crockett, E.; Inhibition of Kupffer cells reduced CXC chemokine production and liver injury; *Journal of Surgical Research*, 2001, 99(2), 201-210
- Mueller, R. H.; *Zetapotential und Partikelladung in der Laborpraxis (Paperback APV)*; Wissenschaftliche Verlagsgesellschaft mbH, Stuttgart, 1996,
- Mueller, R. H. and Heinemann, S.; Surface modeling of microparticles as parenteral systems with high tissue affinity; in *Bioadhesion-possibilities Future Trends, (Paperback APV)*, Wissenschaftliche Verlagsgesellschaft mbH, Stuttgart, 1990, 25, 202-213
- Mutschler, E.; *Arzneimittelwirkungen*; Wissenschaftliche Verlagsgesellschaft mbH, Stuttgart, 2001, 8, 230-231
- Nakada, Y., Fattal, E., Foulquier, M., and Couvreur, P.; Pharmacokinetics and biodistribution of oligonucleotide adsorbed onto poly(isobutylcyanoacrylate) nanoparticles after intravenous administration in mice; *Pharmaceutical Research*, 1996, 13(1), 38-43
- Nozaki, T., Totsuka, E., Takiguchi, M., Yoshida, A., and Sasaki, M.; Attenuation of canine hepatic warm ischemia/reperfusion injury by nitric oxide donor (FK409); *Hirosaki Igaku*, 2003, 54(3-4), 105-116
- O'Farrell, P. H.; High resolution two-dimensional electrophoresis of proteins; *Journal of Biological Chemistry*, 1975, 250(10), 4007-4021
- Ogawara, K. i., Furumoto, K., Nagayama, S., Minato, K., Higaki, K., Kai, T., and Kimura, T.; Pre-coating with serum albumin reduces receptor-mediated hepatic disposition of polystyrene nanosphere: implications for rational design of nanoparticles; *Journal of Controlled Release*, 2004, 100(3), 451-455
- Ogushi, I., Iimuro, Y., Seki, E., Son, G., Hirano, T., Hada, T., Tsutsui, H., Nakanishi, K., Morishita, R., Kaneda, Y., and Fujimoto, J.; Nuclear factor kappa Beta decoy oligodeoxynucleotides prevent endotoxin-induced fatal liver failure in a murine model; *Hepatology*, 2003, 38(2), 335-344
- Owens, D. E. and Peppas, N. A.; Opsonization, biodistribution, and pharmacokinetics of polymeric nanoparticles; *International Journal of Pharmaceutics*, 2006, 307(1), 93-102
- Ponnappa, B. C. and Israel, Y.; Targeting Kupffer cells with antisense oligonucleotides; *Frontiers in Bioscience*, 2002, 7, E223-E233

- Passirani, C. and Benoit, J. P.; Complement activation by injectable colloidal drug carriers; *Biomaterials for Delivery and Targeting of Proteins and Nucleic Acids*, 2005, 187-230
- Patel, H. M.; Serum opsonins and liposomes: their interaction and opsonophagocytosis; *Critical Reviews in Therapeutic Drug Carrier Systems*, 1992, 9(1), 39-90
- Ricciardi, R., Schaffer, B. K., Shah, S. A., Quarfordt, S. H., Banner, B. F., Wheeler, S. M., Donohue, S. E., Meyers, W. C., and Chari, R. S.; Bosentan, an endothelin antagonist, augments hepatic graft function by reducing graft circulatory impairment following ischemia/reperfusion injury; *Journal of Gastrointestinal Surgery*, 2001, 5(3), 322-329
- Righetti, P. G. and Drysdale, J. W.; Small-scale fractionation of proteins and nucleic acids by isoelectric focusing in polyacrylamide gels; *Annals of the New York Academy of Sciences*, 1973, 209, 163-186
- Righetti, P. G.; Bioanalysis: Its past, present, and some future; *Electrophoresis*, 2004, 25(14), 2111-2127
- Romero, E. L., Morilla, M. J., Regts, J., Koning, G. A., and Scherphof, G. L.; On the mechanism of hepatic transendothelial passage of large liposomes; *FEBS Letters*, 1999, 448(1), 193-196
- Roser, M., Fischer, D., and Kissel, T.; Surface-modified biodegradable albumin nano- and microspheres. Part 2. Effect of surface charges on in vitro phagocytosis and biodistribution in rats; *European Journal of Pharmaceutics and Biopharmaceutics*, 1998, 46(3), 255-263
- Scheele, G. A.; Two-dimensional gel analysis of soluble proteins. Characterization of guinea pig exocrine pancreatic proteins; *Journal of Biological Chemistry*, 1975, 250(14), 5375-5385
- Serracino-Inglott, F., Habib, N. A., and Mathie, R. T.; Hepatic ischemia-reperfusion injury; *American Journal of Surgery*, 2001, 181(2), 160-166
- Shiratori, Y., Kiriyaama, H., Fukushi, Y., Nagura, T., Takada, H., Hai, K., and Kamii, K.; Modulation of ischemia-reperfusion-induced hepatic injury by Kupffer cells; *Digestive Diseases and Sciences*, 1994, 39(6), 1265-1272
- Sobotta, J.; *Atlas der Anatomie des Menschen, Band 2*; Urban & Fischer Verlag GmbH, München, 1999, 21, 142-144
- Sperling, K.; From proteomics to genomics; *Electrophoresis*, 2001, 22(14), 2835-2837
- Stolnik, S., Illum, L., and Davis, S. S.; Long circulating microparticulate drug carriers; *Advanced Drug Delivery Reviews*, 1995, 16(2,3), 195-214

- Tan, Y., Zhang, J. S., and Huang, L.; Codelivery of NF-kB decoy-related oligodeoxynucleotide improves LPD-mediated systemic gene transfer; *Molecular Therapy*, 2002, 6(6), 804-812
- Teoh, N. C. and Farrell, G. C.; Hepatic ischemia reperfusion injury: pathogenic mechanisms and basis for hepatoprotection; *Journal of Gastroenterology and Hepatology*, 2003a, 18(8), 891-902
- Teoh, N., Leclercq, I., Pena, A. D., and Farrell, G.; Low-dose TNF-alpha protects against hepatic ischemia-reperfusion injury in mice: implications for preconditioning; *Hepatology*, 2003b, 37(1), 118-128
- Thews, G., Mutschler, E., and Vaupel, P.; Anatomie Physiologie Pathophysiologie des Menschen; Wissenschaftliche Verlag GmbH, Stuttgart, 1999, 5, 145-146
- Thiele, L., Diederichs, J. E., Reszka, R., Merkle, H. P., and Walter, E.; Competitive adsorption of serum proteins at microparticles affects phagocytosis by dendritic cells; *Biomaterials*, 2003, 24(8), 1409-1418
- Uhlmann, D., Witzigmann, H., Senninger, N., Hauss, J., and Spiegel, H. U.; Protective role of an endothelin-converting enzyme inhibitor (FR901533) in hepatic ischemia/reperfusion injury; *Microvascular Research*, 2001, 62(1), 43-54
- Van Leuven, F., Marynen, P., Sottrup-Jensen, L., Cassiman, J. J., and Van den Berghe, H.; The receptor-binding domain of human α 2-macroglobulin. Isolation after limited proteolysis with a bacterial proteinase; *Journal of Biological Chemistry*, 1986, 261(24), 11369-11373
- Van Oss, C. J.; Phagocytosis as a surface phenomenon; *Annual Review of Microbiology*, 1978, 32, 19-39
- Vilatoba, M., Eckstein, C., Bilbao, G., Smyth, C. A., Jenkins, S., Thompson, J. A., Eckhoff, D. E., and Contreras, J. L.; Sodium 4-phenylbutyrate protects against liver ischemia reperfusion injury by inhibition of endoplasmic reticulum-stress mediated apoptosis; *Surgery*, 2005, 138(2), 342-351
- Vogel, W., Bomford, A., Young, S., and Williams, R.; Heterogeneous distribution of transferrin receptors on parenchymal and nonparenchymal liver cells: biochemical and morphological evidence; *Blood*, 1987, 69(1), 264-270
- Vonarbourg, A., Passirani, C., Saulnier, P., and Benoit, J. P.; Parameters influencing the stealthiness of colloidal drug delivery systems; *Biomaterials*, 2006, 27(24), 4356-4373
- Wattiaux, R., Laurent, N., Wattiaux-De Coninck, S., and Jadot, M.; Endosomes, lysosomes: their implication in gene transfer; *Advanced Drug Delivery Reviews*, 2000, 41(2), 201-208

- Wilkins, D. J. and Myers, P. A.; Studies on the relationship between the electrophoretic properties of colloids and their blood clearance and organ distribution in the rat; *British Journal of Experimental Pathology*, 1966, 47(6), 568-576
- Witzigmann, H., Ludwig, S., Escher, E., Armann, B., Gabel, G., Teupser, D., Tannapfel, A., Pietsch, U. C., Hauss, J., and Uhlmann, D.; Administration of a selective endothelin-A receptor antagonist (BSF 208075) improves hepatic warm ischemia/reperfusion injury in pigs; *Transplantation Proceedings*, 2002, 34(6), 2387-2388
- Yabe, Y., Kobayashi, N., Nishihashi, T., Takahashi, R., Nishikawa, M., Takakura, Y., and Hashida, M.; Prevention of neutrophil-mediated hepatic ischemia/reperfusion injury by superoxide dismutase and catalase derivatives; *Journal of Pharmacology and Experimental Therapeutics*, 2001, 298(3), 894-899
- Yan, X., Scherphof, G., and Kamps, J.; Liposome Opsonization; *Journal of Liposome Research*, 2005, 15(1 & 2), 109-139
- Yoshida, M., Yamamoto, N., Uehara, T., Terao, R., Nitta, T., Harada, N., Hatano, E., Iimuro, Y., and Yamaoka, Y.; Kupffer cell targeting by intraportal injection of the HVJ cationic liposome; *European Surgical Research*, 2002, 34(3), 251-259
- Young, D. S. and Tracy, R. P.; Clinical applications of two-dimensional electrophoresis; *Journal of Chromatography, A*, 1995, 698(1 + 2), 163-179
- Zillies, J. and Coester, C.; Evaluating gelatin based nanoparticles as a carrier system for double stranded oligonucleotides; *Journal of Pharmacy & Pharmaceutical Sciences*, 2004, 7(4), 17-21
- Zwacka, R. M., Zhang, Y., Zhou, W., Halldorson, J., and Engelhardt, J. F.; Ischemia/reperfusion injury in the liver of BALB/c mice activates AP-1 and nuclear factor kB independently of Ikb degradation; *Hepatology*, 1998, 28(4), 1022-1030
- Zwiorek, K.; Gelatin nanoparticles as delivery system for nucleotide-based drugs, Dissertation, Ludwig-Maximilians-University Munich; 2006

FINAL CONCLUSION

The present work followed a course of analytical description, formulation development, and practical application of (NF- κ B decoy oligonucleotide-loaded) gelatin nanoparticles. The introduction of asymmetrical flow field-flow fractionation (AF4) in the analysis of colloidal drug carrier systems was exemplarily described for gelatin nanoparticles (**CHAPTER I**), stable freeze-dried formulations of empty and oligonucleotide loaded gelatin nanoparticles were successfully developed (**CHAPTER II**), and gelatin nanoparticles were proven as effective tool for the targeted delivery of an NF- κ B decoy oligonucleotide to Kupffer cells within a hepatic ischemia reperfusion rat model (**CHAPTER III**).

Gelatin bulk material is characterized by inherent heterogeneity of its molecular weight distribution. Selective fractionation yet enables the production of homogeneously size-distributed gelatin nanoparticles, at which asymmetrical flow field-flow fractionation (AF4) analysis revealed a mean molecular weight of the favorable gelatin fraction of $\sim 2,000$ kDa (**CHAPTER I**). This is about one order of magnitude higher than it was determined for the unfractionated gelatin. This two-step desolvation procedure could successfully be simplified towards a one-step desolvation by employing customized gelatin batches. This is remarkable as the mean molecular weight of these batches could be determined ranging in the middle between regularly applied gelatin bulk material and the above mentioned high molecular weight fraction obtained during two-step desolvation. In addition the specification of the customized batches stated a reduced portion of low molecular weight gelatin < 65 kDa below 20 % [w/w]. Thus, the restrictions that have to be made for gelatin bulk material in terms of successful one-step desolvation include a mean molecular weight around 500 kDa and a concurrently reduced portion of low molecular weight fractions. The necessity of reducing the peptide amount below 20 % [w/w] could be proven to be even more decisive than the expanded presence of high molecular weight fractions. Subsequently, the resolving power of AF4 for particulate matter was exemplified. The separation of suspended gelatin nanoparticles from dissolved single- and double-stranded oligonucleotides was demonstrated and the drug loading of a single-stranded oligonucleotide onto the nanoparticles' surface could be quantified via the AUCs of the respective UV

detection signals. A precedent sample preparation was thereby not necessary. The drug loading of a double-stranded oligonucleotide in turn highlighted the methodical limit of this analytical approach. The concept of adverse charged reaction partners enabling drug loading via electrostatic attraction requires in case of double-stranded oligonucleotides clearly stronger charges than for single-stranded oligonucleotides. With respect to reproducible AF4 sample runs these charges are in general compensated by increasing the ionic background within the running buffer. This avoids on the one hand adsorptive tendencies within capillaries and the separation channel but causes on the other hand the release of oligonucleotide from the surface of gelatin nanoparticles due to the weakened electrostatic attraction between the double-stranded oligonucleotide and the nanoparticles. Independent from these considerations the quantification of covalently bound PEG on gelatin nanoparticles could be completed. In an analogous attempt to the single-stranded drug loading the amount of unbound PEG was calculated from its RI detection signals obtained before and after PEGylation. RI detection was imperative due to the poor spectroscopic properties of PEG.

The need for a gelatin nanoparticle formulation that is easy to ship, to store, and to handle especially with regard to future application in clinical studies was addressed during the development of a freeze-dried formulation of gelatin nanoparticles (**CHAPTER II**). Nanoparticles were at first successfully freeze-dried with various amounts of sucrose. Particle size and size distribution were preserved, pertaining residual moisture contents ranged below 1 % and the respective glass transition temperatures matched expectations. For convenient application freeze-dried samples of already drug-loaded gelatin nanoparticles are required. Thus, freeze-drying properties of loaded gelatin nanoparticles were explored for double-stranded DNA and siRNA oligonucleotides. Basically, data from empty nanoparticles could be verified and were supplemented with important results from experiments investigating reduced rehydration volumes. In order to obtain high concentrated suspensions of oligonucleotide-loaded gelatin nanoparticles, samples were rehydrated upon freeze-drying with reduced volumes, whereas sample integrity was not affected. Concomitantly, excipient amounts were adjusted to guarantee isotonicity of the rehydrated samples. By substituting sucrose for dextran 3000, low excipient masses could be circumvented while the osmotic activity was maintained.

Interestingly, dextran 3000 was able to sufficiently stabilize loaded gelatin nanoparticles at its own. Samples combined of four accordingly concentrated NF- κ B decoy oligonucleotide-loaded gelatin nanoparticle preparations were transferred to the hepatic ischemia reperfusion rat model, established during the cooperation work described in chapter 3.4, where a selective NF- κ B inhibition within Kupffer cells could be accomplished: Thus, the concept of concentrating ODN-loaded gelatin nanoparticles by freeze-drying was successfully proving.

In the last part of this chapter the storage stability of empty and oligonucleotide-loaded gelatin nanoparticles was investigated. Formulations containing sucrose, trehalose, mannitol, and mannitol-sucrose in the ratio 4:1 were prepared and held under four different storage conditions. The results revealed good stabilizing properties of sucrose and trehalose, whereas trehalose appears superior at increased storage temperatures due to its higher T_g . If the residual moisture content did not exceed a threshold of 3 %, particle size and size distribution were preserved. Complete sample loss was observed during storage at elevated relative humidity. Despite its crystalline nature even mannitol was able to stabilize empty and oligonucleotide-loaded gelatin nanoparticles at its own, whereas compared to sucrose and trehalose higher excipient amounts were required. The resistance of mannitol against water sorption was expressed in sufficient stabilizing of samples containing the highest amount of mannitol during open storage at 30 % RH. Mannitol-sucrose formulations in turn exhibited poor stabilizing properties. This could be related to amorphous mannitol resulting from freeze-drying that underwent conversion to its crystalline state during storage, which finally corrupted the sample quality. Finally *in vivo* data from stored oligonucleotide-loaded gelatin nanoparticles demonstrated that maintained sample quality at the same time provides maintained biological function of the bound oligonucleotide.

Based on the rapid clearance of colloidal drug carrier systems by cells of the MPS, an exclusive targeting of gelatin nanoparticles within liver to Kupffer cells was proposed (**CHAPTER III**). Loaded with an NF- κ B decoy oligonucleotide, gelatin nanoparticle delivery should enable the selective inhibition of NF- κ B in Kupffer cells. NF- κ B inhibition should in turn contribute to the elucidation of inflammation processes taking place after NF- κ B activation upon hepatic ischemia reperfusion. In cooperation with the chair of Pharmaceutical Biology of the Ludwig-Maximilians-

University Munich a rat model of warm hepatic ischemia reperfusion was established. Before the NF- κ B inhibition could be therein evaluated, the selectivity of the Kupffer cell uptake was scrutinized. Independent from the route of administration, nanoparticles were found to be exclusively distributed within liver to Kupffer cells. Intraportal application thereby increased the portion of nanoparticles detectable within liver compared to other organs. Additionally investigated liposomes were in contrast to a small extent also detectable beyond Kupffer cells in hepatocytes. The biodistribution of gelatin nanoparticles was further investigated with respect to their plasma protein adsorption patterns and compared to solid lipid nanoparticles (SLN). After incubating empty, surface-modified, and oligonucleotide-loaded gelatin nanoparticles with human or rat plasma, adsorbed proteins were qualified and quantified by 2D-PAGE analysis. Different from SLN, mainly adsorbing apolipoproteins, classical opsonins were adsorbed in a comparable manner on all gelatin nanoparticle formulations indicating a rapid clearance from circulation. Findings from 2D-PAGE were confirmed *in vivo* with short plasma half lives below 15 min and an accumulation of gelatin nanoparticles in the organs of the MPS. SLN in turn showed longer circulation times in addition to unspecific organ distribution.

After proving the selective Kupffer cell uptake, NF- κ B decoy oligonucleotide-loaded gelatin nanoparticles were applied in the hepatic ischemia reperfusion rat model. The amount of the delivered oligonucleotide was thereby determined to be decisive for a successful NF- κ B inhibition. Only after applying the concentrated samples obtained from formulation development by freeze-drying, (complete) inhibition of NF- κ B was achieved, suggesting a concentration dependent mechanism. NF- κ B decoy oligonucleotide released from liposomes showed as well certain NF- κ B inhibition. But, with respect to their distribution beyond Kupffer cells the direct correlation between NF- κ B inhibition within Kupffer cells and monitored changes of the downstream processes will be limited. After establishing the *in vivo* model and the targeted delivery of the NF- κ B decoy oligonucleotide to Kupffer cells via gelatin nanoparticles the outcome of the NF- κ B inhibition within Kupffer cells can now be addressed during future studies.

In sum the technological basis of gelatin nanoparticles was further broadened. Besides the advancement in the implementation of AF4, the description of a freeze-dried gelatin nanoparticle formulation provides convenient handling and application

in future. And, the development of gelatin nanoparticles for selective oligonucleotide delivery to Kupffer cells offers a tool to further investigate Kupffer cell related signal transduction within liver, as well beyond hepatic ischemia reperfusion injury.

This Thesis has been Presented and Published in Parts in:

Original Research Articles

Zillies, J. and Coester, C.; Evaluating gelatin based nanoparticles as a carrier system for double stranded oligonucleotides; *Journal of Pharmacy & Pharmaceutical Sciences*, 2004, 7(4), 17-21

Fraunhofer, W., Winter, G., Zillies, J., Coester, C.; Asymmetrical flow field-flow fractionation as new analytical tool in pharmaceutical biotechnology; *New Drugs*, 2003, 2, 16-19

In preparation

Zillies, J., Zwioerek, K., Winter, G., Coester, C.; A New method for quantifying the PEGylation of gelatin nanoparticle drug carrier systems using asymmetrical flow field-flow fractionation (AF4) and refractive index (RI) detection (submitted to *Analytical Chemistry*, November 2006)

Zillies, J., Anchordoquy, T., Winter, G., Coester, C.; Formulation development of freeze-dried gelatin nanoparticles

Patent

Ahlers, M., Coester, C., Zwioerek, K., and Zillies, J.; Biodegradable gelatin nanoparticles and procedure for their production; DE 102004041340 / WO 2006/021367

Oral Presentations

Zillies, J., Winter, G., Coester, C.; Application of asymmetrical flow field-flow fractionation in the analysis of colloidal drug carrier systems; *Pharmaceutical Sciences Fair & Exhibition*, Nice, France, June 12-17, 2005

Zillies, J., Winter, G., Coester, C.; A new delivery system for double stranded siRNA oligonucleotides based on gelatin nanoparticles; *Canada-Japan Nanopharmaceutical Symposium*, Banff, Canada, August 22-26, 2004

Poster Presentations

Zillies, J., Göppert, T. M., Müller, R. H., Hoffmann, F., Vollmar, A., Winter, G., Coester, C.; Correlation of plasma protein adsorption patterns and biodistribution data of different gelatin and solid lipid nanoparticle formulations; *AAPS Annual Meeting & Exposition*, Nashville, USA, November 6-10, 2005

Zillies, J., Nayyar, P., Zwioerek, K., Samuel, J., Coester, C.; Intracellular distribution and trafficking of fluorescent dye loaded gelatin nanoparticles; *CRS Annual Meeting & Exposition*, Miami Beach, USA, June 18-22, 2005

Zillies, J., Winter, G., Coester, C.; New methods for the characterization of different gelatin based nanoparticulate drug carrier systems; *AAPS Annual Meeting and Exposition*, Salt Lake City, USA, October 26-30, 2003

Zillies, J. and Coester, C.; Capillary hydrodynamic fractionation (CHDF) and other semi-chromatographic methods as new analytical tools for the separation and analysis of protein based nanoparticles aside low molecular weight proteins and oligonucleotides; *Annual Meeting Controlled Release Society Local Chapter Germany*, Munich, Germany, April 4, 2003

Curriculum Vitae

Jan Carl Zillies

Personal data

Date of birth April 20, 1976
Place of birth Hamburg
Nationality German

Work experience and academic training

Since 01/2003 Ph.D. studies at the Department of Pharmacy
Pharmaceutical Technology and Biopharmaceutics of the
Ludwig-Maximilians-University Munich, Germany
Supervisor: Prof. Dr. Gerhard Winter
01/2006-04/2006 Research stay at the School of Pharmacy of the University of
Colorado, Denver, CO, USA
Supervisor: Prof. Dr. Thomas J. Anchordoquy
07/2002-12/2002 Pharmacist (retail), Hamburg, Germany

Education

11/2001-04/2002 Practical education in pharmacy (industry), Department of
Regulatory Affairs, AstraZeneca GmbH, Wedel, Germany
05/2001-10/2002 Practical education in pharmacy (retail),
Maria-Louisen-Apotheke, Hamburg, Germany
10/1996-03/2001 Study of pharmacy,
Albert-Ludwigs-University Freiburg, Germany
10/1995-07/1996 Military service at the German Navy,
Fleet Headquarters, Gluecksburg, Germany
1986-1995 High School, Ratsgymnasium Bielefeld, Graduation with
Abitur